UNIVERSITY OF CALIFORNIA

Los Angeles

Polymeric Materials to Improve the Stability and Delivery of Insulin and Glucagon

A dissertation submitted in partial satisfaction of the requirements for the degree Doctor of Philosophy in Chemistry

by

Kathryn Margaret Mansfield Messina

2020

ABSTRACT OF THE DISSERTATION

Polymeric Materials to Improve

the Stability and Delivery of Insulin and Glucagon

by

Kathryn Margaret Mansfield Messina

Doctor of Philosophy in Chemistry

University of California, Los Angeles, 2020

Professor Heather D. Maynard, Chair

Proteins and peptides have become an important class of therapeutics due to their high specificity and general biocompatibility. However, using proteins and peptides as drugs has several intrinsic challenges. These macromolecules are generally cleared rapidly due to renal filtration and enzymatic degradation following administration. Issues of instability during storage due to their chemical composition and specific three-dimensional confirmations necessitate that most protein and peptide therapeutics be stored in the refrigerator or as a lyophilized powder. Additionally, they must be administered through injection and are not responsive to intrinsic biological signals, unlike endogenous processes. Thus, it is important to develop methods to improve characteristics of

protein and peptide therapeutics to improve their stability, pharmacokinetics, and delivery in response to biological stimuli.

Chapter Two describes the investigation of the insulin stabilization properties of trehalose glycopolymer as excipient and conjugate. Addition of a styrenyl backbone trehalose polymer excipient stabilized insulin against aggregation induced by exposure of insulin to heat or mechanical agitation. Conjugation of the trehalose polymer to insulin was achieved by reductive amination and the stability assays were repeated with the conjugate, showing results like the excipient. The conjugation site was identified as GlyA1 and LysB29 by indirect characterization through acid-cleavage of the polymer. While conjugation prolonged the half-life in mice, addition of trehalose polymer excipient did not alter protein pharmacokinetics. The mechanism of insulin stabilization was investigated with a methacrylate backbone trehalose polymer excipient, showing presence of the polymer inhibits both fibrillation and deamidation.

Chapter Three continues the development of a new strategy for site-specific conjugation of a trehalose polymer to insulin for improved stability and bioactivity. Conditions for AGET ATRP under mild, aqueous conditions were optimized. A site-specific insulin macroinitiator was prepared targeting modification at LysB29 utilizing its higher nucleophilicity over the other possible amine conjugation sites and purifying to isolate the desired species. Trehalose monomer was polymerized directly from this site-specific macroinitiator resulting in a conjugate with improved heat stability. A lower dosage of the site-specific conjugate compared to the nonspecific conjugate was needed to achieve the same change in blood glucose.

Chapter Four details the synthesis of blood triggered self-immolative linkers designed for use as spacers for rapid-acting insulin-trehalose glycopolymer conjugates. Linkers triggered by

serum albumin through base-catalyzed β-elimination were first prepared and triggering was characterized. During conjugation, the first linker underwent premature triggering from the primary amines of insulin and the exposed amine catalyzed further triggering. The second linker design underwent base-catalyzed self-immolation over the course of 20 h. Linkers that could be triggered by the thiol concentration in the blood were then synthesized and evaluated. Both aliphatic and aromatic linkers underwent rapid self-immolation with small molecules across the disulfide under relevant glutathione concentrations. Conjugation with trehalose glycopolymer slowed the kinetics of the self-immolation, likely because of the increase in steric bulk.

Chapter Five describes optimization of the background release of insulin from a trehalose glycopolymer hydrogel for improved stability and glucose-responsive delivery of the protein. Several strategies were used to decrease the background release. Two methods to increase the binding affinity of the boronic acid to polyols was used to strengthen the hydrogel network. The influence of pore size/crosslink density was also explored. Finally, incorporation of comonomers for electrostatic attraction to insulin resulted in the lowest background release of insulin without glucose after optimization of gelation procedure.

Chapter Six introduces glucose-responsive materials for regulation of glucagon delivery. Glucose-responsive nanogels are prepared by precipitation polymerization and post-polymerization modification with phenylboronic acid as glucose-sensing unit. Nanogels were thermo- and glucose-responsive through incorporation of thermoresponsive pNIPAM or pPEGMA with glucose acting as an additive that alters the hydration of the polymers. Native glucagon was found to degrade during the loading of the nanogels, so a more stable soluble analog was used that improved to loading.

The Dissertation of Kathryn Margaret Mansfield Messina is approved.

Andrea L. Hevener

Joseph A. Loo

David S. Eisenberg

Heather D. Maynard, Committee Chair

University of California, Los Angeles

2020

TABLE OF CONTENTS

LIST OF FIGURES

LIST OF TABLES

LIST OF SCHEMES

LIST OF ABBREVIATIONS

AA, ascorbic acid

AFM, atomic force microscopy

AGET, activators generated by electron transfer

AIBN, azobisisobutyronitrile

AGET, activators generated by electron transfer

2-APBA, 2-aminophenylboronic acid

APS, ammonium persulfate

ARGET, activators regenerated by electron transfer

ATRP, atom transfer radical polymerization

BSA, bovine serum albumin

BTPA, 2-(butylthiocarbonothioyl)propionic acid

*c*GFP, cyclic green fluorescent protein

CPADB, 4-cyano-4-(phenylcarbonothioylthio)pentanoic acid

CPP, cell-penetrating peptide

CTA, chain-transfer agent

CuAAC, copper-catalyzed azide-alkyne cycloaddition

CuBr, copper(I) bromide

$CuBr_2$, copper(II) bromide

CuCl, copper(I) chloride

Cys, cysteine

DBCO, dibenzocyclooctyl

DCC, *N*,*N*-dicyclohexylcarbodiimide

DLS, dynamic light scattering

DCM, dichloromethane

DMA, *N,N*-dimethylacrylamide

DMAP, 4-dimethylaminopyridine

DMAEMA, 2-(dimethylamino)ethyl methacrylate

DMF, *N*,*N*-dimethylformamide

DNA, deoxyribonucleic acid

Dox, doxorubicin

DTT, dithiothreitol

eATRP, electrochemically-mediated ATRP

EDC, 1-Ethyl-3-(3-dimethylaminopropyl)carbodiimide

ELISA, enzyme-linked immunosorbent assay

ESI-MS, electrospray ionization mass spectrometry

FcMMA, ferrocenyl methyl methacrylate

FPLC, fast protein liquid chromatography

FT-IR, fourier transform infrared spectroscopy

Gd, gadolinium

GFP, green fluorescent protein

GMA, glycidyl methacrylate

GOx, glucose oxidase

GPC, gel-permeation chromatography

Hb, hemoglobin

HEA, hydroxyethyl acrylate

HEMA, 2-hydroxyethyl methacrylate

HPLC, high performance liquid chromatography

HRP, horseradish peroxidase

HSF, horse spleen apoferritin

ICAR, initiators for continuous activator regeneration

IFN-α, interferon-α

LC-MS, liquid chromatography mass spectrometry

LC-MS/MS, tandem liquid chromatography mass spectrometry

LCST, lower critical solution temperature

Lys, lysine

Lyz, lysozyme

MALDI-ToF, matrix assisted laser desorption/ionization time-of-flight

Mb, myoglobin

MES, 2-(*N*-morpholino)ethanesulfonic acid

MOEGMA, methoxy oligo(ethylene glycol) methacrylate

MPC, methacryloyloxyethyl phosphorylcholine

MPEGMA, monomethoxy poly(ethylene glycol)-methacrylate

MSEA, 2-(methylsulfinyl)ethyl acrylate

NaBr, sodium bromide

native PAGE, native polyacrylamide gel electrophoresis

*n*BA, *n*-butyl acrylate

*n*BMA, *n*-butyl methacrylate

NHS, *N*-hydroxysuccinimide

NIPPAm, *N*-isopropyl acrylamide

NMP, nitroxide-mediated polymerization

OEGA, oligo(ethylene glycol) acrylate

OEGMA, oligo(ethylene glycol) methacrylate

PBS, phosphate buffered saline

PDS, pyridyl disulfide

PEG, poly(ethylene glycol)

PEGA, poly(ethylene glycol) acrylate

PEGMA, poly(ethylene glycol) methacrylate

PET-RAFT, photo-induced electron transfer-RAFT

PFP, pentafluorophenyl

Phe, phenylalanine

Photo-ATRP, photo-mediated ATRP

PLP, pyridoxal-5-phosphate

PMDETA, *N,N,N′,N″,N″*-pentamethyldiethylenetriamine

PNA, peptide nucleic acid

PPase, pyrophosphatase

RAFT, reversible addition-fragmentation chain-transfer polymerization

RCM, ring-closing metathesis

RDRP, reversible deactivation radical polymerization

rh-GH, recombinant human growth factor

ROMP, ring-opening metathesis polymerization

ROMPISA, ring-opening metathesis polymerization-induced self-assembly

SAv, streptavidin

sCT, salmon calcitonin

SDS-PAGE, sodium dodecyl sulfate polyacrylamide gel electrophoresis

SEC, size exclusion chromatography

SET-LRP, single electron transfer living radical polymerization

siRNA, small interfering ribonucleic acid

SPAAC, strain-promoted 1,3-dipolar cycloaddition

SPE, screen printed electrode

SP, sodium pyruvate

SPPS, solid-phase peptide synthesis

SrtA, sortase A

ssDNA, single-stranded DNA

*t*BA, *tert*-butyl acrylate

TBAF, tetra-n-butylammonium fluoride

TCEP, tris(2-carboxyethyl)phosphine

tDNA, transfer DNA

TEA, triethylamine

TEA-Br, tetraethylammonium bromide

TEM, transmission electron microscopy

TFA, trifluoroacetic acid

TIPS, triisopropylsilane

TL, *Thermomyces languginosa*

TPMA, tris(2-pyridylmethyl) amine

TPO-Na, (2,4,6-trimethylbenzoyl)phenyl phosphonic acid sodium

TreSA- styrenyl acetal backbone trehalose polymer

TreMA- methacrylate backbone trehalose polymer

VA-044, 2,2'-Azobis[2-(2-imidazolin-2-yl)propane]dihydrochloride

VI, *N*-vinylimidazole

VLP, virus-like nanoparticle

ACKNOWLEDGEMENTS

"It matters not what someone is born, but what they grow to be."

–JK Rowling, *Harry Potter and the Goblet of Fire*

I am so thankful to my family, who have provided an abundance of love and encouragement during my graduate studies and without whom I could not have finished this dissertation. Thank you to my parents, Stan and Lori Mansfield, for their endless support and unconditional love. You are the most wonderful parents and I am so grateful to know you always have my back. Thank you to my sister, brother in law, and adorable niece, Sarah, Aaron, and Eleanor Bobuk, for their love and friendship. Thank you to my grandparents, Merle and Ruthann Loney, who inspire me to achieve my goals and for their generous support of my education.

The person who has been one of my closest confidants and sources of perseverance has been my husband, Marco Messina, who I am so glad to have met during my graduate studies. I am so thankful for his love, humor, support, and encouragement. I am also thankful for his insight and advice with chemistry. Thank you to my wonderful mother in law, Norma Puente, and all my new family for being extremely welcoming and making me feel immediately at home.

I also must thank my advisor Heather Maynard for her mentorship and advocacy. My experience in her group has led to many wonderful professional opportunities. I am truly grateful for her belief in my abilities and championship of my growth as a scientist. Thank you also to my committee members: David Eisenberg, Joseph Loo, Tatiana Segura, and Andrea Hevener.

Thank you to my graduate student mentor, Jeong Hoon Ko, who taught me practically all my laboratory skills and who is a wonderful advocate for me. JK is such an impressive scientist and I'm so grateful for his mentorship. Thank you to my mentees, Warrick Ma and Jane Yang, who are awesome and for some reason listened to what I had to say to them. I'm pleased to leave my project in the hands of capable scientists of Jane and Daniele. Thank you to Priera Panescu for being one of my best friends and bridesmaid. I remember Pri talking about being in the Maynard lab and me thinking "She's so cool and I'll never get in that lab!" but I'm glad I was wrong.

I also am so grateful for all my coworkers in the Maynard group, who have offered their advice and friendship. Thank you to Sam, Uland, Natalie, Jacquelin, Daniele, Emma, Kyle, Neil, Doug, Madeline, Arvind, Kathleen, Mikayla, Nik, Hayden, Grace, Billy, and Omar. Thank you to all my friends in the chemistry department. I'm particularly grateful for Michelle Bradley who has become one of my best friends and bridesmaid, and I'm so glad I sat next to her in orientation!

Thank you to the UCLA Biotechnology Training Program, Helmsley trust, and the UCLA Graduate Division for funding during my graduate studies.

Chapter 1 was reproduced with permission from: Messina, M.S.; Messina, K.M.M.; Bhattacharya, A.; Montgomery, H.R.; Maynard, H.D. "Preparation of biomolecule-polymer conjugates by grafting-from using ATRP, RAFT, or ROMP" *Prog. Poly. Sci.* **2020**, *100*, 101186. Copyright 2019 Elsevier.

Chapter 2 contains portions of an edited version of the following published paper reprinted with permission from: Liu, Y.;† Lee, J.;† Mansfield, K.M.; Ko, J.H.; Sallam, S.; Wesdemiotis, C.; Maynard, H.D. "Trehalose Glycopolymer Enhances Both Solution Stability and Pharmacokinetics

of a Therapeutic Protein." *Bioconjugate Chem.* **2017**, *28*, 836-845. (†Equal contribution). Copyright 2017 American Chemical Society.

Chapter 3 was reprinted with permission from: Mansfield, K.M.; Maynard, H.D. "Site-Specific Insulin-Trehalose Glycopolymer conjugate by Grafting from Strategy Improves Bioactivity." *ACS Macro Lett.* **2018**, *7*, 324-329. Copyright 2018 American Chemical Society.

Chapter 5 contains portions of an edited version of the following published paper reprinted with permission from: Lee, J., Ko, J. H., Mansfield, K.M., Nauka, P. C., Bat, E., Maynard, H. D., "Glucose-Responsive Trehalose Hydrogels for Insulin Stabilization and Delivery," *Macromol. Biosci*, **2018**, *18*, 1700372, 1-7. Copyright 2017 WILEY-VCH Verlag GmbH & Co. KGaA, Weinheim.

VITA

Education

University of California, Los Angeles

Ph.D. Candidate in Chemistry, Specialization in Biophysics, Sept. 2015-June 2020

Advancement to Candidacy & M.S. Chemistry: April 2017

California Polytechnic State University (Cal Poly SLO), San Luis Obispo

B.S. Chemistry, *Magna Cum Laude*, June 2015

Research Experience

Graduate Researcher, Department of Chemistry and Biochemistry, UCLA.

September 2015 to June 2020

Advisor: Heather D. Maynard

Chemistry/Materials Science Intern, HP Inc.

April 2018 to July 2018

Undergraduate researcher, Department of Chemistry, Cal Poly SLO.

March 2014 to June 2015

Advisors: Derek Gragson and Rafael Jimenez-Flores.

Publications

Messina, M. S.; Messina, K. M. M., Bhattacharya, A.; Montgomery, H. R.; Maynard, H. D. "Preparation of Biomolecule-Polymer Conjugates by Grafting-from using ATRP, RAFT, or ROMP" *Prog. Polym. Sci*., **2020**, *100*, 101186.

Lee, J.; Ko, J. H.; Mansfield, K. M.; Nauka, P. C.; Bat, E.; Maynard, H. D. "Glucose-Responsive Trehalose Hydrogel for Insulin Stabilization and Delivery" *Macromol. Biosci*., **2018**, *18*, 1700372.

Mansfield, K. M.; Maynard, H. D. "Site-Specific Insulin-Trehalose Glycopolymer Conjugate by Grafting From Strategy Improves Bioactivity" *ACS Macro Lett.*, **2018**, *7*, 324-329. *Chosen for the cover of that issue

Liu, Y.; Lee, J.; Mansfield, K. M.; Ko, J. H.; Sallam, S.; Wesdemiotis, C.; Maynard, H. D. "Trehalose Glycopolymer Enhances Both Solution Stability and Pharmacokinetics of a Therapeutic Protein" *Bioconjugate Chem*., **2017**, *28*, 836-845. *Highlighted in C&EN News

Awards and Honors

- UCLA Graduate Division Dissertation Year Fellowship (May 2019)
- UCLA Research Showcase Fellowship for Fall 2019 ACS National Meeting (March 2019)
- NIH Biotechnology Training in Biomedical Sciences and Engineering Fellowship (June 2016- June 2018)
- Outstanding Chemistry Student (Cal Poly College of Math and Science Award) (June 2015)
- LAM Research Scholarship for the Sciences (Nov. 2015)
- President's list (3 consecutive quarters on the Dean's list) (2011-2015)

Chapter 1. Introduction: Preparation of Biomolecule-Polymer Conjugates by Grafting-From using ATRP, RAFT, or ROMP

1.1 Introduction

Biomolecule-polymer conjugates represent an important class of macromolecular architectures that combine the advantageous properties inherent to both the biomolecule and synthetic polymer(s) appended to it. The attachment of poly(ethylene glycol) (PEG) to biomolecule therapeutics represents the most utilized form of biomolecule-polymer conjugates in the pharmaceutical realm, and there currently exist 17 PEGylated peptide and protein therapeutics which have garnered approval from the food and drug administration (FDA).[1-8] In this instance, PEG acts to increase the *in vivo* biomolecule half-life by protecting the therapeutic from recognition by the immune system and/or reducing clearance.[2] The development of controlled polymerization techniques has equipped the scientific community with the ability to prepare specially tailored polymers of controlled molecular weights and well-defined architectures from a wide array of monomers.[9-11] This has led to the development of diverse polymers able to invoke unique characteristics such as pH responsiveness, increased storage and *in-vivo* stability, thermo-responsiveness, and in PEG alternatives which exhibit lower immunogenicity.[1, 12-16] Commonly used controlled polymerization techniques for biomolecule-polymer modification are atom-transfer radical polymerization (ATRP), reversible addition-fragmentation chain-transfer polymerization (RAFT), and ring-opening metathesis polymerization (ROMP), which are the focus of this review.[11, 16-18] It is important to note that nitroxide-mediated radical polymerization (NMP) has also been used to great extent to prepare bioactive polymers and conjugates, and interested readers are directed to the many interesting reviews and manuscripts which detail the use of NMP.[19-22]

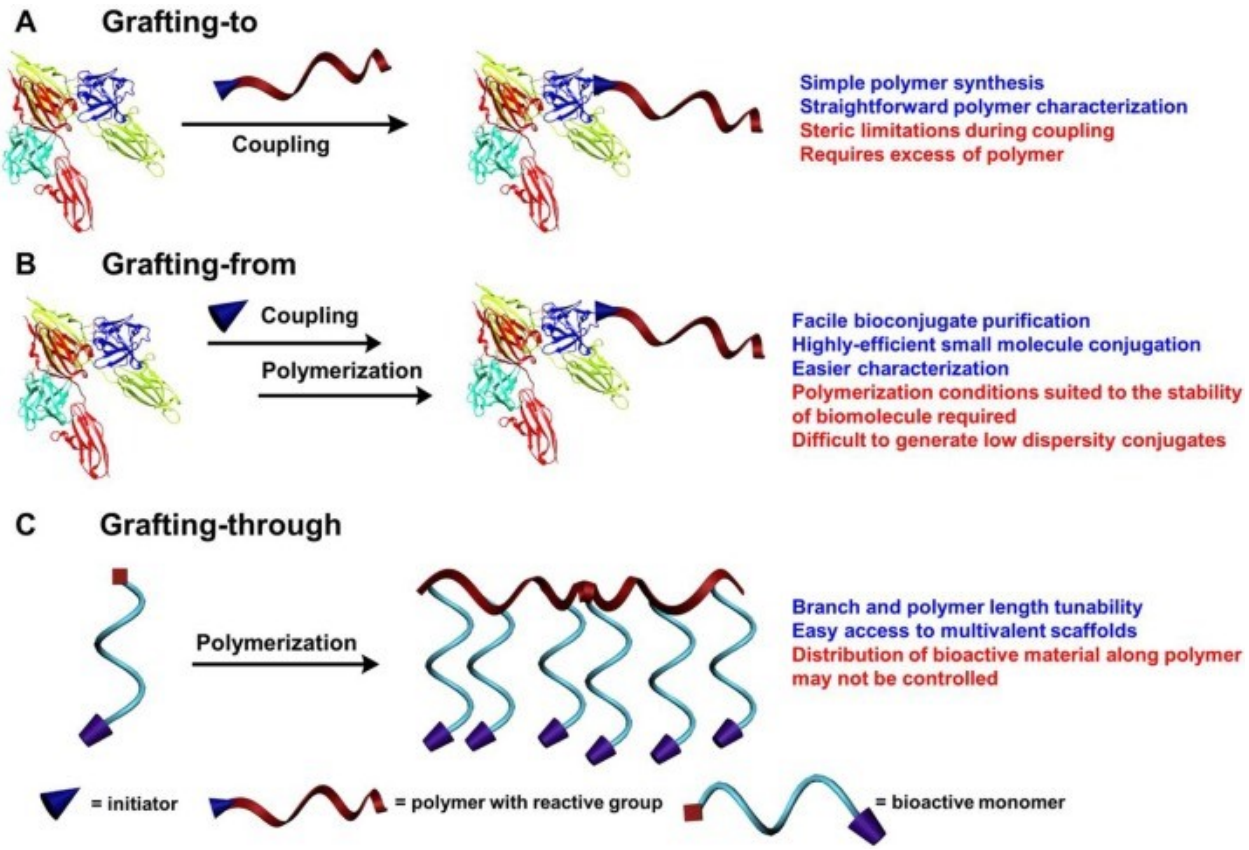

Figure 1-1. Schematic representations depicting different methods of preparing biomolecule-polymer conjugates along with a list of key advantages or disadvantages.

Biomolecule-polymer conjugates prepared using controlled polymerization techniques are typically accessed through three different routes: grafting-to in which a polymer is first synthesized, purified, and subsequently coupled to the biomolecule, grafting-from in which a small-molecule reactive handle is attached to the biomolecule and used as an initiation site to grow the polymer from the surface of the protein, and grafting-through in which monomers functionalized with a specific payload are polymerized (**Figure 1-1**).[15, 23-24] Grafting-through has been used to a great extent in the preparation of bioactive polymers synthesized using ROMP and we will briefly cover a few examples in that area towards the end of the review. The grafting-to

strategy has been employed to a greater extent most likely due to the great advances that have been made in coupling chemistry and the introduction of so-called "click" reactions which are highly versatile and efficient methods to generate bioconjugates (**Figure 1-1A**). However, the grafting-from technique offers many advantages, especially in regard to the purification of the prepared biomolecule-polymer conjugate (**Figure 1-1B**).[15, 23] Using an excess amount of a small-molecule for bioconjugation is a straight-forward process, as any unreacted material can easily be removed either by dialysis or size-exclusion chromatography (SEC) due to the large disparity in molecular weights between the protein and small-molecule. In contrast, using an excess amount of polymer to couple onto a biomolecule can be problematic due to the time intensive nature of polymer synthesis. Purification of polymers from the bioconjugates is also challenging due to similarities in molecular weight. Additionally, in grafting-from limitations due to sterics, which are inherent to the coupling of polymers to biomolecules, are avoided and characterization of the locations of the polymer chains on the conjugate is easier. However, grafting-from techniques require polymerization conditions which are suited to the stability of the biomolecule and it remains challenging to generate low dispersity conjugates.

Over the course of this review, we will cover recent progress in the formation of biomolecule-polymer conjugates which have been prepared using the grafting-from technique. For reading ease, the review is sectioned in terms of the controlled polymerization technique used. The initial section will cover select works using ATRP, the second section will cover RAFT polymerization, and the third will be devoted to ROMP with a brief discussion on grafting-through techniques to develop bioactive polymers (**Figure 1-1C**).

1.2 Conjugation of reactive groups onto biomolecules

Key to the successful implementation of the grafting-from technique is the installation of small molecule reactive handles capable of initiating or mediating polymerization processes from the biomolecule surface. Throughout the years this has taken many forms, with lysine (Lys) and cysteine (Cys) amino acid residues being the most frequently targeted sites for modification on proteins (**Figure 1-2**).[1, 25] For the purposes of grafting-from, Cys amino acid modifications have taken the form of pyridyl disulfide (PDS) exchange and Michael addition using maleimide-modified substrates. The weaknesses of these linkages lie in their inherent instability with disulfide bridges being reversible in the presence of external reductants and the thiol-ether bond from the maleimide being susceptible to retro-Michael processes *in vivo*. However, Cys remains a popular site for conjugation due to the low relative abundance on proteins, thereby allowing for site selectivity.[25] Lys is also a popular site for conjugation of reactive groups with several research groups taking advantage of conjugation through acid-halides, *N*-hydroxysuccinimide (NHS)-esters, nitrophenyl carbonates, and squaric acid containing functionality (**Figure 1-2**).[1, 25-26] However, Lys residues typically have a high abundance on proteins and conjugation methods are generally non-selective, and there are many groups currently working on selective Lys conjugation techniques.[27-29]

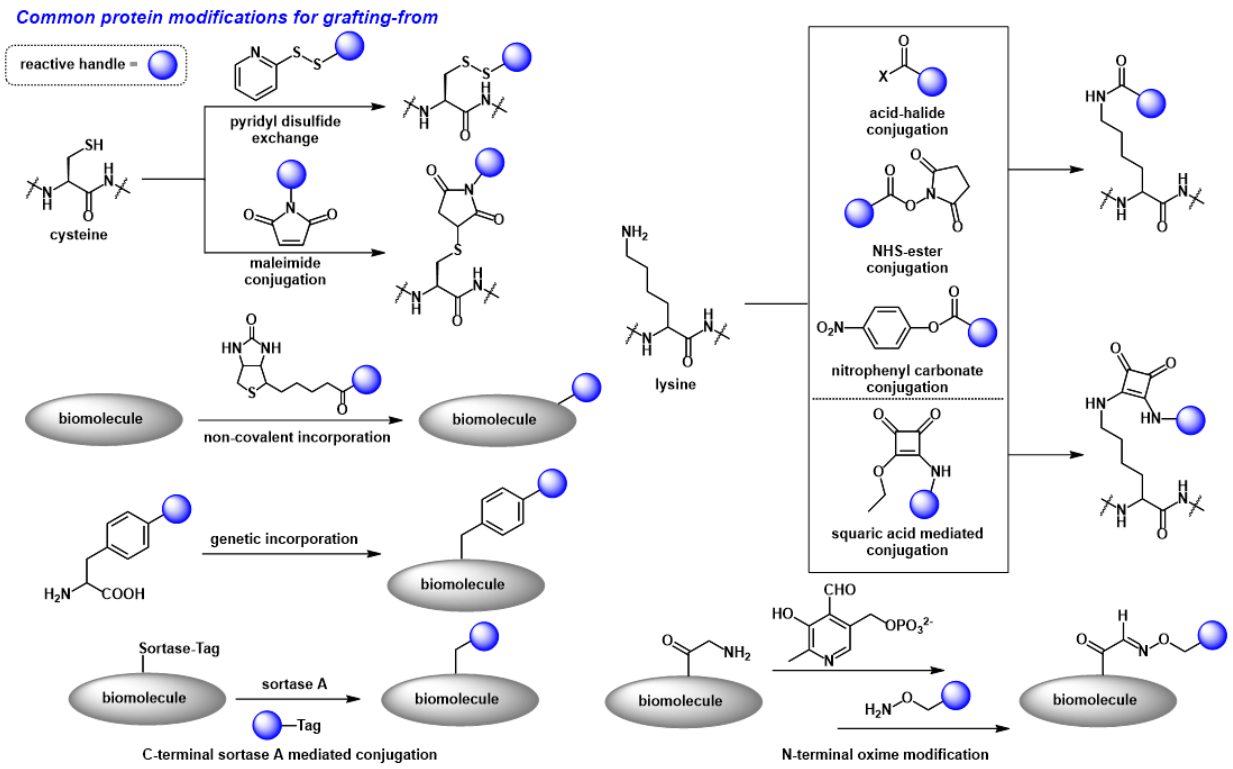

Figure 1-2. Commonly used protein modification techniques for grafting-from.

Other methods of conjugating reactive handles onto protein substrates include non-covalent modification taking advantage of the streptavidin (SAv)-biotin interaction, genetic incorporation of non-native amino acids, sortase A (SrtA)-mediated modifications targeting LPGXTG/A sequences on the proteins C-terminus, and oxime formation after treatment by pyridoxal-5-phosphate (PLP) which targets the protein N-terminus.[1, 23, 30-31] Given the expansion of amino acid modification techniques along with the introduction of transition-metal-mediated conjugation techniques, there remains a wealth of opportunities to modify proteins with reactive handles capable of mediating polymerization.[32-41]

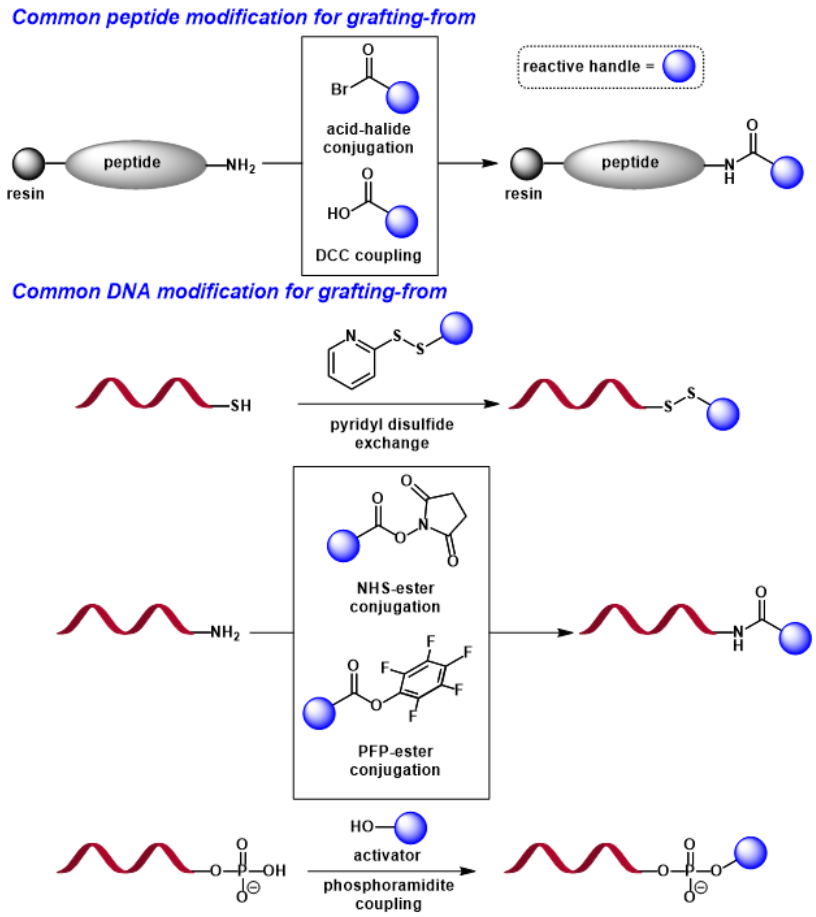

Figure 1-3. Commonly used peptide and nucleic acid modification techniques for grafting-from.

Typical peptide conjugation for grafting-from has been performed *via* on-resin reactions targeting the amine terminus of the peptide by either acid-halide conjugation or *N*,*N*-dicyclohexylcarbodiimide (DCC) coupling of reactive handles.[42-43] Deoxyribonucleic acid (DNA) modification for grafting-from has typically made use of either PDS exchange on a thiol terminated DNA strand, NHS-ester or pentafluorophenyl (PFP)-ester conjugation on amine terminated DNA, and phosphoramidite coupling which targets the phosphoester backbone on DNA (**Figure 1-3**).[24, 44-45]

1.3 Biomolecule-polymer conjugates accessed through ATRP

ATRP is a living and controlled radical polymerization technique, first reported independently by the Matyjaszewski group and the Sawamoto group in 1995, which falls under the category of reversible deactivation radical polymerization (RDRP).[18, 46-47] In the traditional ATRP mechanism, homolytic cleavage of a C(sp^3)-X (where X = Br or Cl) bond on an ATRP initiator is imposed by a reduced metal halide catalyst thereby initiating polymerization (**Figure 1-4**). The then oxidized metal catalyst can reversibly deactivate the radical propagation of the polymer chain transfer of the halide to the end of the propagating polymer chain. This reversible deactivation ultimately imposes control over the polymerization process by decreasing the amount of active radicals in solution thereby minimizing unproductive termination pathways (**Figure 1-4**).[9, 18]

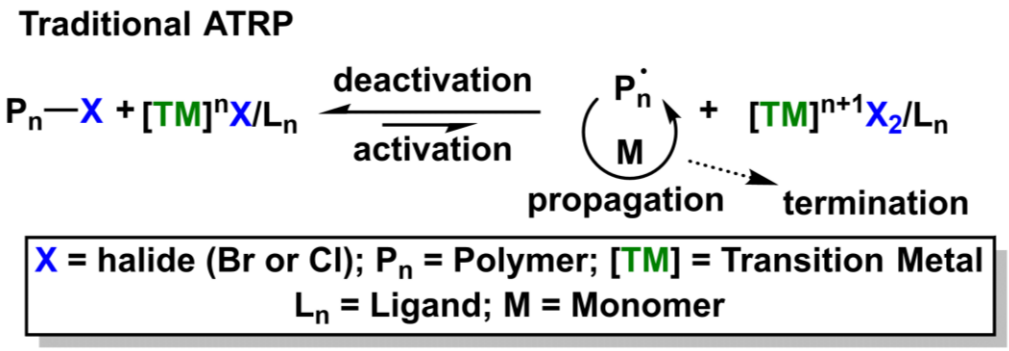

Figure 1-4. Mechanism of the traditional ATRP process.

There are many alternatives to typical ATRP procedures which differ in the method of initiation used. A few commonly used alternative ATRP strategies for grafting-from processes include initiators for continuous activator regeneration (ICAR), activators generated by electron transfer (AGET), activators regenerated by electron transfer (ARGET), and photo-induced ATRP

among others.[18] Though there exist many other ATRP strategies, we will only focus on those used for the grafting-from polymerization.[9, 18]

1.3.1 Traditional ATRP to access protein-polymer conjugates by grafting-from

Workers at Biocompatibles Ltd synthesized hydroxysuccinimide ester substituted ATRP initiators which were then appended onto Lys residues of the protein lysozyme (Lyz).[48] Protein functionalization was performed in borate buffer at room temperature and the resulting protein-macroinitiator was used without purification. A variety of olefin substituted monomers and zwitterionic monomers were polymerized from the protein surface under traditional ATRP conditions in the presence of a copper bromide catalyst and bipyridyl ligand at room temperature. The resulting protein-polymer conjugates could be isolated via capillary electrophoresis.[48]

Our group published grafting-from methodology by employing traditional ATRP to polymerize *N*-isopropylacrylamide (NIPAAm) from both SAv and T4 lysozyme (T4-Lyz) (**Figure 1-5**A and B).[49-50] In our initial disclosure targeting SAv bioconjugates, we developed a biotin functionalized ATRP initiator. The strong binding affinity of biotin to SAv (K_d = 10^{-15} M) was utilized to modify the protein with up to four of the biotin ATRP initiators thereby forming the SAv-macroinitiator (**Figure 1-5**A).[49, 51] The room temperature polymerization of NIPAAm using the SAv-macroinitiator was carried out in an aqueous solution in the presence of copper (I) bromide (CuBr) and the 2,2'-bipyridine ligand.[49] In a follow-up article that same year, our group modified a Cys amino acid residue (Cys-34) on bovine serum albumin (BSA) as well as a Cys residue (Cys-131) on a genetically engineered T4-Lyz protein with an ATRP initiator. The BSA- or T4-Lyz-macroinitiators were prepared using either pyridyl disulfide exchange to modify the proteins with reversible disulfide linkages or by maleimide conjugation (**Figure 1-5**B).[50] Grafting-

from polymerization of NIPAAm was carried out similarly to the previous report grafting-from SAv (**Figure 1-5**B).[49-50] The polymer-conjugates were purified via preparative SEC and characterized using gel permeation chromatography and sodium dodecyl sulfate polyacrylamide gel electrophoresis (SDS-PAGE). Additionally, the T4-Lyz-polymer conjugate retained activity as determined by a commercially available fluorescence assay which monitored lysis of the *Micrococcus lysodeikticus* substrate. Though these works provided a foundation for the introduction of the grafting-from concept, polymerization from the SAv and T4-Lyz bioconjugates required the addition of a 2-bromoisobutyryl-functionalized resin which was introduced in order to increase the concentration of initiating sites **Figure 1-5**A and B).[49-50] The addition of a sacrificial initiator is not needed when there is an abundance of the protein substrate, as is the case with cheaper proteins such as BSA.

Matyjaszewski, Russell, and co-workers also disclosed an example of grafting-from using traditional ATRP from chymotrypsin functionalized at Lys amino acid residues with 2-bromoisobutyramide initiators (**Figure 1-5**C).[52] The authors expanded the monomer scope to include polymerization of monomethoxy poly(ethylene glycol)-methacrylate (MPEGMA), sodium 4-styrenesulfonate, and 2-(dimethylamino)ethyl methacrylate (DMAEMA) from the chymotrypsin macroinitiator, which was carried out in the presence of phosphate buffered saline (PBS) (pH 6.0), CuBr, and 2,2'-bipyridine (**Figure 1-5**C). All of the protein-polymer conjugates retained their bioactivity to varying degrees' dependent on the nature of the polymer, with the poly(MPEGMA) conjugated protein retaining the highest at 76%, as determined by a spectrophotometric assay monitoring enzymatic hydrolysis of an oligopeptide sequence.[52] An important feature represented in this manuscript is that uniform protein-polymer conjugates could be accessed when attaching one initiator onto the protein.[52] Taking further advantage of grafting-from using traditional ATRP

techniques, the groups have gone on to publish manuscripts detailing the tuning of enzyme activity and stability based on the polymers attached to the enzyme.[53] Additionally, redox active polymers have been polymerized from the surface of glucose oxidase (GOx) and exhibited an increase in the efficiency of current generation when testing the GOx-polymer conjugates on the surface of an anode.[54]

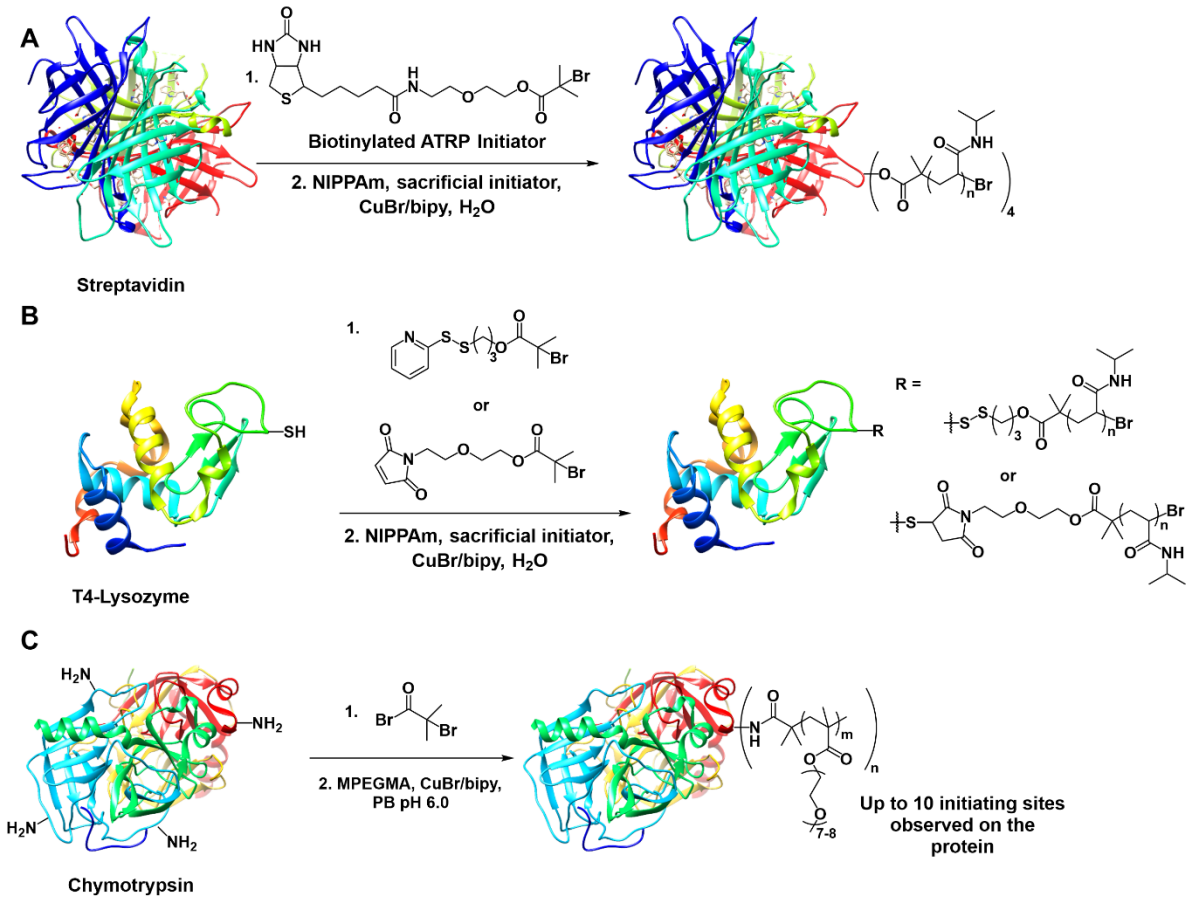

Figure 1-5. Examples of grafting-from polymerization using ATRP. (A) Maynard and co-workers use of SAv-biotin interaction in order to develop a SAv-macroinitiator to be employed in the controlled polymerization of NIPPAm.[49] The Maynard group Cys targeted approaches towards polymer-protein conjugate generation via grafting-from.[50] (C) The Matyjaszewski and Russell groups work in developing a chymotrypsin macroinitiator through Lys conjugation.[52]

The initial reports on grafting-from were followed-up extensively with reports, which demonstrated expansions in the conjugation chemistry, monomer scope, variance in polymer architectures, and the protein substrates used. The Haddleton group developed protein macroinitiators using maleimide conjugation chemistry to target the Cys-34 on BSA and NHS-ester conjugation to target Lys residues on Lyz.[55] They were able to co-polymerize methacrylate-functionalized fluorescent monomers based on either rhodamine B or hostasol along with PEGMA.[55-56] An impressive example of grafting-from is a report by the Velonia group in which they combined copper-catalyzed azide-alkyne cycloaddition (CuAAC) and ATRP which resulted in the polymerization, from a Cys-34 modified BSA, of alkyne-functionalized methacrylate monomers and subsequent attachment of azide-functionalized small-molecules for the *in-situ* production of *giant amphiphiles*.[57] The Klok group has also shown success in using squaric acid mediated conjugation techniques to install ATRP initiators on Lys amino acid residues of BSA.[26]

Mehl, Matyjaszewski, and co-workers devised an elegant approach to installing ATRP initiators within proteins by genetically encoding the ATRP initiator containing unnatural amino acid 4-(2'-bromoisobutyroamido)phenylalanine within green fluorescent protein (GFP).[58] The authors evolved a *Methanococcus jannaschii* tyrosyl-tRNA synthetase/$tRNA_{CUA}$ pair that installed the novel amino acid in the presence of an amber codon. Incredibly, up to 420 mg of the ATRP initiator modified GFP was purified from one liter of medium. Upon purification of the GFP-macroinitiator and characterization by ESI-mass spectrometry, which showed an increase in mass from the wild type GFP corresponding to addition of the ATRP initiator, polymerization was carried out using traditional ATRP techniques in the presence of PBS and methoxy OEG methacrylate monomer (MOEGMA) at room temperature.[58]

The scientific community also gained interest in grafting-from larger types of biomolecule constructs. Wang and co-workers modified Lys residues on horse spleen apoferritin (apo-HSF) with bromoisobutyrate initiators via NHS-ester bioconjugation.[59] Matrix assisted laser desorption/ionization time-of-flight (MALDI-ToF) analysis following tryptic digestion of the apo-HSF macroinitiator revealed modification of Lys-83, Lys-97, Lys-104, and Lys-143, all of which are highly exposed on the surface of the biomolecule. Polymerization of PEGMA from the apo-HSF macroinitiator was carried out in a 4:1 mixture of PBS (pH 8.5) and *N*,*N*-dimethylformamide (DMF) at 4°C upon treatment with CuBr and bipyridine. Hydrogels could be formed in the presence of high monomer loadings (up to 1800 equiv to the macroinitiator) which could be subsequently solubilized in dichloromethane (DCM). The biomolecule-polymer conjugates were characterized via fast protein liquid chromatography (FPLC) and transmission electron microscopy (TEM).[59] The Russell and Emrick research groups also used grafting-from to access horse spleen ferritin (HSF) and poly(methacryloyloxyethyl phosphorylcholine) poly(MPC) conjugates.[60] Poly(MPC) is a biocompatible zwitterionic polymer which is resistant to non-specific protein adsorption, similarly to PEG, though it is much more hydrophilic. The authors used NHS-ester chemistry to conjugate up to 45 bromoisobutyryl ATRP initiators onto Lys residues of HSF and accessed HSF-poly(PEGMA) conjugates in a similar manner to what was previously reported.[59] Notably, the HSF-poly(MPC) and HSF-poly(PEGMA) conjugates exhibited distinct changes in recognition properties due to the presence of the polymers on the protein surface. This was apparent in the decreased ferritin antibody binding as determined by an enzyme-linked immunosorbent assay (ELISA)-based assay.[60] The Ye group has also utilized NHS-ester bioconjugation to develop temperature and pH responsive hybrid biomaterials made by polymerizing NIPAAm from the surface of amelogenin.[61]

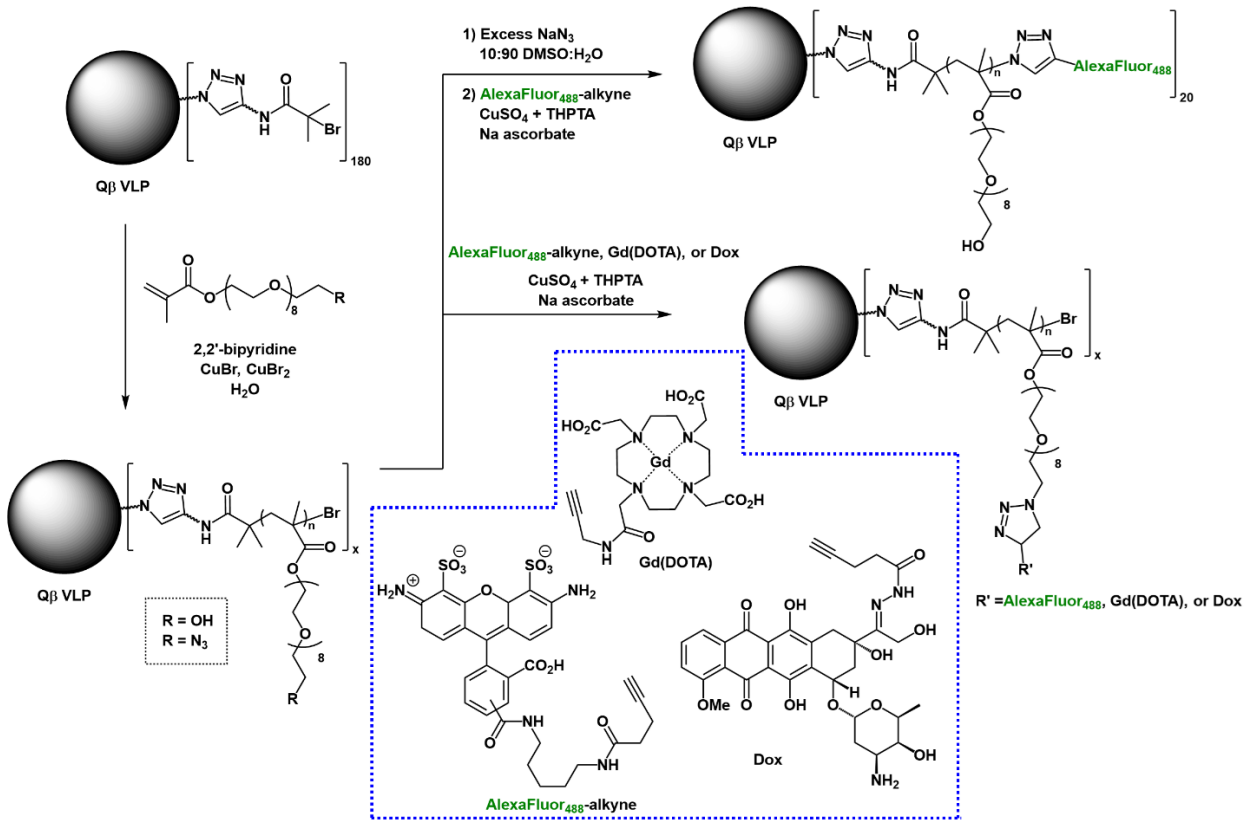

Figure 1-6. Grafting-from example from the Finn group in which they modified QB VLP-macroinitiators to synthesize polymers which could undergo post-polymerization modification with an array of bioactive substrates.[62]

Finn and co-workers demonstrated an elegant example of grafting-from virus-like nanoparticles (VLP's) using traditional ATRP (**Figure 1-6**).[62] The group developed bacteriophage Qβ VLP macroinitiators by reacting azide functionalized NHS-ester linkers to Lys residues on the biomolecule and using CuAAC to add on the alkyl bromide ATRP initiator. It was found by protein digestion and subsequent mass spectrometry analysis that ~180 Lys residues were modified (**Figure 1-6**). Polymerization of oligoethylene glycol methacrylate (OEGMA) was carried out by treating the macroinitiator and monomer solution with 2,2'-bipyridine, CuBr, and $CuBr_2$ in water. The purified conjugates were characterized via dynamic light scattering (DLS) and SEC which

showed that the VLP-polymer conjugates were much larger in size to the Qβ wild-type. Notably, the bromine end-groups present on the polymers of the VLP-poly(OEGMA) conjugates could be modified further through treatment with sodium azide to form azide terminated polymers which could undergo CuAAC with an alkyne bearing AlexaFluor488 fluorescent dye (**Figure 1-6**). Additionally, the authors developed VLP-poly(OEGMA-N_3) conjugates in which each OEGMA repeat unit was modified with a pendent azide. This allowed for post-polymerization modification using CuAAC with the AlexaFluor488 dye, doxorubicin (Dox), or a gadolinium (Gd) complex (**Figure 1-6**). This is a notable achievement given the importance of Gd-modified nanoparticles in magnetic resonance imaging. Through inductively coupled plasma optical emission spectroscopy (ICP-OES), the authors found that the VLP-poly(OEGMA-Gd) particles contained 500-650 Gd complexes per conjugate. Additionally, the authors conjugated Dox via 'click' chemistry on the pendent poly(OEGMA-N_3) and found about 150 Dox molecules appended onto the particle. The drug could be released in the presence of pH 5.5 2-(*N*-morpholino)ethanesulfonic acid (MES) buffer through degradation of the hydrazone linkage present on Dox and were also found to be cytotoxic towards HeLa cells at the same concentrations as free Dox. Interestingly, control experiments in which Dox was loaded directly on the VLP through triazole linkages and subjected to pH 5.5 MES buffer led to complete degradation and subsequent precipitation of the biomolecule indicating that the presence of poly(OEGMA) conjugated to the protein surface is required for stability.[62]

The Chilkoti group has targeted the N-terminus of myoglobin (Mb) to attach an ATRP initiator by-way of oxime ligation chemistry.[31] This modification resulted in a single reactive site on the protein surface. The site-specific conjugation of the ATRP initiator was confirmed by liquid chromatography with tandem mass spectrometry (LC-MS/MS) of peptide fragments after trypsin

digestion of the Mb-macroinitiator. In-situ ATRP of OEGMA from the singly modified Mb-macroinitiator in aqueous conditions resulted in the formation of a Mb-poly(OEGMA) bioconjugate which retained bioactivity and exhibited an increased in vivo half-life compared to native Mb.[31] Chilkoti and coworkers have also used SrtA-mediated conjugation to attach an ATRP initiator on the C-terminus of GFP.[30] GFP harboring a SrtA recognition site was expressed and purified then subsequently treated with an amine functionalized ATRP initiator in the presence of SrtA. This reaction resulted in a singly modified GFP-macroinitiator which was modified exclusively at the C-terminus of the protein. Notably, this methodology proved to be highly efficient with the GFP-macroinitiator purified in >85% yield.[30] SrtA mediated installation of a reactive handle has also been used in the attachment of an ATRP initiator onto the C-terminus of interferon-α (IFN-α) by the Gao group.[63] Using traditional ATRP techniques they were able to polymerize OEGMA thereby developing IFN-α-poly(OEGMA) conjugates which exhibited increased *in-vivo* half-life compared to native IFN-α. Additionally, IFN-α-poly(OEGMA) showed increased anti-proliferative activity in mice compared to IFN-α-PEG conjugates used clinically.[63] The Gao group has also made use of SrtA mediated transformations to produce a cyclized GFP (*c*GFP) derivative and subsequently coupled an ATRP initiator using maleimide chemistry to target an engineered Cys residue on the protein.[64] Polymerization of OEGMA to produce *c*GFP-poly(OEGMA) conjugates resulted in a hybrid protein with increased thermal stability and enhanced tumor retention relative to either native GFP or the non-cyclized GFP-poly(OEGMA) conjugates.[64]

1.3.2 Peptide-polymer conjugates

Traditional ATRP techniques have also been used to access peptide-polymer conjugates via grafting-from. Though it is important to note that peptide-polymer conjugates had been previously prepared by grafting-from using NMP and additionally, ATRP had been previously shown to operate using substrates attached to a Wang resin.[65-66] In 2004, the Washburn group used ATRP to prepare peptide-polymer conjugates via grafting-from to prepare GRGDS-poly(2-hydroxyethyl methacrylate) (poly(HEMA)) conjugates.[67] GRGDS is an oligopeptide sequence within the protein fibronectin, which has been shown to interact with cell surface integrins. The GRGDS sequence was prepared through solid-phase peptide synthesis (SPPS) using Wang resin. The ATRP initiator, 2-bromopropionyl bromide, was introduced in the final coupling step thereby producing an initiator-terminated protected oligopeptide on resin. Polymerization of HEMA was carried out by treatment of the GRGDS-resin initiator with the monomer, CuCl, and 2,2'-bipyridine in the presence of butanone and 1-propanol. Cleavage from the resin and subsequent deprotection of the prepared GRGDS-poly(HEMA) was carried out by treatment with a standard peptide cleavage cocktail (trifluoroacetic acid (TFA), triisopropylsilane (TIPS), H_2O). A cell adhesion assay was carried out using mouse NIH-3T3 fibroblasts and the results indicated successful adhesion of cells to the GRGDS-poly(HEMA) conjugate and cell spreading while no adhesion was detected using the poly(HEMA) control thereby indicating the biocompatibility of the peptide-polymer conjugate and retention of the cell adhesive peptide moiety.[67] The Börner group also disclosed a report detailing their preparation of peptide-polymer conjugates via grafting-from soon after.[43] Incorporation of an ATRP initiator on the amine terminus of an oligopeptide during SPPS using DCC coupling chemistry and subsequent cleavage of the oligopeptide from the resin afforded an oligopeptide-macroinitiator. The authors carried out

polymerization of *n*-butyl acrylate (*n*BA) in the presence of the oligopeptide-macroinitiator and performed an extensive study on the polymerization kinetics. Though the CuBr catalyst was found to interact with the amine functionality on the oligopeptide, this interaction was found not to have an effect on the controlled synthesis of monodisperse polymers.[43]

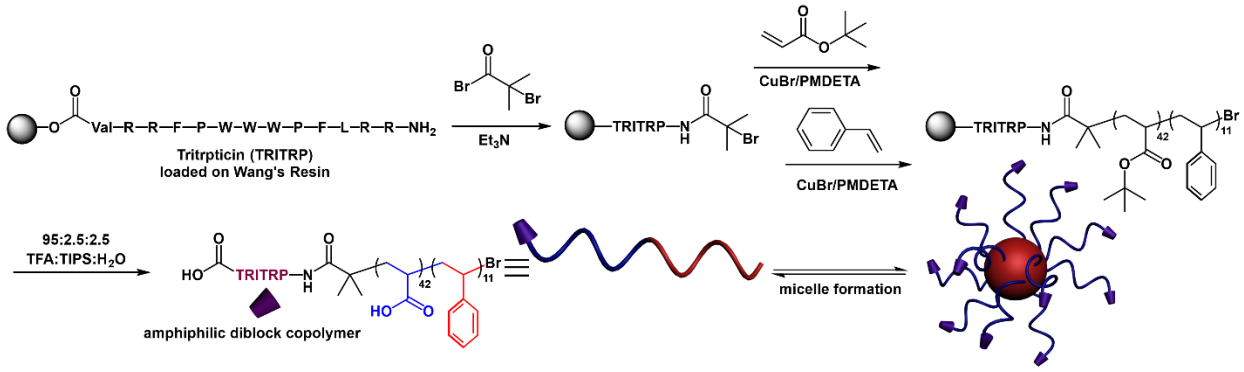

Figure 1-7. Development of peptide containing amphiphilic block copolymers which assemble to form micelles exhibiting a high degree of anti-microbial activity.[42]

The Wooley group was also able to utilize ATRP of protected peptides on-resin, in addition to NMP.[42, 65] They prepared the 13 amino acid residue tritrpticin peptide, an oligopeptide which exhibits anti-microbial activity, using SPPS on Wang resin (**Figure 1-7**). The tritrpticin-resin was treated with bromoisobutyryl bromide to install the ATRP initiator on the oligopeptide end. The group was able to polymerize block co-polymers made from *tert*-butyl acrylate (*t*BA) and styrene monomers by treatment of the tritrpticin-resin with CuBr and *N,N,N′,N″,N″*-pentamethyldiethylenetriamine (PMDETA) in the presence of the monomers. Cleavage and deprotection were carried out to afford the tritrpticin-*b*-poly(acrylic acid-*b*-styrene) conjugate (**Figure 1-7**). Micelles from the peptide-polymer conjugates were generated and found to have improved anti-microbial activity at lower concentration towards *Staphylococcus aureus* and *Escherichia coli* in comparison to tritrpticin alone (**Figure 1-7**).

1.3.3 DNA-Polymer Conjugates

Grafting-from to access DNA-polymer conjugates using traditional ATRP was used by the He group for the amplification of signal to specific DNA sequences.[68] Hybridization and ligation of an ATRP-functionalized single-stranded DNA (ssDNA) onto complementary ssDNA sequences modified on a gold surface led to the formation of DNA-macroinitiators. Polymerization of HEMA from the DNA-macroinitiators led to the surface formation of DNA-poly(HEMA) conjugates which were characterized by atomic force microscopy, ellipsometry, and contact angle measurements. Notably, the formed polymer films could be detected visually without the need for an optical microscope, and the technique allowed for the detection of single point mutations as ATRP modified ssDNA exclusively hybridizes to complementary sequences on the surface.[68] An interesting observation was found that initial polymerization rates from DNA surfaces were considerably accelerated.[69] The authors have attributed this initial rate enhancement to an interaction of Cu with the highly charged phosphate backbones on DNA.[69] Using similar methodology to their previous reports, the He group was also able to develop DNA-polymer conjugate coated core-shell Au nanoparticles using traditional ATRP under aqueous conditions.[70] Again, only nanoparticles harboring the complementary ssDNA strands to the ssDNA-macroinitiator were able to undergo polymerization leading to the visual detection of DNA-polymer conjugate loaded nanoparticles.[70]

1.3.4 AGET and ARGET ATRP

While the effectiveness of traditional ATRP to prepare biomolecule-polymer conjugates via grafting-from has been well established, the main challenges with traditional ATRP techniques include sensitivity to oxygen which may limit its implementation by novice users and low

efficiency in aqueous solutions.[71-72] Activator generated by electron transfer (AGET) ATRP relies on the introduction of an external reducing agent to reduce the transition metal species in solution thereby promoting activation of the initiator or halide terminated polymer chain. AGET ATRP is much more tolerant to low oxygen concentrations which allows for better control over polymerization in aqueous media at lower temperatures. The higher oxygen tolerance arises from the use of oxidatively stable transition metal-based catalysts coupled with the ability for the introduced reductant to remove dissolved oxygen and to reduce the transition metal catalyst (**Figure 1-8**).[18] This important characteristic makes AGET ATRP a more feasible technique for the novice user and a popular approach to access protein-polymer conjugates via ATRP.

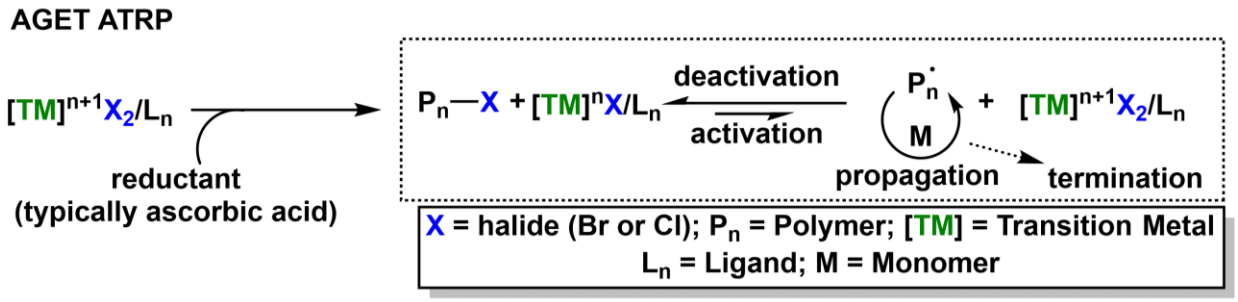

Figure 1-8. Mechanism of AGET ATRP.

In an early example using AGET ATRP to graft-from biomolecules, He and co-workers expanded on their previous work (*vide supra*) but instead used AGET ATRP with water soluble ascorbic acid as a reducing agent, thereby employing an oxygen-tolerant and homogenous method to make DNA and protein sensors based on a unique amplification-by-polymerization strategy.[73] Polymerization of HEMA from an ssDNA macroinitiator following hybridization and ligation to the immobilized complimentary ssDNA strand allowed for detection and determination of DNA concentration, which was proportional to the film thickness. The sensitivity of this method was comparable to that of sensors using traditional ATRP techniques but the turnaround time was

reduced by 2.5 times and a purging step to remove dissolved oxygen was eliminated, making it more attractive for portable applications.[73] The authors extended this work further by the implementation of electrochemical sensors based on polymers harboring pendant ferrocene-based monomers. Post-polymerization modification of ssDNA-polymer conjugates made from either glycidyl methacrylate (GMA) or HEMA was carried out by coupling aminoferrocene to the pendant chains on the polymer thus generating electrochemically active polymers. This method allowed for detection of unlabeled DNA or proteins with sensitivity modulated by the length of the polymer chains and amount of aminoferrocene added to the polymers.[73]

Other groups have also utilized AGET ATRP to graft from oligonucleotides. Das, Matyjaszewski, and co-workers incorporated an acid-stable amide initiator during solid-phase DNA synthesis using phosphoramidite coupling chemistry.[44] A variety of methacrylate monomers were polymerized from the DNA macroinitiator which either remained attached on the solid support or was polymerized from while in solution after cleavage from the solid support. DNA remained stable under the mild polymerization conditions and was able to hybridize with complementary strands. The DNA-polymer hybrids were characterized via gel permeation chromatography (GPC) and fluorescence analysis.

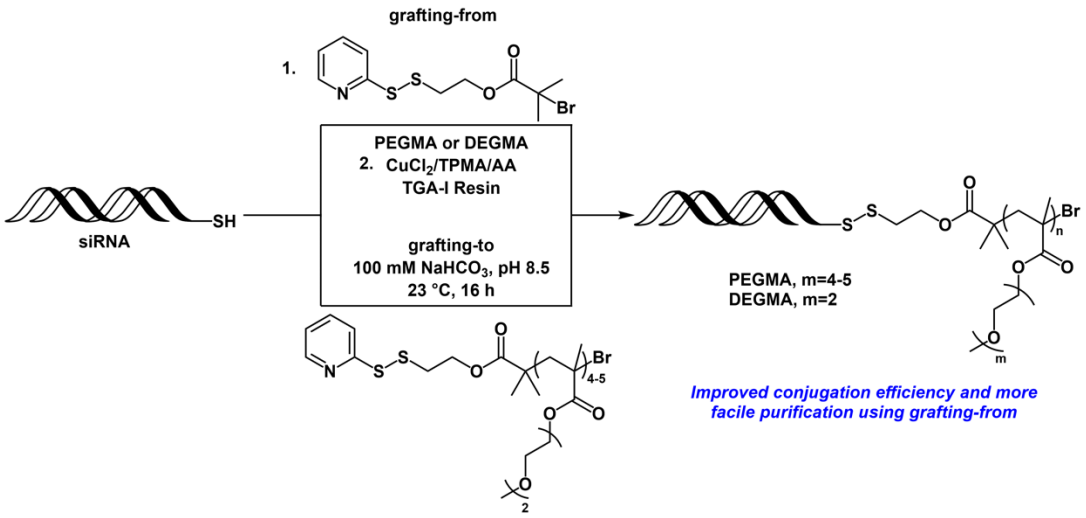

Figure 1-9. Development of siRNA-polymer conjugates via grafting-to or grafting-from. Use of the grafting-from technique exhibited improved conjugation efficiency and easier purification than the grafting-to method.[74]

Lin and Maynard prepared polymer conjugates with small interfering ribonucleic acid (siRNA) using AGET ATRP (**Figure 1-9**).[74] A macroinitiator was prepared by modifying a 5'-thiol siRNA with a PDS-functionalized ATRP initiator. Ethylene glycol methacrylate monomers, which varied in length, were polymerized in the presence of $CuCl_2$, tris(2-pyridylmethyl amine (TPMA), and ascorbic acid (AA) from siRNA in PBS using a sacrificial resin, due to the low quantities of the siRNA-macroinitiator available. The authors compared the grafting-to strategy to prepare siRNA-polymer conjugates by conjugating pyridyl disulfide terminated polymers to siRNA through disulfide exchange reactions. Ultimately, the grafting-from process exhibited improved conjugation efficiency and a more facile purification process (**Figure 1-9**). All siRNA-polymer conjugates were characterized by PAGE analysis.

The groups of Wu and Weil used a bottom-up approach to construct nanoscale polymer patterns by grafting-from ATRP initiator modified DNA origami.[75] Different DNA origami

patterns were formed on a surface and underwent hybridization with ATRP-initiator functionalized complementary strands. AGET ATRP of MPEGMA in the presence of a sacrificial initiator was then performed from the DNA origami initiating sites and polymer growth was followed using atomic force microscopy (AFM). The purified polymer products were characterized by agarose gel electrophoresis which showed a molecular weight increase from the native DNA origami and AFM which showed an increase in the height from the surface. The surface height could be controlled depending on the ratio of monomer to initiator employed which led to differences in the molecular weight of the polymer. Interestingly, after the preparation of cross-linked polymers using similar techniques and the degradation of the DNA origami template under heat stress, the polymers retained their shape. Ultimately, this work showcased the great potential of pairing grafting-from techniques using AGET ATRP with DNA origami templates to create unique 2D and 3D polymer shapes.[75]

Enzyme conjugates have also been prepared by the grafting-from method using AGET ATRP. Liu and coworkers prepared an enzyme-polymer conjugate by polymerizing acrylamide from horseradish peroxidase (HRP) in the presence of air, thus taking advantage of the oxygen tolerance inherent to AGET conditions.[76] Molecular weight was controlled by the ratio of the HRP macroinitiator to monomer and the polymers exhibited low dispersity values. Modification of HRP with the small-molecule ATRP initiators decreased the activity of the protein by nearly 50 %, likely due to the use of dichloromethane during the initial modification step. However, no change in activity after polymerization was detected and the stability of the conjugate to elevated temperatures (55 °C) and enzymatic degradation by trypsin was improved. Magnusson, Alexander, and co-workers prepared thermo-responsive trypsin conjugates using AGET ATRP.[77] The Lys residues on trypsin were modified using a heterobifunctional NHS-ester functionalized

tetraethylene glycol ATRP initiator and MALDI characterization of the trypsin macroinitiator determined there to be an average of 5 initiating sites per protein. Trypsin proteins harboring PEGMA-based copolymers or block copolymers which varied in molecular weight were synthesized through grafting-from under typical AGET ATRP conditions in aqueous buffer solutions at low temperature (4 °C) to form trypsin-polymer conjugates which were characterized by SDS-PAGE. The polymers were analyzed by GPC after cleavage from trypsin using tetra-n-butylammonium fluoride (TBAF) to validate differences in molecular weight. The trypsin-polymer conjugates exhibited different self-assembly behaviors above the lower critical solution temperature (LCST) dependent on the molecular weight of the polymers appended to the protein. Conjugate activity could also be regulated through the phase transition of the conjugated polymers.[77]

Conjugates with therapeutically relevant proteins have also been prepared by grafting-from using AGET ATRP conditions. As an alternative to traditional grafting-to PEGylation, Caliceti and coworkers utilized AGET ATRP to polymerize PEGMA from recombinant human growth factor (rh-GH), a hormone used as a therapeutic for growth deficiency (**Figure 1-10**A).[78] Conjugation of Lys amino acid residues on rhGH was carried out by treatment of the protein with a tetraethylene glycol based heterobifunctional ATRP initiator harboring an NHS ester functional group in the presence of pH 7.5 PBS. MALDI-ToF analysis revealed rh-GH functionalized with 6-8 initiating sites. Polymerization from the rh-GH macroinitiator was performed in phosphate buffer at 4 °C using standard AGET ATRP conditions. This conjugate exhibited improved stability to heating at 37 °C, mechanical agitation, and enzymatic degradation compared to the native protein (**Figure 1-10**A). The rh-GH-polymer conjugates were characterized via SDS-PAGE which indicated a large increase in molecular weight from the native rh-GH. Additionally, acidic

hydrolysis to liberate the polymers from the protein allowed for GPC analysis which showed relatively monodisperse ($Đ$ = 1.2) polymers. The stability of native rh-GH and the rh-GH-polymer conjugate during exposure to heat stress or in the presence of the enzyme pepsin was tested. In each case, the rh-GH-polymer conjugates exhibited a higher degree of stability over native rh-GH. In vivo studies were carried out wherein rats were injected with either native rh-GH or the rh-GH-polymer conjugates. It was found that the rh-GH-polymer conjugates retained biological activity similarly to the native rh-GH as indicated by weight increase following dosage in rats with a daily dosage schedule. Notably, the rh-GH-polymer conjugate retained bioavailability when following a twice weekly dosage schedule as indicated by a weight gain in rats, in contrast to rats injected with native rh-GH which maintained their weight.[78]

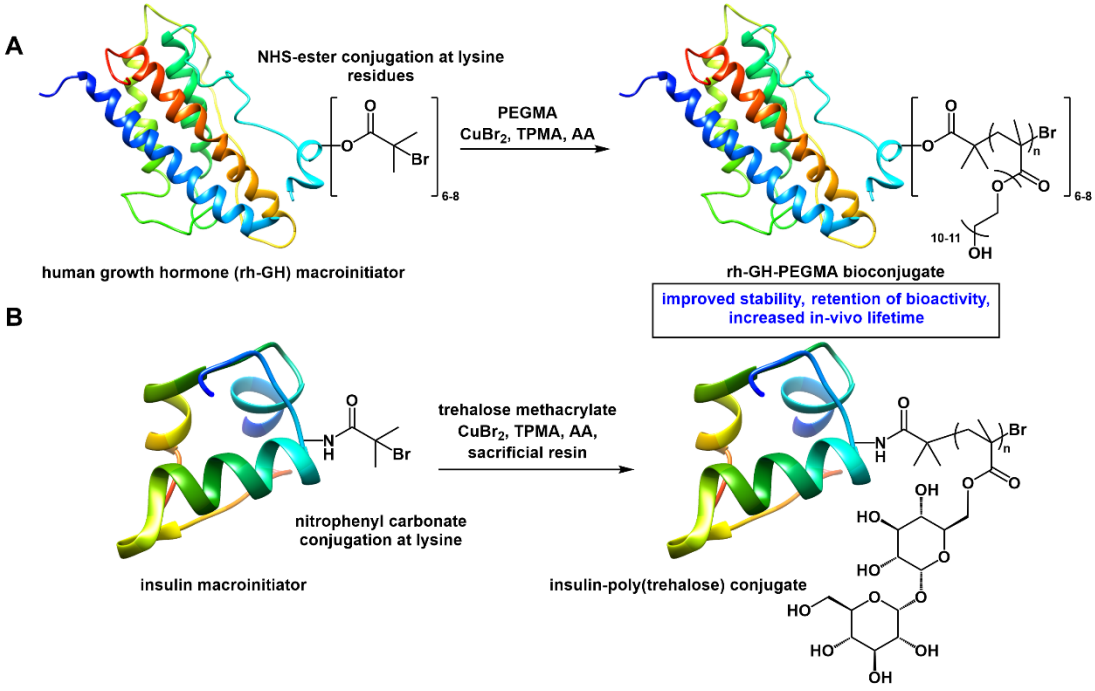

Figure 1-10. (A) Use of grafting-from to develop rh-GH-PEGMA. (B) Generation of insulin-poly(trehalose) conjugates. Both conjugates retained bioactivity and exhibited an increased in-vivo lifetime in comparison to the native proteins.[78-79]

We have previously used AGET ATRP to prepare a trehalose glycopolymer conjugate of insulin (**Figure 1-10**B). Using the grafting-from approach simplified purification and characterization of the insulin-macroinitiator.[79] A site-specific insulin macroinitiator was prepared by treatment of insulin with a nitrophenyl carbonate modified ATRP initiator in the presence of pH 11.0 borate buffer (**Figure 1-10**B). Basic conditions were used in order to favor modification at the Lys residues due to the residues higher nucleophilicity over other N-terminal amines. Purification of the insulin-macroinitiator by HPLC and characterization by MALDI and LC-MS/MS after reduction of the conjugate with DTT revealed a single modification at the LysB29 residue on insulin. A methacrylate trehalose monomer was polymerized from the insulin-macroinitiator in pH 7.4 PBS using AGET ATRP conditions in the presence of a sacrificial resin and the insulin-polymer conjugate was purified via HPLC after polymerization. The purified insulin-polymer conjugate was characterized by SDS-PAGE which appeared as a higher molecular weight band to that of native insulin and the polymer was characterized by GPC after digestion of insulin with proteinase K and found to be well defined. Though a 3-fold increase in dosage was needed in order to achieve similar decreases of blood glucose to native insulin in mice, the insulin-polymer conjugate retained bioactivity to a greater extent than nonspecific insulin-polymer conjugates prepared by grafting-to.[79]

Other groups have prepared nanostructures with covalently incorporated proteins by grafting-from ATRP macroinitiators in the presence of cross-linkers to encapsulate the protein over the course of polymerization. Matyjaszewski and co-workers prepared GFP nanogels wherein GFP was incorporated into a polymer matrix through the course of AGET ATRP in a water-in-oil inverse miniemulsion. GFP containing a genetically incorporated ATRP initiator was expressed through site-directed mutagenesis. Polymerization from the GFP macroinitiator was carried out in

the presence of a PEGMA monomer and a bifunctional methyl methacrylate PEG cross-linker.[80] The GFP-nanogels were characterized by DLS and confocal microscopy. Importantly, it was found that grafting-from was essential for keeping the protein covalently entrapped in the nanogel. Polymerization using similar conditions to form the nanogel in the presence of wt-GFP, which did not contain a genetically incorporated ATRP initiator, resulted in GFP leaching out of the nanogel, as determined by the UV-vis absorption spectrum of the purified product. Liu, Zhao, and co-workers prepared core-corona type nanoparticle with a BSA decorated corona and a cross-linked poly(HEMA) core.[81] The BSA-macroinitiator was prepared through disulfide exchange with a PDS-functionalized ATRP initiator to modify Cys-34 on BSA. Polymerization from the BSA-macroinitiator was carried out in aqueous solutions using typical AGET ATRP conditions in the presence of HEMA and the cross-linker *N,N'*-methylene diacrylamide. Because the protein macroinitiator functioned as a colloidal stabilizer, particle size was controlled by the amount of the BSA-macroinitiator employed: loading of a smaller amount of BSA-macroinitiator resulted in larger nanoparticles. Interestingly, upon treatment of the nanoparticles with dithiothreitol (DTT) in order to reduce disulfide linkages thereby removing BSA from the particle coronas, the nanoparticles underwent aggregation as determined by TEM. This indicated that the BSA-macroinitiator was also important for the stabilization of the nanoparticles in addition to its role in initiating polymerization. Additionally, the authors found that covalently immobilized BSA on the nanoparticle surface retained up to 76% activity in comparison to native BSA as determined by a spectrophotometric assay measuring the hydrolysis of 4-nitrophenyl acetate. The BSA-nanoparticles were also found to be non-toxic when incubated with HepG2 cells and were internalized in the same cell line. These examples illustrate the utility of AGET ATRP grafting from in preparing more complex architectures with retention of protein structure and activity.[81]

Matyjaszewski and coworkers systematically screened conditions to polymerize PEGMA from BSA using ATRP in aqueous conditions resulting in conjugates with good control over molecular weight and dispersity.[71] Conditions were first screened with traditional ATRP methods, then AGET ATRP was then investigated to prepare BSA conjugates. Interestingly, different CuX/ligand conditions were optimal for traditional ATRP compared to AGET ATRP. Additionally, controlled polymerization in PBS buffer, which can be challenging from formation of insoluble phosphate salts and displacement of ligands by chloride, was achieved with different CuX/ligand conditions than was optimal in water. The authors also observed that slow feeding of the ascorbic acid reducing agent resulted in the highest molecular weight and narrowest molecular weight distribution by minimizing termination with very active ligands like TPMA for polymerization of PEGMA under AGET ATRP conditions.

This observation of improved control with slow feeding of reducing agent, or activators regenerated by electron transfer (ARGET) ATRP, was then investigated in depth by the Matyjaszewski group to polymerize from proteins.[82] This technique allows for low catalyst loading and an extra handle of control to start/stop polymerization based on the feed of reducing agent. Systematic optimization of polymerization conditions with OEGMA was first accomplished with a small molecule initiator; addition of halide salt (30-100 mM), increased equiv of ligand (4/1 L/Cu), and altering copper concentration (300 to 100 ppm) resulted in the best control with acceptable rates of polymerization. Additionally, a block copolymer could be prepared with the optimized method and polymerization could be stopped and started with the ascorbic acid feed. Polymerization of OEGMA from a BSA macroinitiator was accomplished in PBS buffer with 300 ppm Cu. Matyjaszewski and coworkers also utilized this technique to polymerize OEGMA from GFP with a genetically encoded, base-cleavable initiator.[83]

1.3.5 ICAR ATRP

During initiators for continuous activator regeneration (ICAR) ATRP, addition of a conventional thermal radical initiator (typically an azo-initiator) generates the active Cu(I)/L complex in situ, enabling use of low (<100 ppm) levels of copper catalyst.[84] Similar to ARGET ATRP, oxidatively stable Cu(II) reagents are used and the technique allows for some tolerance to oxygen. However, continuous feeding to regenerate the active species is not required due to the slow decomposition of the radical initiator. Polymerization conditions are generally mild, although with slightly elevated temperatures to activate the thermal initiator, this method may not be appropriate for more sensitive biomolecules. The Matyjaszewski group was the first to report the use of ICAR ATRP to polymerize from a biomolecule.[85] The group initially optimized aqueous polymerization conditions for homopolymers of oligo(ethylene glycol) acrylate (OEGA) with a small molecule initiator in the presence of TPMA, $CuBr_2$, an excess of tetraethylammonium bromide (TEA-Br, 20-300 mM) to maintain the concentration of the deactivator complex, and 2,2'-azobis[2-(2-imidazolin-2-yl)propane]dihydrochloride (VA-044) as the thermal initiator. Cu catalyst concentrations as low as 20 ppm could be employed while maintaining control over molecular weight and dispersity. Optimized conditions (100 ppm Cu, 44 °C, 8 h) were then used to polymerize OEGA from a BSA macroinitiator, resulting in a conjugate with polymers of controlled molecular weight and molecular weight distribution.[85]

ICAR ATRP has also been used by the Averick group to polymerize homo- and block-copolymers of acrylamide monomers.[86] Conjugates of BSA with a block copolymer of acrylamide, *N,N*-dimethylacrylamide (DMA), and *N*-vinylimidazole (VI) were prepared by ICAR using PBS buffer as the halide source as opposed to TEA-Br. BSA conjugates harboring block copolymers of VI and OEGA underwent cross-linking in the presence of palladium through the metal interaction

with the imidazole containing block, thus forming a biohybrid nanoparticle capable of serving as a catalyst for Suzuki-Miyaura cross-coupling reactions.[86] Further work used ICAR ATRP to explore the effect of conjugation site on *Thermomyces languginosa* lipase (TL)-poly[*N*-(3-(*N*,*N*-dimethylamino)propyl) acrylamide] conjugates.[87] TL was modified with an ATRP initiator at either Lys residues with an NHS-ester or acidic (glutamic and aspartic acid) residues with 1-ethyl-3-(3-dimethylaminopropyl)carbodiimide (EDC) coupling. Enzyme activity was increased by 50 % for conjugates grafted from acidic residues compared to from Lys residues, despite 6 initiating sites for the former compared to 3 for the latter.[87]

1.3.6 SET-LRP

Single electron-transfer living radical polymerization (SET-LRP) or Cu(0)-mediated LRP involves disproportionation of Cu(I) in polar solvents to generate active Cu(0) species and Cu(II) species which deactivate the propagating polymer chains; thus aqueous conditions are well suited for this polymerization method. Haddleton and coworkers utilized SET-LRP to polymerize water soluble monomers from a small library of proteins and peptides.[56] BSA, bovine hemoglobin (Hb), human Lyz, salmon calcitonin (sCT), and bovine insulin were chosen as model proteins and peptides with a variety of molecular weights and properties. Macroinitiators were prepared by reacting ATRP initiators with proteins/peptides through NHS-ester coupling at Lys amino acid residues. Conditions were screened to polymerize NIPAAm, DMA, and OEGA from the protein/peptide-macroinitiators. Synthesis of well-defined BSA conjugates were achieved through an excess of CuBr relative to Me_6TREN ligand to improve control. Conjugates of Hb were obtained, though with broad dispersities ($Đ$ >1.6) likely due to interactions with Cu(II) with the Fe(II) containing heme centers present on the protein. Lyz and sCT macroinitiators were insoluble

in aqueous conditions, but the addition of 0.5% SDS denaturant to solubilize the protein-macroinitiators and sodium bromide (NaBr) to minimize loss of halide anions from SDS resulted in well-defined protein-polymer conjugates. The insulin-macroinitiator formed a stable colloid in aqueous solution but polymerization could be accomplished in this heterogeneous system with the SET-LRP conditions. These conjugates also exhibited interesting self-assembly behavior in solution. Demonstration of the range of conjugates prepared by SET-LRP indicates that this is a versatile method to prepare polymer conjugates by the grafting from method.[56]

In collaboration with the Haddleton group, Joensuu, Milani, Linder and coworkers synthesized protein-polymer conjugates by the grafting from method using Cu(0)-mediated LRP to make antifouling surfaces.[88] A Cys mutant of hydrophobin (NCysHFBI), a protein that self-assembles on hydrophobic surfaces, was used and conjugation with a maleimide modified initiator afforded a site-specific macroinitiator. Growth of poly(PEGA) from the macroinitiator already self-assembled on a hydrophobic surface resulted in a surface with decreased nonspecific binding. Utilization of this method to graft from NcysHFBI enabled facile synthesis of these surfaces.[88]

1.3.7 Photo-mediated ATRP (photo-ATRP)

Photo-ATRP processes have also gained considerable interest due to the high degree of temporal control provided by using light as an external stimulus for the generation of active Cu(I) species. The need for external radical initiators or reducing agents is replaced with the requirement of additional ligands in the system which also serve as reductants under light irradiation.[89] The Matyjaszeski group has recently utilized visible-light (Blue LED) mediated ATRP to graft oligo(ethylene oxide) methyl ether methacrylate (OEOMA) monomers from the surface of BSA and DNA in order to develop BSA- and DNA-polymer conjugates.[90] Notably, polymerization was

carried out in aqueous conditions and in the presence of low ppm of Cu (50-1000 ppm). The deployment of glucose, glucose oxidase, and sodium pyruvate (Glu, GOx, SP) was used to deoxygenate the polymerization mixture, thus precluding the need for N_2 sparging or freeze-pump-thaw procedures.[90] The complete elimination of metal catalysts in order to synthesize protein-polymer conjugates would be a welcome development, especially given the recent progress in metal-free photo-ATRP methodology.[91-94]

1.3.8 Electrochemical ATRP (e-ATRP)

Electrochemically mediated ATRP was first reported by the Matyjaszewski group in 2011 and has garnered attention due to its general tolerance of oxygen, low catalyst loading, removal of chemical reducing agents, and feasibility of temporal control.[95] In the case of eATRP, polymerization is performed in an electrochemical cell with regeneration of the reduced metal species controlled by an applied cathodic current. Application of an anodic current acts to oxidize the metal species thereby terminating the polymerization.[95-97] Many groups have taken advantage of eATRP for a variety of unique applications.[98-100] The Matyjaszewski group recently utilized eATRP for grafting-from initiator functionalized DNA substrates under aqueous conditions.[101] A screen printed electrode (SPE) was used to bypass the large reaction volumes required of electrochemical setups, which would render grafting-from using eATRP an unreasonable method for expensive biomolecules. SPE's are inexpensive substrates that can be smaller than 1 cm^2 and contain a working electrode, counter electrode, and a reference electrode typical of electrochemical setups. Interestingly, the authors were able to decrease reaction volumes down to 75 μL using SPEs. This large decrease in reaction volume necessitated the use of an enzyme degassing system consisting of GOx, glucose, and SP rather than traditional degassing methods. Polymerization of

2-(methylsulfinyl)ethyl acrylate (MSEA) and OEGMA was carried out from the DNA-macroinitiator in the presence of $CuBr_2$ and TPMA under eATRP conditions and an extensive study was carried out to elucidate the effects that different catalyst and ligand loadings had on the reaction outcome. Notably, DNA-polymer conjugates larger than 25 kDa were able to be synthesized in <30 min, despite the low monomer conversion observed.[101]

1.4 Biomolecule-polymer conjugates accessed through RAFT polymerization

RAFT polymerization is a living and controlled radical polymerization technique that quickly garnered popularity after its initial discovery reported in 1998.[102-104] Control during RAFT polymerization is obtained through a degenerative chain transfer process that is mediated by a chain transfer agent (CTA; also referred to as a RAFT agent).[11, 105-106] The RAFT agent is a small molecule organic compound typically composed of a thiocarbonylthiol group, some common architectures include xanthates, trithiocarbonates, dithioesters, and dithiocarbamates.[107-108] The RAFT agent structure is often conceptually split into two parts, the "R" group and the "Z" group (**Figure 1-11**).[105-106] The R group initiates radical polymerization while the Z group is involved in both modulating the reactivity of the thiocarbonyl bond towards radical addition and also in stabilizing the subsequent radical formed on the thiocarbonyl carbon atom (**Figure 1-11**). A useful feature of RAFT polymerization is that both the R and Z groups are incorporated on the polymer chain ends upon termination, allowing for further functionality to be engendered at either end.[105-106, 108]

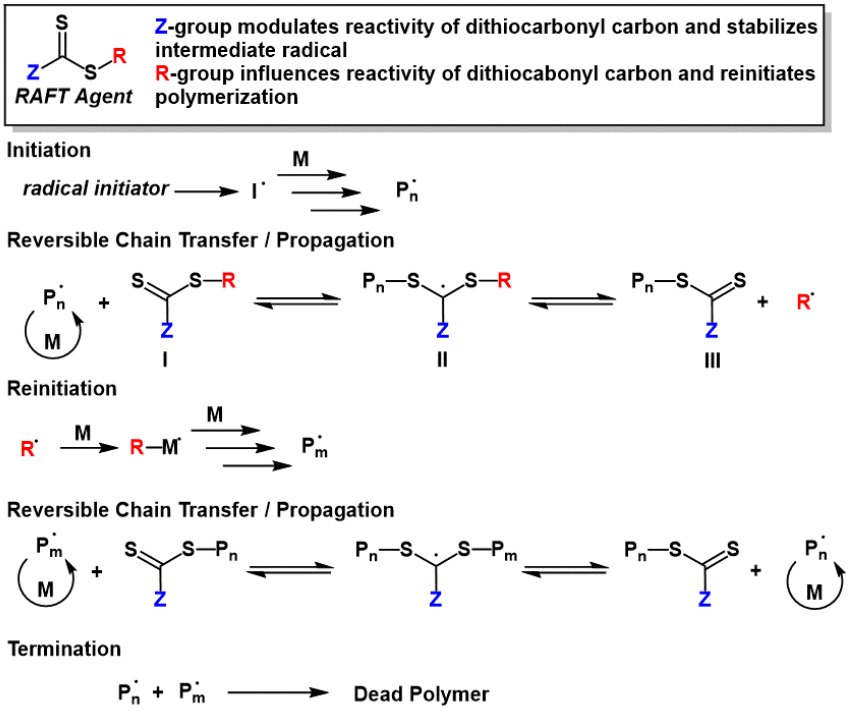

Figure 1-11. RAFT polymerization mechanism.

The widely accepted mechanism for traditional RAFT polymerization involves initiation using a prototypical radical initiator such as the thermally activated initiator azobibsisobutyronitrile (AIBN) (**Figure 1-11**).[11, 106, 109] Photochemical initiation is another popular form of initiation for RAFT polymerization and will be discussed later in the review. Initiation and radical addition to monomers produce propagating oligomeric radicals which can then enter into the RAFT equilibrium whereby the propagating radicals add into the thiocarbonyl bond of the RAFT agent (**I**) and produce a stabilized radical on the thiocarbonylthio carbon atom (**II**) (**Figure 1-11**). During this equilibrium process, (**II**) can fragment back to produce the oligomeric propagating radical and the intact RAFT agent, or homolytic cleavage of the R group can occur whereby the RAFT agent becomes appended to the end of the oligomer (**III**) and the R group radical can then re-initiate polymerization. After this initial equilibrium process, polymer chains

propagate through the addition of monomers and either enter into the RAFT equilibrium process again with the thiocarbonylthio capped polymer chains or continue adding monomers. It is this rapid equilibrium process that affords control over the polymerization because the concentration of stabilized radical intermediates is greater than that of the propagating radicals, thus unproductive termination pathways are greatly limited (**Figure 1-11**). RAFT polymerization is a popular method in the bioconjugation realm due to its wide monomer scope, solvent compatibility, and general avoidance of transition metals (though there are exceptions such as in photo-induced electron transfer-RAFT (PET-RAFT)).[110-111] Although there exist many examples of generating polymers through RAFT with bioactive functionality either at the end of the polymer or as pendant groups, this section of the review will only cover peptide-, protein-, and nucleic acid-polymer conjugates by grafting-from using RAFT.[112-116]

1.4.1 Protein-polymer conjugates

The initial report of grafting-from a protein using RAFT polymerization was by Davis, Bulmus and co-workers where they developed a pyridyl disulfide functionalized trithiocarbonate RAFT agent which could undergo disulfide exchange with Cys-34 on BSA thereby forming a macroRAFT agent where BSA acted as the Z-group. This was planned due to Z-group retention on polymer chain ends (**Figure 1-12**, top).[117] Formation of the macroRAFT agent was monitored by UV-vis spectroscopy to visualize the formation of the 2-pyridinethione byproduct that occurs after PDS exchange and absorbs in the 340-370 nm range. The authors opted to initiate polymerization of PEG-acrylate (PEGA) using γ-irradiation which offered the benefit of room temperature initiation in aqueous conditions suitable to the stability of BSA. Though γ-irradiation can potentially be detrimental to protein structure and function, the authors determined both BSA

and glucose oxidase to retain up to 92 % and 88 % activity after 6 h of γ-irradiation, respectively. Polymerization of PEGA was carried out in the presence of the macroRAFT agent in a mixture of water and DMF under γ-irradiation at room temperature thereby producing BSA-polymer conjugates which were characterized by GPC, MALDI, and non-denaturing PAGE. The BSA-polymer conjugate was treated with tris(2-carboxyethyl)phosphine (TCEP) in order to reduce the disulfide linkage thus facilitating disassembly of the polymer from the protein to allow for characterization of the polymer itself. However, the disulfide bond remained intact upon treatment with TCEP, only demonstrating partial reduction for low molecular weight conjugates which the authors attributed to the shielding of the disulfide bond by the polymer. Treatment of the BSA-poly(PEGA) conjugates in the presence of concentrated TCEP solutions completely denatured the protein but allowed for analysis of the polymers. Characterization of the polymers revealed a few drawbacks: though the molecular weight of the polymers increased linearly with increasing monomer conversion, the polymers exhibited dispersity values of up to 2.0 with increasing molecular weight. This observation was attributed to the steric hindrance imparted by BSA in addition to the growing polymer chains during the equilibrium process. Additionally, there was an observed two-hour inhibition period at the start of polymerization which was attributed to slow fragmentation of the macroRAFT agent. Despite these minor drawbacks, this elegant work paved the way for the expansion of grafting-from using RAFT to generate biomolecule-polymer conjugates (**Figure 1-12**, top).[103]

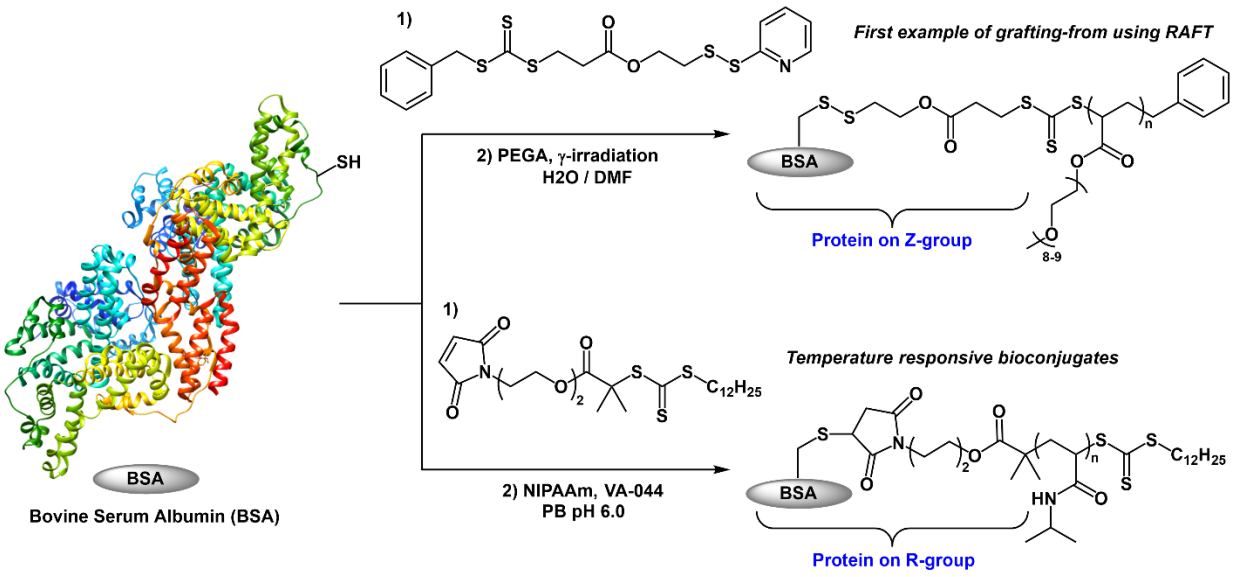

Figure 1-12. (Top) The Davis and Bulmus groups work developing protein Z-group modified macroRAFT agents and polymerization from BSA.[117] (Bottom) Sumerlin group work on developing R-group modified macroRAFT agents to develop thermoresponsive protein-polymer conjugates.[118]

The Davis and Bulmus groups quickly expanded on their initial work by polymerizing NIPAAm and hydroxyethyl acrylate (HEA) in the presence of the BSA-macroRAFT agent using a room temperature and water soluble radical initiator (VA-044).[119] An inhibition period was observed at the beginning stages of polymerization as in their earlier work, however the polymerization exhibited a linear evolution of $Ln[M]_0/[M]$ versus time indicative of a steady concentration of radicals in solution over the course of polymerization. TCEP reduction of the protein-polymer conjugate was carried out and the polymers analyzed via GPC which again showed a linear increase in molecular weight with increasing monomer conversion. Interestingly the poly(NIPAAm) samples were relatively monodisperse exhibiting dispersity values up to 1.3 for the higher molecular weight polymers. This is in stark contrast to their above described grafting-

from polymerization of PEGA which exhibited dispersity values up to 2.0. Activity studies were also carried out to determine the esterase-like activity of BSA to hydrolyze *p*-nitrophenyl acetate. The BSA-macro RAFT agent, BSA incubated with VA-044, and BSA-poly(NIPAAm) conjugates all remained active, while controls in which BSA was heated to 85 °C in buffer for 4 h lost up to 80 % activity. Additionally, BSA-poly(NIPAAm) conjugates displayed increased LCST values in comparison to poly(NIPAAm) alone, which increased as the polymer molecular weight of the conjugate decreased.[119] In an interesting follow-up work, the Davis group was able to employ similar polymerization methodology in the presence of a bifunctional PDS trithiocarbonate RAFT agent to access polymers harboring biomolecules at each end through a combination of grafting-to and grafting-from approaches.[120]

The thermoresponsive properties of BSA-poly(NIPAAm) conjugates were studied further by the Sumerlin group (**Figure 1-12**, bottom).[118] A BSA-macroRAFT agent was developed through attachment of a maleimide functionalized RAFT agent on Cys-34. Instead of attaching BSA to the Z-group portion of the RAFT agent similar to the Bulmus and Davis work mentioned above, Sumerlin and co-workers attached BSA on the R-group portion of the RAFT agent (**Figure 1-12**, bottom). This offers several unique advantages; the thiocarbonyl bond is more accessible for chain transfer thereby improving on the control over polymerization processes. Additionally, having the thiocarbonylthio group at the polymer chain end would allow for post-polymerization modification without interfering with the protein on the other end of the polymer. Polymerization of NIPAAm in the presence of the BSA-macroRAFT agent was carried out in pH 6.0 phosphate buffer using VA-044 as the radical initiator similar to earlier reports. Purification of the BSA-poly(NIPAAm) conjugates was carried out via thermal precipitation at 40 ˚C. The purified BSA-poly(NIPAAm)

conjugates were treated with TCEP and the corresponding polymers characterized via GPC which showed an increase in polymer molecular weight with increasing monomer conversion and high molecular weight polymers (234 kDa) exhibited a dispersity of 1.38. The BSA-macroRAFT agent and the BSA-poly(NIPAAm) conjugate both retained their secondary structure as determined by circular dichroism and also retained esterase-like activity (>90 % activity compared to native BSA). The activity of the protein could be modulated due to the thermally responsive nature of poly(NIPAAm) (**Figure 1-13**). Upon exposure to heating above the LCST of the BSA-poly(NIPAAm) conjugate (40 ˚C), the protein activity was reduced to 75 %. Interestingly, the protein activity was regained upon cooling of the conjugate solution below the LCST and this process was cycled up to 5 times with no apparent loss in protein activity after each cycle (**Figure 1-13**).[118]

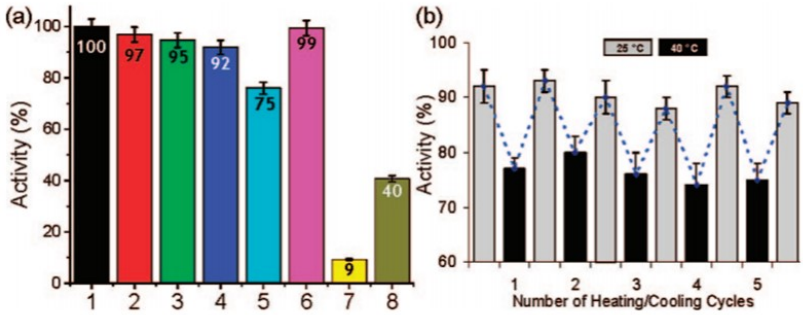

Figure 1-13. "(a) Activity of (1) BSA, (2) BSA-macroCTA, (3) BSA-poly(NIPAAm) (free BSA present) with conjugated polymer of 234,000g/mol, (4)BSA-poly(NIPAAm) thermal precipitate, (5) BSA-poly(NIPAAm) thermal precipitate at 40 °C assay temperature (with respect to BSA at 40 °C), (6) BSA+poly(NIPAAm) physical mixture, (7) poly(NIPAAm), (8) BSA after incubation at 75 °C for 3 h. All assays were conducted with identical [BSA]. (b) Activity of BSA-

poly(NIPAAm) thermal precipitate during thermal cycling between 25 and 40 °C." [118], Copyright 2008. Reproduced with permission from the American Chemical Society.

The Sumerlin group next explored the synthesis of more complex thermoresponsive protein-polymer conjugates through RAFT polymerization by implementing methodology which allowed for the formation of block copolymer architectures through grafting-from.[121-122] In their initial work, the group attached a RAFT agent to Cys-34 on BSA through a maleimide linkage, again appending the protein to the R-group of the RAFT agent.[121] The BSA-poly(NIPAAm) conjugate was synthesized, purified, and subsequently characterized using SDS-PAGE. Retention of the trithiocarbonate end-group could be visualized using UV-vis spectroscopy with the characteristic absorption appearing at ~310 nm. The BSA-poly(NIPAAm) conjugate was then employed as the macroRAFT agent in the subsequent polymerization of DMA using similar conditions to those mentioned above to produce the second block. UV-vis spectroscopy indicated retention of the trithiocarbonate end-group even after addition of the DMA block. Additionally, the thermoresponsive properties were measured using DLS which showed an increase in the hydrodynamic diameter of the protein-polymer conjugate at elevated temperatures.[121] Similar work targeted the seven Lys amino acid residues on Lyz using a NHS-ester functionalized RAFT agent thereby forming a Lyz-macroRAFT agent with the protein on the R-group.[122] Lyz-poly(NIPAAm)-*b*-poly(DMA) conjugates were synthesized using similar polymerization conditions to their previous work and their thermoresponsive solution behavior analyzed.[122]

Konkolewicz, Page, Berberich, and co-workers used RAFT polymerization and a combination of grafting-to and grafting-from procedures to perform a thorough study detailing the effects of different types of polymers of varying lengths and structures on the stability and activity of Lyz

conjugates.[123] The activity of Lyz was tested using a standard spectrophotometric technique that measures lysis of *Micrococcus lysodeikticus* in the presence of Lyz. As might be expected, the Lyz-polymer conjugate activity was reduced as the molecular weight of the polymer increased. Charged polymers attached to Lyz were also studied with negatively charged polymers resulting in reduced enzyme activity due to charge repulsion on the negatively charged *M. lysodeikticus* cell. Cationic polymers had the opposite effect. Additionally, the thermal stability of the Lyz-polymer conjugates was reduced. However, the chemical stability towards treatment with the protein denaturant guanidine HCl was increased with the highest molecular weight conjugates exhibiting the greatest stability, most likely due to a shielding effect imposed by polymers on the enzyme surface.[123]

The establishment of photochemically initiated grafting-from polymerization using RAFT proved to be a significant addition to the practitioners' toolbox which introduced an additional degree of control over the polymerization process. Chen and co-workers used a specially prepared *Escherichia coli* inorganic pyrophosphatase (PPase) protein in which they exchanged the Lys-148 amino acid residue with Cys through site-directed mutagenesis.[124] The Cys amino acid residue was used as the conjugation site for the attachment of a maleimide functionalized RAFT agent, thus generating the PPase-macroRAFT agent with the protein appended as the R-group. Polymerization of NIPAAm was performed in water and at room temperature under visible (420 nm) light irradiation in the presence of (2,4,6-trimethylbenzoyl)phenyl phosphonic acid sodium (TPO-Na) as the photoinitiator. The polymerization exhibited rapid kinetics with molecular weights reaching 150 kDa within 30 min. Notably, the authors were able to control polymerization by either turning the light source 'on' or 'off'. Polymerization was halted upon removal of the light source but

continued when the light source was turned on. This process was cycled and the molecular weight of the PPase-poly(NIPAAm) conjugate was followed by SDS-PAGE. Because the conjugation site of the RAFT agent and the conjugated polymer are near the active site of the protein, the PPase activity was greatly reduced. However, an interesting observation was made when it was determined that PPase-poly(NIPAAm) conjugates harboring higher molecular weight poly(NIPAAm) show an increased activity over the wild-type PPase above the LCST of the conjugate (45 °C).[124]

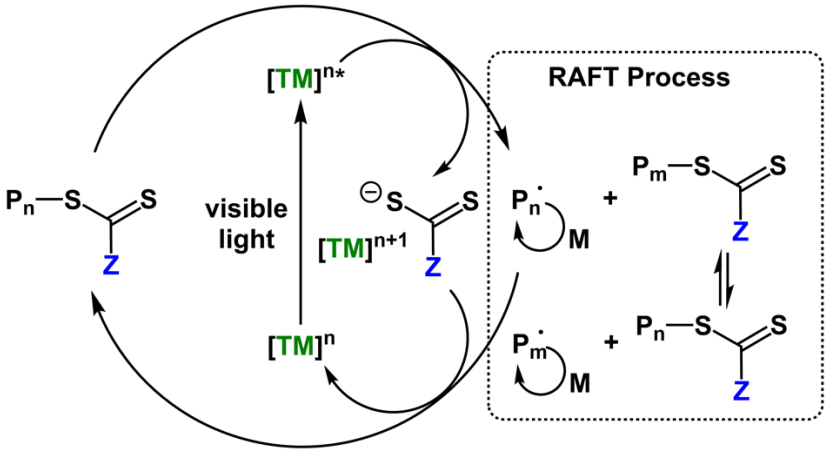

Figure 1-14. Proposed mechanism of a prototypical PET-RAFT polymerization using a transition-metal based chromophore.

Boyer and co-workers reported on using PET-RAFT to graft-from BSA in aqueous conditions (**Figure 1-14**).[125] PDS exchange was used to append a trithiocarbonate-based chain transfer agent on BSA to generate the BSA-macroRAFT agent where BSA was appended as the R-group. Grafting-from polymerization of either DMA or OEGA was carried out in aqueous conditions in the presence of $Ru(bpy)_3Cl_2$, the BSA-macroRAFT agent, and blue LED irradiation and proceeded in a controlled manner to produce monodisperse protein-polymer conjugates. Additionally, the

prepared BSA-polymer conjugates retained identical activity to native BSA as determined by an esterase activity assay.[125] In 2017, the Sumerlin group expanded on PET-RAFT methodology by employing an organophotocatalyst to polymerize an extended class of monomers under visible-light irradiation and also demonstrated the construction of block copolymers grafted-from Lyz.[126]

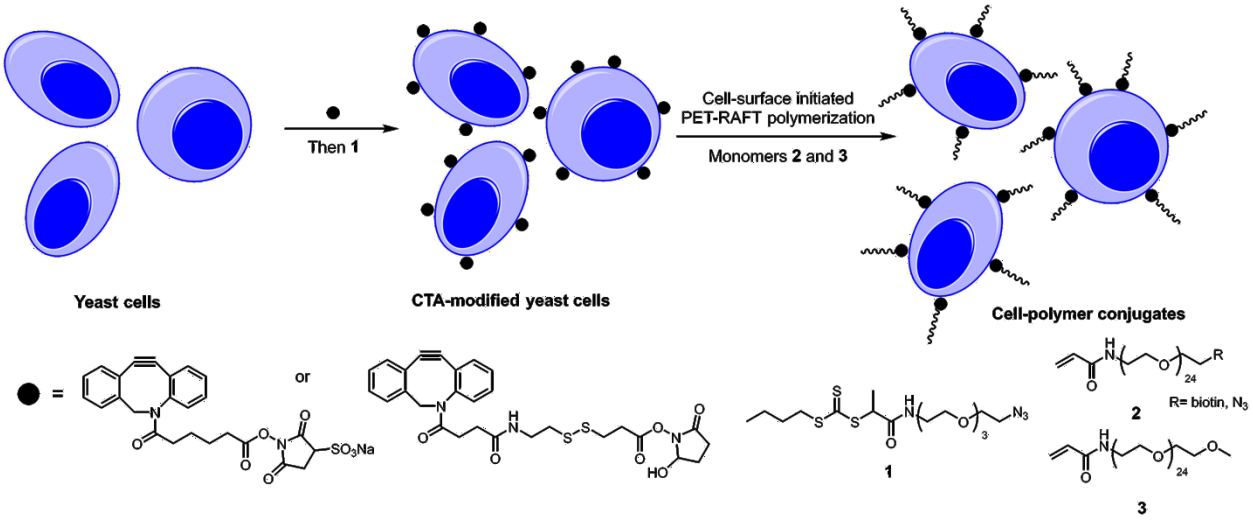

Figure 1-15. Modification of yeast cells with RAFT agents and polymerization from yeast cell surfaces.

Beyond protein-polymer conjugation, the ability to engineer whole live cell surfaces with polymers of controlled molecular weights and architectures represents an important challenge.[127] Seminal work by Soh, Hawker, and coworkers used grafting-from techniques to assemble polymers on live cell surfaces (**Figure 1-15**).[128] Though there were a few previous reports of using grafting-to methods to obtain polymer-functionalized cells, the conjugation efficiencies were often minimal which necessitated the need for a large excess of synthesized polymer. Additionally, uncontrolled polymerization techniques to encapsulate cells resulted in the cells being difficult to access. Polymerization of PEG modified acrylamide monomers was carried out in the presence of

live wild-type *Saccharomyces cerevisiae* (Baker's yeast) cells under PET-RAFT conditions using eosin Y as the photocatalyst and triethanolamine as the co-catalyst **Figure 1-15**). In order to maximize cell viability, the PET-RAFT conditions were modified in order to quicken polymerization kinetics and monomer conversion was kept low in order to maximize end-group retention. Notably, the yeast cells remained intact and were able to undergo cell proliferation after being subjected to polymerization conditions. After these promising initial results, the authors introduced dibenzocyclooctyl (DBCO) functionality on the yeast cell surfaces through NHS-ester conjugation (**Figure 1-15**). This allowed for the efficient conjugation of azide-modified RAFT agents through strain-promoted 1,3-dipolar cycloaddition (SPAAC) thereby producing cell-based macro-RAFT agents. PEG-based acrylamide monomers were then polymerized using the modified PET-RAFT conditions employing the cell-based macro-RAFT agents and also a sacrificial RAFT agent in order to maintain control over polymerization. Additionally, the authors were able to incorporate azide functionality along the polymer chain for post-polymerization functionalization with an Alexa Fluor 647 strained alkyne analogue. Using confocal microscopy of the fluorescently labelled cell-polymer conjugates indicated that fluorescence was localized only on the cell surface. This experiment showcased that cell-surface polymers were able to undergo post-polymerization modification using bioorthogonal methods and that polymerization only occurred on the cell surface without any observable polymer growth occurring inside the cell. Notably, the cell-polymer conjugates derived from grafting-from polymerization exhibited much greater grafting densities than those prepared using the traditional grafting-to technique. The authors were able to carry this technique forward to a mammalian cell line through the non-covalent modification of Jurkat cell membranes with a RAFT agent modified lipid. Cell viability assays performed after polymerization from the cell surface exhibited up to 90 % viability and also

retained their metabolic activity.[128]

1.4.2 Peptide-polymer conjugates

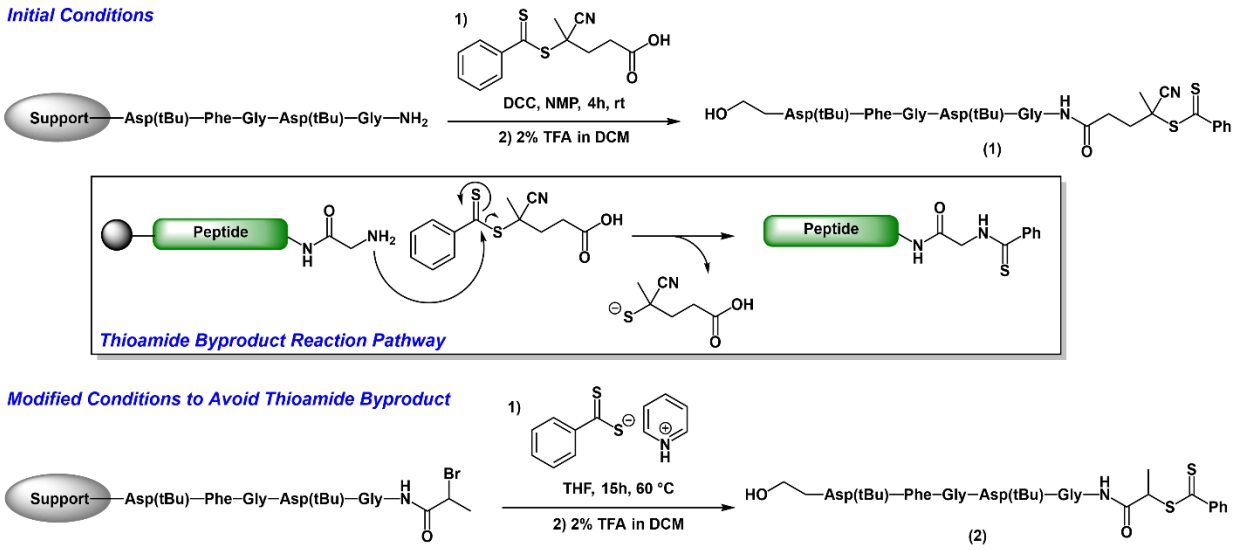

Figure 1-16. Development of oligopeptide-macroRAFT agents.

Some examples of grafting-from oligopeptide sequences using RAFT polymerization were reported by the Perrier and Börner groups.[129-131] Börner and coworkers' first manuscript of this kind describes the SPPS of an oligopeptide in which the N-terminus was modified with a dithiobenzoate-based RAFT agent via DCC coupling while on-resin (**Figure 1-16**).[129] Treatment of the resin-bound peptide with a TFA cleavage cocktail and subsequent precipitation resulted in the production of the oligopeptide-macroRAFT agent (**1**) with the oligopeptide positioned as the R-group. The authors noted the formation of a thioamide byproduct which is due to nucleophilic attack of the peptide amine terminus with the dithioester functionality during the DCC coupling step (**Figure 1-16**). This byproduct was observed via electrospray ionization mass spectrometry (ESI-MS) and is probable given the sensitivity of dithiobenzoate-based RAFT agents towards aminolysis. Despite this, the authors proceeded with polymerization of *n*BA using **1** as the

thioamide byproduct would not interfere with polymerization conditions. However, the authors also developed a second approach to creating oligopeptide-macroRAFT agents by modifying an oligopeptide ATRP macroinitiator on resin. This was then reacted with a pyridinium salt of dithiobenzoic acid to produce **2** without formation of the previously observed thioamide byproduct (**Figure 1-16**). Polymerization of *n*BA employing either of the oligopeptide-macroRAFT agents generated monodisperse polymers and exhibited linear polymerization kinetics typical of a controlled RAFT process. However, it is important to note the significant inhibition observed at the start of polymerization which lasted between 4-8 h depending on the oligopeptide-macroRAFT agent used.[129] In a later report, the authors developed a trithiocarbonate-based GGRGDS oligopeptide-macroRAFT agent (**3**) which was much more stable than the dithiobenzoate derivative published earlier.[130] Notably, polymerization of *n*BA using **3** did not exhibit an inhibition period at the start of the polymerization, though it is not clear if the inhibition period was due to differences in the oligopeptide structure or differences between the dithiobenzoate or trithiocarbonate structures. The authors employed **3** in the polymerization of NIPAAm to produce oligopeptide-poly(NIPAAm) conjugates, the ω-trithiocarbonate group was then reduced to afford a poly(NIPAAm) terminated with a free thiol which could be used for surface functionalization on a gold substrate. Cell adhesion of L929 mouse fibroblasts was examined on the GGRGDS-poly(NIPAAm) functionalized surface and was found to be faster than the corresponding poly(NIPAAm) functionalized surfaces.[130] The Börner group has also developed ABC-triblock co-polymers from oligopeptide-macroRAFT agents synthesized on-resin.[132]

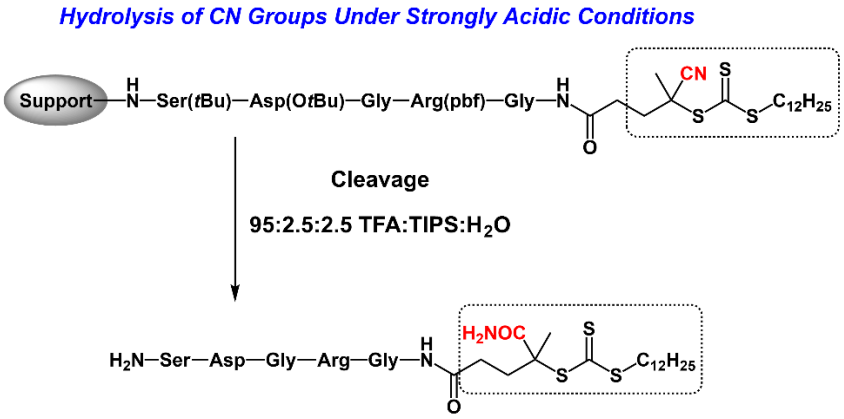

Figure 1-17. Exhibited hydrolysis of nitrile substituted RAFT derivatives after treatment with standard peptide cleavage cocktails.[133]

An important additional consideration in the construction of oligopeptide-macroRAFT agents is hydrolysis of nitrile (CN) groups on the RAFT agent structure during cleavage of resin-bound peptides (**Figure 1-17**).[133] Because typical peptide cleavage cocktails make use of strongly acidic conditions (>95 % TFA), RAFT agents appended to peptide structures during SPPS undergo hydrolysis thereby forming carboxamide functional groups in place of the nitrile substituent (**Figure 1-17**).[133-135] Despite this, Thang and co-workers were still able to perform controlled RAFT polymerization of DMAEMA, OEGMA, and *n*-butyl methacrylate (*n*BMA) monomers employing trithiocarbonate-based oligopeptide-macroRAFT agents in which the nitrile substituent had undergone hydrolysis to the corresponding carboxamide.[133] Though the earlier reports by the Börner group made use of nitrile modified dithiobenzoate RAFT agents in which no carboxamide formation was reported, they used a 2 % TFA in DCM cleavage cocktail which cleaved the oligopeptide from the resin but did not remove the protecting groups present on the amino acid residue side-chains.[129]

1.4.3 Nucleic acid-polymer conjugates

Grafting-from DNA using RAFT was first employed by the He group for purposes of DNA biosensing.[136-137] A few of their reports detailing their use of grafting-from for DNA detection made use of ATRP conditions (vide supra), however the transition metals employed for polymerization formed complexes with DNA molecules which complicated their intended application due to unwanted background noise. RAFT seemed to be a promising alternative due to the absence of transition metals.[136] Complementary oligonucleotide probes were functionalized on a gold surface and a separate complementary oligonucleotide sequences were synthesized with a trithiocarbonate-based RAFT agent attached to the amine terminus of the sequence via NHS-ester chemistry. The strands were allowed to hybridize and ligation was performed using a T4 ligase, thereby affixing the RAFT agent to the complementary strand placed on the gold substrate, forming surface immobilized DNA-macroRAFT agents. RAFT polymerization of OEGMA was performed from the modified surfaces in the presence of water at 30 ˚C using AIBN as the thermal initiator. Film characterization was performed using AFM, ellipsometry, and ATR-FTIR. Notably, the polymer film generated from the DNA-macroRAFT agents were much thicker than those generated by ATRP described in their previous reports and a large reduction in the background signal was observed, most likely due to the absence of transition metals during polymerization.[136] A thorough follow-up report was published soon after detailing the effects of variations in polymerization conditions (initiator concentration, temperature, reaction time, RAFT agent surface density) on film thickness of the DNA-polymer conjugates.[137]

RAFT polymerization from DNA-macro-RAFT agents have also been used for electrochemical target DNA (tDNA) biosensing applications.[138-139] Recently reported

methodology makes use of immobilized peptide nucleic acid (PNA)-DNA duplexes on gold electrode substrates that have been modified with dithiobenzoate-based RAFT agents using Zr^{4+} mediated coupling chemistry targeting the phosphate groups on the PNA-DNA duplexes. Polymerization of ferrocenylmethyl methacrylate (FcMMA) using VA-044 in the presence of the DNA-macroRAFT agent-modified surface was carried out and the electrochemical response of the prepared polymer modified surfaces was tested. Only gold electrodes which contained the tDNA-polymer conjugates exhibited an oxidation peak on the square-wave voltammogram, with a peak potential of 0.3 V. Electrochemical analysis of gold substrates which served as controls (PNA probe, tDNA, Zr^{4+}, RAFT agent, VA-044, or FcMMA) did not exhibit any visible oxidation peaks on the square-wave voltammogram. Notably, oxidation peak currents of the tDNA-polymer substrates increased linearly as the surface concentration of tDNA increased and allowed for the detection of the tDNA at concentrations as low as 3.2 aM.[138-139]

Recently, photo-RAFT processes have also been used to develop DNA-polymer conjugates via grafting-from.[45] Barner-Kowollik, Ng, Weil, and co-workers developed two ssDNA-macroRAFT agents based on either 4-cyano-4-(phenylcarbonothioylthio)pentanoic acid (CPADB) or 2-(butylthiocarbonothioyl)propionic acid (BTPA) with the ssDNA appended as the R-group of the RAFT agent. CPADB and BTPA were functionalized with either a PFP or NHS-ester group and coupled to the amine terminus of the purified ssDNA (NH_2-ssDNA). RAFT polymerization employing the BTPA- or CPADB-DNA macroRAFT agents was performed using acrylamide, acrylate, or methacrylate based monomers in the presence of eosin Y and ascorbic acid under blue LED irradiation. DNA-polymer conjugates could be purified by membrane filtration and were characterized by GPC and native PAGE. While polymerization from the ssDNA-macroRAFT

agent was operative, the polymers were not monodisperse owing to potential side reactions with the ssDNA which produced low molecular weight tailing in the GPC traces of the DNA-polymer conjugates. Additionally, high molecular weight shoulders were observed in the GPC spectra of ssDNA-poly(OEGMA) conjugates most likely due to transesterification or side reactions to the growing polymer backbone.[45, 140] Impressively, the purified ssDNA-polymer conjugates were able to undergo hybridization with a complementary ssDNA sequence which had been modified with a Rhodamine dye on the DNA terminus thereby showcasing that the prepared ssDNA-polymer conjugates maintain functionality.[45]

1.5 Biomolecule-polymer conjugates accessed through ROMP

Ring-opening metathesis polymerization (ROMP) has early roots stemming from the initial discovery of olefin metathesis in the 1950s, unlike the more recently developed ATRP and RAFT methodologies which were reported in the mid-1990s.[17, 46-47, 141-142] The introduction of well-defined single-component carbene complexes based on molybdenum or ruthenium, spearheaded by the Schrock and Grubbs groups, has paved way for significant advances in ROMP thereby enhancing the synthesis of well-defined and monodisperse polymers through the living polymerization of strained cyclic olefin monomers.[10, 17, 143-144] In particular, the augmented functional group tolerance and increased stability in aqueous media of the ruthenium-based carbenes introduced by Grubbs and co-workers expanded the scope of chemical transformations and facilitated expansion of ROMP into the realm of biomolecule-polymer conjugation.[145-148] As such, ROMP bolsters the chemical toolbox available to chemical biologists and materials chemists alike through the expansion of available polymers with unique function, structures, and material properties.[10, 149]

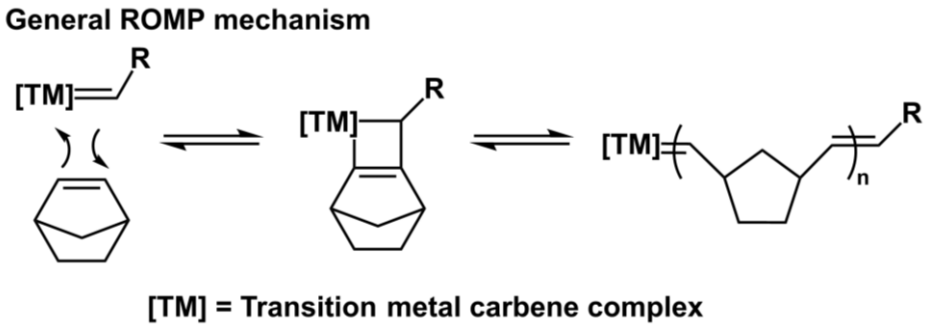

Figure 1-18. General mechanism of ROMP polymerization.

The ROMP mechanism involves coordination of a transition-metal based carbene to a strained cyclic olefin and subsequent [2+2] cycloaddition to form a metallacyclobutane intermediate.[17, 150] The metallacyclobutane then undergoes [2+2] cycloreversion to yield a new olefin and transition-metal carbene which exists on the end of the propagating polymer chain (**Figure 1-18**). The transition-metal carbene catalyst will continue to react with other cyclic olefin monomers with the typical driving force being the release of ring strain from the strained cyclic olefin or an increase an entropy when polymerizing non-strained cyclic olefins. Ruthenium-based transition-metal carbene complexes are the most widely utilized in the context of biomolecule modification due to their stability and functional group tolerance.[17, 39]

1.5.1 Grafting-from proteins using ROMP

Isarov and Pokorski reported the only example of developing protein-polymer conjugates through grafting-from using ROMP (**Figure 1-19**).[151] Because the polymerization needed to be carried out in buffered aqueous solutions compatible with the protein, the authors synthesized a water-soluble Grubbs 3rd generation carbene analogue. Taking inspiration from the Emrick group w0 prepared PEG-functionalized ruthenium carbene derivatives, Isarov and Pokorski synthesized a PEGylated Grubbs 3rd generation derivative (**4**) through a ligand exchange reaction of to displace

the original bromopyridyl groups with PEGylated pyridyl ligands to generate **4** (**Figure 1-19**).[151-152] The catalyst was found to be stable in water for over 10 h as confirmed by ^{1}H NMR monitoring of the alkylidene resonance in D_2O which remained unchanged over the course of the study. Test polymerizations to evaluate catalyst activity were carried out with PEGylated norbornene monomers in both DCM and PBS in order to compare reactivity in both organic and aqueous conditions. Ultimately, polymerization kinetics were found to be slower in aqueous solutions most likely due to a decreased rate of ligand dissociation.[151]

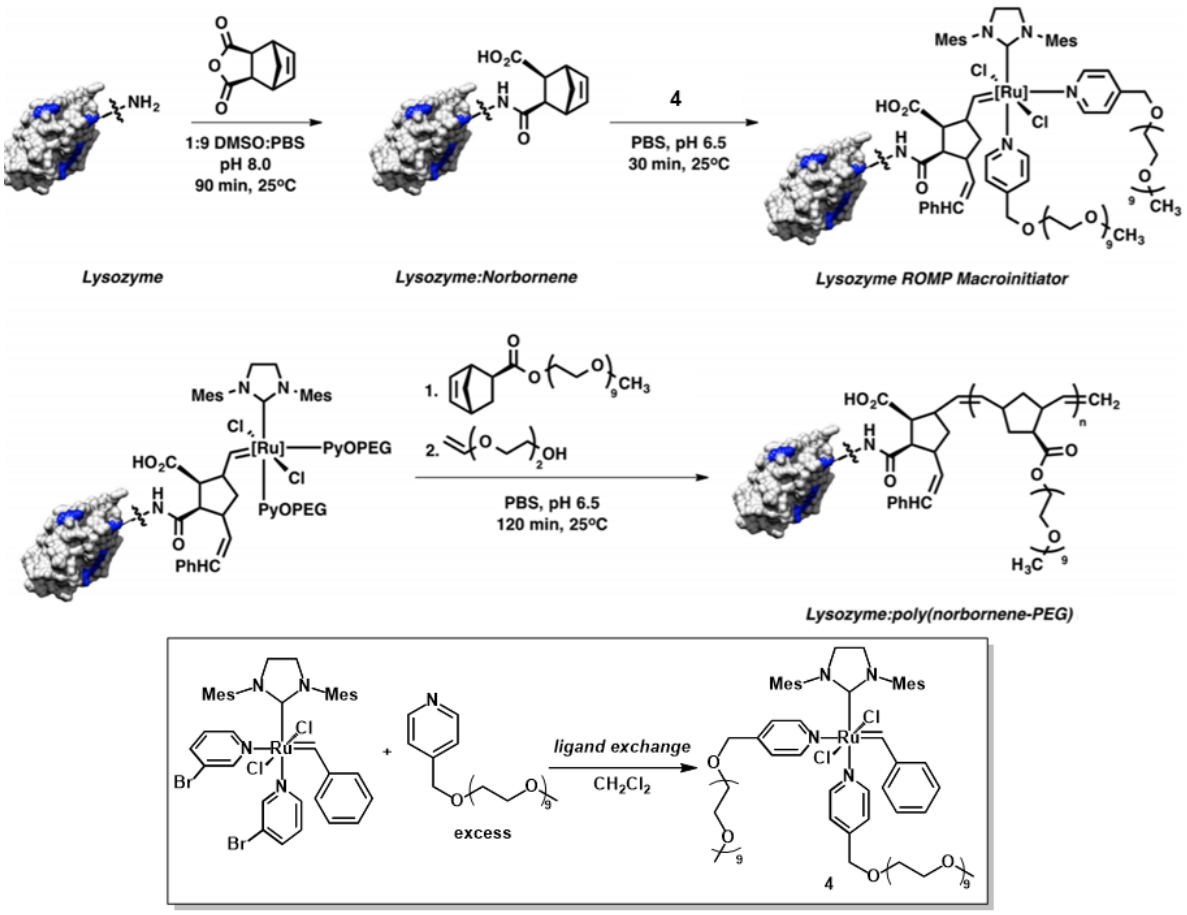

Figure 1-19. ROMP from Lyz to develop Lyz-polymer conjugates using a water-soluble Ru-based carbine. [151], Copyright 2015. Adopted with permission from the American Chemical Society.

Norbornenyl groups were added to reactive Lys residues on the protein surface of Lyz. Treatment of the protein with *exo*-norbornene dicarboxylic anhydride resulted in the modification of up to 5-6 Lys residues per protein. Excess amounts of **4** were then reacted with the norbornenyl modified Lyz to yield the protein macroinitiator which was used for the in-situ growth of PEGylated norbornene monomers from the protein surface. Large monomer loadings (>200 equiv per protein) were ultimately needed to initiate polymerization due to the poor accessibility of the catalytic site on the protein. As a result, only high molecular weights were able to be targeted, since at low monomer concentrations no polymerization could be initiated.[151]

In a follow-up work from the Pokorski group, this challenge was resolved by using a grafting-to approach to instead attach the synthesized polymer to the protein.[153] This allowed for greater control during polymerization and enabled the synthesis of monodisperse polymers of varying molecular weights to be fully characterized and subsequently conjugated to the protein through the Lys residues. The grafting-to strategy is utilized to a greater extent for the conjugation of polymers prepared through ROMP.[12, 154-155] Though grafting-from is under-utilized in the context of ROMP, the initial disclosure from Isarov and Pokorski provides an important foundation with which to develop improved systems through careful tuning of catalyst systems.[151, 153]

1.5.2 Grafting-through approaches with ROMP

The bulk of examples for ROMP in the context of biomolecule modification use the grafting-through strategy. In grafting-through, a biomolecule or bioactive material is attached directly to a monomer (such as norbornene) thus generating a “macromonomer”. The prepared macromonomer can then be polymerized, resulting in a polymer chain with the pendant bioactive cargo attached. Several elegant examples make use of grafting-through using ROMP to prepare

polymer materials with potential therapeutic utility.[156-159] The employment of grafting-through using ROMP in the context of biomolecule modification has been developed extensively for materials bearing nucleic acids or DNA and oligopeptides.

1.5.2.1 Oligopeptides

There exist many examples of grafting-through using ROMP to generate polymer architectures harboring pendant amino acids and oligopeptides. Grubbs and co-workers disclosed many of the initial reports detailing the modification of amino acids and peptides using ruthenium-based carbene complexes. Early manuscripts in the 1990's detailing the extensive use of ring-closing metathesis (RCM) for the generation of cyclic peptides established a foundation for the use of ruthenium-based carbenes to invoke chemical transformations on densely functionalized substrates; interested readers are directed to these literature reports.[160-162] In an early example from Maynard and Grubbs transitioning into ROMP, template directed RCM was used to create cyclic crown ether monomers with a pendent phenylalanine (Phe) amino acid residue.[163] These cyclic monomers were subsequently polymerized through ROMP to yield polyethers with novel olefinic backbone structures and bioactive side chains. Olefin containing polyethers are of interest primarily due to their structural similarity with PEG; however the presence of olefins along the backbone of the polymer introduces a greater degree of synthetic utility making possible the introduction of complex functionality through post-polymerization modification techniques. Polymerization attempts using unprotected phenylalanine substrates were ultimately stymied due to solubility challenges which led to the employment of protected amino acids in earlier approaches.[164-166] Follow-up work focused on developing co-polymers with more complex functionality. Polymers composed of a norbornenyl backbone with pendant oligonucleotide

sequences Gly-Arg-Gly-Asp (GRGD) and Pro-His-Ser-Arg-Asn (PHSRN) were synthesized and their biological activity tested.[167-168] RGD is a peptide sequence on cell surface integrins which mediates the binding of extracellular proteins thereby influencing cell processes. The SRN sequence, physically near the near the RGD sequence in the extracellular matrix protein fibronectin, enhances binding. Norbornene monomers harboring the RGD or SRN oligopeptides were homo- or copolymerized using Grubbs 2nd generation catalyst. Using ROMP allowed for the fine-tuning of the final polymer to incorporate a controlled amount of RGD. The oligopeptide functionalized monomers remained protected over the course of polymerization in order to maintain solubility which necessitated a post-polymerization deprotection strategy resulting in water-soluble polymers to be used in biological assays. Cell adhesion inhibition studies were performed where fibronectin coated surfaces were incubated with human foreskin fibroblast (HFF) cells in the presence of either oligopeptide homo- and co-polymers, the oligopeptides alone, or buffer. Interestingly, the co-polymers consisting of pendant GRGDS and PHSRN sequences inhibited HFF adhesion to fibronectin to a greater degree than homopolymers with pendant GRGDS and the GRGDS or PHSRN peptides alone, highlighting the synergistic effect of the two oligopeptide sequences and underscoring the utility of ROMP to prepare bioactive materials.

Several groups sought to expand or improve upon the use of ROMP to access pendant oligopeptide polymer architectures in order to better understand structure/function relationships of oligopeptide grafted polymers. The Muthukumar and Emrick groups used ROMP to generate polyelectrolytes through the polymerization of OEG or pentalysine oligopeptide functionalized cyclooctene monomers thereby accessing homo- or co-polymers which differed in charge density.[169] Solution behavior could be modulated based on the length of the OEG or Lys blocks and on the graft density of Lys blocks. Additionally, it was found that poly(cyclooctene)-graft-

pentalysine polymers underwent complexation with DNA under acidic conditions but was disrupted under basic conditions. This characteristic can potentially be utilized in plasmid DNA transfection applications.[169] Conrad and Grubbs also utilized ROMP to develop polymers bearing the pendant VPGVG elastin oligopeptide attached to a norbornene monomer.[170] An OEG functionalized norbornene comonomer was also included to varying degrees along the polymer chain. The LCSTs of each polymer were then studied as a function of the polymer concentration in solution, degree of polymerization, or OEG comonomer feed. Ultimately it was found that the LCST depended greatly on the ratio of oligopeptide versus OEG monomers along the copolymer chain and on the concentration of the copolymer in solution, but to a lesser degree on the molecular weight of the copolymer.[170]

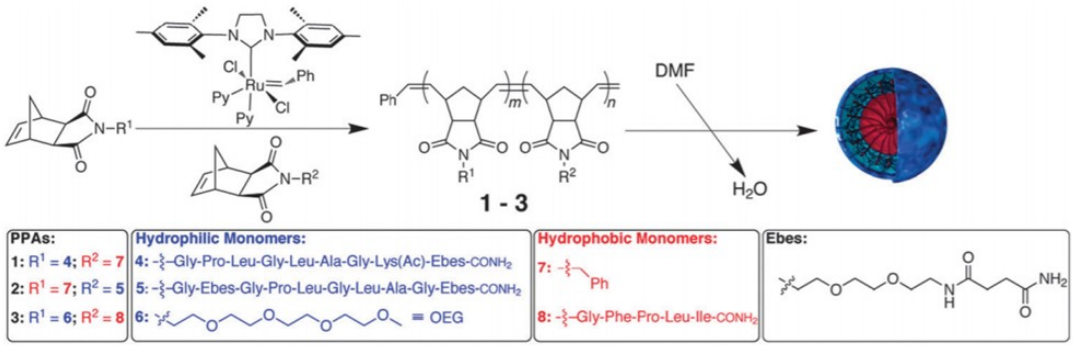

Figure 1-20. Development of copolymers containing pendent oligopeptides via ROMP for the generation of peptide-containing nanoparticles. [171], Copyright 2013. Reproduced with permission from The Royal Society of Chemistry.

The Gianneschi group has greatly expanded on the development of oligopeptide containing homo- or block- (co)polymers prepared via grafting-through using ROMP. In their earliest examples, copolymerization of either hydrophilic or hydrophobic norbornene-based monomers functionalized with oligopeptides was achieved via ROMP which resulted in the formation of

bioactive nanoparticles (**Figure 1-20**).[171] The Gianneschi group has also been successful in developing protecting-group free strategies towards accessing polymers harboring pendant oligopeptides using ROMP.[172] These initial works served as a foundation to understand proteolytic stability of peptide-based nanoparticles and established a set of synthetic principles to better develop polymers harboring pendant oligopeptide functionality. Expansion of this platform led to the development of polymer brushes harboring pendant cell-penetrating peptides (CPPs) which were resistant to proteolysis and also maintained their cell penetration activity.[173-174] The elegant use of ROMP has also allowed for facile tuning of polymer architectures and grafting densities which has made possible unique nanoparticle materials for drug delivery, fluorescence imaging, and for either the evasion or uptake of macrophages.[175-176] The ring-opening metathesis polymerization-induced self-assembly (ROMPISA) ushered in by the Gianneschi group has also proven to be an extremely useful method for the generation of well-defined nanostructures.[177-178]

1.5.2.2 Nucleic acids

ROMP has been used to great extent in the polymerization of nucleic acid containing polymers. Initial reports by Williams and co-workers have utilized ROMP to develop polymers with pendant nucleic acid functionality via grafting-through of norbornene monomers substituted with either thymine, adenine, cytosine, guanine, or uracil.[179-180] The monomers were poorly soluble, however, and polymerization of the monomers was only able to produce short oligomers due to precipitation over the course of the reaction. Bazzi and Sleiman were able to successfully synthesize homopolymers and copolymers containing adenine side chains via ROMP using a succinimide additive to solubilize the resulting polymer through hydrogen bonding interactions.[181]

Work by Weck and co-workers has also developed template-directed strategies to carry out ROMP of nucleic acid based monomers.[182-183]

Expanding further on this, Herrmann and co-workers recently reported a strategy to solubilize DNA in the organic phase by exchanging counter-ions on the backbone with quaternary ammonium surfactants.[184] These DNA-side chains are then modified with norbornene and polymerized via ROMP to yield DNA homopolymers of varying architectures. This strategy allowed for higher yields for DNA-based conjugates and overcame challenges of nucleic acid modification in organic solvents.[184]

Gianneschi and co-workers have shown recent progress in preparing nucleic acid brush polymers and co-polymers from PNA functionalized norbornene monomers.[185] Homopolymers made from the oligonucleotide substituted monomers or amphiphilic brush copolymers made up of a pendant oligonucleotide block and a benzyl-substituted poly(norbornene) block were synthesized through ROMP. The authors were able to develop spherical nanoparticles from the synthesized brush copolymers which harbored the oligonucleotide block exposed as the outer shell of the sphere. Notably the oligonucleotides present on the nanoparticle surface were able to undergo hybridization with complementary DNA oligonucleotide sequences thereby showcasing post-polymerization functionality.[185]

1.6 Summary and outlook

Utilizing controlled polymerization methods to graft-from biomolecules has enabled rapid access to biomolecule-polymer conjugates which combine the unique traits of both the biomolecule and the synthetic polymer attached to it. Over the course of the review, we have examined recent developments in the generation of biomolecule-polymer conjugates synthesized

using grafting-from techniques tracing back from the initial discoveries employing ATRP, RAFT, or ROMP. There are many advantages to utilizing grafting-from techniques with purification and small molecule coupling efficiencies being the two most critical. Additionally, each controlled polymerization process holds inherent advantages and disadvantages in the context of grafting-from biomolecules. While an advantage of ATRP is the high degree of flexibility offered by the availability of many different variations based on the polymerization process, this also presents a challenge as the correct choice of ATRP method to use may not always be straightforward to the novice user. The deployment of transition-metal based reagents and the need for oxygen-free conditions also presents a challenge in the context of grafting-from. RAFT polymerization is an incredibly versatile method which allows for the polymerization of a wide range of monomers in a variety of solvent conditions, and the absence of transition-metal based reagents is also a significant advantage of the technique. However, RAFT in the context of grafting-from suffers from relatively slow reaction kinetics or long inhibition periods which may be dependent on the structure of the biomolecule-macroCTA, the amount of oxygen in the reaction mixture, or on the reagent concentrations. On the other hand, ROMP typically exhibits fast polymerization kinetics and allows access to polymers made from monomers which may not be readily polymerized using controlled radical techniques. However, the need to employ transition-metal based reagents, especially from the biomolecule surface represents a significant challenge. Fortunately, all together these methods provide scientists with a plethora of opportunities to prepare protein-polymer conjugates of choice.

We anticipate continued interest in grafting-from processes, given the recent resurgence and creativity by many groups to investigate new bioconjugation techniques which have expanded the scope of targetable amino acid residues and increased the conjugation yields.[6, 36-38, 41, 186-190]

The relatively recent highly-efficient methods to label methionine and histidine residues on proteins provide additional, less abundant, amino acid residues with which to polymerize from, if reagents bearing ATRP initiators can be accessed.[36-37, 191-193] Additionally, the rapid progress of metal-free and photo-induced controlled polymerization techniques paves way for the synthesis of polymers from more therapeutically relevant biomolecules that exhibit greater sensitivity to reaction conditions.[91-93, 126, 194-195] It would be an exciting and much needed addition to identify water-soluble organic photo-reductants capable of promoting ATRP processes in purely aqueous solutions in the absence of transition metals.[196-197] Oxygen tolerant polymerization techniques that can operate at low volumes also represent a significant breakthrough that may play a role in further development of grafting-from techniques.[198-200] Combined altogether, newly developed polymerization and conjugation techniques may soon allow for rapid access and high-throughput screening of constructs to develop new biomolecule-polymer conjugates with vastly unique properties that would give additional insights into structure-property relationships of complex bioconjugates.

1.7 References

(1) Russell, A. J.; Baker, S. L.; Colina, C. M.; Figg, C. A.; Kaar, J. L.; Matyjaszewski, K.; Simakova, A.; Sumerlin, B. S. Next generation protein-polymer conjugates. *AIChE J.* **2018,** *64*, 3230-3245.

(2) Pelegri-O'Day, E. M.; Lin, E.-W.; Maynard, H. D. Therapeutic protein–polymer conjugates: advancing beyond PEGylation. *J. Am. Chem. Soc.* **2014,** *136*, 14323-14332.

(3) Abuchowski, A.; Van Es, T.; Palczuk, N.; Davis, F. Alteration of immunological properties of bovine serum albumin by covalent attachment of polyethylene glycol. *J. Biol. Chem.* **1977,** *252*, 3578-3581.

(4) Pfister, D.; Morbidelli, M. Process for protein PEGylation. *J. Control. Release* **2014,** *180*, 134-149.

(5) Alconcel, S. N.; Baas, A. S.; Maynard, H. D. FDA-approved poly (ethylene glycol)–protein conjugate drugs. *Polym. Chem.* **2011,** *2*, 1442-1448.

(6) Ko, J. H.; Maynard, H. D. A guide to maximizing the therapeutic potential of protein–polymer conjugates by rational design. *Chem. Soc. Rev.* **2018,** *47*, 8998-9014.

(7) G de la Torre, B.; Albericio, F. The pharmaceutical industry in 2018. An analysis of FDA drug approvals from the perspective of molecules. *Molecules* **2019,** *24*, 809.

(8) Ramos-de-la-Peña, A. M.; Aguilar, O. Progress and Challenges in PEGylated Proteins Downstream Processing: A Review of the Last 8 Years. *Int. J. Pept. Res. Ther.* **2019**, 1-16.

(9) Braunecker, W. A.; Matyjaszewski, K. Controlled/living radical polymerization: Features, developments, and perspectives. *Prog. Polym. Sci.* **2007,** *32*, 93-146.

(10) Bielawski, C. W.; Grubbs, R. H. Living ring-opening metathesis polymerization. *Prog. Polym. Sci.* **2007,** *32*, 1-29.

(11) Moad, G.; Rizzardo, E.; Thang, S. H. Living radical polymerization by the RAFT process–a third update. *Aust. J. Chem.* **2012,** *65*, 985-1076.

(12) Pelegri-O'Day, E. M.; Matsumoto, N. M.; Tamshen, K.; Raftery, E. D.; Lau, U. Y.; Maynard, H. D. PEG Analogs Synthesized by Ring-Opening Metathesis Polymerization for Reversible Bioconjugation. *Bioconjugate Chem.* **2018,** *29*, 3739-3745.

(13) Messina, M. S.; Ko, J. H.; Yang, Z.; Strouse, M. J.; Houk, K.; Maynard, H. D. Effect of trehalose polymer regioisomers on protein stabilization. *Polym. Chem.* **2017,** *8*, 4781-4788.

(14) Mancini, R. J.; Lee, J.; Maynard, H. D. Trehalose glycopolymers for stabilization of protein conjugates to environmental stressors. *J. Am. Chem. Soc.* **2012,** *134*, 8474-8479.

(15) Sumerlin, B. S., Proteins as initiators of controlled radical polymerization: grafting-from via ATRP and RAFT. ACS Publications: 2011.

(16) Pelegri-O'Day, E. M.; Maynard, H. D. Controlled radical polymerization as an enabling approach for the next generation of protein–polymer conjugates. *Acc. Chem. Res.* **2016,** *49*, 1777-1785.

(17) Trnka, T. M.; Grubbs, R. H. The development of L2X2Ru CHR olefin metathesis catalysts: an organometallic success story. *Acc. Chem. Res.* **2001,** *34*, 18-29.

(18) Matyjaszewski, K. Atom transfer radical polymerization (ATRP): current status and future perspectives. *Macromolecules* **2012,** *45*, 4015-4039.

(19) Chenal, M.; Boursier, C.; Guillaneuf, Y.; Taverna, M.; Couvreur, P.; Nicolas, J. First peptide/protein PEGylation with functional polymers designed by nitroxide-mediated polymerization. *Polym. Chem.* **2011,** *2*, 1523-1530.

(20) Nicolas, J.; Guillaneuf, Y.; Lefay, C.; Bertin, D.; Gigmes, D.; Charleux, B. Nitroxide-mediated polymerization. *Prog. Polym. Sci.* **2013,** *38*, 63-235.

(21) Hawker, C. J.; Bosman, A. W.; Harth, E. New polymer synthesis by nitroxide mediated living radical polymerizations. *Chem. Rev.* **2001,** *101*, 3661-3688.

(22) Vinciguerra, D.; Denis, S.; Mougin, J.; Jacobs, M.; Guillaneuf, Y.; Mura, S.; Couvreur, P.; Nicolas, J. A facile route to heterotelechelic polymer prodrug nanoparticles for imaging, drug delivery and combination therapy. *J. Control. Release* **2018,** *286*, 425-438.

(23) Heredia, K. L.; Maynard, H. D. Synthesis of protein–polymer conjugates. *Org. Biomol. Chem.* **2006,** *5*, 45-53.

(24) Sun, H.; Yang, L.; Thompson, M. P.; Schara, S.; Cao, W.; Choi, W.; Hu, Z.; Zang, N.; Tan, W.; Gianneschi, N. C. Recent Advances in Amphiphilic Polymer-Oligonucleotide Nanomaterials via Living/Controlled Polymerization Technologies. *Bioconjugate Chem.* **2019,** *30*, 1889–1904.

(25) Wang, Y.; Wu, C. Site-specific conjugation of polymers to proteins. *Biomacromolecules* **2018,** *19*, 1804-1825.

(26) Steinbach, T.; Wurm, F.; Klok, H.-A. Squaric acid mediated bioconjugation expanded to polymers prepared by ATRP. *Polym. Chem.* **2014,** *5*, 4039-4047.

(27) Miller, S.; Janin, J.; Lesk, A. M.; Chothia, C. Interior and surface of monomeric proteins. *J. Mol. Biol.* **1987,** *196*, 641-656.

(28) Carmali, S.; Murata, H.; Amemiya, E.; Matyjaszewski, K.; Russell, A. J. Tertiary structure-based prediction of how atrp initiators react with proteins. *ACS Biomater. Sci. Eng.* **2017,** *3*, 2086-2097.

(29) Matos, M. J.; Oliveira, B. L.; Martínez-Sáez, N.; Guerreiro, A.; Cal, P. M.; Bertoldo, J.; Maneiro, M.; Perkins, E.; Howard, J.; Deery, M. J. Chemo-and regioselective lysine modification on native proteins. *J. Am. Chem. Soc.* **2018,** *140*, 4004-4017.

(30) Qi, Y.; Amiram, M.; Gao, W.; McCafferty, D. G.; Chilkoti, A. Sortase-catalyzed initiator attachment enables high yield growth of a stealth polymer from the C terminus of a protein. *Macromol. Rapid Commun.* **2013,** *34*, 1256-1260.

(31) Gao, W.; Liu, W.; Mackay, J. A.; Zalutsky, M. R.; Toone, E. J.; Chilkoti, A. In situ growth of a stoichiometric PEG-like conjugate at a protein's N-terminus with significantly improved pharmacokinetics. *Proc. Natl. Acad. Sci. U. S. A.* **2009,** *106*, 15231-15236.

(32) Messina, M. S.; Stauber, J. M.; Waddington, M. A.; Rheingold, A. L.; Maynard, H. D.; Spokoyny, A. M. Organometallic gold (III) reagents for cysteine arylation. *J. Am. Chem. Soc.* **2018,** *140*, 7065-7069.

(33) Vinogradova, E. V.; Zhang, C.; Spokoyny, A. M.; Pentelute, B. L.; Buchwald, S. L. Organometallic palladium reagents for cysteine bioconjugation. *Nature* **2015,** *526*, 687–691.

(34) Vinogradova, E. V. Organometallic chemical biology: an organometallic approach to bioconjugation. *Pure Appl. Chem.* **2017,** *89*, 1619-1640.

(35) Hanaya, K.; Ohata, J.; Miller, M. K.; Mangubat-Medina, A. E.; Swierczynski, M. J.; Yang, D. C.; Rosenthal, R. M.; Popp, B. V.; Ball, Z. T. Rapid Nickel (II)-Promoted Cysteine S-Arylation with Arylboronic Acids. *Chem. Comm.* **2019,** *55*, 2841-2844.

(36) Jia, S.; He, D.; Chang, C. J. Bioinspired Thiophosphorodichloridate Reagents for Chemoselective Histidine Bioconjugation. *J. Am. Chem. Soc.* **2019,** *141*, 7294–7301.

(37) Lin, S.; Yang, X.; Jia, S.; Weeks, A. M.; Hornsby, M.; Lee, P. S.; Nichiporuk, R. V.; Iavarone, A. T.; Wells, J. A.; Toste, F. D. Redox-based reagents for chemoselective methionine bioconjugation. *Science* **2017,** *355*, 597-602.

(38) deGruyter, J. N.; Malins, L. R.; Baran, P. S. Residue-specific peptide modification: a chemist's guide. *Biochemistry* **2017,** *56*, 3863-3873.

(39) Isenegger, P. G.; Davis, B. G. Concepts of Catalysis in Site-Selective Protein Modifications. *J. Am. Chem. Soc.* **2019,** *141*, 8005–8013.

(40) Hoyt, E. A.; Cal, P. M.; Oliveira, B. L.; Bernardes, G. J. Contemporary approaches to site-selective protein modification. *Nat. Rev. Chem.* **2019,** *3*, 147–171.

(41) Zhang, C.; Vinogradova, E. V.; Spokoyny, A. M.; Buchwald, S. L.; Pentelute, B. L. Arylation chemistry for bioconjugation. *Angew. Chem., Int. Ed.* **2019,** *58*, 4810-4839.

(42) Becker, M. L.; Liu, J.; Wooley, K. L. Functionalized micellar assemblies prepared via block copolymers synthesized by living free radical polymerization upon peptide-loaded resins. *Biomacromolecules* **2005,** *6*, 220-228.

(43) Rettig, H.; Krause, E.; Börner, H. G. Atom transfer radical polymerization with polypeptide initiators: A general approach to block copolymers of sequence-defined polypeptides and synthetic polymers. *Macromol. Rapid Commun.* **2004,** *25*, 1251-1256.

(44) Averick, S. E.; Dey, S. K.; Grahacharya, D.; Matyjaszewski, K.; Das, S. R. Solid-phase incorporation of an ATRP initiator for polymer–DNA biohybrids. *Angew. Chem., Int. Ed.* **2014,** *53*, 2739-2744.

(45) Lueckerath, T.; Strauch, T.; Koynov, K.; Barner-Kowollik, C.; Ng, D. Y.; Weil, T. DNA–Polymer Conjugates by Photoinduced RAFT Polymerization. *Biomacromolecules* **2018,** *20*, 212-221.

(46) Kato, M.; Kamigaito, M.; Sawamoto, M.; Higashimura, T. Polymerization of methyl methacrylate with the carbon tetrachloride/dichlorotris-(triphenylphosphine) ruthenium (II)/methylaluminum bis (2, 6-di-tert-butylphenoxide) initiating system: possibility of living radical polymerization. *Macromolecules* **1995,** *28*, 1721-1723.

(47) Wang, J.-S.; Matyjaszewski, K. Controlled/" living" radical polymerization. atom transfer radical polymerization in the presence of transition-metal complexes. *J. Am. Chem. Soc.* **1995,** *117*, 5614-5615.

(48) Lewis, A. L.; Leppard, S. W., Conjugation reactions. Google Patents: 2011.

(49) Bontempo, D.; Maynard, H. D. Streptavidin as a macroinitiator for polymerization: in situ protein− polymer conjugate formation. *J. Am. Chem. Soc.* **2005,** *127*, 6508-6509.

(50) Heredia, K. L.; Bontempo, D.; Ly, T.; Byers, J. T.; Halstenberg, S.; Maynard, H. D. In situ preparation of protein−"smart" polymer conjugates with retention of bioactivity. *J. Am. Chem. Soc.* **2005,** *127*, 16955-16960.

(51) Weber, P. C.; Ohlendorf, D.; Wendoloski, J.; Salemme, F. Structural origins of high-affinity biotin binding to streptavidin. *Science* **1989,** *243*, 85-88.

(52) Lele, B. S.; Murata, H.; Matyjaszewski, K.; Russell, A. J. Synthesis of uniform protein−polymer conjugates. *Biomacromolecules* **2005,** *6*, 3380-3387.

(53) Cummings, C.; Murata, H.; Koepsel, R.; Russell, A. J. Tailoring enzyme activity and stability using polymer-based protein engineering. *Biomaterials* **2013,** *34*, 7437-7443.

(54) Campbell, A. S.; Murata, H.; Carmali, S.; Matyjaszewski, K.; Islam, M. F.; Russell, A. J. Polymer-based protein engineering grown ferrocene-containing redox polymers improve current generation in an enzymatic biofuel cell. *Biosens. Bioelectron.* **2016,** *86*, 446-453.

(55) Nicolas, J.; San Miguel, V.; Mantovani, G.; Haddleton, D. M. Fluorescently tagged polymer bioconjugates from protein derived macroinitiators. *Chem. Comm.* **2006**, 4697-4699.

(56) Zhang, Q.; Li, M.; Zhu, C.; Nurumbetov, G.; Li, Z.; Wilson, P.; Kempe, K.; Haddleton, D. M. Well-defined protein/peptide–polymer conjugates by aqueous Cu-LRP: synthesis and controlled self-assembly. *J. Am. Chem. Soc.* **2015,** *137*, 9344-9353.

(57) Droumaguet, B. Multifunctional Giant Amphiphiles via simultaneous copper (i)-catalyzed azide–alkyne cycloaddition and living radical polymerization. *Chem. Comm.* **2012,** *48*, 1586-1588.

(58) Peeler, J. C.; Woodman, B. F.; Averick, S.; Miyake-Stoner, S. J.; Stokes, A. L.; Hess, K. R.; Matyjaszewski, K.; Mehl, R. A. Genetically encoded initiator for polymer growth from proteins. *J. Am. Chem. Soc.* **2010,** *132*, 13575-13577.

(59) Zeng, Q.; Li, T.; Cash, B.; Li, S.; Xie, F.; Wang, Q. Chemoselective derivatization of a bionanoparticle by click reaction and ATRP reaction. *Chem. Comm.* **2007**, 1453-1455.

(60) Hu, Y.; Samanta, D.; Parelkar, S. S.; Hong, S. W.; Wang, Q.; Russell, T. P.; Emrick, T. Ferritin–polymer conjugates: Grafting chemistry and integration into nanoscale assemblies. *Adv. Funct. Mater.* **2010,** *20*, 3603-3612.

(61) Jiang, L.; Bonde, J. S.; Ye, L. Temperature and pH Controlled Self-Assembly of a Protein–Polymer Biohybrid. *Macromol. Chem. Phys.* **2018,** *219*, 1700597.

(62) Pokorski, J. K.; Breitenkamp, K.; Liepold, L. O.; Qazi, S.; Finn, M. Functional virus-based polymer–protein nanoparticles by atom transfer radical polymerization. *J. Am. Chem. Soc.* **2011,** *133*, 9242-9245.

(63) Hu, J.; Wang, G.; Zhao, W.; Liu, X.; Zhang, L.; Gao, W. Site-specific in situ growth of an interferon-polymer conjugate that outperforms PEGASYS in cancer therapy. *Biomaterials* **2016,** *96*, 84-92.

(64) Hu, J.; Zhao, W.; Gao, Y.; Sun, M.; Wei, Y.; Deng, H.; Gao, W. Site-specific in situ growth of a cyclized protein-polymer conjugate with improved stability and tumor retention. *Biomaterials* **2015,** *47*, 13-19.

(65) Becker, M. L.; Liu, J.; Wooley, K. L. Peptide-polymer bioconjugates: hybrid block copolymers generated via living radical polymerizations from resin-supported peptides. *Chem. Comm.* **2003**, 180-181.

(66) Angot, S.; Ayres, N.; Bon, S. A.; Haddleton, D. M. Living radical polymerization immobilized on Wang resins: synthesis and harvest of narrow polydispersity poly (methacrylate) s. *Macromolecules* **2001,** *34*, 768-774.

(67) Mei, Y.; Beers, K. L.; Byrd, H. M.; VanderHart, D. L.; Washburn, N. R. Solid-phase ATRP synthesis of peptide− polymer hybrids. *J. Am. Chem. Soc.* **2004,** *126*, 3472-3476.

(68) Lou, X.; Lewis, M. S.; Gorman, C. B.; He, L. Detection of DNA point mutation by atom transfer radical polymerization. *Anal. Chem.* **2005,** *77*, 4698-4705.

(69) Lou, X.; He, L. DNA-accelerated atom transfer radical polymerization on a gold surface. *Langmuir* **2006,** *22*, 2640-2646.

(70) Lou, X.; Wang, C.; He, L. Core− Shell Au Nanoparticle Formation with DNA− Polymer Hybrid Coatings Using Aqueous ATRP. *Biomacromolecules* **2007,** *8*, 1385-1390.

(71) Averick, S.; Simakova, A.; Park, S.; Konkolewicz, D.; Magenau, A. J.; Mehl, R. A.; Matyjaszewski, K. ATRP under biologically relevant conditions: grafting from a protein. *ACS Macro Lett.* **2011,** *1*, 6-10.

(72) Jakubowski, W.; Matyjaszewski, K. Activator generated by electron transfer for atom transfer radical polymerization. *Macromolecules* **2005,** *38*, 4139-4146.

(73) Wu, Y.; Liu, S.; He, L. Electrochemical biosensing using amplification-by-polymerization. *Anal. Chem.* **2009,** *81*, 7015-7021.

(74) Lin, E.-W.; Maynard, H. D. Grafting from small interfering ribonucleic acid (siRNA) as an alternative synthesis route to siRNA–polymer conjugates. *Macromolecules* **2015,** *48*, 5640-5647.

(75) Tokura, Y.; Jiang, Y.; Welle, A.; Stenzel, M. H.; Krzemien, K. M.; Michaelis, J.; Berger, R.; Barner-Kowollik, C.; Wu, Y.; Weil, T. Bottom-Up Fabrication of Nanopatterned Polymers on DNA Origami by In Situ Atom-Transfer Radical Polymerization. *Angew. Chem.* **2016,** *128*, 5786-5791.

(76) Zhu, B.; Lu, D.; Ge, J.; Liu, Z. Uniform polymer–protein conjugate by aqueous AGET ATRP using protein as a macroinitiator. *Acta Biomater.* **2011,** *7*, 2131-2138.

(77) Yaşayan, G.; Saeed, A. O.; Fernández-Trillo, F.; Allen, S.; Davies, M. C.; Jangher, A.; Paul, A.; Thurecht, K. J.; King, S. M.; Schweins, R. Responsive hybrid block co-polymer conjugates of proteins–controlled architecture to modulate substrate specificity and solution behaviour. *Polym. Chem.* **2011,** *2*, 1567-1578.

(78) Magnusson, J. P.; Bersani, S.; Salmaso, S.; Alexander, C.; Caliceti, P. In Situ Growth of Side-Chain PEG Polymers from Functionalized Human Growth Hormone: A New Technique for Preparation of Enhanced Protein- Polymer Conjugates. *Bioconjugate Chem.* **2010,** *21*, 671-678.

(79) Mansfield, K. M.; Maynard, H. D. Site-specific insulin-trehalose glycopolymer conjugate by grafting from strategy improves bioactivity. *ACS Macro Lett.* **2018,** *7*, 324-329.

(80) Averick, S. E.; Magenau, A. J.; Simakova, A.; Woodman, B. F.; Seong, A.; Mehl, R. A.; Matyjaszewski, K. Covalently incorporated protein–nanogels using AGET ATRP in an inverse miniemulsion. *Polym. Chem.* **2011,** *2*, 1476-1478.

(81) Wang, J.-T.; Hong, Y.; Ji, X.; Zhang, M.; Liu, L.; Zhao, H. In situ fabrication of PHEMA–BSA core–corona biohybrid particles. *J. Mater. Chem. B* **2016,** *4*, 4430-4438.

(82) Simakova, A.; Averick, S. E.; Konkolewicz, D.; Matyjaszewski, K. Aqueous ARGET ATRP. *Macromolecules* **2012,** *45*, 6371-6379.

(83) Averick, S. E.; Bazewicz, C. G.; Woodman, B. F.; Simakova, A.; Mehl, R. A.; Matyjaszewski, K. Protein–polymer hybrids: Conducting ARGET ATRP from a genetically encoded cleavable ATRP initiator. *Eur. Polym. J.* **2013,** *49*, 2919-2924.

(84) Matyjaszewski, K.; Jakubowski, W.; Min, K.; Tang, W.; Huang, J.; Braunecker, W. A.; Tsarevsky, N. V. Diminishing catalyst concentration in atom transfer radical polymerization with reducing agents. *Proc. Natl. Acad. Sci. U. S. A.* **2006,** *103*, 15309-15314.

(85) Konkolewicz, D.; Magenau, A. J.; Averick, S. E.; Simakova, A.; He, H.; Matyjaszewski, K. ICAR ATRP with ppm Cu Catalyst in Water. *Macromolecules* **2012,** *45*, 4461-4468.

(86) Cohen-Karni, D.; Kovaliov, M.; Ramelot, T.; Konkolewicz, D.; Graner, S.; Averick, S. Grafting challenging monomers from proteins using aqueous ICAR ATRP under bio-relevant conditions. *Polym. Chem.* **2017,** *8*, 3992-3998.

(87) Kovaliov, M.; Cheng, C.; Cheng, B.; Averick, S. Grafting-from lipase: utilization of a common amino acid residue as a new grafting site. *Polym. Chem.* **2018,** *9*, 4651-4659.

(88) Liu, Y.; Nevanen, T. K.; Paananen, A.; Kempe, K.; Wilson, P.; Johansson, L.-S.; Joensuu, J. J.; Linder, M. B.; Haddleton, D. M.; Milani, R. Self-Assembling Protein–Polymer Bioconjugates for Surfaces with Antifouling Features and Low Nonspecific Binding. *ACS Appl. Mater. Interfaces* **2018,** *11*, 3599-3608.

(89) Pan, X.; Malhotra, N.; Simakova, A.; Wang, Z.; Konkolewicz, D.; Matyjaszewski, K. Photoinduced atom transfer radical polymerization with ppm-level Cu catalyst by visible light in aqueous media. *J. Am. Chem. Soc.* **2015,** *137*, 15430-15433.

(90) Fu, L.; Wang, Z.; Lathwal, S.; Enciso, A. E.; Simakova, A.; Das, S. R.; Russell, A. J.; Matyjaszewski, K. Synthesis of Polymer Bioconjugates via Photoinduced Atom Transfer Radical Polymerization under Blue Light Irradiation. *ACS Macro Lett.* **2018,** *7*, 1248-1253.

(91) Discekici, E. H.; Anastasaki, A.; Read de Alaniz, J.; Hawker, C. J. Evolution and Future Directions of Metal-Free Atom Transfer Radical Polymerization. *Macromolecules* **2018,** *51*, 7421-7434.

(92) Treat, N. J.; Sprafke, H.; Kramer, J. W.; Clark, P. G.; Barton, B. E.; Read de Alaniz, J.; Fors, B. P.; Hawker, C. J. Metal-free atom transfer radical polymerization. *J. Am. Chem. Soc.* **2014,** *136*, 16096-16101.

(93) Pan, X.; Lamson, M.; Yan, J.; Matyjaszewski, K. Photoinduced metal-free atom transfer radical polymerization of acrylonitrile. *ACS Macro Lett.* **2015,** *4*, 192-196.

(94) Miyake, G. M.; Theriot, J. C. Perylene as an organic photocatalyst for the radical polymerization of functionalized vinyl monomers through oxidative quenching with alkyl bromides and visible light. *Macromolecules* **2014,** *47*, 8255-8261.

(95) Magenau, A. J.; Strandwitz, N. C.; Gennaro, A.; Matyjaszewski, K. Electrochemically mediated atom transfer radical polymerization. *Science* **2011,** *332*, 81-84.

(96) Fantin, M.; Park, S.; Wang, Y.; Matyjaszewski, K. Electrochemical atom transfer radical polymerization in miniemulsion with a dual catalytic system. *Macromolecules* **2016,** *49*, 8838-8847.

(97) Magenau, A. J.; Bortolamei, N.; Frick, E.; Park, S.; Gennaro, A.; Matyjaszewski, K. Investigation of electrochemically mediated atom transfer radical polymerization. *Macromolecules* **2013,** *46*, 4346-4353.

(98) Li, B.; Yu, B.; Huck, W. T.; Liu, W.; Zhou, F. Electrochemically mediated atom transfer radical polymerization on nonconducting substrates: controlled brush growth through catalyst diffusion. *J. Am. Chem. Soc.* **2013,** *135*, 1708-1710.

(99) Sun, Y.; Du, H.; Lan, Y.; Wang, W.; Liang, Y.; Feng, C.; Yang, M. Preparation of hemoglobin (Hb) imprinted polymer by Hb catalyzed eATRP and its application in biosensor. *Biosens. Bioelectron.* **2016,** *77*, 894-900.

(100) Liu, Q.; Ma, K.; Wen, D.; Wang, Q.; Sun, H.; Liu, Q.; Kong, J. Electrochemically mediated ATRP (eATRP) amplification for ultrasensitive detection of glucose. *J. Electroanal. Chem.* **2018,** *823*, 20-25.

(101) Sun, Y.; Lathwal, S.; Wang, Y.; Fu, L.; Olszewski, M.; Fantin, M.; Enciso, A. E.; Szczepaniak, G.; Das, S.; Matyjaszewski, K. Preparation of Well-Defined Polymers and DNA–Polymer Bioconjugates via Small-Volume eATRP in the Presence of Air. *ACS Macro Lett.* **2019,** *8*, 603-609.

(102) Chiefari, J.; Chong, Y.; Ercole, F.; Krstina, J.; Jeffery, J.; Le, T. P.; Mayadunne, R. T.; Meijs, G. F.; Moad, C. L.; Moad, G. Living free-radical polymerization by reversible addition− fragmentation chain transfer: the RAFT process. *Macromolecules* **1998,** *31*, 5559-5562.

(103) Boyer, C.; Bulmus, V.; Davis, T. P.; Ladmiral, V.; Liu, J.; Perrier, S. Bioapplications of RAFT polymerization. *Chem. Rev.* **2009,** *109*, 5402-5436.

(104) Moad, G.; Rizzardo, E.; Thang, S. H. RAFT polymerization and some of its applications. *Chem. - Asian J.* **2013,** *8*, 1634-1644.

(105) Moad, G.; Rizzardo, E.; Thang, S. H. Toward living radical polymerization. *Acc. Chem. Res.* **2008,** *41*, 1133-1142.

(106) Perrier, S. b. 50th Anniversary Perspective: RAFT Polymerization- A User Guide. *Macromolecules* **2017,** *50*, 7433-7447.

(107) Skey, J.; O'Reilly, R. K. Facile one pot synthesis of a range of reversible addition–fragmentation chain transfer (RAFT) agents. *Chem. Comm.* **2008**, 4183-4185.

(108) Keddie, D. J.; Moad, G.; Rizzardo, E.; Thang, S. H. RAFT agent design and synthesis. *Macromolecules* **2012,** *45*, 5321-5342.

(109) Monteiro, M. J. Design strategies for controlling the molecular weight and rate using reversible addition–fragmentation chain transfer mediated living radical polymerization. *J. Polym. Sci., Part A: Polym. Chem.* **2005,** *43*, 3189-3204.

(110) Bulmus, V. RAFT polymerization mediated bioconjugation strategies. *Polym. Chem.* **2011,** *2*, 1463-1472.

(111) Shanmugam, S.; Xu, J.; Boyer, C. Photoinduced Electron Transfer–Reversible Addition–Fragmentation Chain Transfer (PET-RAFT) Polymerization of Vinyl Acetate and N-Vinylpyrrolidinone: Kinetic and Oxygen Tolerance Study. *Macromolecules* **2014,** *47*, 4930-4942.

(112) Bathfield, M.; D'Agosto, F.; Spitz, R.; Charreyre, M.-T.; Delair, T. Versatile precursors of functional RAFT agents. Application to the synthesis of bio-related end-functionalized polymers. *J. Am. Chem. Soc.* **2006,** *128*, 2546-2547.

(113) Lutz, J.-F.; Börner, H. G. Modern trends in polymer bioconjugates design. *Prog. Polym. Sci.* **2008,** *33*, 1-39.

(114) Hong, C.-Y.; Pan, C.-Y. Direct synthesis of biotinylated stimuli-responsive polymer and diblock copolymer by RAFT polymerization using biotinylated trithiocarbonate as RAFT agent. *Macromolecules* **2006,** *39*, 3517-3524.

(115) Messina, M. S.; Graefe, C. T.; Chong, P.; Ebrahim, O. M.; Pathuri, R. S.; Bernier, N. A.; Mills, H. A.; Rheingold, A. L.; Frontiera, R. R.; Maynard, H. D. Carborane RAFT agents as tunable and functional molecular probes for polymer materials. *Polym. Chem.* **2019,** *10*, 1660-1667

(116) Robin, M. P.; Jones, M. W.; Haddleton, D. M.; O'Reilly, R. K. Dibromomaleimide end functional polymers by raft polymerization without the need of protecting groups. *ACS Macro Lett.* **2011,** *1*, 222-226.

(117) Liu, J.; Bulmus, V.; Herlambang, D. L.; Barner-Kowollik, C.; Stenzel, M. H.; Davis, T. P. In situ formation of protein–polymer conjugates through reversible addition fragmentation chain transfer polymerization. *Angew. Chem., Int. Ed.* **2007,** *46*, 3099-3103.

(118) De, P.; Li, M.; Gondi, S. R.; Sumerlin, B. S. Temperature-regulated activity of responsive polymer− protein conjugates prepared by grafting-from via RAFT polymerization. *J. Am. Chem. Soc.* **2008,** *130*, 11288-11289.

(119) Boyer, C.; Bulmus, V.; Liu, J.; Davis, T. P.; Stenzel, M. H.; Barner-Kowollik, C. Well-defined protein− polymer conjugates via in situ RAFT polymerization. *J. Am. Chem. Soc.* **2007,** *129*, 7145-7154.

(120) Liu, J.; Liu, H.; Bulmus, V.; Tao, L.; Boyer, C.; Davis, T. P. A simple methodology for the synthesis of heterotelechelic protein–polymer–biomolecule conjugates. *J. Polym. Sci., Part A: Polym. Chem.* **2010,** *48*, 1399-1405.

(121) Li, M.; Li, H.; De, P.; Sumerlin, B. S. Thermoresponsive Block Copolymer–Protein Conjugates Prepared by Grafting-from via RAFT Polymerization. *Macromol. Rapid Commun.* **2011,** *32*, 354-359.

(122) Li, H.; Li, M.; Yu, X.; Bapat, A. P.; Sumerlin, B. S. Block copolymer conjugates prepared by sequentially grafting from proteins via RAFT. *Polym. Chem.* **2011,** *2*, 1531-1535.

(123) Lucius, M.; Falatach, R.; McGlone, C.; Makaroff, K.; Danielson, A.; Williams, C.; Nix, J. C.; Konkolewicz, D.; Page, R. C.; Berberich, J. A. Investigating the impact of polymer functional groups on the stability and activity of lysozyme–polymer conjugates. *Biomacromolecules* **2016,** *17*, 1123-1134.

(124) Li, X.; Wang, L.; Chen, G.; Haddleton, D. M.; Chen, H. Visible light induced fast synthesis of protein–polymer conjugates: controllable polymerization and protein activity. *Chem. Comm.* **2014,** *50*, 6506-6508.

(125) Xu, J.; Jung, K.; Corrigan, N. A.; Boyer, C. Aqueous photoinduced living/controlled polymerization: tailoring for bioconjugation. *Chem. Sci.* **2014,** *5*, 3568-3575.

(126) Tucker, B. S.; Coughlin, M. L.; Figg, C. A.; Sumerlin, B. S. Grafting-from proteins using metal-free PET–RAFT polymerizations under mild visible-light irradiation. *ACS Macro Lett.* **2017,** *6*, 452-457.

(127) Fakhrullin, R. F.; Zamaleeva, A. I.; Minullina, R. T.; Konnova, S. A.; Paunov, V. N. Cyborg cells: functionalisation of living cells with polymers and nanomaterials. *Chem. Soc. Rev.* **2012,** *41*, 4189-4206.

(128) Niu, J.; Lunn, D. J.; Pusuluri, A.; Yoo, J. I.; O'Malley, M. A.; Mitragotri, S.; Soh, H. T.; Hawker, C. J. Engineering live cell surfaces with functional polymers via cytocompatible controlled radical polymerization. *Nat. Chem.* **2017,** *9*, 537–545.

(129) Ten Cate, M. G.; Rettig, H.; Bernhardt, K.; Börner, H. G. Sequence-Defined Polypeptide− Polymer Conjugates Utilizing Reversible Addition Fragmentation Transfer Radical Polymerization. *Macromolecules* **2005,** *38*, 10643-10649.

(130) Hentschel, J.; Bleek, K.; Ernst, O.; Lutz, J.-F.; Börner, H. G. Easy access to bioactive peptide− polymer conjugates via RAFT. *Macromolecules* **2008,** *41*, 1073-1075.

(131) Zhao, Y.; Perrier, S. Synthesis of well-defined conjugated copolymers by RAFT polymerization using cysteine and glutathione-based chain transfer agents. *Chem. Comm.* **2007**, 4294-4296.

(132) ten Cate, M. G.; Börner, H. G. Synthesis of ABC-Triblock Peptide-Polymer Conjugates for the Positioning of Peptide Segments within Block Copolymer Aggregates. *Macromol. Chem. Phys.* **2007,** *208*, 1437-1446.

(133) Chen, C.; Kong, F.; Wei, X.; Thang, S. H. Syntheses and effectiveness of functional peptide-based RAFT agents. *Chem. Comm.* **2017,** *53*, 10776-10779.

(134) Moorthy, J. N.; Singhal, N. Facile and highly selective conversion of nitriles to amides via indirect acid-catalyzed hydration using TFA or AcOH− H2SO4. *J. Org. Chem.* **2005,** *70*, 1926-1929.

(135) Fuchs, A. V.; Thurecht, K. J. Stability of trithiocarbonate RAFT agents containing both a cyano and a carboxylic acid functional group. *ACS Macro Lett.* **2017,** *6*, 287-291.

(136) He, P.; Zheng, W.; Tucker, E. Z.; Gorman, C. B.; He, L. Reversible addition− fragmentation chain transfer polymerization in DNA biosensing. *Anal. Chem.* **2008,** *80*, 3633-3639.

(137) He, P.; He, L. Synthesis of Surface-Anchored DNA− Polymer Bioconjugates Using Reversible Addition− Fragmentation Chain Transfer Polymerization. *Biomacromolecules* **2009,** *10*, 1804-1809.

(138) Hu, Q.; Han, D.; Gan, S.; Bao, Y.; Niu, L. Surface-initiated-reversible-addition–fragmentation-chain-transfer polymerization for electrochemical DNA biosensing. *Anal. Chem.* **2018,** *90*, 12207-12213.

(139) Hu, Q.; Kong, J.; Han, D.; Niu, L.; Zhang, X. Electrochemical DNA Biosensing via Electrochemically Controlled Reversible Addition–Fragmentation Chain Transfer Polymerization. *ACS Sens.* **2019,** *4*, 235-241.

(140) Robinson, K.; Khan, M.; de Paz Banez, M.; Wang, X.; Armes, S. Controlled polymerization of 2-hydroxyethyl methacrylate by ATRP at ambient temperature. *Macromolecules* **2001,** *34*, 3155-3158.

(141) Eleuterio, H. Olefin metathesis: chance favors those minds that are best prepared. *J. Mol. Catal.* **1991,** *65*, 55-61.

(142) Le, T.; Moad, G.; Rizzardo, E.; Thang, S. In *PCT Int. Appl. WO 9801478 A1 980115*, Chem. Abstr, 1998; p 115390.

(143) Hilf, S.; Kilbinger, A. F. Functional end groups for polymers prepared using ring-opening metathesis polymerization. *Nat. Chem.* **2009,** *1*, 537–546.

(144) Schrock, R. R. Living ring-opening metathesis polymerization catalyzed by well-characterized transition-metal alkylidene complexes. *Acc. Chem. Res.* **1990,** *23*, 158-165.

(145) Lynn, D. M.; Mohr, B.; Grubbs, R. H. Living ring-opening metathesis polymerization in water. *J. Am. Chem. Soc.* **1998,** *120*, 1627-1628.

(146) Lynn, D. M.; Kanaoka, S.; Grubbs, R. H. Living ring-opening metathesis polymerization in aqueous media catalyzed by well-defined ruthenium carbene complexes. *J. Am. Chem. Soc.* **1996,** *118*, 784-790.

(147) Strong, L. E.; Kiessling, L. L. A general synthetic route to defined, biologically active multivalent arrays. *J. Am. Chem. Soc.* **1999,** *121*, 6193-6196.

(148) Kanai, M.; Mortell, K. H.; Kiessling, L. L. Varying the size of multivalent ligands: the dependence of concanavalin A binding on neoglycopolymer length. *J. Am. Chem. Soc.* **1997,** *119*, 9931-9932.

(149) Frenzel, U.; Nuyken, O. Ruthenium-based metathesis initiators: Development and use in ring-opening metathesis polymerization. *J. Polym. Sci., Part A: Polym. Chem.* **2002,** *40*, 2895-2916.

(150) Jean-Louis Hérisson, P.; Chauvin, Y. Catalyse de transformation des oléfines par les complexes du tungstène. II. Télomérisation des oléfines cycliques en présence d'oléfines acycliques. *Makromol. Chem.* **1971,** *141*, 161-176.

(151) Isarov, S. A.; Pokorski, J. K. Protein ROMP: Aqueous graft-from ring-opening metathesis polymerization. *ACS Macro Lett.* **2015,** *4*, 969-973.

(152) Breitenkamp, K.; Emrick, T. Amphiphilic ruthenium benzylidene metathesis catalyst with PEG-substituted pyridine ligands. *J. Polym. Sci., Part A: Polym. Chem.* **2005,** *43*, 5715-5721.

(153) Isarov, S. A.; Lee, P. W.; Pokorski, J. K. "Graft-to" Protein/Polymer Conjugates Using Polynorbornene Block Copolymers. *Biomacromolecules* **2016,** *17*, 641-648.

(154) Chen, B.; Metera, K.; Sleiman, H. F. Biotin-terminated ruthenium bipyridine ring-opening metathesis polymerization copolymers: Synthesis and self-assembly with streptavidin. *Macromolecules* **2005,** *38*, 1084-1090.

(155) Carrillo, A.; Gujraty, K. V.; Rai, P. R.; Kane, R. S. Design of water-soluble, thiol-reactive polymers of controlled molecular weight: a novel multivalent scaffold. *Nanotechnology* **2005,** *16*, S416.

(156) Johnson, J. A.; Lu, Y. Y.; Burts, A. O.; Xia, Y.; Durrell, A. C.; Tirrell, D. A.; Grubbs, R. H. Drug-Loaded, Bivalent-Bottle-Brush Polymers by Graft-through ROMP. *Macromolecules* **2010,** *43*, 10326-10335.

(157) Burts, A. O.; Gao, A. X.; Johnson, J. A. Brush-First Synthesis of Core-Photodegradable Miktoarm Star Polymers via ROMP: Towards Photoresponsive Self-Assemblies. *Macromol. Rapid Commun.* **2014,** *35*, 168-173.

(158) Gao, A. X.; Liao, L.; Johnson, J. A. Synthesis of Acid-Labile PEG and PEG-Doxorubicin-Conjugate Nanoparticles via Brush-First ROMP. *ACS Macro Lett.* **2014,** *3*, 854-857.

(159) Johnson, J. A.; Lu, Y. Y.; Burts, A. O.; Lim, Y.-H.; Finn, M. G.; Koberstein, J. T.; Turro, N. J.; Tirrell, D. A.; Grubbs, R. H. Core-Clickable PEG-Branch-Azide Bivalent-Bottle-Brush Polymers by ROMP: Grafting-Through and Clicking-To. *J. Am. Chem. Soc.* **2011,** *133*, 559-566.

(160) Clark, T. D.; Ghadiri, M. R. Supramolecular design by covalent capture. Design of a peptide cylinder via hydrogen-bond-promoted intermolecular olefin metathesis. *J. Am. Chem. Soc.* **1995,** *117*, 12364-12365.

(161) Miller, S. J.; Grubbs, R. H. Synthesis of conformationally restricted amino acids and peptides employing olefin metathesis. *J. Am. Chem. Soc.* **1995,** *117*, 5855-5856.

(162) Miller, S. J.; Blackwell, H. E.; Grubbs, R. H. Application of ring-closing metathesis to the synthesis of rigidified amino acids and peptides. *J. Am. Chem. Soc.* **1996,** *118*, 9606-9614.

(163) Maynard, H. D.; Grubbs, R. H. Synthesis of Functionalized Polyethers by Ring-Opening Metathesis Polymerization of Unsaturated Crown Ethers. *Macromolecules* **1999,** *32*, 6917-6924.

(164) Coles, M. P.; Gibson, V. C.; Mazzariol, L.; North, M.; Teasdale, W. G.; Williams, C. M.; Zamuner, D. Amino acid derived homochiral polymers via ring-opening metathesis polymerisation. *J. Chem. Soc., Chem. Commun.* **1994**, 2505-2506.

(165) Biagnini, S. C. G.; Coles, M. P.; Gibson, V. C.; Giles, M. R.; Marshall, E. L.; North, M. Living ring-opening metathesis polymerisation of amino ester functionalised norbornenes. *Polymer* **1998,** *39*, 1007-1014.

(166) C. G. Biagini, S.; Gareth Davies, R.; North, M.; C. Gibson, V.; R. Giles, M.; L. Marshall, E.; A. Robson, D. The synthesis and ring-opening metathesis polymerization of peptide functionalized norbornenes. *Chem. Comm.* **1999**, 235-236.

(167) Maynard, H. D.; Okada, S. Y.; Grubbs, R. H. Synthesis of Norbornenyl Polymers with Bioactive Oligopeptides by Ring-Opening Metathesis Polymerization. *Macromolecules* **2000,** *33*, 6239-6248.

(168) Maynard, H. D.; Okada, S. Y.; Grubbs, R. H. Inhibition of Cell Adhesion to Fibronectin by Oligopeptide-Substituted Polynorbornenes. *J. Am. Chem. Soc.* **2001,** *123*, 1275-1279.

(169) Breitenkamp, R. B.; Ou, Z.; Breitenkamp, K.; Muthukumar, M.; Emrick, T. Synthesis and Characterization of Polyolefin-graft-oligopeptide Polyelectrolytes. *Macromolecules* **2007,** *40*, 7617-7624.

(170) Conrad, R. M.; Grubbs, R. H. Tunable, Temperature-Responsive Polynorbornenes with Side Chains Based on an Elastin Peptide Sequence. *Angew. Chem., Int. Ed.* **2009,** *48*, 8328-8330.

(171) Hahn, M. E.; Randolph, L. M.; Adamiak, L.; Thompson, M. P.; Gianneschi, N. C. Polymerization of a peptide-based enzyme substrate. *Chem. Comm.* **2013,** *49*, 2873-2875.

(172) Kammeyer, J. K.; Blum, A. P.; Adamiak, L.; Hahn, M. E.; Gianneschi, N. C. Polymerization of protecting-group-free peptides via ROMP. *Polym. Chem.* **2013,** *4*, 3929-3933.

(173) Blum, A. P.; Kammeyer, J. K.; Gianneschi, N. C. Activating peptides for cellular uptake via polymerization into high density brushes. *Chem. Sci.* **2016,** *7*, 989-994.

(174) Blum, A. P.; Kammeyer, J. K.; Yin, J.; Crystal, D. T.; Rush, A. M.; Gilson, M. K.; Gianneschi, N. C. Peptides displayed as high density brush polymers resist proteolysis and retain bioactivity. *J. Am. Chem. Soc.* **2014,** *136*, 15422-15437.

(175) Adamiak, L.; Touve, M. A.; LeGuyader, C. L.; Gianneschi, N. C. Peptide brush polymers and nanoparticles with enzyme-regulated structure and charge for inducing or evading macrophage cell uptake. *ACS Nano* **2017,** *11*, 9877-9888.

(176) Proetto, M. T.; Callmann, C. E.; Cliff, J.; Szymanski, C. J.; Hu, D.; Howell, S. B.; Evans, J. E.; Orr, G.; Gianneschi, N. C. Tumor Retention of Enzyme-Responsive Pt (II) Drug-Loaded Nanoparticles Imaged by Nanoscale Secondary Ion Mass Spectrometry and Fluorescence Microscopy. *ACS Cent. Sci.* **2018,** *4*, 1477-1484.

(177) Wright, D. B.; Touve, M. A.; Adamiak, L.; Gianneschi, N. C. ROMPISA: Ring-Opening Metathesis Polymerization-Induced Self-Assembly. *ACS Macro Lett.* **2017,** *6*, 925-929.

(178) Wright, D. B.; Thompson, M. P.; Touve, M. A.; Carlini, A. S.; Gianneschi, N. C. Enzyme-Responsive Polymer Nanoparticles via Ring-Opening Metathesis Polymerization-Induced Self-Assembly. *Macromol. Rapid Commun.* **2019,** *40*, 1800467.

(179) C. Gibson, V.; L. Marshall, E.; North, M.; A. Robson, D.; J. Williams, P. Thymine functionalised polymers via living ring-opening metathesis polymerisation. *Chem. Comm.* **1997**, 1095-1096.

(180) Davies, R. G.; Gibson, V. C.; Hursthouse, M. B.; Light, M. E.; Marshall, E. L.; North, M.; Robson, D. A.; Thompson, I.; White, A. J.; Williams, D. J. Synthesis of nucleic-acid base containing norbornene derivatives as monomers for ring-opening-metathesis–polymerization. *J. Chem. Soc., Perkin Trans. 1* **2001**, 3365-3381.

(181) Bazzi, H. S.; Sleiman, H. F. Adenine-Containing Block Copolymers via Ring-Opening Metathesis Polymerization: Synthesis and Self-Assembly into Rod Morphologies. *Macromolecules* **2002,** *35*, 9617-9620.

(182) Burd, C.; Weck, M. Self-sorting in polymers. *Macromolecules* **2005,** *38*, 7225-7230.

(183) South, C. R.; Weck, M. Template-Enhanced Ring-Opening Metathesis Polymerization. *Macromolecules* **2007,** *40*, 1386-1394.

(184) Liu, K.; Zheng, L.; Liu, Q.; de Vries, J. W.; Gerasimov, J. Y.; Herrmann, A. Nucleic acid chemistry in the organic phase: from functionalized oligonucleotides to DNA side chain polymers. *Journal of the American Chemical Society* **2014,** *136*, 14255-14262.

(185) James, C. R.; Rush, A. M.; Insley, T.; Vuković, L.; Adamiak, L.; Král, P.; Gianneschi, N. C. Poly(oligonucleotide). *J. Am. Chem. Soc.* **2014,** *136*, 11216-11219.

(186) Seki, Y.; Ishiyama, T.; Sasaki, D.; Abe, J.; Sohma, Y.; Oisaki, K.; Kanai, M. Transition metal-free tryptophan-selective bioconjugation of proteins. *J. Am. Chem. Soc.* **2016,** *138*, 10798-10801.

(187) Alvarez-Dorta, D.; Thobie-Gautier, C.; Croyal, M.; Bouzelha, M.; Mével, M.; Deniaud, D.; Boujtita, M.; Gouin, S. G. Electrochemically Promoted Tyrosine-Click-Chemistry for Protein Labeling. *J. Am. Chem. Soc.* **2018,** *140*, 17120-17126.

(188) Ban, H.; Gavrilyuk, J.; Barbas III, C. F. Tyrosine bioconjugation through aqueous ene-type reactions: a click-like reaction for tyrosine. *J. Am. Chem. Soc.* **2010,** *132*, 1523-1525.

(189) Rosen, C. B.; Francis, M. B. Targeting the N terminus for site-selective protein modification. *Nat. Chem. Biol.* **2017,** *13*, 697-705.

(190) Ohata, J.; Martin, S. C.; Ball, Z. T. Metal-Mediated Functionalization of Natural Peptides and Proteins: Panning for Bioconjugation Gold. *Angew. Chem., Int. Ed.* **2018**.

(191) Taylor, M. T.; Nelson, J. E.; Suero, M. G.; Gaunt, M. J. A protein functionalization platform based on selective reactions at methionine residues. *Nature* **2018,** *562*, 563.

(192) Christian, A. H.; Jia, S.; Cao, W.; Zhang, P.; Meza, A. T.; Sigman, M. S.; Chang, C. J.; Toste, F. D. A Physical Organic Approach to Tuning Reagents for Selective and Stable Methionine Bioconjugation. *J. Am. Chem. Soc.* **2019,** *141*, 12657–12662.

(193) Chen, X.; Ye, F.; Luo, X.; Liu, X.; Zhao, J.; Wang, S.; Zhou, Q.; Chen, G.; Wang, P. Histidine-Specific Peptide Modification via Visible-Light-Promoted CH Alkylation. *J. Am. Chem. Soc.* **2019,** *141*, 18230–18237.

(194) Ogawa, K. A.; Goetz, A. E.; Boydston, A. J. Metal-free ring-opening metathesis polymerization. *J. Am. Chem. Soc.* **2015,** *137*, 1400-1403.

(195) Xu, J.; Shanmugam, S.; Duong, H. T.; Boyer, C. Organo-photocatalysts for photoinduced electron transfer-reversible addition–fragmentation chain transfer (PET-RAFT) polymerization. *Polym. Chem.* **2015,** *6*, 5615-5624.

(196) Theriot, J. C.; Lim, C.-H.; Yang, H.; Ryan, M. D.; Musgrave, C. B.; Miyake, G. M. Organocatalyzed atom transfer radical polymerization driven by visible light. *Science* **2016,** *352*, 1082-1086.

(197) McCarthy, B. G.; Pearson, R. M.; Lim, C.-H.; Sartor, S. M.; Damrauer, N. H.; Miyake, G. M. Structure–property relationships for tailoring phenoxazines as reducing photoredox catalysts. *J. Am. Chem. Soc.* **2018,** *140*, 5088-5101.

(198) Gormley, A. J.; Yeow, J.; Ng, G.; Conway, Ó.; Boyer, C.; Chapman, R. An Oxygen-Tolerant PET-RAFT Polymerization for Screening Structure–Activity Relationships. *Angew. Chem., Int. Ed.* **2018,** *57*, 1557-1562.

(199) Shanmugam, S.; Xu, J.; Boyer, C. Aqueous RAFT photopolymerization with oxygen tolerance. *Macromolecules* **2016,** *49*, 9345-9357.

(200) Enciso, A. E.; Fu, L.; Russell, A. J.; Matyjaszewski, K. A Breathing Atom-Transfer Radical Polymerization: Fully Oxygen-Tolerant Polymerization Inspired by Aerobic Respiration of Cells. *Angew. Chem., Int. Ed.* **2018,** *57*, 933-936.

Chapter 2. Solution Stability of Insulin is Improved by Addition or Conjugation of Trehalose Glycopolymer

This chapter contains portions of an edited version of the following published paper reprinted with permission from: Liu, Y.;† Lee, J.;† Mansfield, K.M.; Ko, J.H.; Sallam, S.; Wesdemiotis, C.; Maynard, H.D. "Trehalose Glycopolymer Enhances Both Solution Stability and Pharmacokinetics of a Therapeutic Protein." *Bioconjugate Chem.* **2017**, *28*, 836-845. (†Equal contribution).

2.1 Introduction

Diabetes mellitus affects 29.1 million people in the United States alone and estimates for the incidence of diabetes continue to rise.[1-2] The disease leads to a higher risk of secondary conditions including kidney disease, heart disease, stroke, blindness, and the need for amputations.[2] Diabetes is a high management disease and type I diabetes requires the use of insulin replacement therapy with 3-4 injections per day of the therapeutic protein. However, insulin must be refrigerated while stored and it has been shown to degrade under conditions observed during storage and transportation such as heat and mechanical agitation.[3-4] Patients with diabetes must make special considerations for activities and routines to take the required insulin injections while avoiding conditions that would cause the protein to degrade.

However, if insulin degrades from exposure to deleterious environmental conditions, it must be discarded. Decreasing the frequency of insulin disposal due to protein degradation could save an estimated $1 billion dollars in the US.[5] More importantly, degradation can lead to patients taking less than their required dose or immune responses to degradation products, which poses a risk to patient safety and may even lead to life threatening situations. Improved stability could prevent these incidents. In addition to improving safety, enhanced stability would decrease dependence on the cold chain and associated costs required during transportation and storage of protein therapeutics such as inulin.

Patient compliance could potentially be improved by more convenient storage requirements. Strategies to stabilize insulin have been reported in the literature using alteration of the amino acid sequence,[6] addition of small molecule excipients,[7-9] and delivery in liposomes or polymer nanoparticles.[10-13] Additionally, several insulin analogs are available clinically with

alterations in the time of onset for tighter control of blood glucose.[14-15] However, diabetes prevalence continues to grow and the disease remains challenging to manage.[1-2, 16] Thus, further investigation into improving the ease of storage and use of insulin to maintain glucose homeostasis is imperative.

In this chapter, we demonstrate that the trehalose polymer can stabilize a protein therapeutic at elevated temperature and under mechanical stress and pharmacokinetics can be altered based on whether or not the trehalose glycopolymer is conjugated to the protein. Insulin was chosen as a model protein because of its importance in clinical usage and established structure and bioactivity assays.[17]

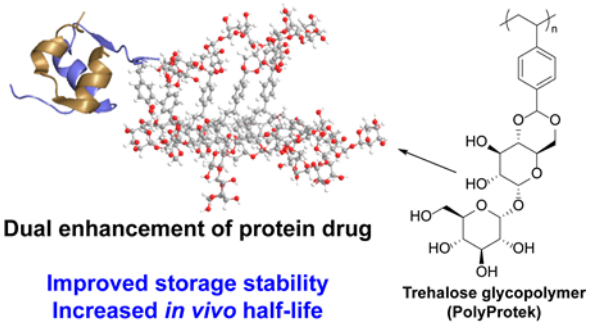

Figure 2-1. Insulin-trehalose glycopolymer conjugate where the polymer improves both the storage stability and in vivo plasma half-life (protein structure from the Protein Data Bank 4INS). Figure reprinted with permission from the previously published report.[18]

2.2 Results

Insulin loses its potency when stored at room temperature, thus storage at 2-8 °C is reccomended.[19-21] The protein is also prone to aggregation during mechanical agitation associated with transportation.[22] Aggregation of insulin exposed to these stressors decreases the activity and

poses a risk of diabetic ketoacidosis and other complications for patients.[20] Thus, we examined whether or not the trehalose glycopolymer with a polystyrene backbone and acetal-linked trehalose (TreSA) could stabilize insulin to thermal and mechanical stress. In our initial tests we added the polymer as an excipient (**Figure 2-1**). An accelerated thermal stability study of insulin was carried out by comparing insulin heated with and without the TreSA for 30 min. High performance liquid chromatography (HPLC) was employed to evaluate the percent of intact insulin because this technique is established as a way to quantify and distinguish intact insulin from its degradation products caused by aggregation.[19] HPLC analysis of the stressed insulin showed that while insulin significantly degraded after heating or agitation, adding 2 mol equiv of the TreSA stabilized the protein to a much greater extent (**Figure 2-2 a**). Though the addition of 2 mol equiv of PEG during heating extended the initial time to denaturation of insulin, the insulin in the presence of PEG eventually degraded to the same extent as the insulin alone at 30 min. Dynamic light scattering (DLS) was employed to study whether or not the trehalose glycopolymer prevented aggregation of insulin. The analysis showed that before stress, the diameter of insulin alone was 4 ± 1 nm and with TreSA was 7 ± 1 nm. After heating, the diameter increased to 1291 ± 189 nm for the insulin sample, while it remained at 6 ± 2 nm when the trehalose glycopolymer was present (**Figure 2-2 b**). The mechanical stress stability study was carried out by agitation at 250 rpm and 37 °C for 3 h. Both the HPLC and DLS analyses showed that TreSA as an excipient (2 mol equiv) completely prevented aggregation of the protein (**Figure 2-2 c** and **d**). Interestingly, the addition of PEG resulted in destabilization of insulin during agitation (**Figure 2-2 c**). This may be due to the hydrophobic interactions of PEG with exposed hydrophobic residues of insulin, which has been previously reported for PEG with other proteins.[23-24] These results demonstrated that the trehalose glycopolymer effectively prevents insulin aggregation induced by both heat and mechanical stress,

which are major mechanisms of insulin degradation.[9, 25] The data further suggested that the polymer was a good candidate for conjugation to insulin.

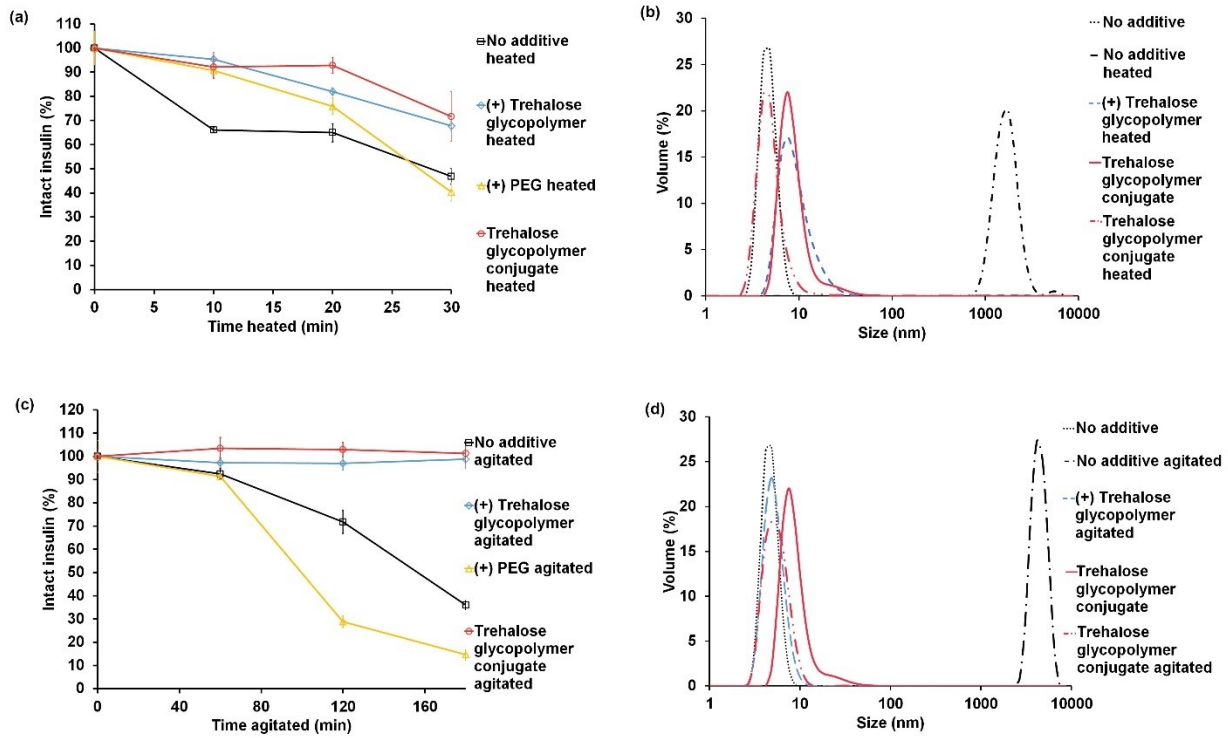

Figure 2-2. In vitro stabilization of insulin (0.5 mg/mL) by trehalose glycopolymer. (a) HPLC AUC (area under the curve) of insulin peak during heating (90 °C), n = 3. (b) Insulin aggregation upon heating (90 °C, 30 min) measured by DLS (n = 3, representative image shown). (c) HPLC AUC of insulin peak during agitation (250 rpm, 37 °C), n = 3. (d) Insulin aggregation upon agitation (250 rpm, 37 °C, 3 h) measured by DLS (n = 3, representative image shown).

Insulin stability with a methacrylate backbone trehalose polymer (TreMA) excipient was also explored. Closer examination of the analytical HPLC traces after the heating assay revealed more information about the mechanism of insulin stabilization by the trehalose polymer. After heating to 90 °C for 30 min, the area under the curve of the intact insulin peak decreased

dramatically (**Figure 2-3 a**). Two additional peaks also appeared in the HPLC trace, corresponding to aspartyl derivatives that are products of deamidation consistent with the literature.[26] In the presence of trehalose polymer as excipient, a significantly greater amount of intact insulin remains. Additionally, the aspartyl derivative peaks are less intense than for no additive. These results indicate that the polymer inhibits insulin degradation by deamidation and aggregation.

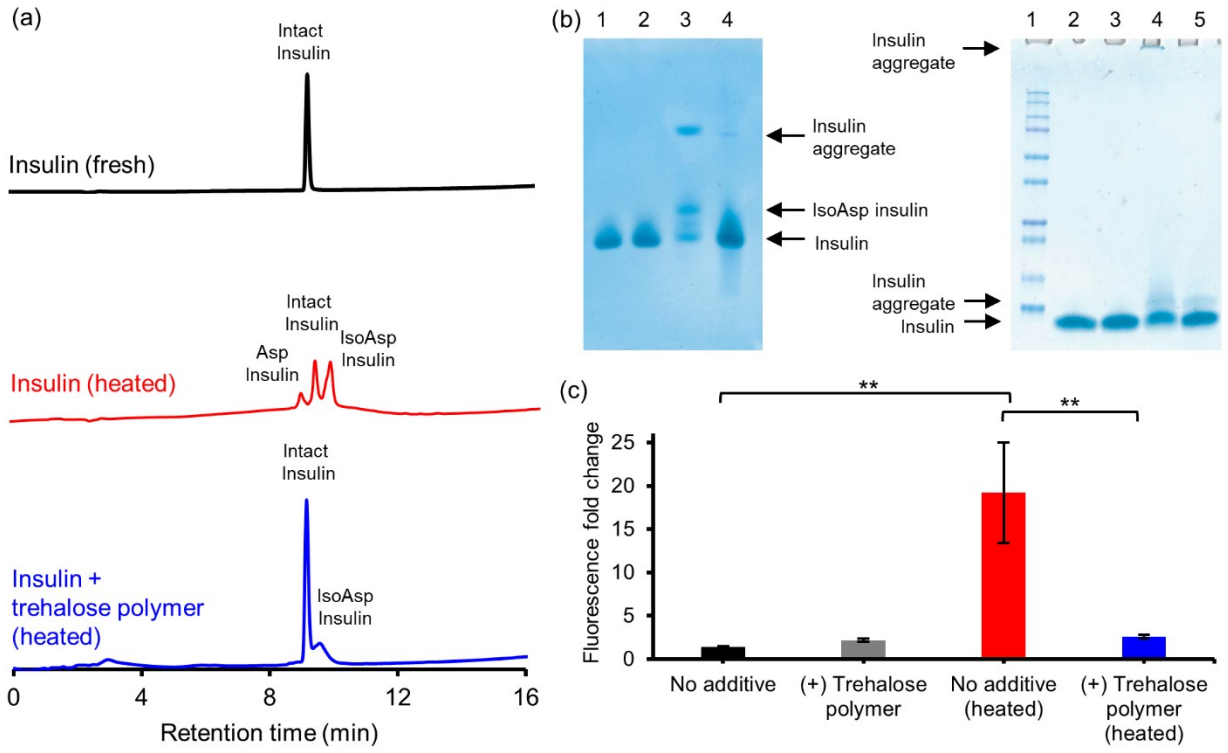

Figure 2-3. In vitro characterization of insulin stabilization by trehalose polymer. (a) Analytical HPLC traces comparing insulin before and after heating (90 °C, 30 min) with or without 2 mol equiv trehalose polymer and (b) Native (lane 1: fresh insulin, lane 2: fresh insulin + 2 mol. equiv trehalose polymer, lane 3: insulin heated 90 °C, 30 min, lane 4: insulin + 2 mol equiv trehalose polymer heated 90 °C, 30 min) and SDS PAGE (lane 1: ladder, lane 2, fresh insulin, lane 3: fresh insulin + 2 mol. equiv trehalose polymer, lane 4: insulin heated 90 °C, 30 min, lane 5: insulin + 2

mol equiv trehalose polymer heated 90 °C, 30 min) with Coomassie staining, and (c) ThT assay comparing insulin before and after heating (90 °C, 30 min) with or without 2 mol. equiv trehalose polymer (** $p < 0.01$).

The insulin stabilization mechanism was further explored by biochemical assays. Native and SDS PAGE agree with the analytical HPLC results (**Figure 2-3 b**). The presence of the trehalose polymer as an excipient preserved the intensity of the intact insulin band and decreased the intensity of bands corresponding to insulin degradation products (aspartyl derivatives and aggregates). Thioflavin T (ThT) assay was used to assess the effect of trehalose polymer on insulin fibrillation. Without additive, a large fold change in fluorescence was observed from the binding of ThT dye to insulin fibrils (**Figure 2-3 c**). No significant change in fluorescence intensity was observed for insulin heated in the presence of trehalose polymer, indicating that trehalose polymer inhibits fibrillation of insulin during heating.

A trehalose polymer for conjugation to insulin was prepared through reversible addition-fragmentation chain transfer (RAFT) polymerization using an aldehyde-functionalized chain transfer agent (M_n = 9.9 kDa and Đ = 1.10) and subsequently conjugated to the amines of insulin by reductive amination (**Figure 2-4**).[27-28] The trithiocarbonate of the RAFT polymer was not reduced under these reductive amination conditions as demonstrated by UV-vis spectroscopy (Appendix A: **Figure 2-9**). If required, the trithiocarbonate could be removed using standard protocols.[29] Conjugation was confirmed by native gel and Western blot (**Figure 2-5 c** and **d**) and the conjugate was purified via fast protein liquid chromatography (FPLC).

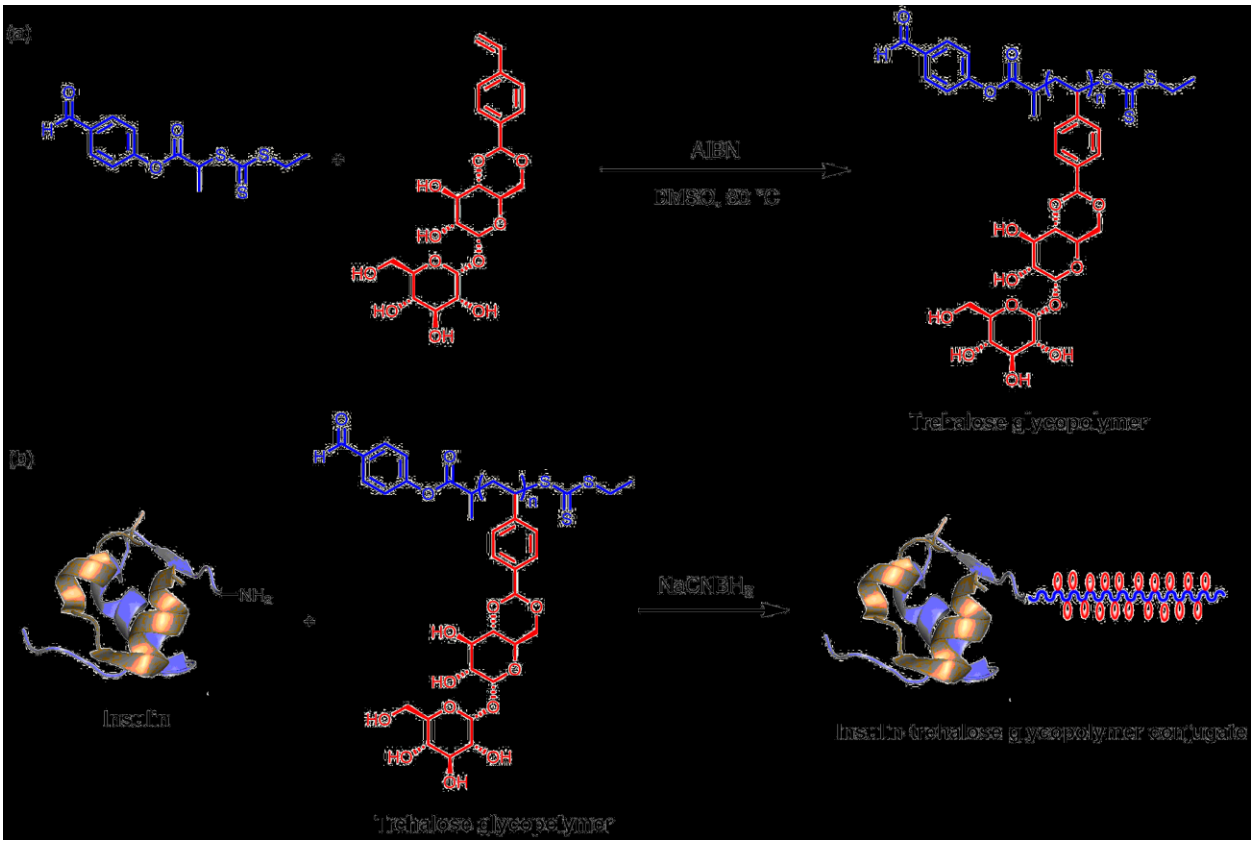

Figure 2-4. Synthesis of insulin-trehalose glycopolymer conjugate. (a) RAFT polymerization and (b) subsequent conjugation of trehalose glycopolymer to insulin (PDB: 4INS) by reductive amination. Revised figure from previously published report.[18]

The conjugates were also characterized by mass spectrometry. We have observed that the trehalose glycopolymer inhibits evaluation by mass spectrometry and prevents protein ionization even when added to samples; thus, a two-step treatment of the sample was necessary for its analysis. First, the trehalose glycopolymer-insulin was treated with formic acid to cleave the polymer chain at the ester leaving a 106 Da linker (corresponding to the 4-hydroxybenzaldehyde moiety) attached to the conjugation site. Second, dithiothreitol (DTT) or *tris*(2-carboxyethyl)phosphine (TCEP) was used to reduce the disulfide bridges of insulin to release chain

A (2382 Da) and chain B (3427 Da) plus the mass of the attached linker. The matrix-assisted laser desorption/ionization time-of-flight (MALDI-TOF) mass spectrum of the conjugate (Appendix A: **Figure 2-10**) shows two species with 106 and 212 Da greater mass than insulin, suggesting the presence of mono- and disubstituted conjugates. Note that trace amount of insulin in the conjugate, although not detectable by Coomassie stain and Western blot, was visible in the spectrum due to very high ionization efficiency of insulin and nonquantitative nature of polymer cleavage from insulin. Nevertheless, the formic acid treatment was sufficient for characterization of the conjugate. Electrospray ionization mass spectrometry (ESI-MS) of the conjugate confirmed the MALDI results (**Figure 2-5 a** and **b**). Both chain A and chain B exhibited a peak that corresponded to modification with a single polymer. These results suggest that the trehalose glycopolymer was conjugated to the N-terminal glycine of chain A (GlyA1) and to N-terminal phenylalanine or lysine of chain B (PheB1 or LysB29). Since the previously reported reactivity of these amines followed the order GlyA1 > LysB29 >> PheB1,[30] we expected LysB29 to be the modification site on the chain B. To confirm this, tandem mass spectrometry experiments were performed on the chain B ion of both native and conjugated insulin (Appendix A: **Figure 2-11**). The spectrum of the conjugate exhibited y_3 + 106 Da (m/z 451.20) ion, which confirmed that the linker was attached to LysB29 adjacent to the C-terminus. This analysis indicates that the trehalose glycopolymer was conjugated to GlyA1 and LysB29, consistent with the literature report that these two amine functionalities are shown to be much more reactive toward conjugation than PheB1.[30] The conjugate was also confirmed by native gel and Western blot (**Figure 2-5 c** and **d**).

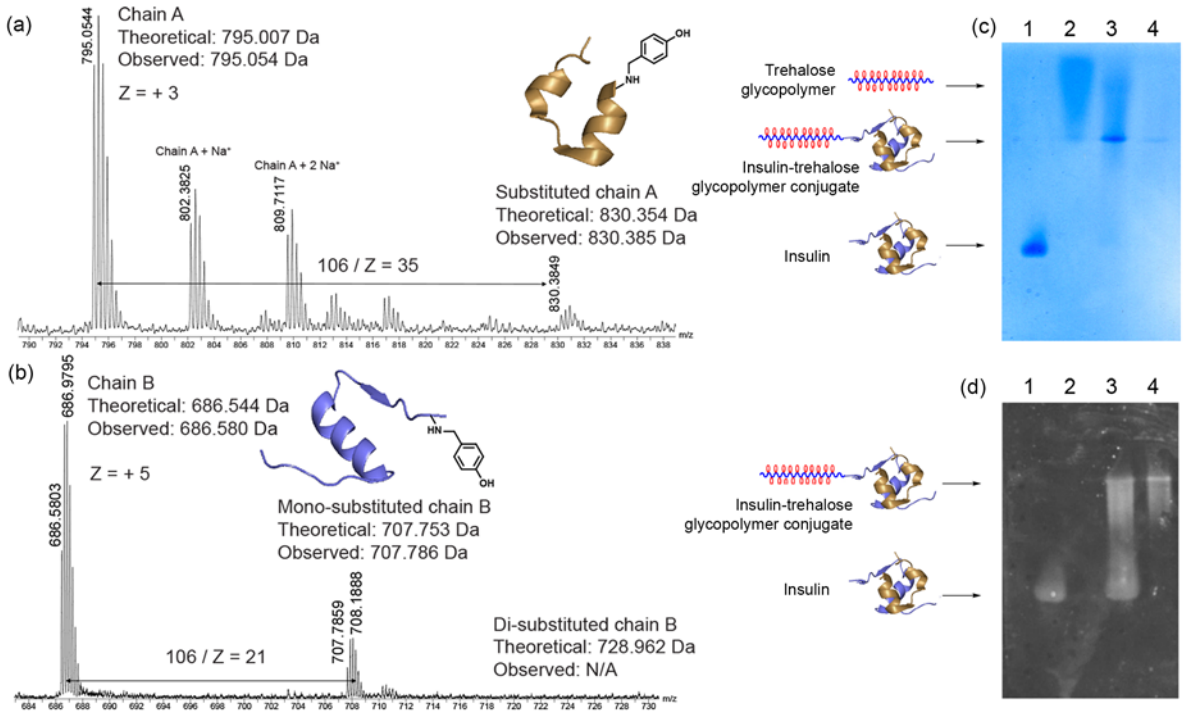

Figure 2-5. Characterization of insulin-trehalose glycopolymer conjugate. ESI-MS spectra of (a) chain A and (b) chain B after acid treatment and disulfide reduction each show modification with a single polymer. Native-PAGE after (c) Coomassie staining and (d) western blot show conjugation of aldehyde-functionalized trehalose glycopolymer to insulin (lane 1: insulin, lane 2: trehalose glycopolymer, lane 3: unpurified insulin-trehalose glycopolymer conjugation mixture, lane 4: purified insulin-trehalose glycopolymer, PDB: 4INS).

Once conjugation was confirmed, the thermal and mechanical stability of the insulin-trehalose glycopolymer was evaluated as described above for the added polymer. In both cases, the conjugated polymer stabilized the protein in its monomeric form as shown by both HPLC and DLS. Further, the results of the conjugate closely resembled that of the excipient data for HPLC, demonstrating that conjugated polymer stabilized insulin as well as excess polymer excipient (**Figure 2-2 a** and **c**). DLS analysis showed that before stress the diameter of the insulin-trehalose

glycopolymer conjugate was 6.4 ± 1.2 nm (**Figure 2-2 b** and **d**). The diameter did not increase after stress like insulin itself (≥1000 nm) and remained low at 4.7 ± 0.7 nm after heating and 6.5 ± 1.3 nm after agitation. Bioactivity was also retained significantly more for excipient and conjugate than no additive after the heating assay, found using insulin tolerance test in mice.[18] Therefore, covalently conjugating two trehalose glycopolymer chains stabilized the monomeric form of insulin as well as adding 2 mol equiv (10 weight equiv) of the polymer as an excipient.

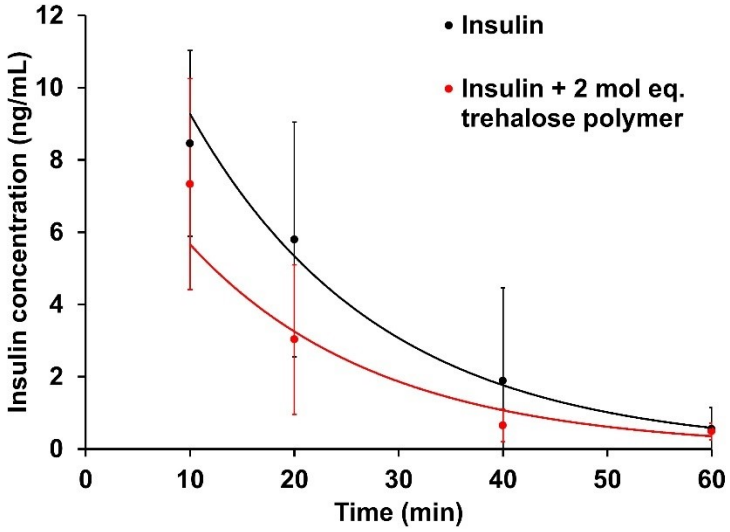

Figure 2-6. Pharmacokinetics of insulin (120 µg/kg dosage) with or without TreMA (2 mol equiv to insulin) as excipient (n = 4, $p > 0.05$ at all timepoints).

Conjugation of the TreSA to insulin enhanced the plasma lifetime of insulin in mice.[18] Influence of TreMA as excipient on pharmacokinetics was tested to determine if presence of the polymer without conjugation could affect the half-life of insulin. CD-1 mice were injected intravenously with 120 µg /kg insulin or insulin with 2 molar equiv TreMA and the amount of

insulin in the blood was measured by ELISA. No significant difference was detected between groups at all timepoints. Additionally, insulin dosage required to detect native insulin in the blood was the same with and without polymer, while previously 7.5x dosage was needed compared to insulin conjugates to detect native insulin in the blood.[18] This data shows that addition of trehalose polymer as excipient does not alter pharmacokinetics.

2.3 Discussion

Our results demonstrate that trehalose glycopolymer is promising for stabilization of the therapeutic protein insulin to prevent aggregation and deamidation. Additionally, conjugation of the trehalose polymer also stabilizes the protein in addition to extending the half-life in vivo. Extending the circulation time is desirable for basal insulin to control blood glucose throughout the day. However, some applications require fast action, like for rapid-acting insulins, so alteration of pharmacokinetics is not desirable. Addition of trehalose polymer excipient improved stability without alteration of protein pharmacokinetics. Prevention of degradation upon exposure to heat and mechanical agitation is also helpful to maintain stability during storage and transportation. Thus, this data demonstrates the utility of trehalose polymer as a means to improve storage stability of therapeutic proteins with or without enhancement of pharmacokinetics. Research of stabilizing formulations for protein therapeutics is important to move away from dependence on the cold chain.

We chose insulin as the model therapeutic protein since insulin instability is clinically relevant and has been reported to cause dangerous emergencies with protein degradation.[20] Work stabilizing insulin using insulin analogs,[6] small-molecule excipients,[7-9] liposomes,[10] and polymeric vehicles[11-13] has been reported, but the high demand and growing prevalence of diabetes

worldwide warrants exploration of new strategies. Our research shows that adding trehalose glycopolymer as an excipient can prevent heat and mechanically induced aggregation and heat induced deamidation. These data suggest trehalose polymer as an excipient for stabilization of proteins should be investigated further.

2.4 Conclusion

This chapter describes research on a trehalose polymer that can enhance the solution stability of insulin upon exposure to heat and mechanical agitation. Addition of trehalose polymer as an excipient or conjugated to the protein decreased the aggregation of insulin. Investigation of the mechanism of the polymer's stabilization of insulin revealed that it inhibits both aggregation and deamidation during heating. Finally, conjugation of the trehalose glycopolymer is needed to alter pharmacokinetics. Addition of trehalose polymer excipient did not alter insulin half-life in vivo, enabling a stabilized rapid-acting insulin. Together, this research demonstrates that the trehalose polymer should be explored for formulation of protein therapeutics because of its ability to enhance aqueous stability.

2.5 Appendix A

Materials

Materials were purchased from Sigma Aldrich or Fisher Scientific without purification unless otherwise noted. Azobis(isobutyronitrile) (AIBN) was recrystallized from acetone. Trehalose was purchased from The Healthy Essential Management Corporation (Houston, TX), azeotropically dried with ethanol, and stored under vacuum before use. Recombinant human insulin was purchased from Sigma Aldrich. Human insulin ELISA kit for quantification of insulin was purchased from Mercodia (Uppsala, Sweden). 2-(Ethyltrithiocarbonate)propionic acid was

synthesized by Jeong Hoon Ko by a previously reported procedure.[31] PEG without end group (20 kDa) was purchased from Sigma-Aldrich. Styrenyl acetal trehalose monomer and trehalose glycopolymer (styrenyl acetal trehalose polymer without end-group synthesized by free radical polymerization, M_n = 29.5 kDa, Đ = 2.11 by GPC) were prepared by Juneyoung Lee using previously reported procedure.[32] Methacrylate trehalose monomer was prepared using a previously reported procedure.[33] Benzaldehyde CTA was prepared by Jeong Hoon Ko as reported previously.[34]

Analytical techniques

Nuclear Magnetic Resonance (NMR) spectra were recorded on a Bruker AV 400 MHz spectrometer. Trehalose monomer was purified by preparatory reverse phase HPLC on a Shimadzu HPLC system equipped with a UV detector using a Luna 5 μm C18 100A column (preparatory: 5 μm, 250 x 21.2 mm) with monitoring at λ = 215 nm and 254 nm. Isocratic solvent system (water:methanol = 50:50) was used as the mobile phase at a flow rate of 20 mL/min. Analytical HPLC for detection of insulin was conducted on an Agilent 1200 HPLC system equipped with an Agilent Quadrupole 6130 ESI-MS detector, using a gradient solvent system (water:acetonitrile = 70:30 to 60:40 + 0.1 % trifluoroacetic acid over 15 min at 1 mL/min). Gel permeation chromatography (GPC) was conducted on a Shimadzu HPLC system equipped with a refractive index detector RID-10A and two Polymer Laboratories PLgel 5 μm mixed D columns (with guard column). Lithium bromide (0.1 M) in N,N-dimethylformamide (DMF) at 40 °C was used as the eluent (flow rate: 0.6 mL/min). Near-monodisperse poly(methyl methacrylate) standards (Polymer Laboratories) were employed for calibration. UV-vis absorbance was measured using a microplate reader ELx800 (BioTek Instruments, Winooski, VT). Matrix-assisted laser desorption/ionization

(MALDI)-MS analysis of insulin was performed on a Voyager DE-STR (Applied Biosystems, Forster City, CA) in linear positive ion mode. For the insulin-trehalose glycopolymer conjugate, a Bruker Ultraflex III MALDI-TOF mass spectrometer was used in reflectron mode. The conjugate was dissolved in water:acetonitrile 1:1 (v/v) to prepare a 10 mg/ml solution, to which 10 % formic acid was added; this solution was then mixed with a solution of either dithiothreitol (DTT) or *tris*(2-carboxyethyl)phosphine (TCEP) for disulfide bond cleavages. 2,5-Dihydroxyacetophenone (DHAP) served as a matrix. For ESI-MS analysis, the insulin-trehalose glycopolymer conjugate was diluted with water:acetonitrile 1:1 (v/v) at a final concentration of 0.025 mg/ml, and the solution was injected into Waters Synapt HDMS quadrupole/time-of-flight (Q/ToF) mass spectrometer (Waters, Milford, MA) after treating it with formic acid and 10 mM DTT. Instrument parameters were adjusted as follows: ESI capillary voltage, 3.5 kV; sample cone voltage, 30 V; extraction cone voltage, 3.2 V; desolvation gas flow, 550 L h^{-1} (N2); trap collision energy (CE), 6.0 eV; transfer CE, 4.0 eV; trap gas flow, 1.5 mL min^{-1} (Ar); sample flow rate, 10 µL min^{-1}; source temperature, 80 °C; desolvation temperature, 150 °C; for tandem mass spectrometry analysis, the trap CE was adjusted to 20 eV to cause fragmentation by collisionally activated dissociation.

RAFT polymerization of trehalose monomer with benzaldehyde CTA

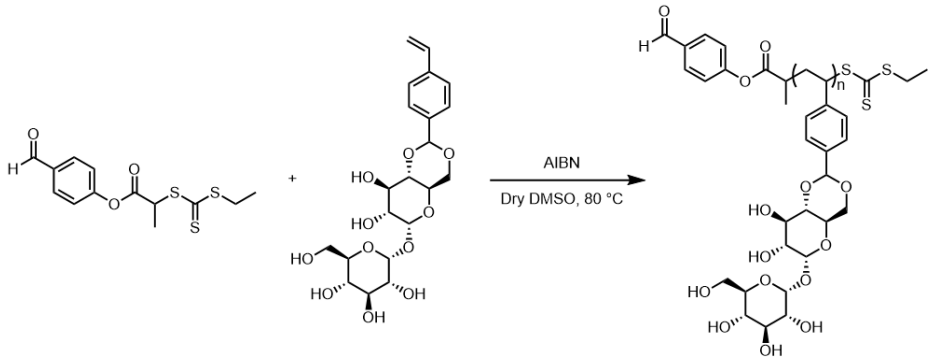

A stock solution of azobisisobutyronitrile (AIBN) was created in DMSO. A portion of the stock (for 0.15 mg AIBN, 0.9 µmol) was added to the benzaldehyde CTA (2.88 mg, 9 µmol). This stock solution was used to dissolve styrenyl acetal trehalose monomer (113.12 mg, 0.247 mmol), and the mixture was transferred to a Schlenk flask. The vial was washed with additional DMSO for total volume of 0.49 mL and then transferred to the Schlenk flask. The mixture was freeze-pump-thawed four times, and then stirred under argon at 80 °C for 3.4 hours. After stopping the polymerization with liquid nitrogen at 80% conversion, the crude was purified by dialysis (MWCO: 3.5 kDa) against water for 2 days and recovered by lyophilization yielding 73 mg product. ^{1}H NMR (400 MHz in D_6DMSO) δ: 9.92, 7.59, 7.15, 6.52, 5.44, 5.17, 4.92, 4.79, 4.37, 4.08, 3.95, 3.75, 3.67, 3.55, 3.46, 3.14, 1.49. M_n = 8.2 kDa (by GPC), Đ = 1.14.

Free radical polymerization of methacrylate trehalose monomer

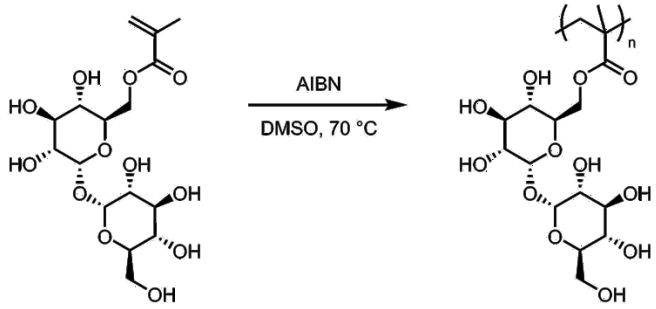

A stock solution of AIBN was created in anhydrous DMSO. A portion of this stock (0.1 mL for 3.4 mg, 0.02 mmol AIBN) was used to dissolve methacrylate trehalose monomer (214.6 mg, 0.52 mmol) and this was added to an dry Schlenk flask. More anhydrous DMSO (total volume 1.9 mL) was added into the Schlenk flask. The mixture was freeze-pump-thawed 3 times before initiation at 70 °C. After 5 hours, the polymerization was stopped at 96% conversion by ^{1}H-NMR. The polymer was purified by purified by dialyzing against H_2O (MWCO 3.5 kDa). ^{1}H NMR (500

MHz in D_6DMSO) δ: 5.91, 5.10, 5.06, 4.24, 4.03, 3.94, 3.75, 3.53, 3.35, 1.83, 1.51, 1.61, 0.96, 0.80. M_n = 19.2 kDa (by GPC), Đ = 4.02.

Preparation of insulin-trehalose glycopolymer conjugate

Insulin (4 mg, 0.259μmol), sodium cyanoborohydride (4 mg, 63.8 μmol), and benzaldehyde end-functionalized styrenyl acetal backbone trehalose polymer (31 mg, 3.1 μmol, 12 molar eq to insulin) were dissolved in 1 mL of 200 mM phosphate buffer, pH 8.0. The mixture was incubated at 4 ºC water bath for 24 h, and the buffer was exchanged to D-PBS pH 7.4, by centriprep ultrafiltration (MWCO 3 kDa) several times before purification by FPLC using anion exchange chromatography. The amount of insulin was determined using ELISA. To determine if the trithiocarbonate could be reduced under these conditions, benzaldehyde end-functionalized trehalose polymer (15.5 mg, 1.5 μmol) was dissolved in 0.5 mL 200 mM phosphate buffer, pH 8.0 with and without sodium cyanoborohydride (2 mg, 31.9 μmol) and incubated at 37 °C 12 h before absorption spectra were obtained.

Styrenyl acetal backbone trehalose polymer stability study

Free insulin, insulin with the styrenyl acetal backbone trehalose glycopolymer or PEG (20 kDa without end-group, 2 mol equiv to insulin), and insulin-trehalose glycopolymer conjugate were incubated at 90 °C in PBS at a concentration of 0.5 mg/mL and total volume of 100 μL. At predetermined time interval, each sample was collected and subjected to further analysis. Free insulin, insulin with the trehalose glycopolymer or PEG (20 kDa without end-group, 2 mol equiv to insulin), and insulin-trehalose glycopolymer conjugate were agitated in PBS at 250 rpm and 37 °C at a concentration of 0.5 mg/mL and total volume of 100 μL in glass vials secured horizontally.

At predetermined time intervals, each sample was collected and subjected to further analysis. For RP-HPLC analysis, each sample was filtered and the concentration of insulin that remained in the sample was determined. Mobile phase consisted of aqueous phase (Solvent A) and organic phase (Solvent B). Solvent A was 0.1% v/v trifluoroacetic acid (TFA) in deionized distilled water and solvent B was acetonitrile. The solvent gradient used was 30% Solvent A to 40% Solvent A in 15 min. The insulin was detected with a UV detector at a wavelength of 215 nm. The measurements of the average size of the aqueous suspensions of insulin formulation were carried out on a Malvern Zetasizer Nano-ZS dynamic light-scattering (DLS) analyzer (Malvern Instruments Ltd., Malvern, Worcestershire, UK).

Pharmacokinetics study

CD-1 mice (5-6 weeks, male, Charles River Laboratories) were used for the pharmacokinetics studies (n = 4). A single dose of insulin (120 μg/kg) with or without methacrylate trehalose polymer (2 mol. eq. to insulin) was administered by injection through the tail vein. Blood samples were taken from the saphenous vein (30-50 μL) at 10, 20, and 40 minutes and by cardiac puncture after euthanasia by inhalation of CO_2 at 60 minutes following administration. Blood was collected using a pipette with ETDA-coated tips into LoBind tubes coated with EDTA. Blood was stored on ice until separation of the plasma by centrifugation (2000 x g, 15 minutes). The amount of insulin in plasma samples was determined by ELISA (Mercodia) according to the manufacturer's protocol.

Methacrylate backbone trehalose polymer stability study

Insulin was dissolved at 2 mg/mL in DPBS pH 7.4. Trehalose polymer (28.1 kDa) was dissolved at 19 mg/mL (2 mol equiv to insulin). Solutions were added 1:1 to a total volume of 100 µL in a LoBind tube for insulin and insulin with trehalose polymer (n = 3). Samples were stored at 4 °C or heated to 90 °C for 30 min. Aliquots of each insulin sample were used directly for SDS and native PAGE. Samples were filtered (0.22 µm) to remove insulin aggregates and analyzed by RP-HPLC. Thioflavin T (ThT) was prepared at 50 µM (0.0159 mg/mL) in 20 mM DPBS pH 7.4. Into a black 96-well plate, 50 µL each insulin sample was pipetted. To these was added 250 µL ThT solution and the plate was incubated at room temperature (21 °C) for 20 min. Fluorescence intensity was measured on a Tecan M1000 plate reader (λ_{ex} = 450 nm, λ_{em} = 482 nm).

Statistical analysis

For assessment of the statistical significance of differences, Student's t-test assuming unequal sample variance was employed. Results were considered significantly different if $p < 0.05$.

Figures and tables

Figure 2-7. ^{1}H NMR spectrum of benzaldehyde end-functionalized styrenyl acetal backbone trehalose polymer from RAFT polymerization (D_6DMSO).

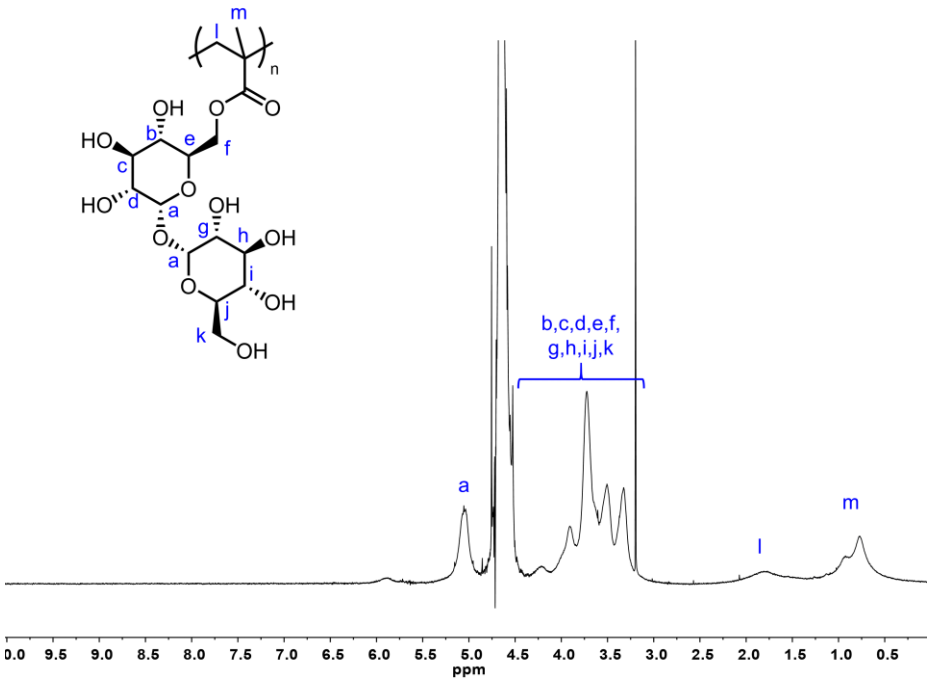

Figure 2-8. ^{1}H-NMR spectrum of methacrylate backbone trehalose polymer from free radical polymerization (DMSO- D_6).

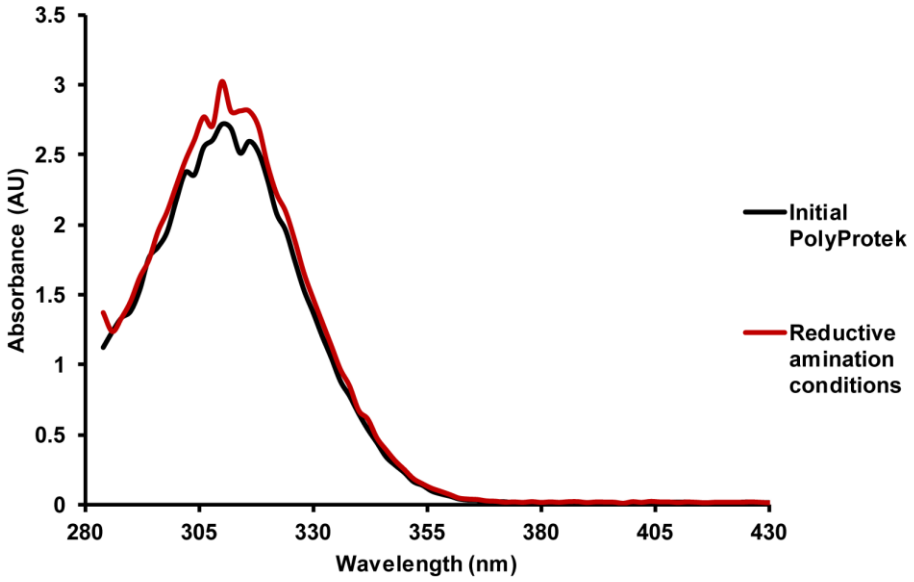

Figure 2-9. UV-vis absorption spectrum of trehalose glycopolymer before (black) and after (red) exposure to reductive amination conditions.

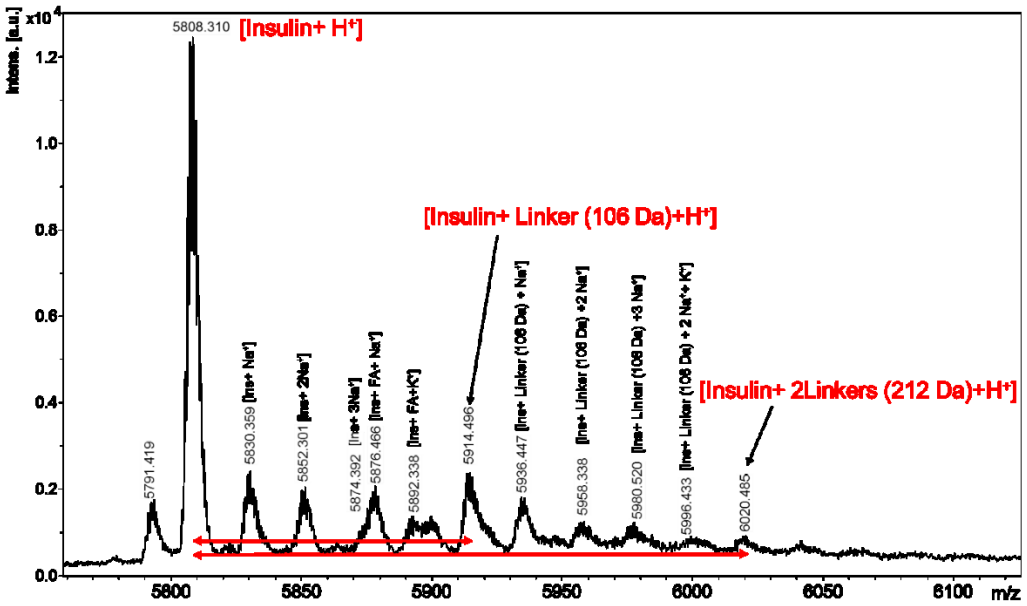

Figure 2-10. MALDI-TOF mass spectrum of insulin-trehalose glycopolymer conjugate after addition of formic acid.

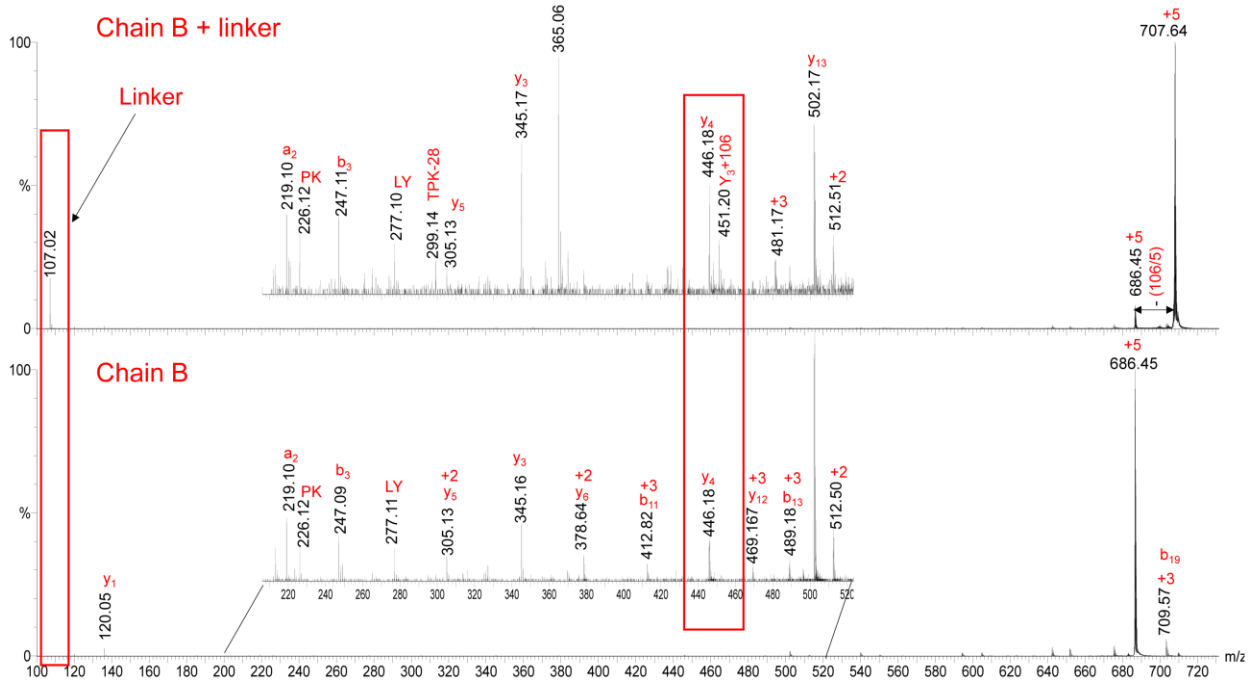

Figure 2-11. Tandem mass spectrum of insulin-trehalose glycopolymer conjugate (top) and native insulin (bottom). Tandem mass spectrometry fragmentation of chain B charge state +5 from the conjugate (m/z 707.64) and insulin (m/z 686.45) mainly gave rise to b_n and y_n ion series fragments.

2.6 References

(1) Guariguata, L.; Whiting, D. R.; Hambleton, I.; Beagly, J.; Linnenkamp, U.; Shaw, J. E. Global estimates of diabetes prevalence for 2013 and projections for 2035. *Diabetes Res. Clin. Pract.* **2014,** *103*, 137-149.

(2) Centers for Disease Control, National diabetes statistics report: estimates of diabetes and its burden in the United States, 2014. In *Atlanta, GA: US Department of Health and Human Services*, 2014.

(3) Pryce, R. Diabetic ketoacidosis caused by exposure of insulin pump to heat and sunlight. *Br. Med. J.* **2009,** *338*, a2218.

(4) Olivia, A.; Farina, J. B.; Llabres, M. Influence of temperature and shaking on stability of insulin preparations: Degradation kinetics. *Int. J. Pharm.* **1996,** *143*, 163-170.

(5) Weiss, R. C.; van Amerongen, D.; Bazalo, G.; Aagren, M.; Bouchard, J. R. Economic Benefits of Improved Insulin Stability In Insulin Pumps. *Managed Care* **2011,** *20*, 42-47.

(6) Karas, J. A.; Patil, N. A.; Tailhades, J.; Sani, M. A.; Scanlon, D. B.; Forbes, B. E.; Gardiner, J.; Separovic, F.; Wade, J. D.; Hossain, M. A. Total Chemical Synthesis of an Intra-A-Chain Cystathionine Human Insulin Analogue with Enhanced Thermal Stability. *Angew. Chem., Int. Ed.* **2016,** *55*, 14743-14747.

(7) Hovgaard, L.; Mack, E. J.; Kim, S. W. Insulin stabilization and GI absorption. *J. Control. Release* **1992,** *19*, 99-108.

(8) Hovgaard, L.; Jacobs, H.; Mazer, N. A.; Kim, S. W. Stabilization of insulin by alkylmaltosides. A. Spectroscopic evaluation. *Int. J. Pharm.* **1996,** *132*, 107-113.

(9) Sluzky, V.; Klibanov, A. M.; Langer, R. Mechanism of insulin aggregation and stabilization in agitated aqueous solutions. *Biotechnol. Bioeng.* **1992,** *40*, 895-903.

(10) Park, S.-J.; Choi, S. G.; Davaa, E.; Park, J.-S. Encapsulation enhancement and stabilization of insulin in cationic liposomes. *Int. J. Pharm.* **2011,** *415*, 267-272.

(11) Leobandung, W.; Ichikawa, H.; Fukumori, Y.; Peppas, N. A. Preparation of stable insulin-loaded nanospheres of poly (ethylene glycol) macromers and N-isopropyl acrylamide. *J. Control. Release* **2002,** *80*, 357-363.

(12) Chalasani, K. B.; Russell-Jones, G.; Yandrapu, S. K.; Diwan, P. V.; Jain, S. K. A novel vitamin B 12-nanosphere conjugate carrier system for peroral delivery of insulin. *J. Control. Release* **2007,** *117*, 421-429.

(13) Akiyoshi, K.; Kobayashi, S.; Shichibe, S.; Mix, D.; Baudys, M.; Kim, S. W.; Sunamoto, J. Self-assembled hydrogel nanoparticle of cholesterol-bearing pullulan as a carrier of protein drugs: complexation and stabilization of insulin. *J. Control. Release* **1998,** *54*, 313-320.

(14) Freeman, J. S. Insulin analog therapy: improving the match with physiologic insulin secretion. *J. Am. Osteopath. Assoc.* **2009,** *109*, 26-36.

(15) Evans, M.; Schumm-Draeger, P.; Vora, J.; King, A. A review of modern insulin analogue pharmacokinetic and pharmacodynamic profiles in type 2 diabetes: improvements and limitations. *Diabetes, Obes. Metab.* **2011,** *13*, 677-684.

(16) Association, A. D. Standards of medical care in diabetes—2017 abridged for primary care providers. *Clinical Diabetes* **2017,** *35*, 5-26.

(17) Pickup, J. C. Insulin-Pump Therapy for Type 1 Diabetes Mellitus. *N. Engl. J. Med.* **2012,** *366*, 1616-1624.

(18) Liu, Y.; Lee, J.; Mansfield, K. M.; Ko, J. H.; Sallam, S.; Wesdemiotis, C.; Maynard, H. D. Trehalose Glycopolymer Enhances Both Solution Stability and Pharmacokinetics of a Therapeutic Protein. *Bioconjugate Chem.* **2017,** *28*, 836-845.

(19) Oliva, A.; Farina, J. B.; Llabres, M. Influence of temperature and shaking on stability of insulin preparations: Degradation kinetics. *Int. J. Pharm.* **1996,** *143*, 163-170.

(20) Pryce, R. Diabetic ketoacidosis caused by exposure of insulin pump to heat and sunlight. *Br. Med. J.* **2009,** *338*, a2218.

(21) Gregory, R.; Edwards, S.; Yateman, N. A. Demonstration of Insulin Transformation Products in Insulin Vials by High-Performance Liquid-Chromatography. *Diabetes Care* **1991,** *14*, 42-48.

(22) Sluzky, V.; Tamada, J. A.; Klibanov, A. M.; Langer, R. Kinetics of insulin aggregation in aqueous solutions upon agitation in the presence of hydrophobic surfaces. *Proc. Natl. Acad. Sci. U. S. A.* **1991,** *88*, 9377-9381.

(23) Lee, L. L. Y.; Lee, J. C. Thermal-Stability of Proteins in the Presence of Poly(Ethylene Glycols). *Biochemistry* **1987,** *26*, 7813-7819.

(24) Senske, M.; Tork, L.; Born, B.; Havenith, M.; Herrmann, C.; Ebbinghaus, S. Protein stabilization by macromolecular crowding through enthalpy rather than entropy. *J. Am. Chem. Soc.* **2014,** *136*, 9036-41.

(25) Bohidar, H. B. Light scattering and viscosity study of heat aggregation of insulin. *Biopolymers* **1998,** *45*, 1-8.

(26) Brange, J.; Langkj, L.; Havelund, S.; Vølund, A. Chemical stability of insulin. 1. Hydrolytic degradation during storage of pharmaceutical preparations. *Pharm. Res.* **1992,** *9*, 715-726.

(27) Kinstler, O. B.; Brems, D. N.; Lauren, S. L.; Paige, A. G.; Hamburger, J. B.; Treuheit, M. J. Characterization and stability of N-terminally PEGylated rhG-CSF. *Pharm. Res.* **1996,** *13*, 996-1002.

(28) Dou, H.; Zhang, M.; Zhang, Y.; Yin, C. Synthesis and Purification of Mono-PEGylated Insulin. *Chem. Biol. Drug Des.* **2007,** *69*, 132-138.

(29) Willcock, H.; O'Reilly, R. K. End group removal and modification of RAFT polymers. *Polym. Chem.* **2010,** *1*, 149-157.

(30) Uchio, T.; Baudys, M.; Liu, F.; Song, S. C.; Kim, S. W. Site-specific insulin conjugates with enhanced stability and extended action profile. *Adv. Drug Delivery Rev.* **1999,** *35*, 289-306.

(31) Wood, M. R.; Duncalf, D. J.; Rannard, S. P.; Perrier, S. Selective One-Pot Synthesis of Trithiocarbonates, Xanthates, and Dithiocarbamates for Use in RAFT/MADIX Living Radical Polymerizations. *Org. Lett.* **2006,** *8*, 553-556.

(32) Lee, J.; Lin, E. W.; Lau, U. Y.; Hedrick, J. L.; Bat, E.; Maynard, H. D. Trehalose Glycopolymers as Excipients for Protein Stabilization. *Biomacromolecules* **2013,** *14*, 2561-2569.

(33) Boehnke, N.; Kammeyer, J. K.; Damoiseaux, R.; Maynard, H. D. Stabilization of Glucagon by Trehalose Glycopolymer Nanogels. *Adv. Funct. Mater.* **2018,** *28*, 1705475.

(34) Liu, Y.; Lee, J.; Mansfield, K. M.; Ko, J. H.; Sallam, S.; Wesderniotis, C.; Maynard, H. D. Trehalose Glycopolymer Enhances Both Solution Stability and Pharmacokinetics of a Therapeutic Protein. *Bioconjugate Chem.* **2017,** *28*, 836-845.

Chapter 3. Site-Specific Insulin-Trehalose Glycopolymer Conjugate by Grafting from Strategy Improves Bioactivity

3.1 Introduction

Diabetes is a growing worldwide problem, affecting over 30 million people[1] in the United States alone, with its prevalence continuing to rise.[1-2] Insulin is an important therapeutic protein for the treatment of diabetes; type I diabetes requires several injections or infusions of insulin daily.[3] However, exposure to environmental stressors such as heat and mechanical agitation encountered during storage and transportation can lead to protein degradation and aggregation.[4-6] Inadequate dosing resulting from degradation increases risk to the patient. For example, diabetic ketoacidosis can result from degradation of insulin from exposure to heat and extended hyperglycemia can increase risk for complications such as retinal damage and kidney disease.[4]

Our group has synthesized polymers with trehalose side chains that stabilize a variety of proteins to stressors such as lyophilization, heat, and mechanical agitation.[7-11] We have shown that conjugating insulin with a trehalose glycopolymer stabilized the protein to heat and mechanical agitation and also improved its pharmacokinetics.[9] However, the bioactivity was significantly lower than the native protein, requiring 5-fold dosage to achieve the same decrease in blood glucose as the native protein. The conjugate was synthesized by reductive amination at pH 8.0 using a benzaldehyde-functionalized trehalose polymer resulting in modification at both GlyA1 and LysB29; it has been shown that under similar pH conditions, the relative reactivity of the three amines in insulin is GlyA1>LysB29>>PheB1.[12] We hypothesized that this non-specific "grafting to" conjugation strategy resulting in modification at both GlyA1 and LysB29 contributed to the observed decrease in activity. Modification of GlyA1 decreases insulin affinity for its receptor and even conjugation of a 2000 Da poly(ethylene glycol) (PEG) can decrease bioactivity.[12] Modification at either PheB1 or LysB29 does not impact bioactivity to the same extent.[12-13]

Furthermore, PheB1 has been shown to react more slowly than the other two amines of insulin and modification at lysine can be favored by increasing the pH of the reaction above pH 9.5, taking advantage of its higher nucleophilicity than the N-terminal amines.[12] Therefore, we decided to target modification with the trehalose glycopolymer at LysB29 by conducting an initiator conjugation at higher pH and purifying the macroinitiator to contain only the LysB29 modification.

Polymerizing directly from a protein, or "grafting from" a protein, is a strategy that facilitates characterization of conjugation site and purification of the conjugate. Our group was the first to report this strategy by modifying biotin with an initiator, forming a biotin/streptavidin macroinitiator, and polymerizing *N*-isopropylacrylamide (NIPAAm) from the protein.[14] Subsequently, our group grafted NIPAAm directly from bovine serum albumin (BSA) and lysozyme macroinitiators, with the latter remaining active.[15] In addition, Matyjaszewski and Russell prepared polymers by first modifying amines and polymerizing poly(ethylene glycol) methacrylate (PEGMA).[16] Many examples of grafting from proteins have followed. Matyjaszewski and co-workers used activators generated by electron transfer atom transfer radical polymerization (AGET ATRP) to polymerize oligo(ethylene glycol) methacrylate (OEGMA) from BSA in phosphate buffer.[17] Bulmus and Davis were the first to demonstrate reversible addition–fragmentation chain transfer (RAFT) polymerization from a protein by conjugating the Z-group of a thiol-reactive chain transfer agent (CTA) to BSA and polymerizing acrylate and acrylamide monomers from the protein.[18-19] Sumerlin and co-workers subsequently employed RAFT to polymerize NIPAAm from BSA by conjugating the R-group of the CTA to the protein.[20] Additionally, Haddleton and coworkers polymerized acrylate and acrylamide monomers from a variety of proteins under mild, aqueous conditions.[21]

We devised a strategy to synthesize the insulin-trehalose glycopolymer conjugate involving targeted modification of LysB29 with an initiator. We envisioned that modification with a small molecule would also facilitate characterization of the conjugation site because the trehalose glycopolymer is not directly amenable to mass spectral analysis and purification of the LysB29 only species. It was expected that polymerizing from this insulin macroinitiator with trehalose monomer in mild, aqueous conditions would result in a conjugate with improved bioactivity compared to our previous approach, while retaining stabilization properties (**Figure 3-1**). The results are described herein.

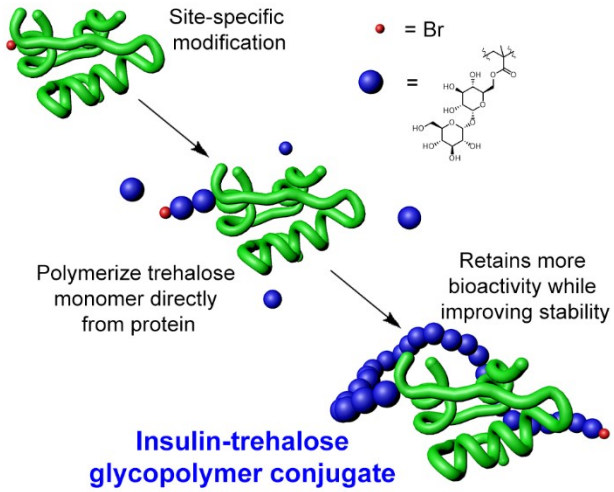

Figure 3-1. Scheme of experimental design.

3.2 Results and discussion

The designed approach required polymerization of a trehalose monomer under mild, aqueous conditions. AGET ATRP is a technique that has been performed in aqueous buffer at room temperature,[17] and our group used this technique to polymerize OEGMA monomers from siRNA.[22] A methacrylate trehalose monomer (**Figure 3-2A**) was selected to facilitate controlled

polymerization at room temperature in place of the styrenyl acetal trehalose monomer used in previous work.[8-9] First, the polymerization was explored under the conditions that would be suitable for the protein. Polymerization in DPBS with the small molecule initiator 2-hydroxyethyl-2-bromoisobutyrate (HEBIB), tris(2-pyridylmethyl)amine (TPMA) as the ligand, and ascorbic acid as the reducing agent was accomplished at 23 °C. Complete conversion was observed within 4 h and dispersity was low (**Figure 3-2B**). This polymer exhibited excipient stabilization of insulin to heating with 93 ± 3% intact insulin (**Figure S8**) compared to 68 ± 2% intact insulin remaining with the styrenyl trehalose glycopolymer used in our previous work,[9] demonstrating that the polymethacrylate backbone polymer also prevented heat-induced aggregation of insulin.

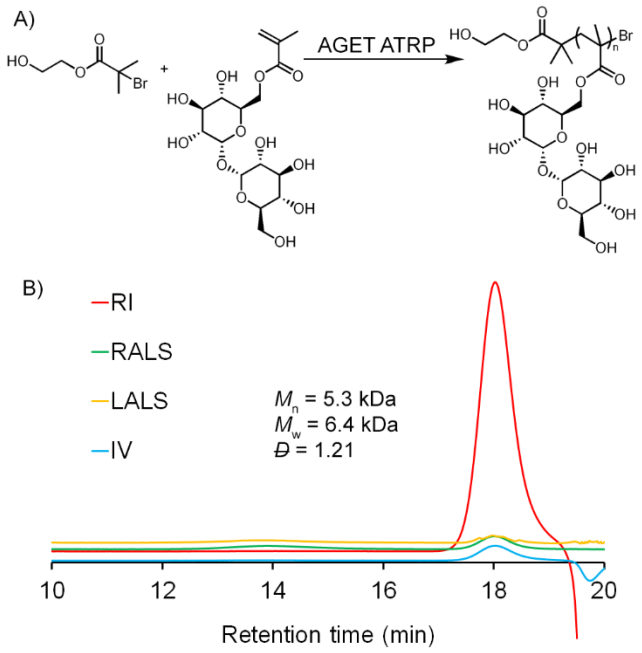

Figure 3-2. Aqueous polymerization of methacrylate trehalose. (A) Reaction scheme to polymerize trehalose monomer by AGET ATRP ([HEBIB]/[M]/[CuBr2]/[TPMA]/[AA] = 1/23/1/1/0.6) in DPBS pH 7.4 at 23 °C 3.5 h and (B) SEC trace of trehalose glycopolymer.

With the success of the trehalose monomer polymerization and resulting polymer stabilization of insulin, the protein was then modified with an initiator. Specifically, the insulin macroinitiator was synthesized with a nitrophenyl carbonate-activated initiator (NPC initiator) in borate buffer at pH 11 (**Figure 3-3A**). Even at this high pH, modification of multiple amines in addition to the desired product and unmodified insulin was observed after 1 h (**Figure S9 and S10**). No increase in the 40% conversion to the desired product was observed for longer reaction times and this yield is consistent with other site-selective modifications for insulin.[23-24] The singly modified product was separated from unmodified insulin and multiply modified products and recovered after semipreparative HPLC. The purified macroinitiator exhibited a single peak by analytical HPLC and matrix-assisted laser desorption ionization mass spectrometry (MALDI MS; **Figure 4A and B**). Further, the macroinitiator was reduced with dithiothreitol (DTT) for analysis by MALDI MS and modification was observed only on the B chain (**Figure S11**). To confirm the modification site, electrospray ionization (ESI) tandem MS was performed on the insulin macroinitiator, which showed fragments consistent with modification on LysB29 and not PheB1 (**Table S1**). Although only one species was observed for the insulin macroinitiator by HPLC, MALDI MS, and sodium dodecyl sulfate polyacrylamide gel electrophoresis (SDS PAGE), two bands were observed for the macroinitiator after purification by native PAGE (**Figure 4D and S13**). To determine if insulin was degrading during synthesis or purification of the macroinitiator, the insulin macroinitiator was run on a highly cross-linked Tris-Tricine gel under reducing and nonreducing conditions (**Figure S13**). Insulin and the insulin macroinitiator both exhibited one band near 6 kDa under nonreducing conditions and shifted bands near 3 kDa, indicating reduction of the interchain disulfide bonds. These results indicate that insulin does not degrade by disulfide reduction once modified. Insulin readily forms dimers near neutral pH at which the native gel was

run. LysB29 is involved in facilitating dimerization and monomeric rapid-acting insulin analogues have been prepared by mutating the amino acid at this position.[25-26] These two bands may be due to dissociation of insulin dimers into monomers with modification at LysB29 in the macroinitiator interfering with this interaction.

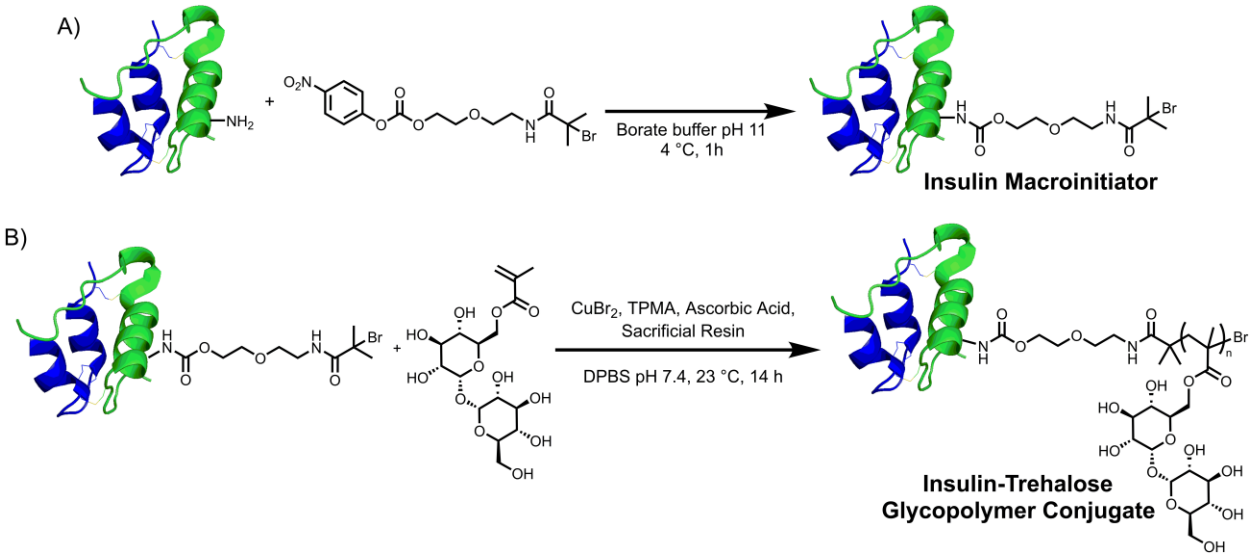

Figure 3-3. Synthesis of insulin-trehalose glycopolymer conjugate. (A) Preparation of the insulin macroinitiator and (B) grafting from the macroinitiator with AGET ATRP ([Resin]/[M]/[$CuBr_2$]/[TPMA]/[AA] = 1/30/1/10/0.6).

Attempts to polymerize from the macroinitiator were initially unsuccessful under a range of AGET ATRP conditions, likely due to the low concentration of initiating sites from the small amount of insulin macroinitiator. To facilitate polymerization from the insulin macroinitiator, a sacrificial resin was prepared as described previously.[22] This resin was modified with an initiator and increased the concentration of initiating sites. With the addition of the resin, the trehalose monomer was then successfully polymerized using AGET ATRP in DPBS pH 7.4 at 23 °C (**Figure 3-3B**) although it took 14 h to polymerize indicating that the reaction was slower for the macroinitiator

than the small molecule initiator. Also, a large molecular weight peak was observed in addition to the main peak by the right-angle light scattering detector equipped on the SEC that was not observed during polymerization with the small molecule initiator. This peak had also been detected during preparation of the monomer if the temperature was high or pressure too low when removing water and observed when insulin was added at 1 mg/mL to the polymerization mixture for the small molecule initiator HEBIB (**Figure S14**). We expected that this peak resulted from uncontrolled polymerization of the monomer. Increasing the amount of TPMA from 1 to 10 mol equiv with respect to copper eliminated this peak (**Figure S15**). We hypothesize that adding excess ligand displaces copper from interactions with insulin that result in uncontrolled polymerization.

The polymerization product exhibited a shift by native and SDS PAGE and this band contained insulin by Western blot analysis (**Figure 3-4C, D, and S12**). To determine if this band formed without the macroinitiator, several control polymerizations were performed. Unmodified insulin was substituted for the insulin macroinitiator, initiator was excluded with unmodified insulin included, or no insulin or initiator was included under the standard AGET ATRP conditions. No new bands were observed when the polymerization mixtures were analyzed by native PAGE (**Figure S16**). Polymer formed ($Đ$ >1.6) for conditions without insulin or initiator, which was likely due to autopolymerization. It is interesting to note that the trehalose glycopolymer did not stain by Coomassie except when these large molecular weight species were present (**Figure 3-4C and S12**).

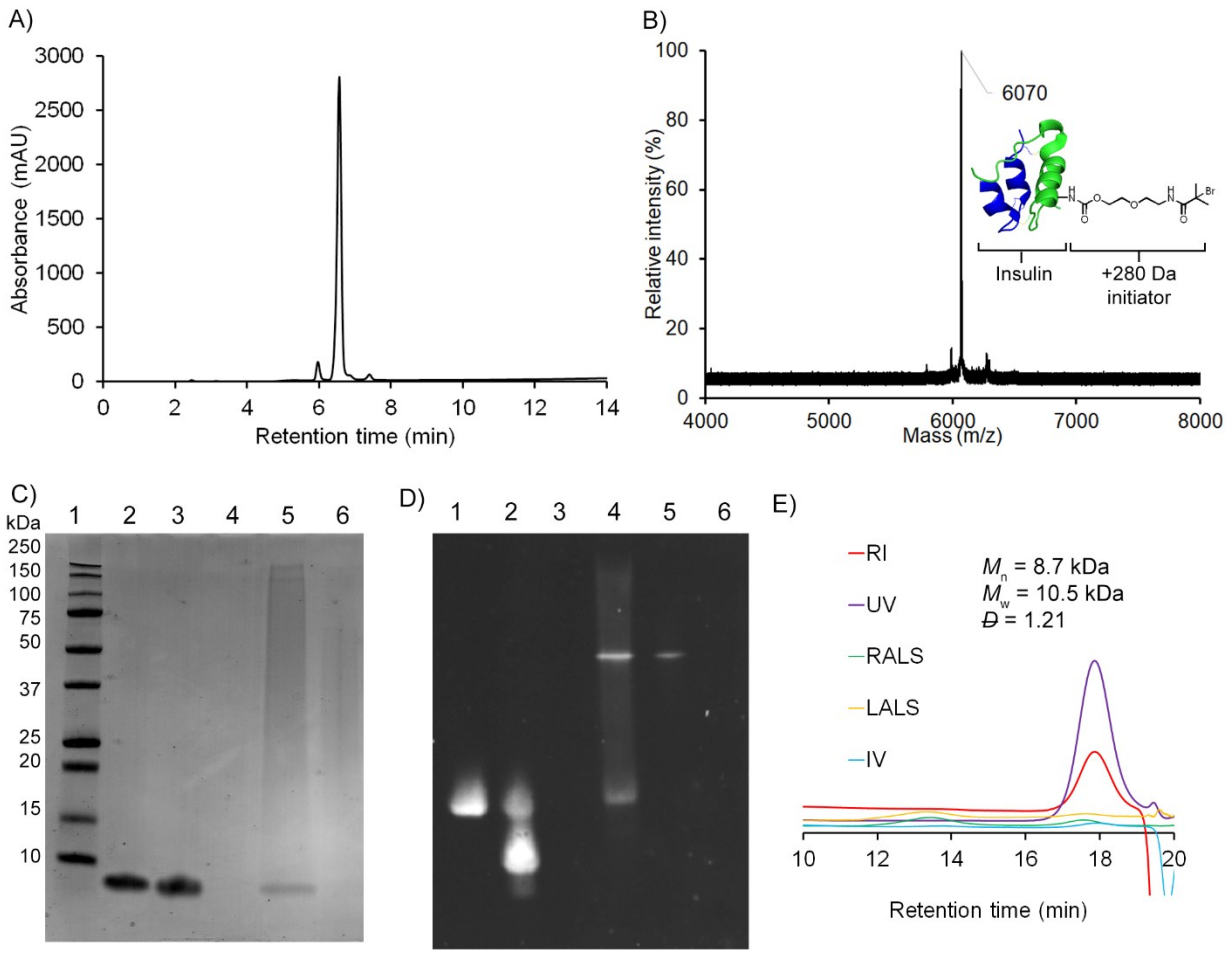

Figure 3-4. Characterization of insulin macroinitiator and insulin-trehalose glycopolymer conjugate. (A) Analytical HPLC and (B) MALDI MS after purification of the insulin macroinitiator, (C) Coomassie stained SDS PAGE (Lane 1: Ladder, Lane 2: Insulin, Lane 3: Purified insulin macroinitiator, Lane 4: Trehalose glycopolymer, Lane 5: Crude insulin-trehalose glycopolymer conjugate, Lane 6: Purified insulin-trehalose glycopolymer conjugate), (D) native PAGE with Western blot analysis (Lane 1: Insulin, Lane 2: Purified insulin macroinitiator, Lane 3: Trehalose glycopolymer, Lane 4: Crude insulin-trehalose glycopolymer conjugate, Lane 5: Purified insulin-trehalose glycopolymer conjugate Lane 6: Insulin-trehalose glycopolymer

conjugate after digestion with Proteinase K), and (E) SEC trace of trehalose glycopolymer after digestion of insulin with Proteinase K.

When the crude conjugate mixture was analyzed by analytical HPLC, peaks corresponding to free polymer likely hydrolyzed from the resin, insulin-trehalose glycopolymer conjugate, and residual insulin macroinitiator were observed (**Figure S17**). The insulin-trehalose glycopolymer conjugate could be separated using the same HPLC method as was used to purify the macroinitiator, yielding the final purified product. To characterize the polymer formed when grafting from the insulin macroinitiator, insulin was digested using Proteinase K as described in literature.[27] Polymer alone in the presence of Proteinase K did not change dispersity or molecular weight (**Figure S18**) showing that Proteinase K does not degrade the polymer or overlap with the polymer signal. By SEC analysis, the polymer was 8.7 kDa and exhibited similar dispersity ($\cancel{Đ}$ =1.21) as with the small molecule initiator (**Figure 3-4**B). The analogous insulin-PEG conjugate was also prepared with a 10 kDa methoxyPEG nitrophenyl carbonate in borate buffer pH 11. The singly modified species was separated by semipreparative HPLC. The insulin-PEG conjugate exhibited single a band at approximately 16 kDa by SDS PAGE, which is consistent with one site modification (**Figure S19**). Additionally, analytical HPLC of the purified insulin-PEG conjugate also exhibited a single peak (**Figures S21**). This was corroborated by MALDI MS (**Figure S20A**) and modification was confirmed on the B chain following reduction of the disulfides with DTT (**Figure S20B**). The modification is most likely at LysB29 because of the similarity of conditions to the macroinitiator and the reportedly higher reactivity of LysB29 over PheB1 under analogous conditions.[12]

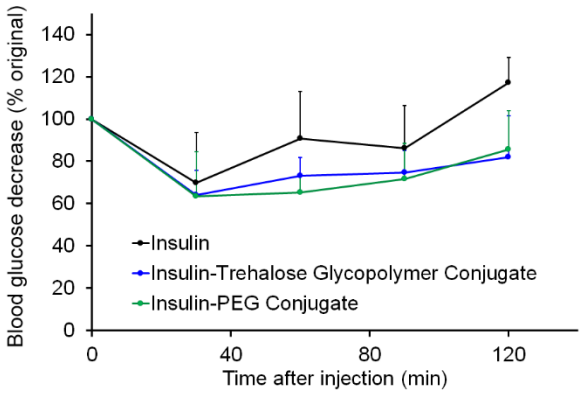

Figure 3-5. ITT in mice with insulin (16 µg/kg), insulin-PEG conjugate (48 µg/kg), and insulin-trehalose glycopolymer conjugate (48 µg/kg) (n=4, $p > 0.05$ at all points between insulin and conjugates).

To evaluate the bioactivity of the conjugates, insulin tolerance test (ITT) was performed in mice (**Figure 3-5**). Animals were injected with insulin, insulin-trehalose glycopolymer conjugate, and the analogous insulin-PEG conjugate. Insulin remained active after exposure to HPLC purification conditions, exhibiting a decrease in blood glucose 30 min after injection. Both the insulin-trehalose glycopolymer conjugate and insulin-PEG conjugate required only a 3-fold dosage relative to insulin alone (48 vs 16 µg/kg) to achieve the same change in blood glucose, which is a significant improvement over the 5-fold dosage (48 vs 80 µg/kg) required previously with a non-selective conjugate prepared by reductive amination at pH 8.0. Insulin conjugated to 20 kDa PEG through LysB29 had significantly lower binding affinity to the receptor than insulin alone.[28] Additionally, 2000 Da PEG-insulin conjugates showed decreased *in vivo* bioactivity, while 600 Da PEG-insulin conjugates retained bioactivity.[12] Thus, tuning the length of the polymer may further improve the retention of bioactivity.[10] A balance between stabilization properties and

bioactivity may be necessary, yet the site-specific conjugation strategy described herein clearly significantly improved retention of bioactivity.

Next, the stability of the insulin-trehalose glycopolymer was evaluated using an accelerated heating assay. Insulin and the insulin-trehalose glycopolymer conjugate were heated for 90 °C for 30 min and the amount of intact insulin was determined by measuring the area under the curve (AUC) of the insulin peak. The amount of intact insulin remaining for the conjugate after heating was found to be significantly greater than for insulin without the trehalose glycopolymer (**Figure 3-6**). This demonstrates that one polymer chain may be conjugated in a site-specific manner and yet still stabilize the protein to heat-induced aggregation.

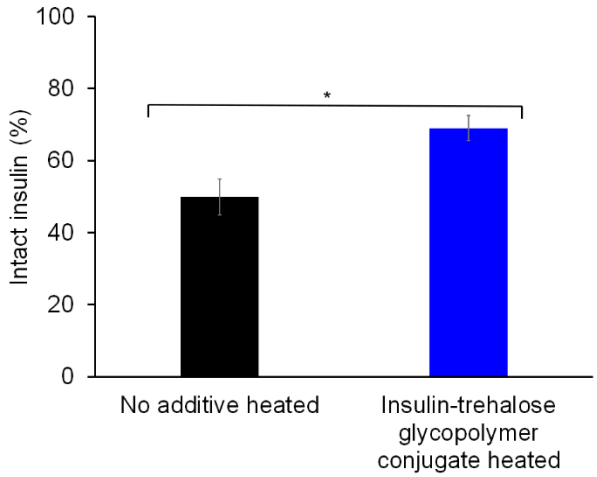

Figure 3-6. Biochemical stability assay of insulin and insulin-trehalose glycopolymer conjugate after heating to 90 °C for 30 min by HPLC AUC (n=3, * p = 0.0056).

3.3 Conclusion

In conclusion, we synthesized a site-specific trehalose glycopolymer conjugate with improved bioactivity retention compared to nonspecific conjugation. An insulin macroinitiator

was prepared at high pH to favor modification at LysB29. Following separation by HPLC, modification at the desired position was confirmed with tandem MS. Trehalose glycopolymer was polymerized directly from this macroinitiator with AGET ATRP under mild, aqueous conditions. The insulin-trehalose glycopolymer conjugate had greater retention of bioactivity than the nonspecific conjugate, requiring just over half the dosage used to achieve the same decrease in blood glucose. Moreover, the insulin-trehalose glycopolymer conjugate retained its stabilization properties by HPLC monitoring of intact insulin after heating.

3.4 Appendix B

Materials and methods

All chemicals were purchased from Sigma-Aldrich and Fisher Scientific and were used without purification unless otherwise noted. Methoxy poly(ethylene glycol) nitrophenyl carbonate (10.5 kDa by MALDI, $Đ$ = 1.02) was purchased from JenKem Technology (Plano, TX). Trehalose was purchased from The Healthy Essential Management Corporation (Houston, TX) and was azeotropically dried with ethanol and kept under vacuum until use. Recombinant human insulin was purchased from Sigma-Aldrich (Lot no. 17A061-D). Methacrylate trehalose monomer synthesis is described below. The sacrificial resin was synthesized as previously described with 93% modification by ^{1}H-NMR (Figure S4).[22] Cuprisorb was purchased from Amazon.com. Glucometer and glucose test strips (TrueTrack) were purchased from RiteAid.

Analytical techniques

Nuclear Magnetic Resonance (NMR) spectra were recorded on a Bruker AV 400 MHz spectrometer. Size exclusion chromatography (SEC) was conducted on a Malvern Viscotek

GPCmax equipped with a TDA 305-040 Quadruple Detector Array (RI + Viscosity + LALS/RALS + UV) and 0.05 M sodium sulfate in water + 10 % methanol as eluent at a flow rate of 1.0 mL/min. Molecular weight was calculated using conventional PEG standards. Trehalose monomer was purified by preparatory reverse phase HPLC on a Shimadzu HPLC system equipped with a UV detector using a Luna 5 μm C18 100A column (preparatory: 5 μm, 250 x 21.2 mm) with monitoring at λ = 215 nm and 254 nm. Gradient solvent system (water:methanol = 90:10 to 40:60 over 20 min) was used as the mobile phase at a flow rate of 20 mL/min. Semi-preparative HPLC to purify the insulin macroinitiator was conducted on an Agilent 1260 Infinity II LC System equipped with a UV detector and Zorbax 300SB C-18 column with a gradient solvent system (water:acetonitrile = 70:30 to 0:100 + 0.1 % trifluoroacetic acid over 20 min at 3 mL/min unless otherwise noted). Analytical HPLC for detection of insulin was conducted on an Agilent 1260 Infinity II LC System equipped with a UV detector using Zorbax SB300 C-3 column and a gradient solvent system (water:acetonitrile = 90:10 to 0:100 + 0.1 % trifluoroacetic acid over 17 min at 0.6 mL/min). Matrix-assisted laser desorption/ionization (MALDI)-MS analysis of the insulin macroinitiator was performed on a Voyager DE-STR (Applied Biosystems, Forster City, CA) in linear positive ion mode. The insulin macroinitiator was desalted by centriprep ultrafiltration (MWCO 3 kDa) and mixed 1:1 with sinapinic acid dissolved in 50 % acetonitrile with 0.1 % trifluoroacetic acid on the MALDI target plate. Tandem MS was performed with static positive ion electrospray ionization mass spectrometry on LTQ-FT Ultra and data was analyzed with Prosight PC 4.0. Insulin-trehalose glycopolymer was reduced with 100 mM DTT and cleaned up by stop-and-go extraction (StaGE) tip SPE before mass spectral analysis.

Synthesis of 2-bromo-N-(2-(2-hydroxyethoxy)ethyl)-2-methylpropanamide

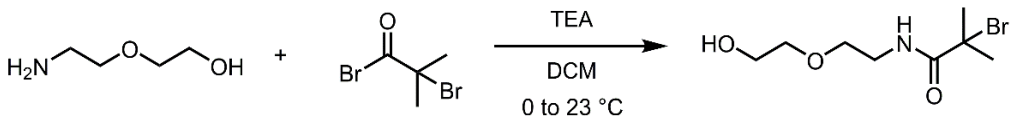

2-(2-Aminoethoxy)ethanol (0.57 mL, 5.73 mmol) was dissolved in anhydrous DCM (12 mL) in an oven-dried round bottom flask under argon. Anhydrous TEA (0.60 mL, 4.30 mmol) was added and this was stirred at 0 °C for 10 min. α-Bromoisobutyryl bromide (0.3 mL, 2.69 mmol) was added dropwise. The reaction mixture was allowed to rise to 23 °C and stirred for a total of 14 h. The mixture was purified by silica gel flash chromatography with a gradient of 0-10% methanol in diethyl ether (product R_f ~0.65) to afford 618 mg product (90% yield) as a pale yellow oil. ^{1}H NMR (400 MHz in $CDCl_3$) δ: 7.07 (s, 1H), 3.78-3.74 (m, 2H), 3.62-3.59 (m, 4 H), 3.51-3.47 (dt, J = 5.41, 5.73 Hz, 2 H), 1.96 (s, 6H). ^{13}C NMR (400 MHz in $CDCl_3$) δ: 172.4, 72.4, 69.6, 63.0, 61.9, 40.3, 32.7. IR: ν = 3336, 2932, 2869, 1652, 1525, 1455, 1370, 1291, 1193, 1111, 1060, 931, 926, 891, 797 cm^{-1}. HRMS (ESI) calculated for $C_8H_{16}BrNO_3Na$ ([M + Na]$^+$) 276.0211, found 276.0216.

Synthesis of nitrophenyl carbonate initiator (NPC initiator)

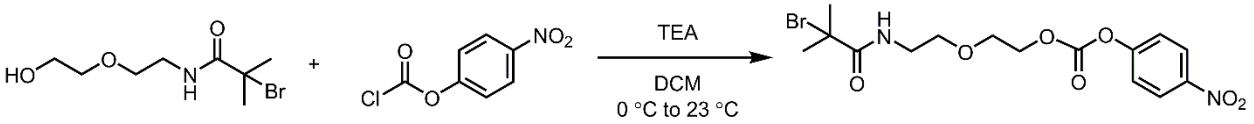

In a flame-dried round bottom flask, 2-bromo-*N*-(2-(2-hydroxyethoxy)ethyl)-2-methylpropanamide (200 mg, 0.79 mmol) was dissolved in anhydrous DCM (0.79 mL) under argon. Anhydrous TEA (0.16 mL, 1.18 mmol) was added and stirred at 0 °C for 10 min. Nitrophenyl chloroformate (316 mg, 1.57 mmol) was added and stirred at 0 °C. The reaction mixture was allowed to rise to 23 °C and stirred for additional 14 h. The mixture was purified by silica gel flash chromatography with a gradient of 20-100% diethyl ether with hexanes (product R_f

~0.48 in 3:1 diethyl ether:hexanes) and 281 mg (85% yield) of product was recovered as a pale yellow oil. ^{1}H NMR (400 MHz in $CDCl_3$) δ: 8.29 (d, J = 8.19 Hz, 2H), 7.40 (d, J = 9.91 Hz, 2H), 7.07 (s, 1H), 4.47-4.44 (m, 2H), 3.81-3.79 (m, 2H), 3.64 (t, J = 4.89 Hz, 2H), 3.52-3.48 (dt, J = 5.41, 4.69 Hz, 2H), 1.96 (s, 6H). ^{13}C NMR (400 MHz in $CDCl_3$) δ: 172.1, 155.4, 152.7, 145.5,125.6, 121.9, 69.6, 68.5, 68.1, 63.0, 40.2, 32.7. IR: ν = 3413, 3120, 3079, 2973, 2929, 2869, 1764, 1663, 1617, 1594, 1522, 1454, 1348, 1258, 1207, 1110, 1061, 1011, 901, 859, 774, 723, 663 cm^{-1}. HRMS (ESI) calculated for $C_{15}H_{19}BrN_2O_7Na$ ($[M + Na]^+$) 443.0255, found 443.0265.

Synthesis of 2-hydroxyethyl 2-bromoisobutyrate (HEBIB)

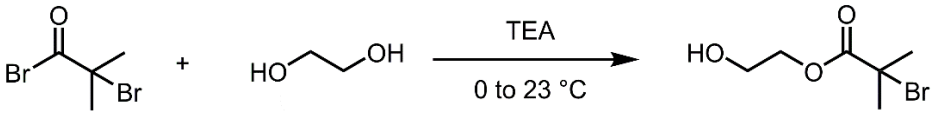

HEBIB was synthesized slightly modified from literature procedure.[29] α-Bromoisobutyryl bromide (0.5 mL, 4.05 mmol) was added dropwise to a cold solution of ethylene glycol (1.33 mL, 23.8 mmol, anhydrous) and anhydrous triethylamine (0.66 mL, 4.74 mmol) at 0 °C for 2 h. The reaction was continued at 23 °C for another 12 hrs. The reaction mixture was added to 10 mL of water and extracted with chloroform three times. The chloroform layer was washed successively with dilute HCl, saturated $NaHCO_3$, and water. The organic layer was dried over anhydrous magnesium sulfate and evaporated for the product. The product was further purified silica gel flash chromatography with a gradient of 16-100% diethyl ether with hexanes and 407 mg (47.6% yield) was recovered as a clear oil. ^{1}H NMR (400 MHz in $CDCl_3$) δ: 4.32 (t, J = 4.65 Hz, 2H), 3.88 (t, J = 4.68 Hz, 2H), 1.96 (s, 6H), 1.58 (s, 1H). ^{1}H-NMR agreed with that reported for this compound.[29]

Synthesis of methacrylate trehalose monomer

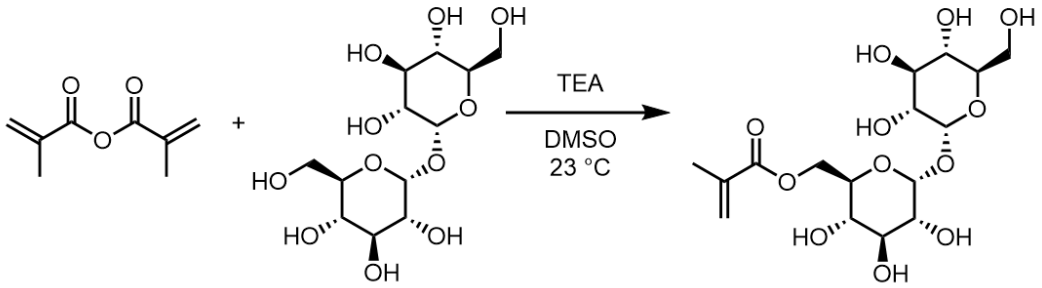

Trehalose (4.6 g, 13.44 mmol) was dissolved in 60 mL anhydrous DMSO in a flame-dried round bottom flask under argon. Anhydrous TEA (5.6 mL, 40.18 mmol) and methacrylic anhydride (400 µL, 2.69 mmol) were added. This was stirred for 15 h at room temperature (23 °C). The solution was precipitated into cold (0 °C ice water bath) 1400 mL 8:2 Hex/DCM. The organic layer was decanted and the viscous liquid was dissolved in water for a total volume of 70 mL. After removing organics by rotary evaporation, the crude product was purified by HPLC with 10-60% MeOH/H_2O over 20 min. To this was added 150 ppm MEHQ as an inhibitor to prevent autopolymerization. Methanol and water were removed by rotary evaporation using a 2-neck flask equipped with a septa and long needle directly into the water to prevent autopolymerization by providing a source of oxygen. The product (340 mg, 31% yield) was recovered after lyophilization. ^{1}H NMR (400 MHz in D_2O) δ: 6.03 (s, 1H), 5.63, (s, 1H), 5.07 (d, J = 3.99, 1H), 5.03 (d, J = 3.87 Hz, 1H), 4.39-4.36 (dd, J = 12.43, 2.19 Hz, 1H), 4.26-4.23 (dd, J = 12.61, 5.27 Hz, 1H), 3.98-3.94 (qd, J = 15.51, 4.98, 2.02, 1H), 3.76-3.68 (m, 4H), 3.65-3.60 (m, 1H), 3.57-3.54 (dd, J = 9.80, 3.90 Hz, 1H), 3.52-3.49 (dd, J = 9.89, 3.88 Hz, 1H), 3.42 (t, J = 9.67 Hz, 1H), 3.32 (t, J = 9.52 Hz, 1H), 1.82 (s, 3H). ^{1}H-NMR agreed with that previously reported.[30]

AGET ATRP of methacrylate trehalose monomer with HEBIB

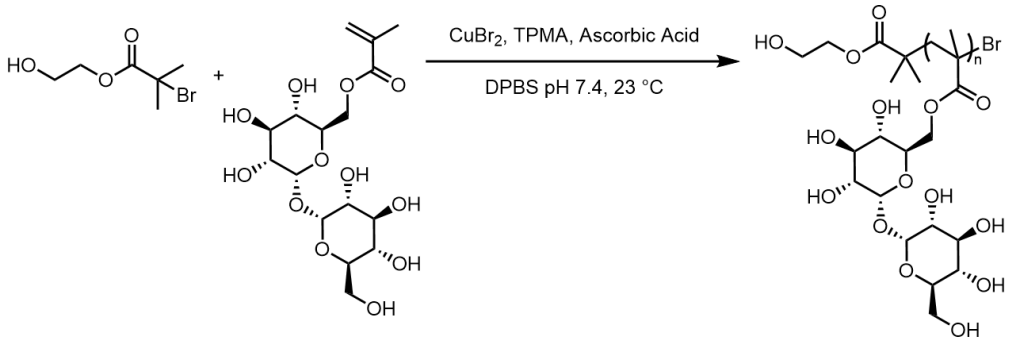

200 mM Dulbecco's phosphate-buffered saline (DPBS) pH 7.4 was degassed by sparging with argon for 40 min. Methacrylate trehalose monomer (100 mg, 0.24 mmol) was placed in a Schlenk flask, which was evacuated and refilled with argon 4 times. $CuBr_2$ (2.36 mg, 10.6 μmol) and tris(2-pyridylmethyl)amine (TPMA) (3.08 mg, 10.6 μmol) were dissolved in degassed DPBS pH 7.4. This was used to dissolve HEBIB (2.24 mg, 10.6 μmol) and transferred to the flask. The vial was washed with additional degassed DPBS for a total volume of 0.54 mL (monomer concentration of 0.45 M). Ascorbic acid (AA) was dissolved in degassed DPBS and a portion of this stock solution (for 1.12 mg, 6.4 μmol AA in 40 μL) was added to the flask to initiate polymerization. The polymerization proceeded at 23 °C for 3.5 h under argon. The polymerization was quenched by exposure to air (>99% conversion by ^{1}H NMR) and the polymer was purified by dialysis against water (MWCO 3.5 kDa, with 100 mL Cuprisorb for 1 day to eliminate copper[31]) for 2 days. The polymer was recovered after lyophilization as a fluffy white solid. ^{1}H NMR (400 MHz in D_2O) δ: 5.10, 5.06, 4.24, 4.03, 3.94, 3.75, 3.53, 3.35, 1.83, 1.51, 1.61, 0.96, 0.80. Number-average molecular weight (M_n) = 5.3 kDa (by size exclusion chromatography (SEC) with PEG standards), molecular weight dispersity ($Đ$) = 1.21.

Preparation of insulin macroinitiator

Insulin (15 mg, 2.5 μmol) was weighed into a vial equipped with a stir bar and dissolved in 15 mL borate buffer pH 11 in a 0 °C ice bath. Nitrophenyl carbonate activated initiator (NPC initiator) (3.25 mg, 7.8 μmol) dissolved in 150 μL DMSO was added and the solution gradually turned yellow. The solution was stirred for 1 h in a 0 °C ice bath. The solution was buffer exchanged by centriprep ultracentrifugation (MWCO 3 kDa) into DPBS pH 7.4 several times until no yellow color remained. The singly modified macroinitiator was purified using semi-preparative (Zorbax 300SB C-18 column) with a gradient of 30-90% acetonitrile/water + 0.1% TFA over 20 min (eluting at 9.5 min). Fractions were pooled and buffer exchanged into DPBS pH 7.4 using centriprep ultracentrifugation (MWCO 3 kDa). Concentration was determined by analytical HPLC AUC compared to a standard curve. MS (MALDI) expected 6073 Da, found 6070 Da.

Grafting trehalose glycopolymer from insulin macroinitiator

DPBS pH 7.4 was degassed by sparging with argon for 30 min. Methacrylate trehalose monomer (50.0 mg, 122 mmol) and the sacrificial resin (16.9 mg, 4.1 μmol) were placed in a Schlenk tube, and this was evacuated and refilled with argon 3 times. Stock solutions of $CuBr_2$ (0.91 mg, 4.1 μmol) with TPMA (11.8 mg, 41 μmol) in 100 μL degassed DPBS and added to the flask. Ascorbic acid (0.43 mg, 2.4 μmol) in 170 μL degassed DPBS was prepared and used to dissolve the insulin macroinitiator (1.2 mg lyophilized from 300 μL DPBS) and transferred to the Schlenk flask. The polymerization proceeded at 23 °C for 14 h before being quenched by exposure to air. The mixture was stirred with pre-rinsed Cuprisorb for 1 h before purification by centriprep ultracentrifugation (MWCO 3 kDa) buffer exchanging into DPBS. The conjugate was further purified from residual macroinitiator using semi-preparative HPLC (Zorbax 300SB C-18 column) with a gradient of 30-90% acetonitrile/water + 0.1% TFA over 20 min (eluting at 8.8 min).

Fractions were pooled and buffer exchanged into DPBS pH 7.4 using centriprep ultracentrifugation (MWCO 3 kDa). The polymer was characterized by size exclusion chromatography (SEC) after digestion of insulin by Proteinase K.[27] Briefly, insulin-trehalose glycopolymer conjugate was buffer exchanged by centriprep ultracentrifugation (MWCO 3 kDa) to digestion buffer (10 mM Tris HCl, 2 mM $CaCl_2$ pH 7.4) and to 100 µL of this was added 100 µL Proteinase K at 2 mg/mL in digestion buffer. The solution was incubated in a 50 °C water bath for 24 h. Peptide fragments were removed by centriprep ultracentrifugation (MWCO 3 kDa) before analysis by size exclusion chromatography (SEC). Number-average molecular weight (M_n) = 8.7 kDa (with PEG standards), molecular weight dispersity ($Đ$) = 1.21.

Preparation of insulin-PEG conjugate

Insulin (1.5 mg, 0.26 µmol) and methoxyPEG nitrophenyl carbonate (10 kDa, 25.8 mg, 2.6 µmol) were dissolved in 1.5 mL 100 mM borate buffer pH 11. This solution was incubated for 1 hour at 4 °C on a rocker. The solution was filtered before purification using semi-preparative HPLC (Zorbax 300SB C-18 column) with a gradient of 30-80% acetonitrile/water + 0.1% TFA over 30 min (eluting at 10.5 min). Fractions were pooled and buffer exchanged into DPBS pH 7.4 using centriprep ultracentrifugation (MWCO 3 kDa).

Determination of concentration by BCA assay

Insulin conjugate concentrations were determined using Pierce BCA assay kit (ThermoFisher Scientific) according to manufacturer specifications. Briefly, 10 µL each sample and insulin standard were pipetted into a 96-well plate. To this was added 200 µL working reagent

(50 parts A + 1 part B). The plate was incubated at 37 °C for 30 min then cooled to room temperature before measuring absorbance at 562 nm.

Bioactivity Study

Bioactivity was determined by insulin tolerance test (ITT) using standard protocols.[9, 32] Specifically, CD1 mice (6−8 wks, female, n = 4, Charles River Laboratories) were fasted for 4−6 h to reduce variability in baseline blood glucose. Mice were injected through the tail vein with insulin that had been exposed to the HPLC purification conditions used for the macroinitiator (16 μg/kg), insulin-trehalose glycopolymer conjugate (48 μg/kg of insulin), or insulin-PEG conjugate (48 μg/kg of insulin). Blood glucose was measured at prescribed timepoints by pricking the tail vein of conscious mice with a needle and sampling the approximately 2 μL droplet formed with a commercial glucometer.

Stability Study

Insulin and insulin-trehalose glycopolymer conjugate were prepared at 0.1 mg/mL. These solutions were aliquoted 100 μL into 1.5 mL LoBind tubes and heated in a dry heat block at 90 °C for 30 min. Samples were cooled in a 4 °C freezer before filtering with 0.22 μm PTFE filters. Heated and unheated samples were analyzed by HPLC using a Zorbax 300 SB-C3 column with a gradient of 0-100% MeCN/water + 0.1% TFA over 17 min. The area under the curve was used to determine the amount of intact insulin.

Statistical Analysis

For assessment of the statistical significance of differences, two-tailed Student's t-test assuming unequal sample variance was employed. Results were considered significantly different if $p < 0.05$.

Figures and tables

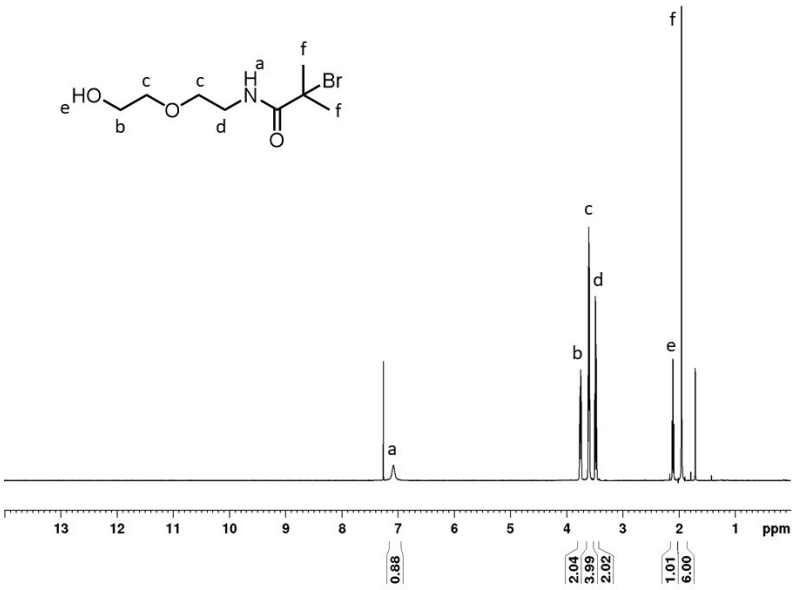

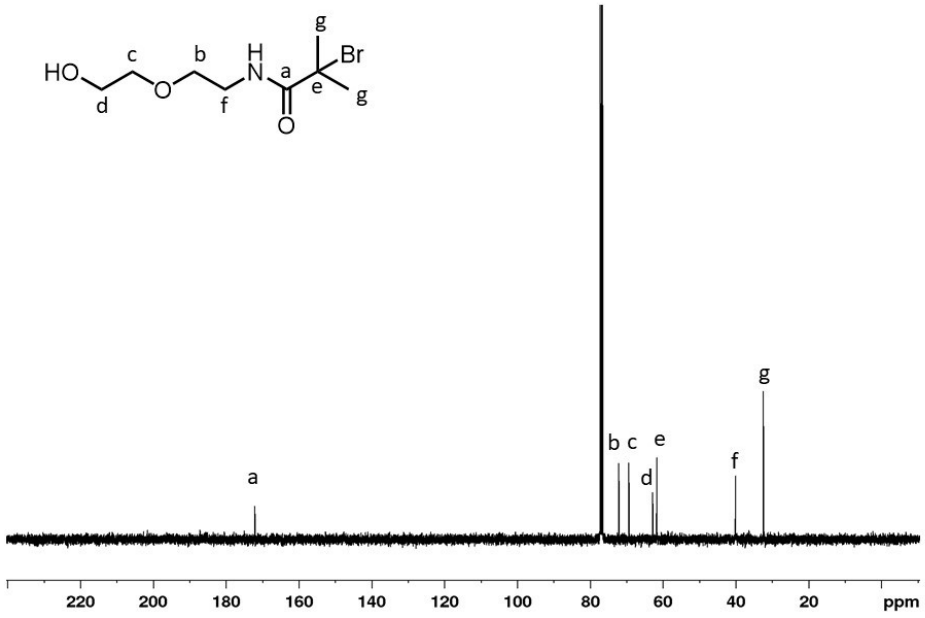

Figure 3-7. ^{1}H and ^{13}C NMR spectra of 2-bromo-N-(2-(2-hydroxyethoxy)ethyl)-2-methylpropanamide ($CDCl_3$).

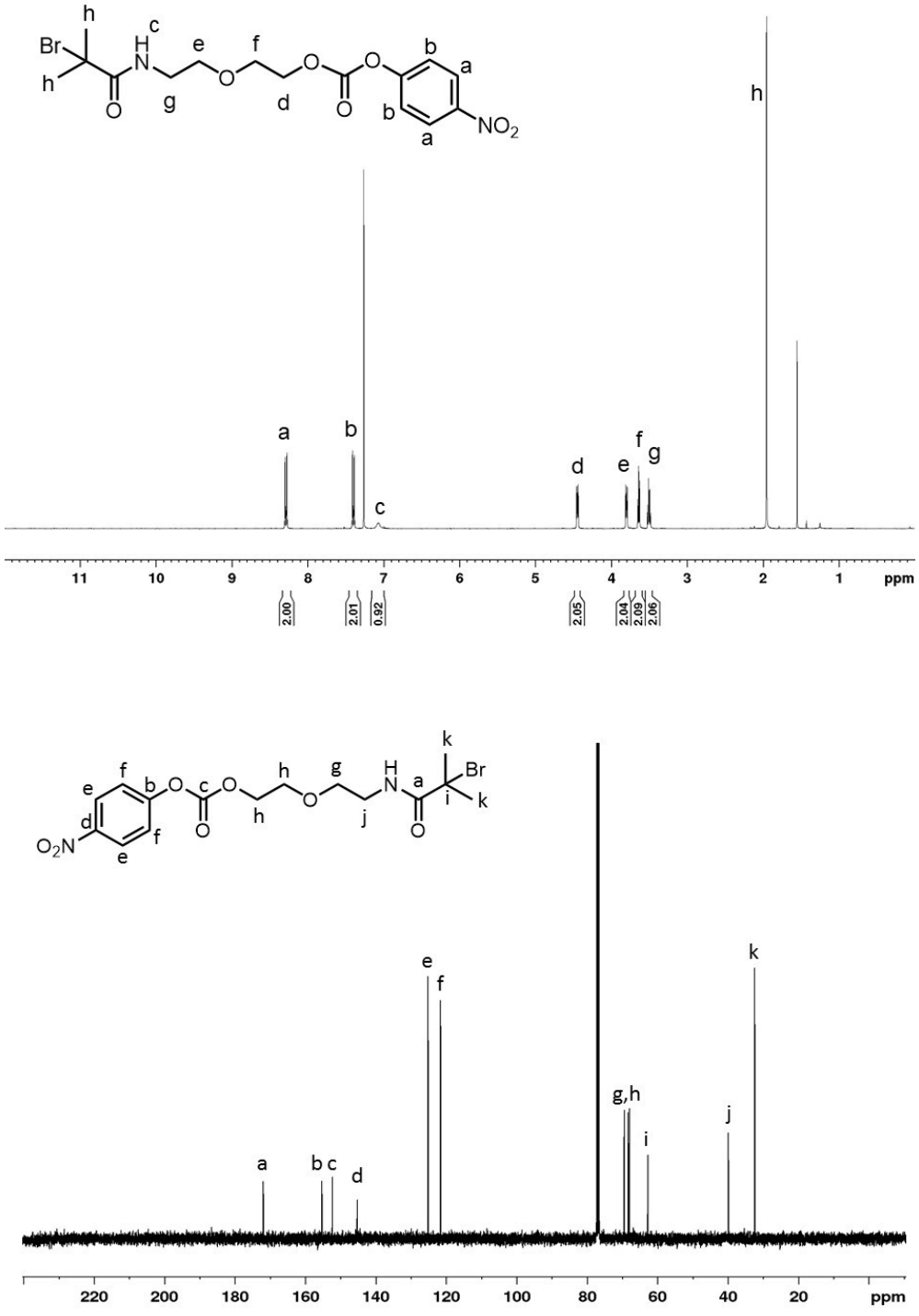

Figure 3-8. ^{1}H and ^{13}C NMR spectra of NPC initiator ($CDCl_3$).

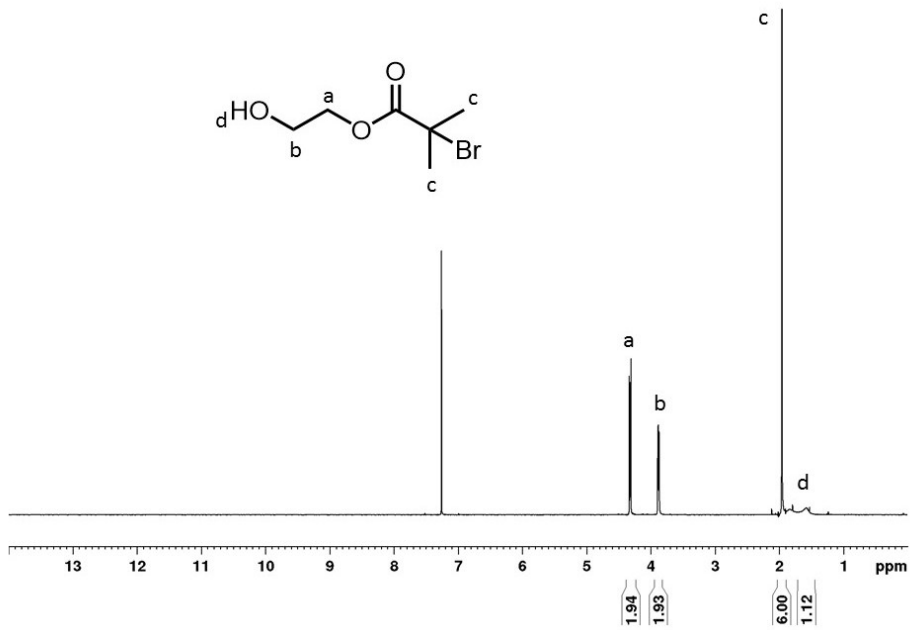

Figure 3-9. ^{1}H NMR spectrum of 2-hydroxyethyl 2-bromoisobutyrate ($CDCl_3$).

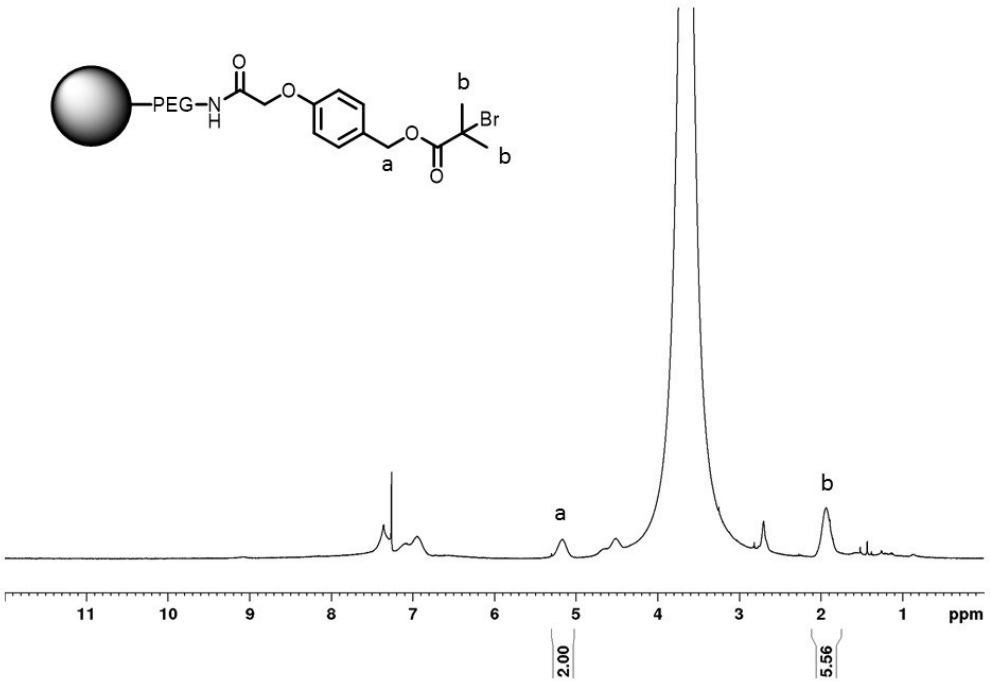

Figure 3-10. ^{1}H NMR spectrum of sacrificial resin ($CDCl_3$).

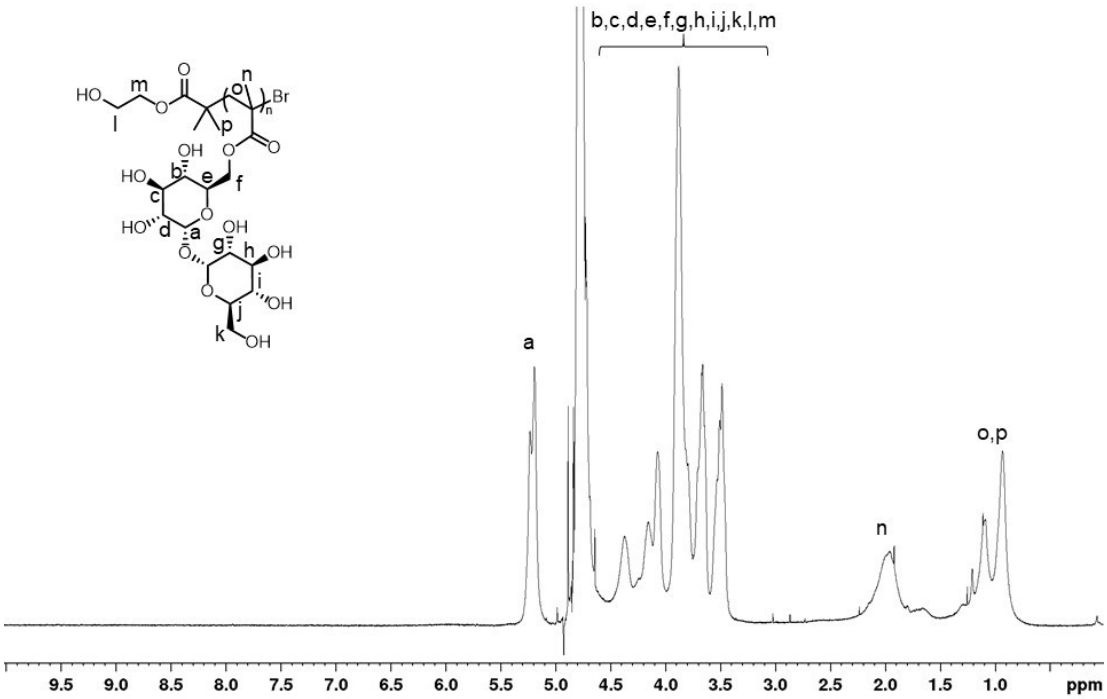

Figure 3-11. ^{1}H NMR of trehalose glycopolymer prepared by AGET ATRP (D_2O).

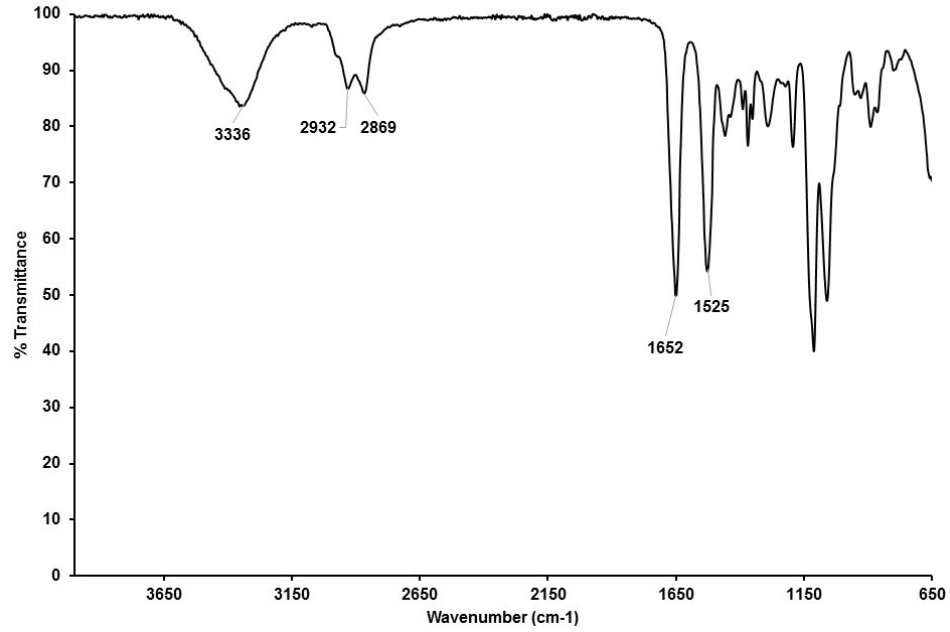

Figure 3-12. FTIR spectrum of 2-bromo-*N*-(2-(2-hydroxyethoxy)ethyl)-2-methylpropanamide.

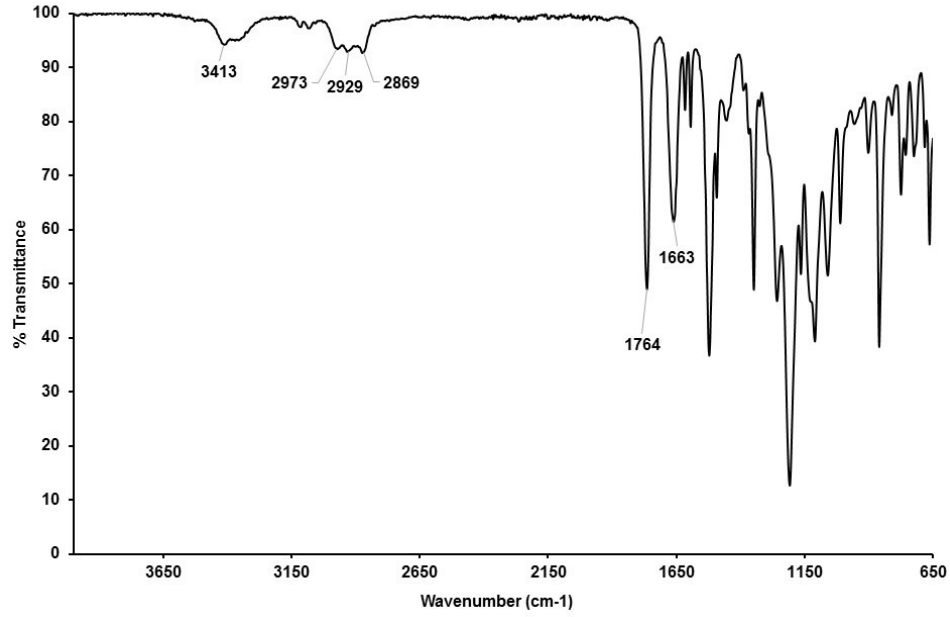

Figure 3-13. FTIR spectrum of NPC initiator.

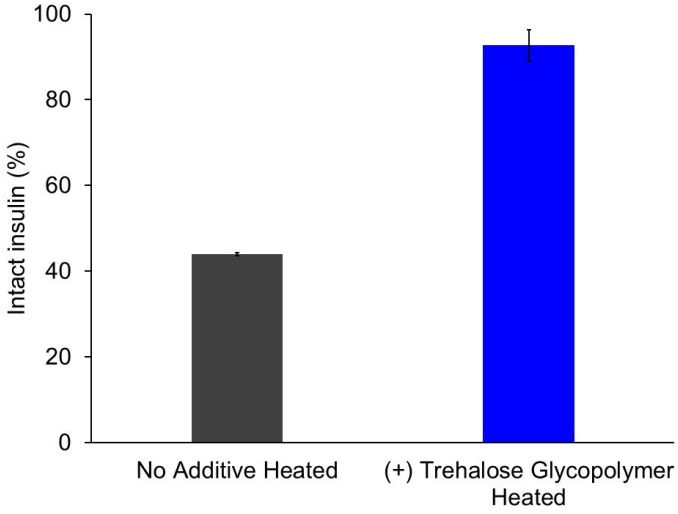

Figure 3-14. Amount of intact insulin by area under the curve (AUC) after heating insulin to 90 °C for 30 min with and without 2 mol equiv trehalose glycopolymer as excipient.

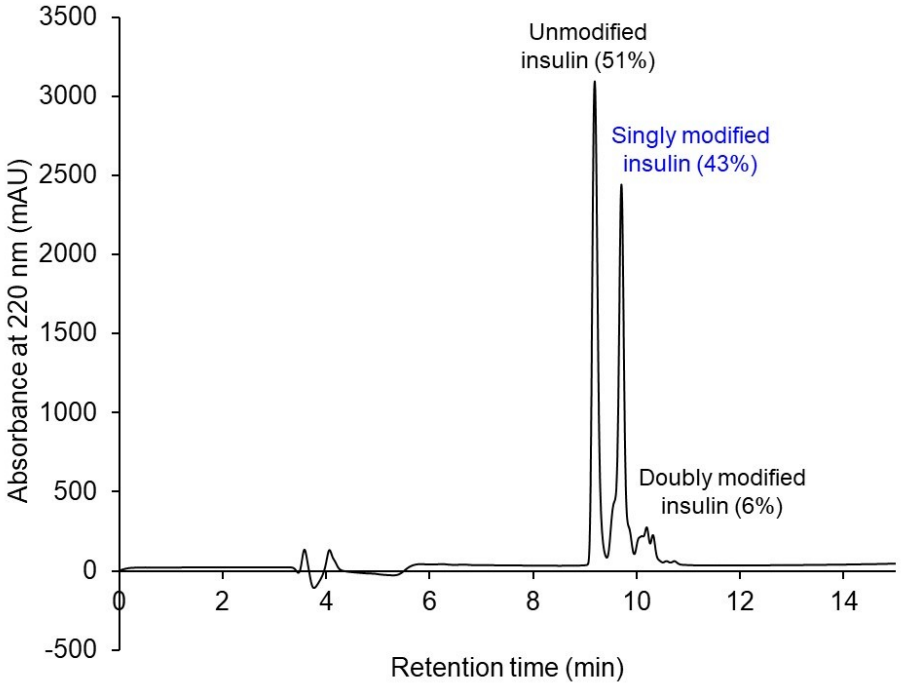

Figure 3-15. HPLC trace of insulin macroinitiator during purification with percent yield determined by relative AUC.

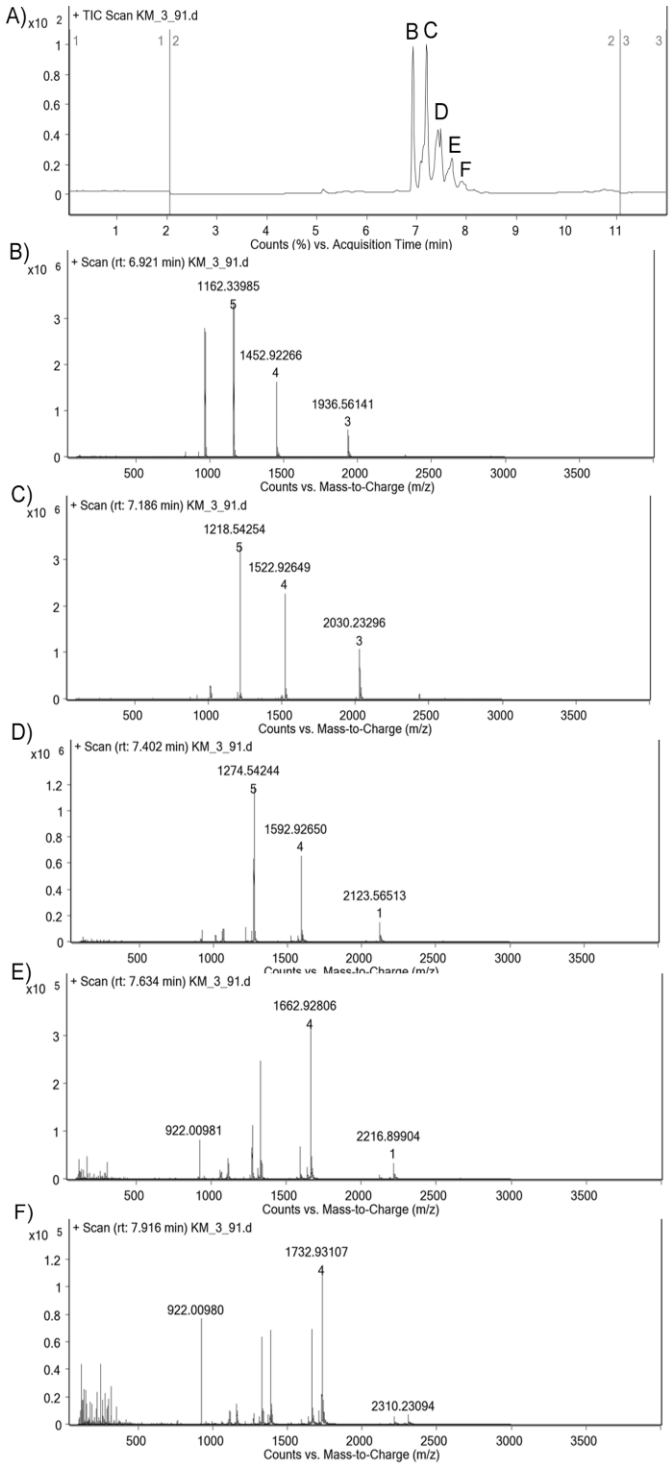

Figure 3-16. LC-MS of crude insulin macroinitiator. (A) TIC trace with mass spectra showing (B) no modification (C) one modification (D) two modifications (E) three modifications (F) four modifications (from deamidation).

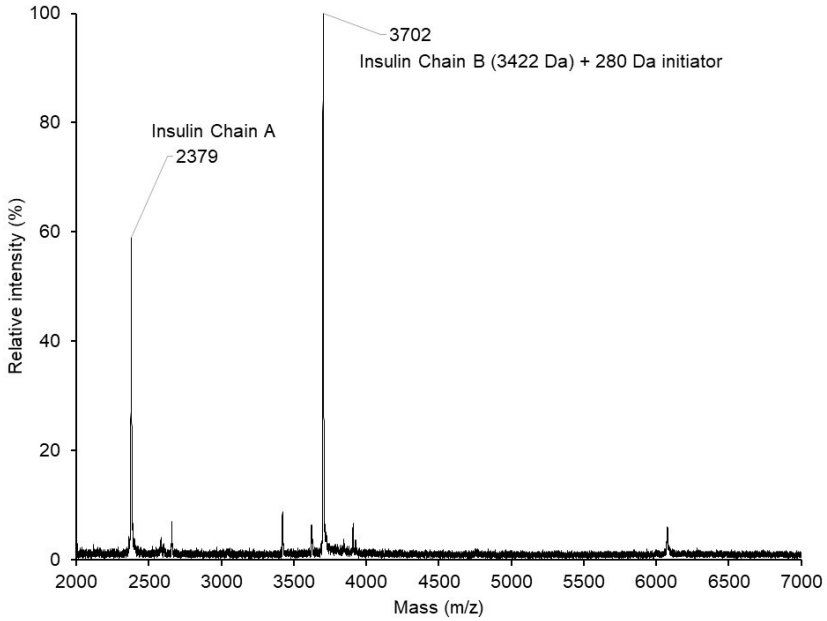

Figure 3-17. MALDI MS of purified insulin macroinitiator reduced with DTT.

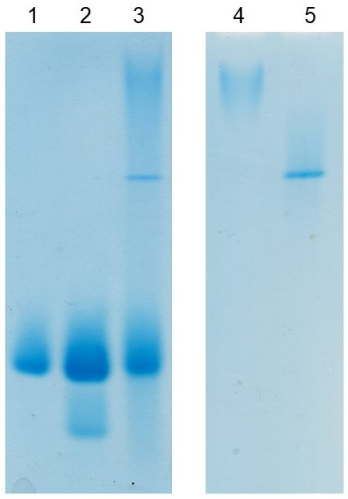

Figure 3-18. Native PAGE of insulin-trehalose glycopolymer conjugate, Coomassie stained (Lane 1: Insulin, Lane 2: Insulin macroinitiator, Lane 3: Insulin-trehalose glycopolymer polymerization mixture, Lane 4: Trehalose glycopolymer with large MW species, Lane 5: Purified insulin-trehalose glycopolymer conjugate).

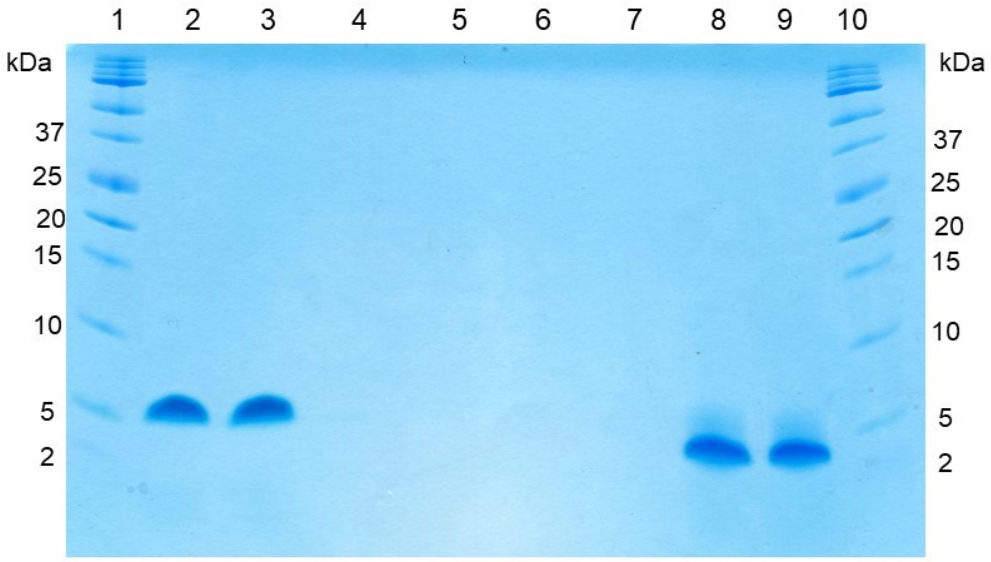

Figure 3-19. SDS PAGE with 16.5% Tris-Tricine Gel under non-reducing and reducing conditions (Nonreducing: Lane 1: Ladder, Lane 2: Insulin, Lane 3: Insulin macroinitiator, Reducing, Lane 8: Insulin macroinitiator, Lane 9: Insulin, Lane 10: Ladder).

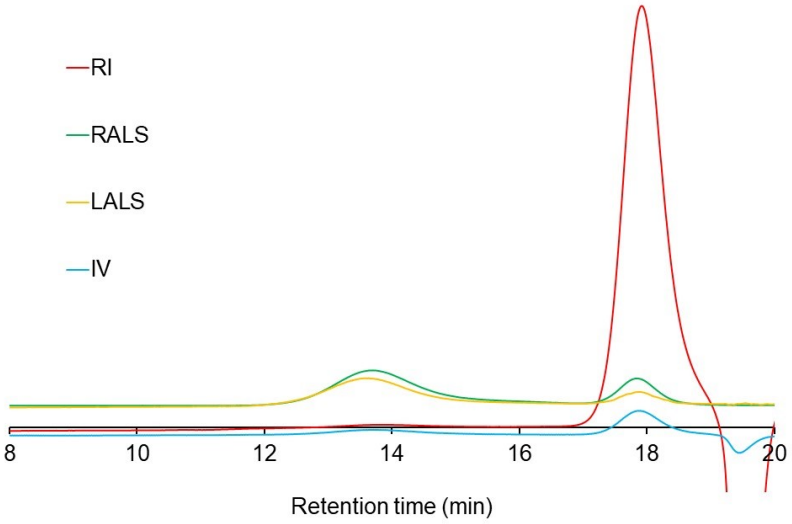

Figure 3-20. SEC trace of polymerization by AGET ATRP with trehalose monomer, 1 mg/mL added insulin, and 1 equiv TPMA : 1 equiv $CuBr_2$.

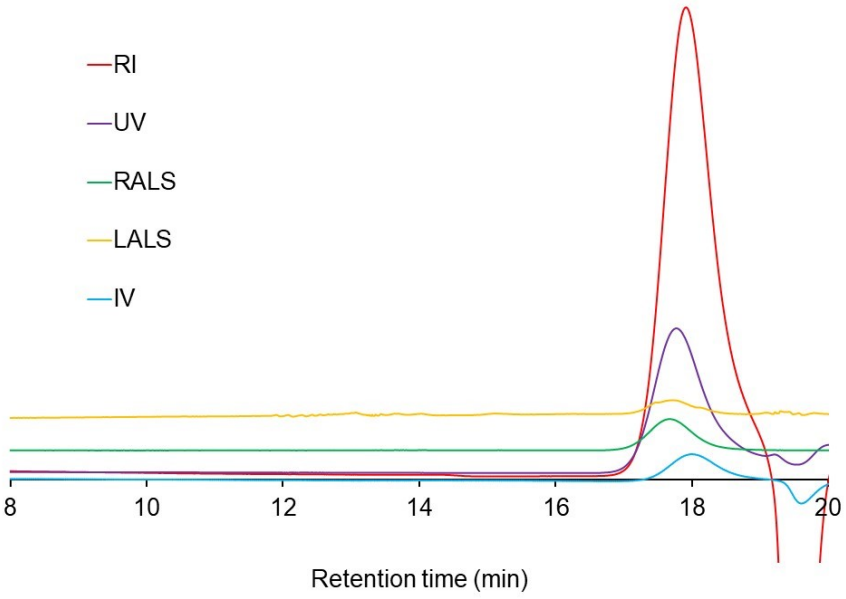

Figure 3-21. SEC trace of polymerization by AGET ATRP with trehalose monomer, 1 mg/mL insulin, and 10 equiv TPMA : 1 equiv $CuBr_2$.

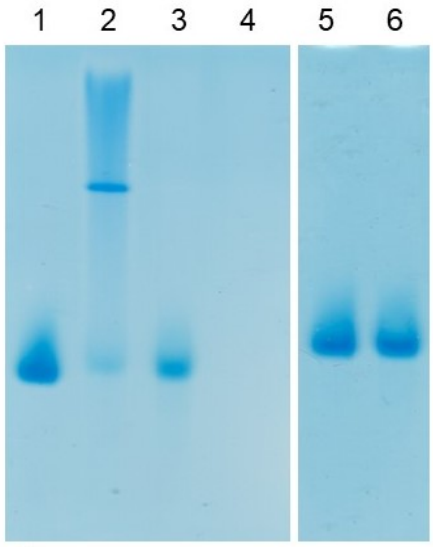

Figure 3-22. Native PAGE with control polymerizations (Lane 1: Insulin, Lane 2: Insulin-trehalose glycopolymer polymerization mixture, Lane 3: AGET ATRP conditions without initiator

and with insulin, Lane 4: AGET ATRP conditions without initiator or insulin, Lane 5: Insulin, Lane 6: AGET ATRP conditions with resin and insulin).

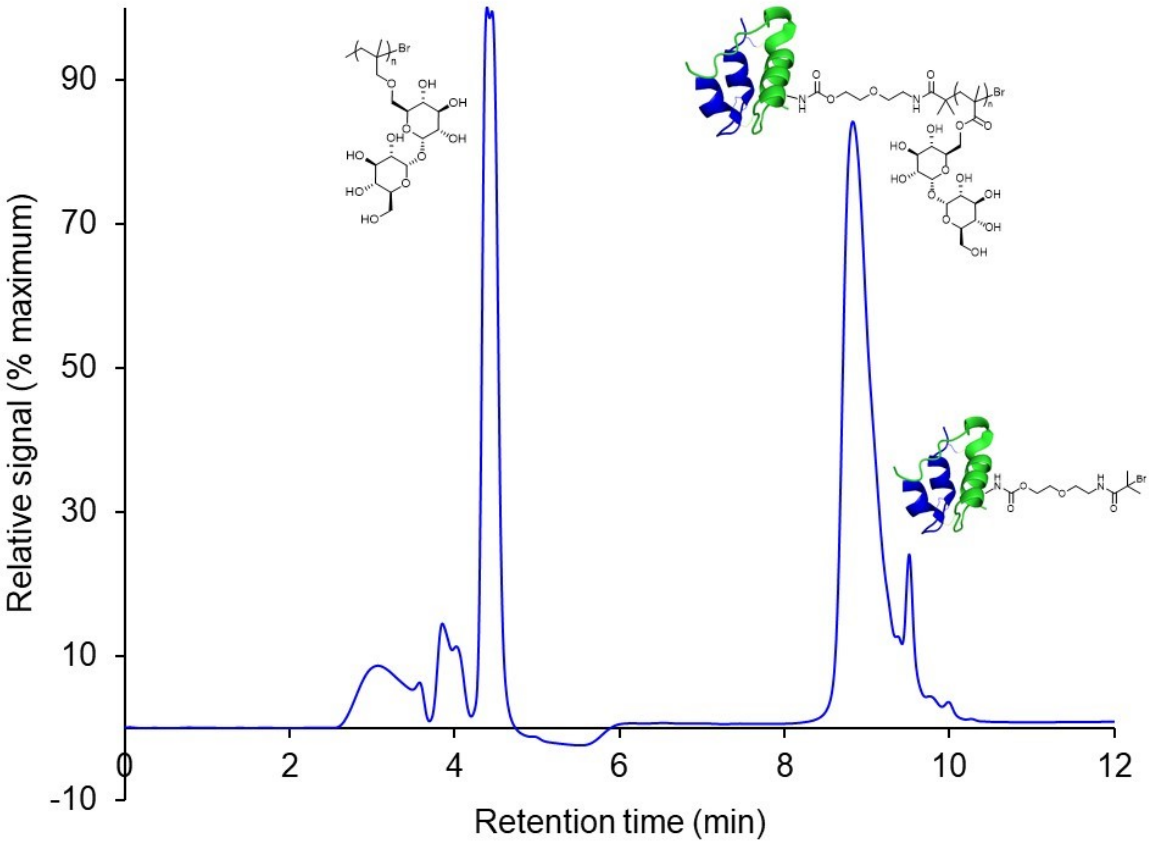

Figure 3-23. HPLC trace of insulin-trehalose glycopolymer polymerization mixture.

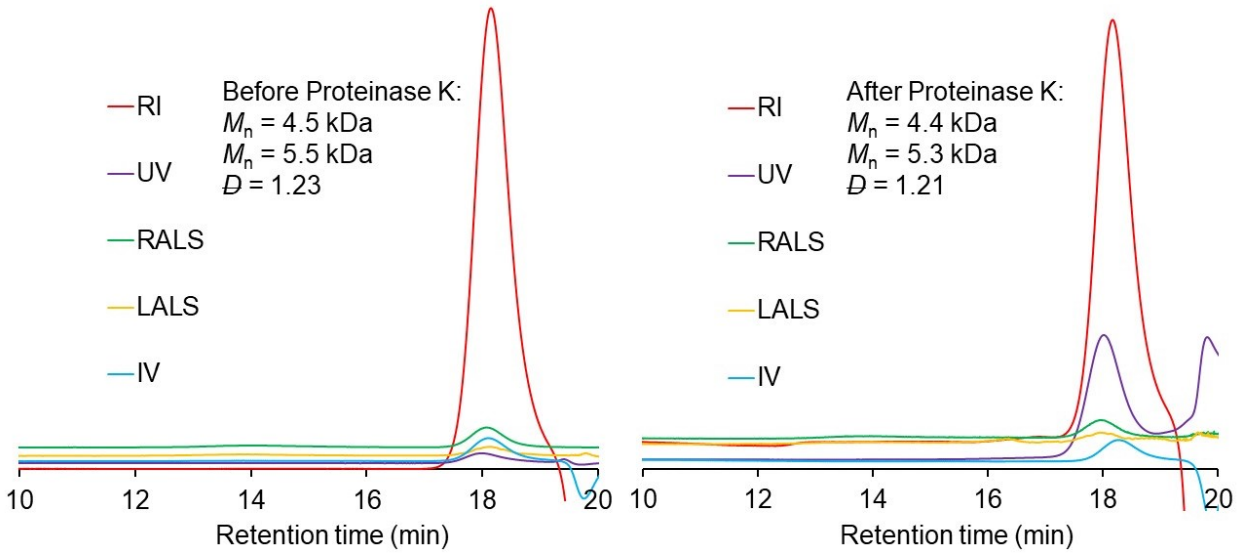

Figure 3-24. SEC traces of trehalose glycopolymer itself before and after incubation with Proteinase K.

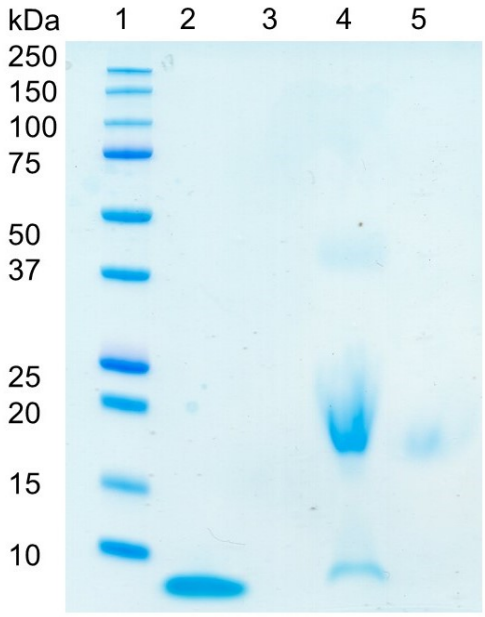

Figure 3-25. SDS PAGE of insulin-PEG conjugate (Lane 1: Ladder, Lane 2: Insulin, Lane 3: PEG, Lane 4: Crude insulin-PEG conjugate, Lane 5: Purified insulin-PEG conjugate).

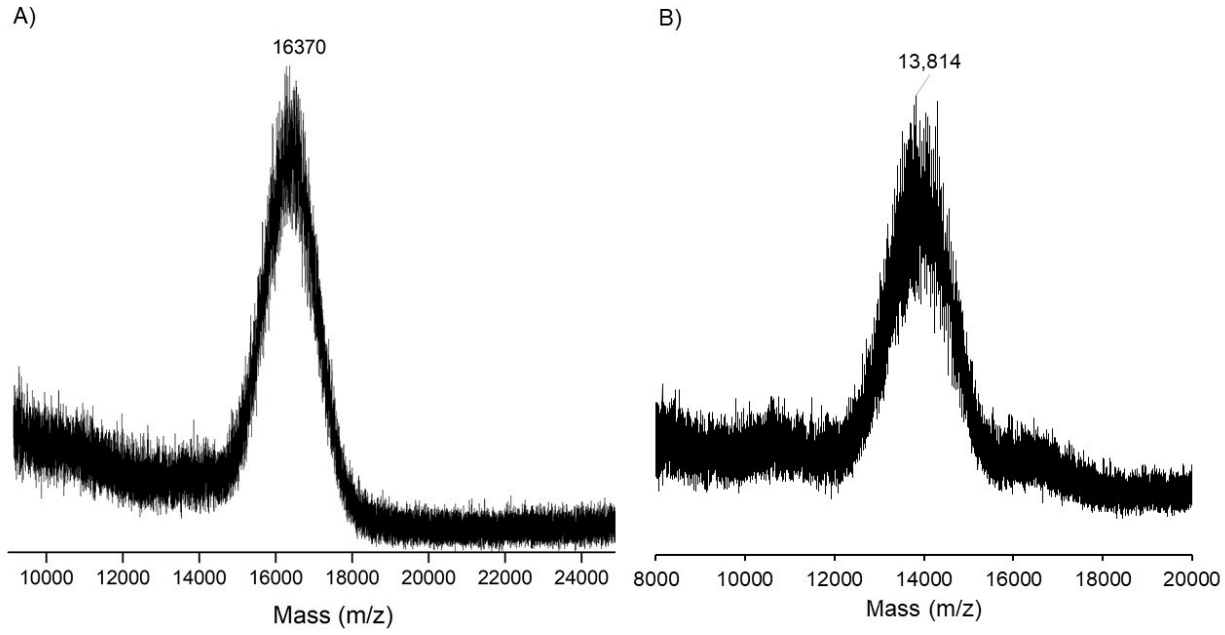

Figure 3-26. MALDI MS of insulin-PEG conjugate (A) intact and (B) reduced with 100 mM DTT.

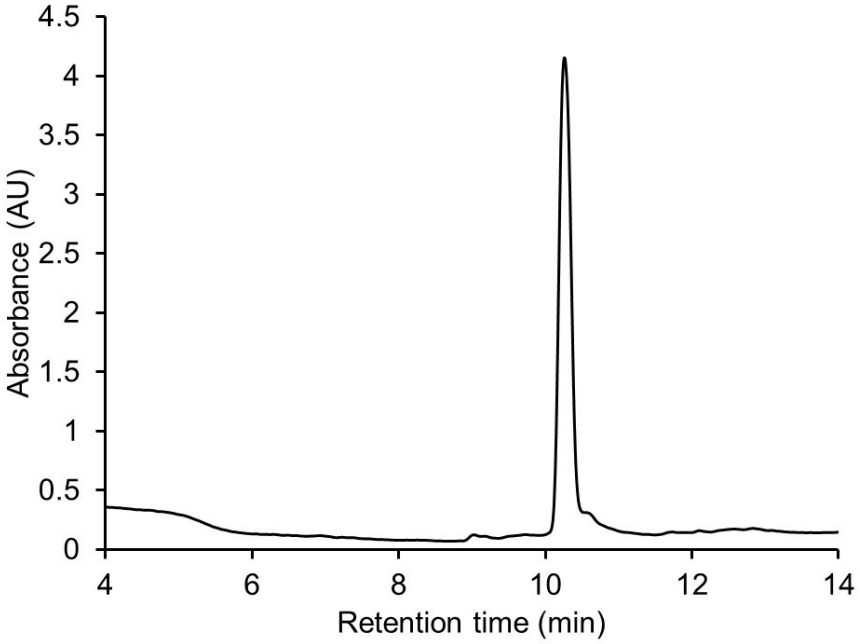

Figure 3-27. Analytical HPLC trace of insulin-PEG conjugate.

Table 3-1. Tandem MS results from purified insulin macroinitiator

Name	Monoisotopic mass (Da)	Intensity	Theoretical Mass (Da)	Error (Da)	Error (ppm)
LysB29					
B18	2023.0146	2.9358e+002	2023.0349	-0.0203	-10.0354
B21	2312.1042	2.7218e+002	2312.1082	-0.0040	-1.7136
B23	2525.1977	3.2198e+002	2525.2307	-0.0330	-13.0717
B24	2672.3277	4.7271e+003	2672.2991	0.0285	10.6788
B26	2982.4270	1.3868e+004	2982.4309	-0.0039	-1.3110
B27	3082.4512	1.1113e+004	3083.4786	-0.0273	-8.8656
Y3	623.2110	5.2549e+002	623.2177	-0.0067	-10.6785
Y4	724.2676	7.8433+002	724.2653	0.0023	3.1715
Y5	887.3322	6.0729e+002	887.3287	0.0035	3.9557
Y6	1034.4029	7.9903+002	1034.3971	0.0058	5.6535
PheB1					
N/A	N/A	N/A	N/A	N/A	N/A

3.5 References

(1) Centers for Disease Control, National diabetes statistics report: estimates of diabetes and its burden in the United States, 2014. In *Atlanta, GA: US Department of Health and Human Services*, 2014.

(2) Guariguata, L.; Whiting, D. R.; Hambleton, I.; Beagley, J.; Linnenkamp, U.; Shaw, J. E. Global estimates of diabetes prevalence for 2013 and projections for 2035. *Diabetes Res. Clin. Pract.* **2014,** *103*, 137-149.

(3) Association, A. D. Standards of medical care in diabetes—2017 abridged for primary care providers. *Clinical Diabetes* **2017,** *35*, 5-26.

(4) Pryce, R. Diabetic ketoacidosis caused by exposure of insulin pump to heat and sunlight. *Br. Med. J.* **2009,** *338,* a2218.

(5) Sluzky, V.; Tamada, J. A.; Klibanov, A. M.; Langer, R. Kinetics of insulin aggregation in aqueous solutions upon agitation in the presence of hydrophobic surfaces. *Proc. Natl. Acad. Sci. U. S. A.* **1991,** *88*, 9377-9381.

(6) Oliva, A.; Fariña, J.; Llabrés, M. Influence of temperature and shaking on stability of insulin preparations: degradation kinetics. *Int. J. Pharm.* **1996,** *143*, 163-170.

(7) Mancini, R. J.; Lee, J.; Maynard, H. D. Trehalose Glycopolymers for Stabilization of Protein Conjugates to Environmental Stressors. *J. Am. Chem. Soc.* **2012,** *134*, 8474-8479.

(8) Lee, J.; Lin, E. W.; Lau, U. Y.; Hedrick, J. L.; Bat, E.; Maynard, H. D. Trehalose Glycopolymers as Excipients for Protein Stabilization. *Biomacromolecules* **2013,** *14*, 2561-2569.

(9) Liu, Y.; Lee, J.; Mansfield, K. M.; Ko, J. H.; Sallam, S.; Wesdemiotis, C.; Maynard, H. D. Trehalose Glycopolymer Enhances Both Solution Stability and Pharmacokinetics of a Therapeutic Protein. *Bioconjugate Chem.* **2017,** *28*, 836-845.

(10) Pelegri-O'Day, E. M.; Paluck, S. J.; Maynard, H. D. Substituted Polyesters by Thiol–Ene Modification: Rapid Diversification for Therapeutic Protein Stabilization. *J. Am. Chem. Soc.* **2017,** *139*, 1145–1154.

(11) Messina, M. S.; Ko, J. H.; Yang, Z.; Strouse, M. J.; Houk, K. N.; Maynard, H. D. Effect of trehalose polymer regioisomers on protein stabilization. *Polym. Chem.* **2017,** *8*, 4781-4788.

(12) Uchio, T.; Baudyš, M.; Liu, F.; Song, S. C.; Kim, S. W. Site-specific insulin conjugates with enhanced stability and extended action profile. *Adv. Drug Delivery Rev.* **1999,** *35*, 289-306.

(13) Gliemann, J.; Gammeltoft, S. The biological activity and the binding affinity of modified insulins determined on isolated rat fat cells. *Diabetologia* **1974,** *10*, 105-113.

(14) Bontempo, D.; Maynard, H. D. Streptavidin as a Macroinitiator for Polymerization: In Situ Protein−Polymer Conjugate Formation. *J. Am. Chem. Soc.* **2005,** *127*, 6508-6509.

(15) Heredia, K. L.; Bontempo, D.; Ly, T.; Byers, J. T.; Halstenberg, S.; Maynard, H. D. In Situ Preparation of Protein−"Smart" Polymer Conjugates with Retention of Bioactivity. *J. Am. Chem. Soc.* **2005,** *127*, 16955-16960.

(16) Lele, B. S.; Murata, H.; Matyjaszewski, K.; Russell, A. J. Synthesis of Uniform Protein−Polymer Conjugates. *Biomacromolecules* **2005,** *6*, 3380-3387.

(17) Averick, S.; Simakova, A.; Park, S.; Konkolewicz, D.; Magenau, A. J. D.; Mehl, R. A.; Matyjaszewski, K. ATRP under Biologically Relevant Conditions: Grafting from a Protein. *ACS Macro Lett.* **2012,** *1*, 6-10.

(18) Liu, J.; Bulmus, V.; Herlambang, D. L.; Barner-Kowollik, C.; Stenzel, M. H.; Davis, T. P. In situ formation of protein–polymer conjugates through reversible addition fragmentation chain transfer polymerization. *Angew. Chem., Int. Ed.* **2007,** *46*, 3099-3103.

(19) Boyer, C.; Bulmus, V.; Liu, J.; Davis, T. P.; Stenzel, M. H.; Barner-Kowollik, C. Well-Defined Protein−Polymer Conjugates via in Situ RAFT Polymerization. *J. Am. Chem. Soc.* **2007,** *129*, 7145-7154.

(20) De, P.; Li, M.; Gondi, S. R.; Sumerlin, B. S. Temperature-Regulated Activity of Responsive Polymer−Protein Conjugates Prepared by Grafting-from via RAFT Polymerization. *J. Am. Chem. Soc.* **2008,** *130*, 11288-11289.

(21) Zhang, Q.; Li, M.; Zhu, C.; Nurumbetov, G.; Li, Z.; Wilson, P.; Kempe, K.; Haddleton, D. M. Well-Defined Protein/Peptide–Polymer Conjugates by Aqueous Cu-LRP: Synthesis and Controlled Self-Assembly. *J. Am. Chem. Soc.* **2015,** *137*, 9344-9353.

(22) Lin, W.; Ma, G.; Ji, F.; Zhang, J.; Wang, L.; Sun, H.; Chen, S. Biocompatible long-circulating star carboxybetaine polymers. *J. Mater. Chem. B* **2015,** *3*, 440-448.

(23) Baudyš, M.; Uchio, T.; Mix, D.; Kim, S. W.; Wilson, D. Physical stabilization of insulin by glycosylation. *J. Pharm. Sci.* **1995,** *84*, 28-33.

(24) Liu, F.; Kim, S. W.; Baudys, M. Synthesis of insulin derivatives. US 6323311 B1, 2001.

(25) Hirsch, I. B. Insulin analogues. *N. Engl. J. Med.* **2005,** *352*, 174-183.

(26) Evans, M.; Schumm-Draeger, P.; Vora, J.; King, A. A review of modern insulin analogue pharmacokinetic and pharmacodynamic profiles in type 2 diabetes: improvements and limitations. *Diabetes, Obes. Metab.* **2011,** *13*, 677-684.

(27) Zhang, L.; Zhao, W.; Liu, X.; Wang, G.; Wang, Y.; Li, D.; Xie, L.; Gao, Y.; Deng, H.; Gao, W. Site-selective in situ growth of fluorescent polymer–antibody conjugates with enhanced antigen detection by signal amplification. *Biomaterials* **2015,** *64*, 2-9.

(28) Beals, J. M.; Cutler, G. B.; Doyle, B. L.; Hansen, R. J.; Li, S.; Shirani, S.; Zhang, L. Pegylated Insulin Lispro Compounds. US 20110105392 A1, 2011.

(29) Ren, L.; Zhang, J.; Hardy, C. G.; Doxie, D.; Fleming, B.; Tang, C. Preparation of cobaltocenium-labeled polymers by atom transfer radical polymerization. *Macromolecules* **2012,** *45*, 2267-2275.

(30) Boehnke, N.; Kammeyer, J. K.; Damoiseaux, R.; Maynard, H. D. Stabilization of Glucagon by Trehalose Glycopolymer Nanogels. *Adv. Funct. Mater.* **2018,** *28*, 1705475.

(31) Anastasaki, A.; Haddleton, A. J.; Zhang, Q.; Simula, A.; Droesbeke, M.; Wilson, P.; Haddleton, D. M. Aqueous Copper-Mediated Living Radical Polymerisation of N-Acryloylmorpholine, SET-LRP in Water. *Macromol. Rapid Commun.* **2014,** *35*, 965-970.

(32) Ayala, J. E.; Samuel, V. T.; Morton, G. J.; Obici, S.; Croniger, C. M.; Shulman, G. I.; Wasserman, D. H.; McGuinness, O. P. Standard operating procedures for describing and performing metabolic tests of glucose homeostasis in mice. *Dis. Models & Mech.* **2010,** *3*, 525-534.

Chapter 4. Preparation of Self-Immolative Linkers for Blood Releasable Insulin-Trehalose Polymer Conjugate

4.1 Introduction

Insulin is an important protein therapeutic for the management of type I diabetes mellitus. To improve glycemic control, several insulin analogs with altered pharmacokinetics are available for clinical use.[1-3] Long-acting (or basal) insulin analogs alter the protein's solubility to precipitate upon subcutaneous injection, creating a depot for extended half-life, or include serum albumin binding domains to increase the circulation time. Long-acting insulin analogs are used to control baseline glucose throughout a full day, thus are more easily stored in conditions amenable to insulin stability. Rapid-acting insulin analogs decrease the protein's propensity to self-associate, enabling action onset within 15 min,[2] and are used to control blood glucose spikes near mealtimes. Issues of safety and efficacy stem from instability of insulin when the protein is exposed to elevated temperatures or mechanical agitation.[4-5] Because regular and rapid-acting insulins are administered on-the-go near mealtimes to lower blood glucose, often without the ability to refrigerate the protein, there is an interest in stabilized formulations without alteration of pharmacokinetics.

We previously reported the preparation of trehalose-glycopolymer conjugates in chapters 2 and 3 as a potentially extended action insulin that has improved stability to heat and mechanical agitation. In the first design, a trehalose glycopolymer was conjugated nonspecifically to 1-2 amines of insulin through reductive amination.[6] To improve the bioactivity of the conjugate, the synthesis strategy was redesigned to achieve a site-specific conjugate by a grafting from method.[7] While both conjugates exhibited stability to environmental stressors, covalent conjugation of a polymer increases the circulation time, resulting in an extended action insulin to control baseline blood glucose. To achieve the same stability as these conjugates without alteration of the protein's pharmacokinetics, we envisioned a strategy where conjugation of trehalose glycopolymer to

insulin would result in stable insulin, preventing aggregation during storage, while the polymer could be quickly released once administered.

Self-immolative linkers have been used to better control kinetics in prodrugs, sensors, and other materials.[8-10] These linkers consist of a protecting group (PG) that is removed by a trigger to activate elimination through an electronic cascade or cyclization of the spacer, releasing the molecule of interest (**Figure 4-1**). Linker kinetics can be tuned based on their mechanism.[8] For elimination, addition of electron density on the aromatic ring speeds up the kinetics of self-immolation because it stabilizes the quinone methide intermediate and facilitates dearomatization. For cyclization, increasing steric bulk of strategically placed substituents on the spacer speeds the cyclization due to the Thorpe-Ingold effect. In general, elimination is faster than cyclization because it does not involve a conformational change. The most common use for self-immolative linkers in biomolecule conjugates is to make antibody-drug conjugates that couple anticancer drugs to targeting antibodies.[11] Additionally, self-immolative linkers have been used in protein-polymer conjugates to prepare conjugates that release native protein in response to a variety of triggers.[12] However, these linkers are primarily designed for slow, controlled release of protein over time. To our knowledge, protein-polymer conjugates with fast-releasing self-immolative linkers have not yet been reported.

Scheme 4-1. Overview of self-immolative spacers and mechanisms used for linker designs. Protecting group (PG) is removed during activation to release molecule of interest (MI).

Herein, self-immolative spacers between insulin and a trehalose glycopolymer were designed and synthesized for use as linkers capable of being triggered for release by common components of blood. Specifically, linkers were designed to be triggered by albumin or reducing conditions in the blood using either elimination or cyclization mechanism. The kinetics of self-immolation and release were tested for each linker design.

4.2 Results and Discussion

Albumin is a major component of blood and is known to catalyze several proton-transfer reactions including Kemp elimination and β-elimination.[13-16] Shabat and coworkers have used 4-hydroxy-2-butanone as a trigger responsive to bovine and human serum albumins in self-immolative polymers for signal amplification.[17-18] With this inspiration, we designed the self-immolative linker **1** that would be triggered by base-catalyzed β-elimination by serum albumin. Synthesis of a polymer conjugate with this linker would be accomplished by grafting from an initiating site substituted on the benzyl ring.

Figure 4-1. Designs of blood-triggerable linkers screened.

The 1,4-elimination linker **1** was synthesized with an amine-reactive nitrophenyl carbonate for conjugation to insulin in order to assess preliminarily release kinetics. However, an unexpected molecular weight species were detected by LC-MS during initial conjugation attempts (**Figure 4-2 A**). After 30 min reaction time, insulin modified with 150 Da small molecules were detected that did not correspond to the expected 264 Da modifications. With an additional 2.5 h of reaction time, another 70 Da modification could be observed in the mass spectra. Upon closer examination, we hypothesized that the free amines on insulin catalyze the β-elimination to expose more primary amines, which also catalyze the self-immolation (**Figure 4-2 B**). The alkene byproduct may then modify the protein through Michael addition, resulting in insulin modified with 70 and 150 Da small molecules. To further probe this hypothesis, small molecule model studies were undertaken. Exposure of the linker to borate buffer pH 9.0 used during conjugation only showed a small amount of hydrolysis of the carbonate (Appendix C: **Figure 4-28**). In the presence of phenylalanine (Phe) as a source of free amine, a rapid decrease in the starting material peak was observed, with minimal hydrolysis as observed with buffer alone (Appendix C: **Figure 4-29**).

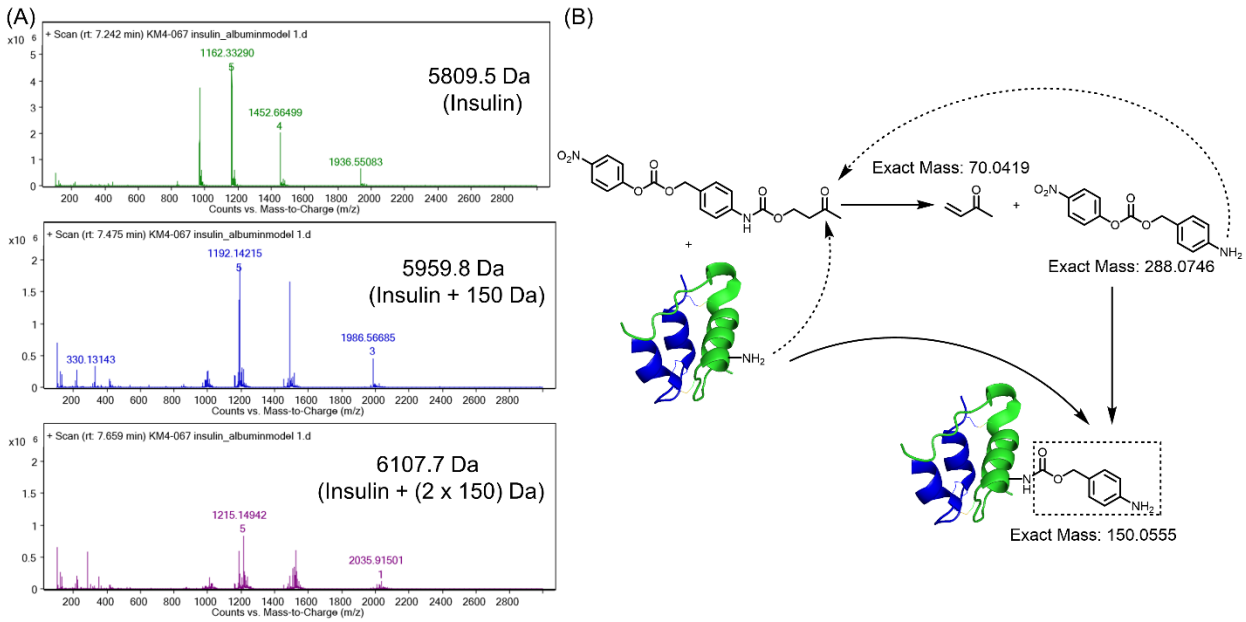

Figure 4-2. Unexpected product of conjugation with albumin-triggered linker **1**. (A) Characterization by LC-MS and (B) scheme of byproduct formation.

To mitigate the premature triggering of the linker during conjugation, the albumin-triggered linker **2** was designed to release a less basic thiol, which was expected not to further catalyze the β-elimination. To test this hypothesis, linker **1** was first incubated in the presence of 2-mercaptoethanol as a model free thiol to determine if the elimination could be catalyzed by any premature release of thiol. No significant change in the starting material peak was observed, indicating that a thiol does not catalyze the β-elimination (Appendix C: **Figure 4-30**). The kinetics of self-immolation of linker **2** before conjugation was first tested with Phe as a small molecule trigger. The starting material was slowly converted to the desired product, only reaching 22% conversion over 50 min and 66% conversion over 20 h (**Figure 4-3**). This is too slow for use with insulin. Yet, the slower kinetics of self-immolation than linker **1** may be because linker **2** lacked

the driving force of CO_2 formation. However, this linker may have utility for applications requiring a longer persisting conjugate.

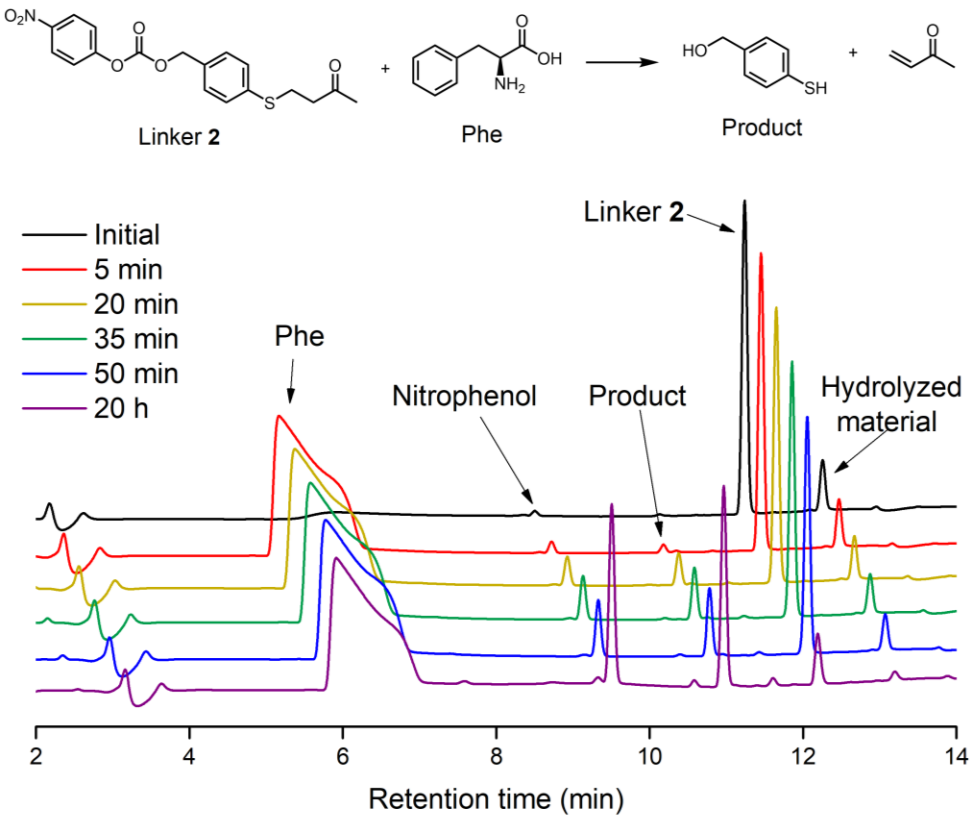

Figure 4-3. HPLC trace of albumin triggered linker **2** during reaction with Phe.

Free thiols including glutathione, cysteine, and albumin have a concentration of approximately 0.6 mM in the blood and glutathione has a concentration of 7 mM in the liver.[19-20] Additionally, some antibody-drug conjugates using disulfides as linkers have had issues with premature release of cargo from reduction during circulation.[21-22] Thus, we hypothesized thiols in the blood and liver could be used as a trigger to release insulin from a conjugate.

Thus, the thiol-triggered linker **3**, utilizing a cyclization mechanism, was prepared with pyridyl disulfide (PDS) as a model small molecule and conjugated to insulin through an amine-

reactive nitrophenyl activated carbonate. The kinetics were first tested with the small molecule conjugate under physiologically relevant thiol concentrations of 0.6 mM (blood) or 7 mM (liver) glutathione, monitoring the reaction by UV-vis and analytical HPLC (**Figure 4-4** and Appendix C: **Figure 4-31**). Absorbance at 343 nm rapidly increased from the formation of 2-pyridylthione following reduction of the disulfide. By HPLC, the fraction of insulin modified with multiple linkers rapidly decreased while the amount of free insulin peaked within 40 min for 0.6 mM glutathione and 20 min for 7 mM glutathione. These results were within the desired time range for insulin release, so linker **3** was studied further.

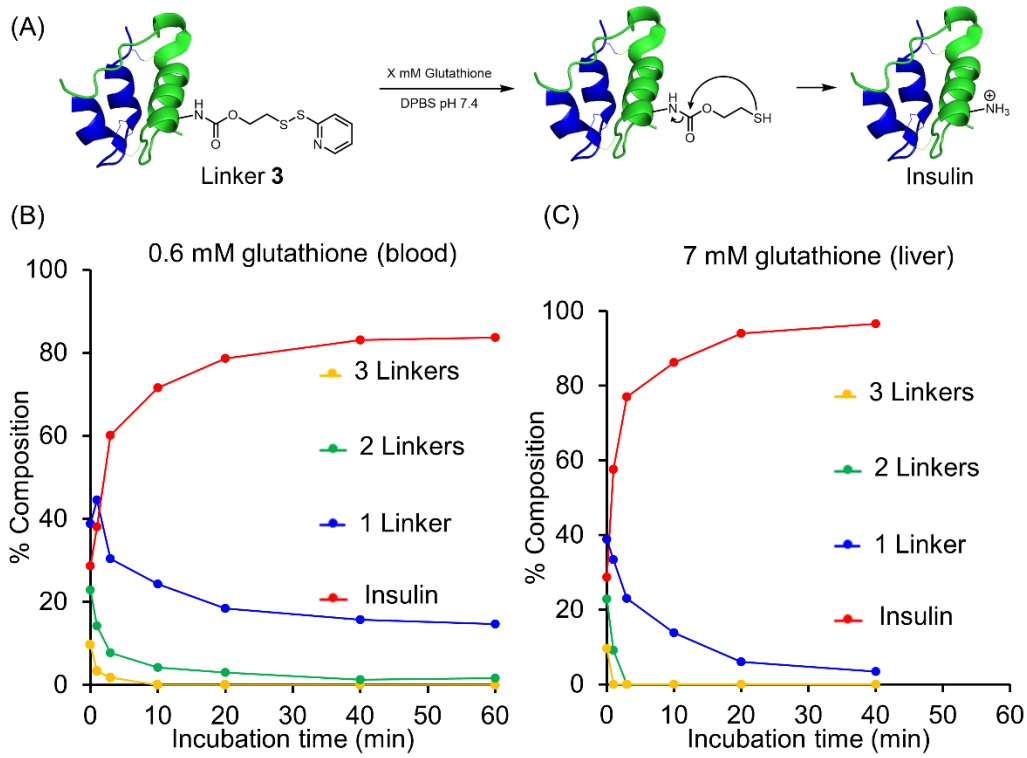

Figure 4-4. Kinetics of (A) insulin release conjugate of linker **3** with glutathione concentrations from (B) blood (0.6 mM) and (C) liver (7 mM).

An insulin-trehalose glycopolymer conjugate was then prepared to compare kinetics with the polymer (**Scheme 4-2**). An insulin macroinitiator was first prepared by reacting insulin with

an initiator derivative of linker **3**. The conjugate was then prepared by polymerizing from the insulin macroinitiator using conditions reported previously.[7] The conjugate was purified by semi-preparative HPLC and characterized by native PAGE and analytical HPLC (Appendix C: **Figure 4-34** and **Figure 4-35**). However, upon reduction with 7 mM glutathione (liver), no appreciable amount of insulin was released from the conjugate over 85 min, though a new peak possibly corresponding to reduction of one or more linkers on the conjugate appeared (Appendix C: **Figure 4-36**). This is most likely due to the increased steric bulk of the polymer slowing kinetics of disulfide exchange by hindering the attacking thiol.[23]

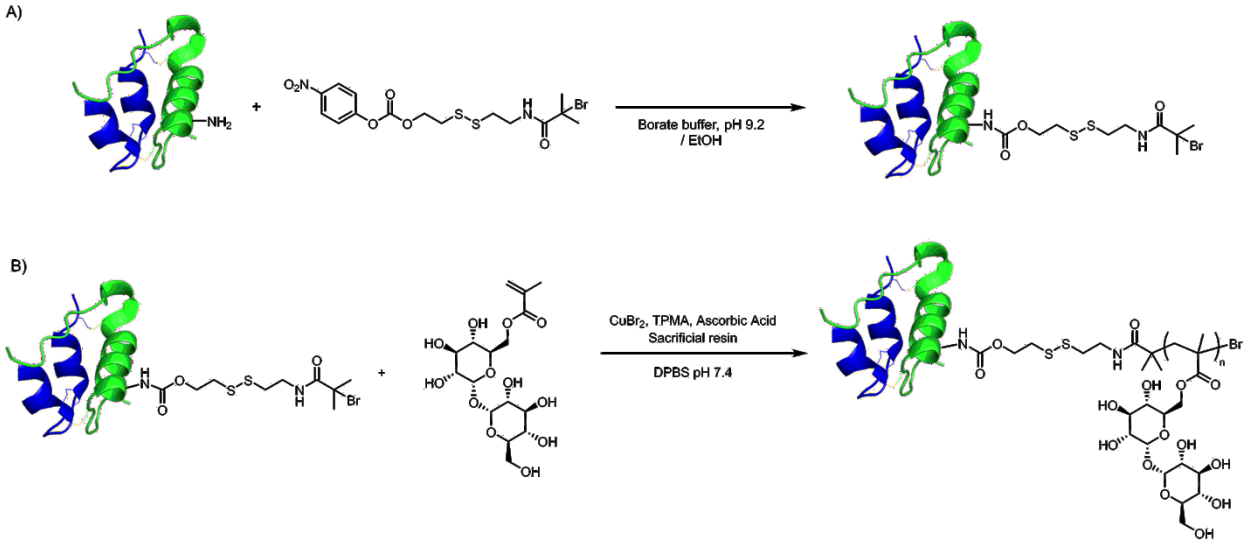

Scheme 4-2. Synthesis of insulin-linker **3** conjugate. (A) Synthesis of insulin-linker **3** macroinitiator and (B) polymerization from insulin-linker **3** macroinitiator.

To minimize the impact of polymer bulk on the triggering step of disulfide exchange, linker **4** was designed with the goal of polymer conjugation across the benzyl linker core to maintain a small molecule across the disulfide. Linker **4** was synthesized with nitrophenyl carbonate as conjugation handle for insulin and PDS across the disulfide as a model compound. The model linker **4** was exposed to reducing conditions (0.6 mM glutathione, blood) and kinetics were

monitored over time by analytical HPLC (**Figure 4-5**). A rapid decrease in the height of the starting material peak was observed within the first 5 minutes. Similar kinetics were observed following conjugation to insulin, though aqueous solubility and stability of the protein was lowered by modification with the hydrophobic small molecule (Appendix C: **Figure 4-38**).

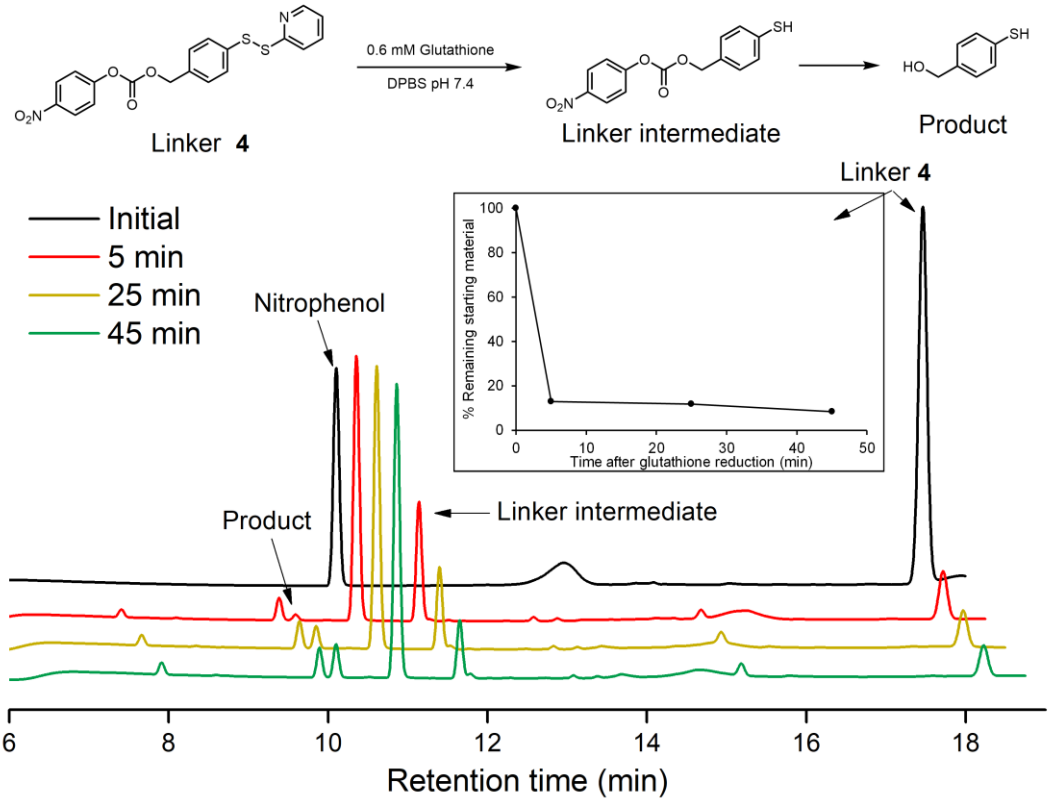

Figure 4-5. HPLC trace of benzyl disulfide linker **4** during reduction with 0.6 mM glutathione and (inset) kinetics of benzyl disulfide linker reduction.

Efforts to synthesize linker **4** with an initiator site substituted on the benzyl ring were ultimately unsuccessful. The presence of the thiol on the benzyl core complicated synthesis by poisoning catalysts and altering expected reactivity on the benzyl ring, resulting in no reaction or undesired side products. Additionally, it was decided that polymer added to the insulin as an excipient (not conjugated) would be a viable route to stabilize rapid-acting insulin because

trehalose added a 2 molar equivalent stabilized as well as conjugated at 1-2 sites.[24] Thus, this work was not pursued. Yet what was learned with regard to various linker designs having different kinetics of release triggered by relevant conditions in the blood that may be useful for other applications.

4.3 Conclusion

Herein, we have reported the synthesis of several blood-triggered self-immolative linkers for conjugation to insulin. Linkers were either triggered by serum albumin-catalyzed β-elimination or disulfide exchange with thiols in the blood or liver. Linker **1** was shown to self-catalyze the electronic cascade during conjugation to insulin. Linker **2** was designed to eliminate this self-triggering, but kinetics was slower because the linker did not possess the production of CO_2 as a driving force. Kinetics of release for linker **3** was rapid for small molecules but was too slow with the addition of the steric bulk of trehalose polymer across the disulfide. Linker **4** also exhibited fast kinetics as small molecule and conjugated to insulin. However, synthetic challenges limited access to addition of an initiator across the benzyl ring. Though these linkers are not suited for preparing rapid-acting stabilized insulin conjugates, they may be useful for other applications requiring trigger upon injection.

4.4 Appendix C

Analytical techniques

Nuclear Magnetic Resonance (NMR) spectra were recorded on a Bruker AV 400 MHz spectrometer. Trehalose monomer was purified by preparatory reverse phase HPLC on a Shimadzu HPLC system equipped with a UV detector using a Luna 5 μm C18 100A column (preparatory: 5 μm, 250 x 21.2 mm) with monitoring at λ = 215 nm and 254 nm. Gradient solvent system

(water:methanol = 90:10 to 40:60 over 20 min) was used as the mobile phase at a flow rate of 20 mL/min. Analytical HPLC for detection of insulin was conducted on an Agilent 1260 Infinity II LC System equipped with a UV detector using Zorbax SB300 C-3 column and a gradient solvent system (water:acetonitrile = 90:10 to 0:100 + 0.1 % trifluoroacetic acid over 17 min at 0.6 mL/min). Analytical HPLC to monitor reaction kinetics was conducted on an Agilent 1260 Infinity II LC System equipped with a UV detector using a Poroshell C18 column and a gradient solvent system (water:acetonitrile = 90:10 to 5:95 + 0.1 % trifluoroacetic acid over 17 min at 1.2 mL/min). Semi-preparative HPLC to purify the insulin macroinitiator was conducted on an Agilent 1260 Infinity II LC System equipped with a UV detector and Zorbax 300SB C18 column with a gradient solvent system (water:acetonitrile = 70:30 to 0:100 + 0.1 % trifluoroacetic acid over 20 min at 3 mL/min unless otherwise noted). LCMS was conducted on an Agilent 6530 Q-TOF LC/MS with 1260 Infinity LC equipped with Zorbax SB300 C-3 column and solvent gradient system (water:acetonitrile = 90:10 to 5:95 + 0.1 % formic acid over 17 min at 1.2 mL/min).

Methods and Materials

All materials were purchased from Sigma Aldrich or Fisher Scientific unless otherwise noted. Recombinant human insulin was purchased from Sigma-Aldrich (Lot no. 17A061-D). 4-Mercaptobenzyl alcohol was purchased from Combi-Blocks. Methacrylate trehalose monomer was synthesized as previously reported.[7] PDS alcohol was synthesized as previously reported.[25] Trehalose was purchased from The Healthy Essential Management Corporation (Houston, TX) and was azeotropically dried with ethanol and kept under vacuum until use.

Synthesis of phenyl (4-(hydroxymethyl)phenyl)carbamate

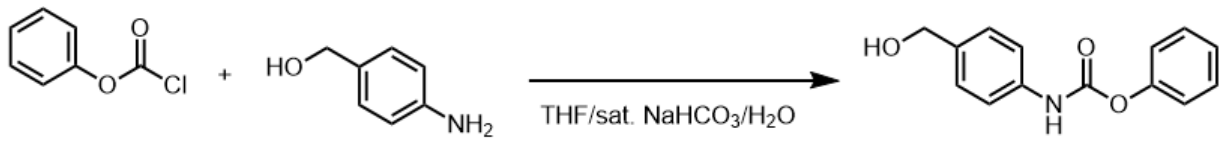

Synthesis was based on previously published literature protocol.[17] 4-Aminobenzyl alcohol (500 mg, 4.1 mmol, 1 eq.) was suspended in a 15 mL mixture of THF: sat. $NaHCO_3$: water (ratio 2:2:1). Phenyl chloroformate (638 µL, 4.5 mmol, 1.1 eq.) was added drop wise over 5 minutes. The solution was stirred at room temperature (21 °C) for 2 h. The solution was extracted with EtOAc and the organic phase washed twice with sat. NH_4Cl solution, dried with $MgSO_4$, and filtered. The solvent was removed under reduced pressure and the crude product purified by column chromatography on silica gel (8-100% acetone/hexanes) to give the product (987.5 mg, quant. yield) as a white solid. ^{1}H NMR (400 MHz, acetone-d6) δ 9.11 (s, 1H), 7.60 – 7.50 (m, 2H), 7.42 – 7.34 (m, 2H), 7.34 – 7.26 (m, 2H), 7.25 – 7.15 (m, 3H), 4.56 (d, J = 5.9 Hz, 2H), 4.10 (t, J = 5.8 Hz, 1H). IR: ν 3399, 3367, 3064, 3044, 2932, 2880, 1727, 1590, 1593, 1523, 1484, 1456, 1411, 1316, 1195, 1112, 1107, 1003, 937, 913, 890, 812, 787, 723, 726, 691, 630, 612 cm^{-1}.

Synthesis of 3-oxobutyl (4-(hydroxymethyl)phenyl)carbamate

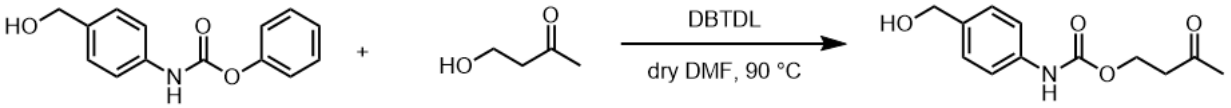

Synthesis was based on a similar procedure in the literature.[17] Phenyl (4-(hydroxymethyl)phenyl) carbamate (70 mg, 0.28 mmol, 1 eq.) was dissolved in dry DMF (2 mL), pre-heated to 90 °C. Dibutyltin dilaurate (DBTDL, 4 µL, 6.9 µmol, 0.024 eq,) and 4-hydroxy-2-butanone (248 µL, 2.8 mmol, 10 eq.) were immediately added. The reaction was monitored to completion by TLC (4:1 EtOAc:Hex) for 3 h. The solvent was removed under reduced pressure

and the crude product purified by column chromatography on silica gel (EtOAc:Hex 20-100%). The product was recovered as a yellow solid (58.1 mg, 88% yield). ^{1}H NMR (400 MHz, chloroform-d) δ 7.38 – 7.27 (m, 4H), 6.67 (d, J = 16.8 Hz, 1H), 4.64 (s, 1H), 4.43 (t, J = 6.1 Hz, 2H), 4.12 (q, J = 7.2 Hz, 2H), 2.82 (t, J = 6.1 Hz, 2H), 2.04 (s, 3H). ^{13}C NMR (400 MHz, Chloroform-*d*) δ 206.05, 137.29, 136.25, 129.56, 128.08, 65.02, 60.08, 42.77, 30.35. IR: ν 3320, 3262, 2977, 2923, 2872, 1728, 1704, 1615, 1595, 1542, 1471, 1416, 1391, 1361, 1323, 1247, 1224, 1166, 1100, 1071, 1012, 823, 794,771, 740 cm^{-1}.

Synthesis of linker 1

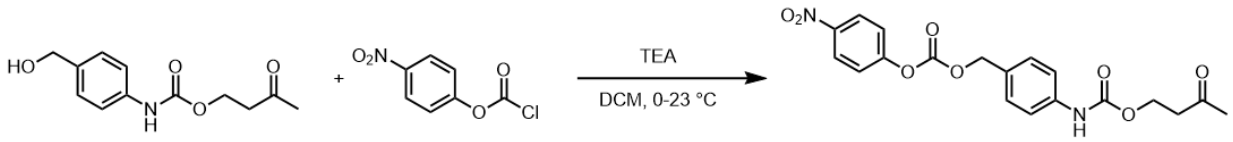

In a flame-dried round bottom flask under argon, 3-oxobutyl (4-(hydroxymethyl)phenyl)carbamate (100 mg, 0.42 mmol, 1 eq.) was dissolved in 0.5 mL anhydrous DCM with anhydrous TEA (88 µL, 0.63 mmol, 1.5 eq.) in a 0 °C ice bath. To this was added nitrophenyl chloroformate (170 mg, 0.84 mmol, 2 eq.). The reaction was left to rise to room temperature 23 °C and stirred 4 h. The reaction mixture was diluted with DCM and washed with 0.1 M HCl, water, and brine, dried with $MgSO_4$, and purified with silica gel chromatography (8-66% EtOAc/Hexanes). The product was isolated as a yellow solid (40.0 mg, 24% yield). ^{1}H NMR (400 MHz, chloroform-d) δ 8.27 (d, J = 9.2 Hz, 2H), 7.42 – 7.33 (m, 4H), 6.64 (s, 1H), 5.24 (s, 2H), 4.45 (t, J = 6.1 Hz, 2H), 2.83 (t, J = 6.1 Hz, 2H), 2.21 (s, 3H). ^{13}C NMR (400 MHz, acetonitrile-d_3) δ 206.14, 155.72, 153.50, 152.49, 139.46, 129.62, 129.23, 125.29, 122.27, 118.46, 70.47, 59.97, 42.08, 29.34. IR: ν 3353, 3123, 3084, 2966, 2920, 1755, 1729, 1704,1602, 1598,

1522, 1491, 1416, 1348, 1285, 1235, 1207, 1163, 1096, 1066, 1036, 923, 863, 836, 805, 768, 751, 714, 664 cm^{-1}.

Conjugation of linker 1 to insulin

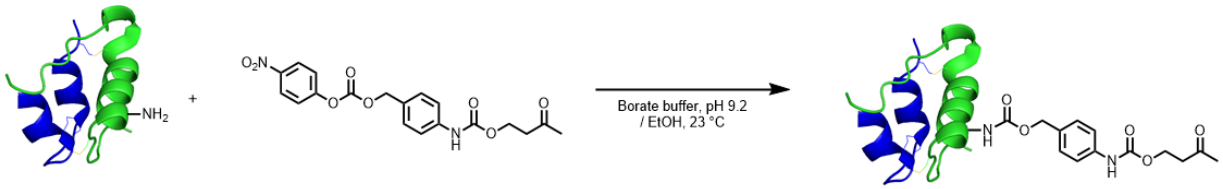

Insulin (0.2 mg, 3.4 x 10^{-5} mmol, 1 eq.) was dissolved in 40 µL borate buffer pH 9.0 and 60 µL EtOH. Linker **1** (0.69 mg, 1.7 µmol, 50 eq.) was dissolved in 100 µL EtOH and to this was added the insulin solution. The solution was stirred and monitored by LC-MS over 3 hours. MS (LC-MS) Expected 5808 (insulin), 6072 (insulin + 1 linker), 6336 (insulin + 2 linkers), 6600 (insulin + 3 linkers), Found 5809 (insulin), 5959 (insulin + 1 byproduct), 6107 (insulin + 2 byproducts) (**Figure 4-2**).

Synthesis of 4-tosyloxy-2-butanone

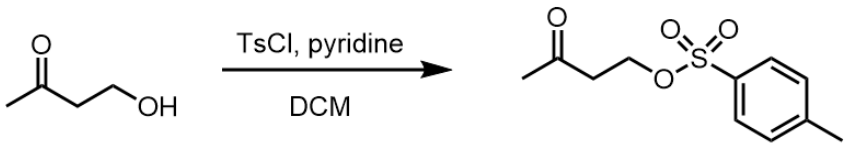

The procedure was based on a previously published protocol.[26] To a solution of 4-toluenesulfonyl chloride (1660 mg, 8.7 mmol, 1.5 eq.) and 4-hydroxy-2-butanone (0.5 mL, 5.8 mmol, 1 eq.) in dry DCM (11.6 ml) at 0 °C was added pyridine (1.4 mL, 17.4 mmol, 3 eq.). The mixture was stirred overnight (21 °C) while warming up to room temperature naturally. The solution was washed with water, and the organic layer was dried over magnesium sulfate. The

organic phase was concentrated under reduced pressure, and the residue was purified by silica gel column (2-20% EtOAc/Hexanes, Rf ~0.37 in 1:9 EtOAc/Hexanes) to afford the product as a clear oil at room temperature? or white solid in freezer (765.5 mg) in 55% yield. ^{1}H NMR (400 MHz, chloroform-*d*) δ 7.79 (d, J = 8.4 Hz, 2H), 7.35 (d, J = 7.9 Hz, 2H), 4.25 (t, J = 6.4 Hz, 2H), 2.83 (t, J = 6.4 Hz, 2H), 2.45 (s, 3H), 2.15 (s, 3H).

Synthesis of 4-((4-(hydroxymethyl)phenyl)thio)butan-2-one

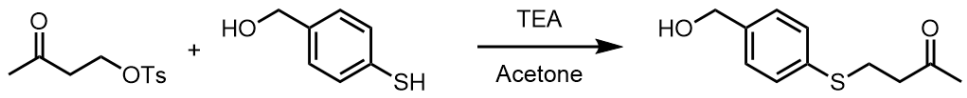

To a solution of 4-mercaptobenzyl alcohol (100 mg, 0.71 mmol, 1 eq.) and 4-tosyloxy-2-butanone (190 mg, 0.79 mmol, 1.1 eq.) in 4 mL anhydrous acetone was added TEA (200 µL, 1.4 mmol, 2 eq.). The reaction mixture was stirred for 2 h at room temperature (21 °C). Solvent was removed by rotary evaporation and the crude was purified by column chromatography (10-65% EtOAc/Hexanes). Solvent was removed to yield the product as a yellow oil (119.3 mg, 80% yield). ^{1}H NMR (400 MHz, Chloroform-*d*) δ 7.37 – 7.16 (m, 2H), 4.66 (s, 1H), 3.12 (dd, *J* = 7.6, 6.9 Hz, 1H), 2.75 (t, *J* = 7.3 Hz, 1H), 2.14 (s, 1H). ^{13}C NMR (400 MHz, Chloroform-*d*) δ 206.64, 139.17, 134.97, 129.82, 127.73, 64.87, 43.08, 30.12, 27.60. IR ν 3398, 2927, 2864, 1709, 1600, 1493, 1405, 1361, 1279, 1206, 1160, 1090, 1011, 892, 819, 798, 741 cm^{-1}. HRMS (ESI) calculated for $C_{11}H_{14}O_2S$ ($[M]^+$) 210.0892, found 210.0314.

Synthesis of linker 2

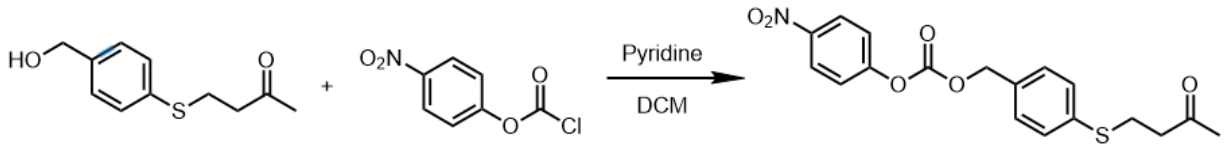

4-((4-(hydroxymethyl)phenyl)thio)butan-2-one (100 mg, 0.48 mmol, 1 eq.) was dissolved in DCM (1 mL) and pyridine (58 µL, 0.71 mmol, 1.5 eq.) and cooled with an ice bath to 0 °C. To this was added 4-nitrophenyl chloroformate (115 mg, 0.57 mmol, 1.2 eq) in DCM (1 mL) dropwise over 15 min. The reaction was stirred another 15 h, monitoring by TLC (3:1 DCM/EtOAc). The mixture was washed with sat. NH_4Cl, water, and brine, dried with $MgSO_4$, and filtered before solvent was removed by rotary evaporation. The crude was further purified by silica gel chromatography (0-40% EtOAc/DCM gradient) to afford the product as a yellow solid (77.1 mg, 44% yield). ^{1}H NMR (400 MHz, Chloroform-*d*) δ 8.27 (d, J = 9.2 Hz, 2H), 7.42 – 7.27 (m, 4H), 6.64 (s, 1H), 5.25 (s, 2H), 3.16 (t, J = 7.3 Hz, 2H), 2.78 (t, J = 7.2 Hz, 2H), 2.16 (s, 3H). ^{13}C NMR (400 MHz, Chloroform-*d*) δ 206.37, 155.50, 152.44, 145.46, 137.47, 131.96, 129.44, 129.27, 129.03, 125.33, 121.77, 70.52, 42.90, 30.12, 26.98. IR ν 3118, 3082, 2929, 2854, 1769, 1715, 16151596, 1520, 1493, 1408, 1348, 1256, 1216, 1160, 1090, 1032, 1012, 954, 933, 862, 801, 797, 727, 730, 686, 669 cm^{-1}.

Kinetics of self-immolation of linker 2

To 1 mg/mL linker **2** in EtOH was added an equal volume of 15 mg/mL phenylalanine in EtOH/DPBS pH 7.4. The mixture was monitored over time by HPLC (Poroshell column, 10-95% MeCN/water +0.1% TFA over 15 min) (**Figure 4-3**).

Synthesis of linker 3

Synthesis was based on previous reports in the literature.[27-28] PDS alcohol (300 mg, 1.60 mmol, 1 eq.) and triethylamine (0.25 mL, 1.76 mmol, 1.1 eq.) was dissolved in 9 mL ACN and cooled to 0 °C. Nitrophenyl chloroformate (355 mg, 1.76 mmol, 1 eq.) was added. The solution was left to rise to 23 °C and stirred for 5 hours. Solvent was removed en vacuo and the product was purified by column chromatography (10-60% EtOAc/Hexanes gradient) to afford a yellow oil (372.2 mg). The product was further purified by column chromatography (DCM) to remove nitrophenol impurity to yield the product as a clear oil (246.6 mg, 44% yield). ^{1}H NMR (400 MHz, Chloroform-*d*) δ 8.47 (ddd, J = 4.8, 1.8, 1.0 Hz, 2H), 7.68 – 7.56 (m, 2H), 7.52 (d, J = 8.3 Hz, 2H), 7.31 (d, J = 8.5 Hz, 2H), 7.09 (ddd, J = 6.7, 4.8, 1.7 Hz, 1H), 4.66 (d, J = 4.5 Hz, 2H), 1.67 (t, J = 5.5 Hz, 1H).

Synthesis of insulin-linker 3 conjugate

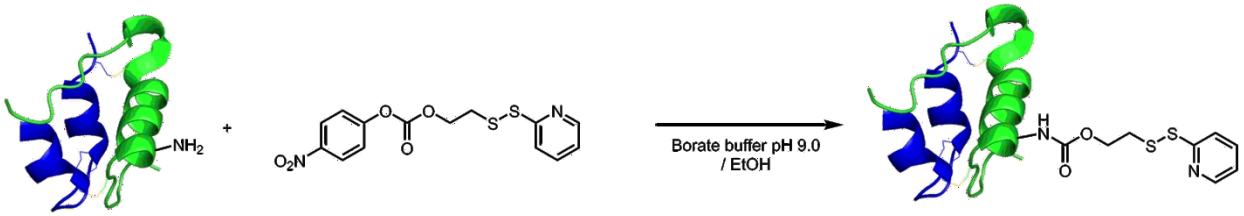

Insulin (1mg, 0.17 µmol, 1 eq.) was dissolved in 500 µL borate buffer pH 9 and 100 µL EtOH. Linker **3** (0.6 mg, 1.7 µmol, 10 eq.) was dissolved in 200 µL EtOH and to this was added the insulin solution. The solution was stirred for 0.5 hour, then another aliquot of linker **3** initiator (0.6 mg, 1.7 µmol, 10 eq.) dissolved in 200 µL EtOH was added. The solution was stirred for an additional 1 hour before desalting with PD-10 desalting column (centrifuge protocol with DPBS

pH 7.4) then concentration and buffer exchange with centriprep (MWCO 3 kDa) and DPBS pH 7.4 buffer. Macroinitiator was lyophilized after analytical HPLC characterization (Recovered: ~1 mg). MS (LC-MS) Expected 5808 (insulin), 6022 (insulin + 1 linker), 6236 (insulin + 2 linkers), 6450 Da (insulin + 3 linkers), Found 5809 (insulin), 6023 (insulin + 1 linker), 6237 (insulin + 2 linkers), 6450 Da (insulin + 3 linkers).

Kinetics of self-immolation of insulin-linker 3 conjugate

Stock solutions of glutathione were prepared in DPBS pH 7.4 at 1.2 mM or 14 mM glutathione. 100 µL Insulin-linker **3** conjugate (0.6 mg/mL) or DPBS pH 7.4 buffer was pipetted into a 96-well plate. Additional 100 µL DPBS buffer with or without glutathione was added to each well and the absorbance at 343 nm was monitored at 37 °C over time. Absorbance was background corrected using buffer or buffer + glutathione. Similarly, 50 µL insulin-linker **3** conjugate (0.6 mg/mL) was pipetted into an HPLC vial. Additional 50 µL DPBS buffer with glutathione was added and the AUC of insulin peaks were monitored over time (**Figure 4-4**).

Synthesis of cystamine bis initiator

In a flame-dried round bottom flask, cystamine dihydrochloride (800 mg, 3.55 mmol, 1 eq.) was dissolved in anhydrous DCM (5.5 mL) and anhydrous TEA (1.24 mL, 8.88 mmol, 2.5 eq.) and stirred for 10 minutes in a 10 °C ice bath. Bromoisobutyryl bromide (1.11 mL, 10.66 mmol, 3 eq.) was added dropwise to the stirring solution. This solution was stirred at room temperature 23 °C for 16 h. The solution was filtered and washed successively with 1 M HCl, sat.

sodium bicarbonate and sat. ammonium chloride solutions. The DCM layer was dried with $MgSO_4$, filtered, and the solvent was removed by rotary evaporation. The product was further purified by column chromatography (8-100% diethyl ether / hexanes gradient). The product (final peak) was recovered as a white solid (770.0 mg, 48% yield). ^{1}H NMR (400 MHz, chloroform-*d*) δ 7.14 (s, 2H), 3.61 (q, *J* = 6.2 Hz, 4H), 2.87 (t, *J* = 6.4 Hz, 4H), 1.96 (s, 12H). ^{13}C NMR (400 MHz, chloroform-*d*) δ 172.33, 62.59, 39.20, 37.41, 32.50. IR ν 3340, 2972, 2919, 1650, 1529, 1435, 1433, 1366, 1293, 1194, 1108, 1031, 928, 831, 730 cm^{-1}.

Synthesis of 2-bromo-N-(2-((2-hydroxyethyl)disulfaneyl)ethyl)-2-methylpropanamide

Cystamine bis initiator (300 mg, 0.67 mmol, 1 eq.) was dissolved in DCM (1.9 mL) and TEA was added (187 µL, 1.34 mmol, 2 eq.). To this was added 2-mercaptoethanol (61 µL, 0.87 mmol, 1.3 eq.) and the mixture was stirred for 16 h. The organic solution was washed with water 2x and brine, dried with $MgSO_4$, and filtered. The product was further purified by column chromatography (8-66% EtOAc/Hexanes gradient, last peak). The product was recovered as a clear oil (112.5 mg, 56% yield). ^{1}H NMR (400 MHz, Chloroform-*d*) δ 7.10 (s, 1H), 3.89 (t, J = 5.7 Hz, 2H), 3.62 (td, J = 6.5, 5.9 Hz, 2H), 2.89 (t, J = 5.8 Hz, 2H), 2.85 (t, J = 6.5 Hz, 2H), 1.95 (s, 6H). ^{13}C NMR (400 MHz, Chloroform-*d*) δ 172.40, 62.77, 60.25, 41.72, 39.25, 37.19, 32.54. IR ν 3340, 2980, 2927, 2871, 1651, 1523, 1437, 1369, 1280, 1194, 1112, 1044, 1000, 913, 851, 748, 730 cm^{-1}.

Synthesis of linker 3 initiator

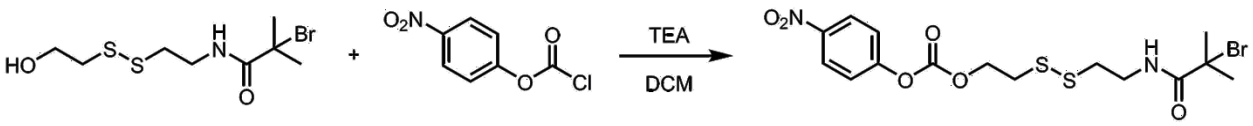

In a dry round bottom flask, 2-bromo-N-(2-((2-hydroxyethyl)disulfaneyl)ethyl)-2-methylpropanamide (170 mg, 0.56 mmol) was dissolved in 3.4 mL anhydrous DCM with 87 µL anhydrous TEA (0.62 mmol) and stirred at 0 °C for 10 minutes. To this was added nitrophenyl chloroformate (170 mg, 0.85 mmol). The solution was left to rise to 23 °C and then stirred for 15 h. The solution was washed with sat. ammonium chloride and brine. The aqueous washes were extracted with DCM, the organic phases were collected, dried with $MgSO_4$, and filtered. The solvent was removed by rotary evaporation and the product was further purified by column chromatography (16-100% DCM/hexanes). Solvent was removed en vacuo and the product was recovered as a yellow oil (105.4 mg, 40.4% yield). ^{1}H NMR (400 MHz, Chloroform-*d*) δ 8.29 (d, J = 9.2 Hz, 2H), 7.40 (d, J = 9.2 Hz, 2H), 7.07 (s, 1H), 4.56 (t, J = 6.5 Hz, 2H), 3.63 (q, J = 6.2 Hz, 2H), 3.05 (t, J = 6.6 Hz, 2H), 2.90 (t, J = 6.3 Hz, 2H), 1.95 (s, 6H). ^{13}C NMR (400 MHz, chloroform-*d*) δ 172.31, 155.39, 152.35, 145.53, 125.37, 121.81, 66.81, 62.74, 39.17, 37.58, 36.58, 32.52. IR ν 3301, 3127, 3060, 2933, 2859, 1763, 1643, 1594, 1520, 1512, 1449, 1381, 1345, 1262, 1221, 1193, 1163, 1102, 1062, 1040, 1036, 934, 856, 772, 748, 666 cm^{-1}.

Synthesis of insulin-linker 3 macroinitiator

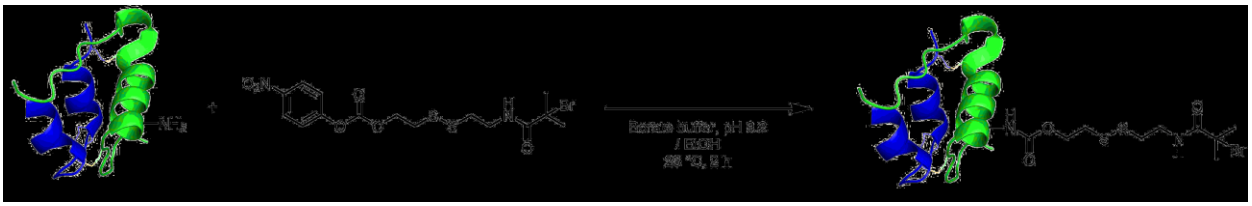

Insulin (10 mg, 1.7 mmol, 1 eq.) was dissolved in 10 mL borate buffer pH 9.0. Linker **3** initiator (8.0 mg, 25 mmol, 10 eq.) was dissolved in 100 µL EtOH and to this was added the insulin

solution. 3 mL EtOH was added to further solubilize the initiator. The solution was stirred for 1 hour, then another aliquot of linker **3** initiator (8.0 mg, 17 mmol, 10 eq.) dissolved in 100 µL EtOH was added. The solution was stirred for an additional 1 hour before centriprep (MWCO 3 kDa) buffer exchange into DPBS pH 7.4 with ~50% EtOH then into DPBS pH 7.4. Insulin-linker **3** macroinitiator was lyophilized after analytical HPLC characterization for grafting from (Recovered: 6.82 mg). MS (LC-MS) expected 5808, 6136, 6464, 6792 Da, found 5808, 6139, 6467, 6796 Da.

Synthesis of insulin-linker 3 trehalose polymer conjugate

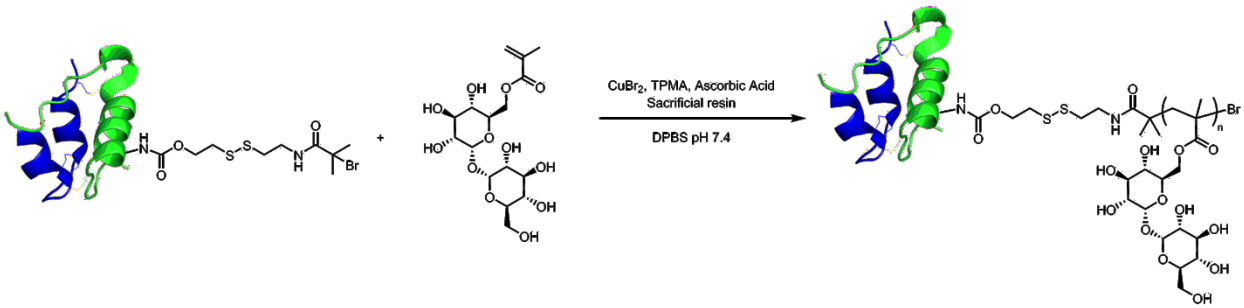

DPBS pH 7.4 was degassed by sparging with argon for 30 minutes. Methacrylate trehalose monomer (80.0 mg, 195 mmol, 30 eq.) and the sacrificial resin (23.4 mg, 6.5 µmol, 1 eq.) were placed in a Schlenk tube and this was evacuated and refilled with argon 3 times. A stock solution of $CuBr_2$ (1.45 mg, 6.5 µmol, 1 eq.) and TPMA (18.9 mg, 65 µmol, 10 eq.) was prepared in 100 µL degassed buffer and added to the flask. Ascorbic acid (0.69 mg, 3.9 µmol, 0.6 eq.) in 330 µL degassed DPBS was prepared and used to dissolve the insulin-linker **3** macroinitiator (~3.1 mg) and transfer it to the Schlenk flask. This initiated polymerization which was run at 23 °C for 16 h. The mixture was purified by centriprep (MWCO 3 kDa) into DPBS pH 7.4 (Stir with rinsed Cuprisorb with resin for 1 h before centriprep). Conjugate was isolated with semi-preparative

HPLC using Zorbax SB300-C18 column (3.0 mL/min, ACN/water + 0.1% TFA gradient: 30% for 1 min, 30-100% for 17 min, 30% 7 min). Fractions were desalted using spin columns then buffer exchanged to DPBS pH 7.4. Concentration was determined by BCA assay.

Kinetics of self-immolation of insulin-linker 3-trehalose polymer conjugate

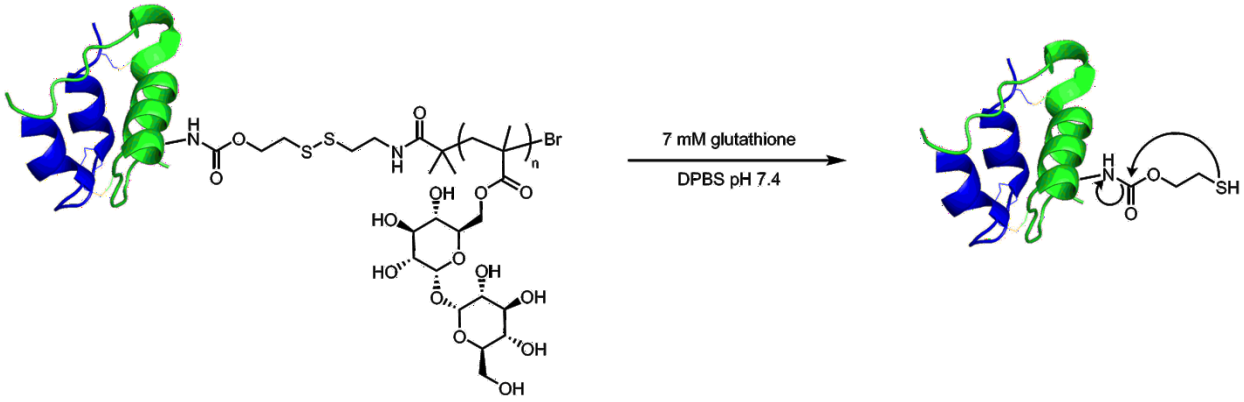

To 75 µL of the insulin-linker **3** trehalose polymer conjugate (0.27 mg/mL in DPBS) was added an equal volume glutathione (34.4 mg/mL in DPBS) for a final concentration of 7 mM. Release of insulin was monitored over time with HPLC (ACN/water + 0.1% TFA gradient: 1 min at 10%, 15 min 10-80%) (**Figure 4-36**).

Synthesis of PDS benzyl alcohol

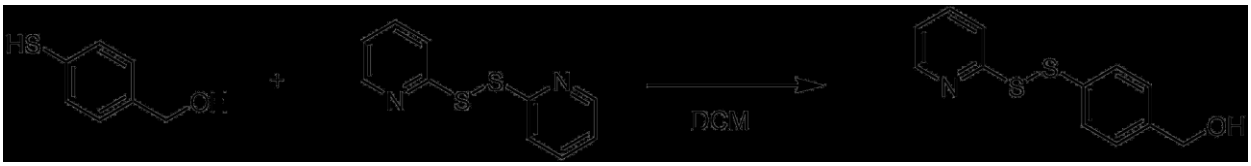

Synthesis was based on previous reports in the literature.[27] 4-Mercaptobenzyl alcohol (200 mg, 1.4 mmol, 1 eq.) was dissolved in DCM (1 mL) and mixed with a solution of 2,2′-dithiodipyridine (629 mg, 2.8 mmol, 2 eq.) in DCM (1 mL). After stirring for 3 h, the excess

solvent was removed by rotary evaporation, and the crude was purified by silica gel chromatography (ethyl acetate/hexane gradient 20-100%, for 1/1 (v/v) Rf = 0.35). After drying under vacuum, 4-(2-pyridyldithio)benzyl alcohol was obtained as a yellow oil (279.5 mg, 80% yield). ^{1}H NMR (400 MHz, chloroform-*d*) δ 8.47 (ddd, *J* = 4.8, 1.8, 1.0 Hz, 1H), 7.68 – 7.56 (m, 2H), 7.56 – 7.48 (m, 2H), 7.35 – 7.27 (m, 2H), 7.09 (ddd, *J* = 6.7, 4.8, 1.7 Hz, 1H), 4.66 (d, *J* = 4.5 Hz, 2H), 1.67 (d, *J* = 5.9 Hz, 1H). IR ν 3300, 3044, 2918, 2863, 1732, 1573, 1489, 1446, 1417, 1277, 1241, 1148, 1104, 1116, 1058, 1043, 1012, 987, 797, 757, 717 cm^{-1}.

Synthesis of linker 4

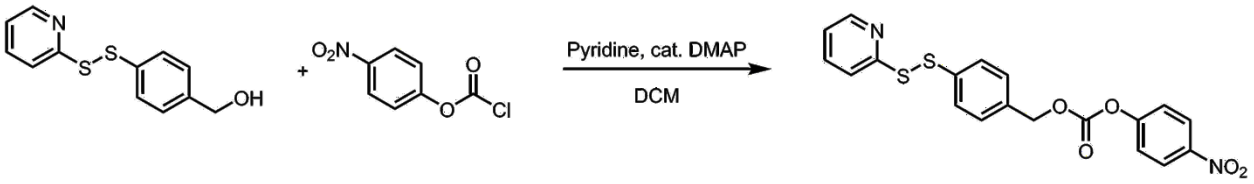

4-(2-Pyridyldithio)benzyl alcohol (150 mg, 0.6 mmol, 1 eq.) and catalytic DMAP (7 mg, 0.06 mmol, 0.1 eq.) was dissolved in anhydrous DCM (5 mL) and pyridine (97 µL, 1.2 mmol) and cooled with an ice bath. To this was added a solution containing 4-nitrophenyl chloroformate (242 mg, 1.2 mmol, 2 eq.) in anhydrous DCM (5 mL). After overnight stirring (14 h), the reaction mixture was washed with 2 N HCl (aq.), brine, and dried over $MgSO_4$. After removal of excess solvent by evaporation, the product was purified by silica gel chromatography (ethyl acetate/ hexane = 1/4 (v/v), R_f = 0.23, then another time with DCM) to obtain 4-nitrophenyl 4-(2-pyridyldithio)benzyl carbonate as a pale yellow oil (yield: 205.9 mg, 83%). ^{1}H NMR (400 MHz, Chloroform-*d*) δ 8.51 – 8.45 (m, 1H), 8.27 (d, J = 9.3 Hz, 2H), 7.65 – 7.59 (m, 1H), 7.56 (d, J = 8.3 Hz, 2H), 7.38 (d, J = 6.2 Hz, 2H), 7.36 (d, J = 7.0 Hz, 2H), 7.12 (td, J = 4.9, 3.5 Hz, 1H), 5.25

(s, 2H). IR ν 3083, 2959, 1762, 1616, 1592, 1521, 1491, 1446,1418, 1376, 1335, 1270, 1253, 1202, 1110, 1044, 1013, 986, 917, 862, 802, 753, 669 cm^{-1}.

Kinetics of self-immolation of linker 4

To 1 mg/mL linker **4** in EtOH was added and equal volume 1.2 mM glutathione in DPBS pH 7.4. The mixture was monitored over time by HPLC (Poroshell column, 10-95% MeCN/water +0.1% TFA over 15 min) (**Figure 4-5**).

Conjugation of linker 4 to insulin

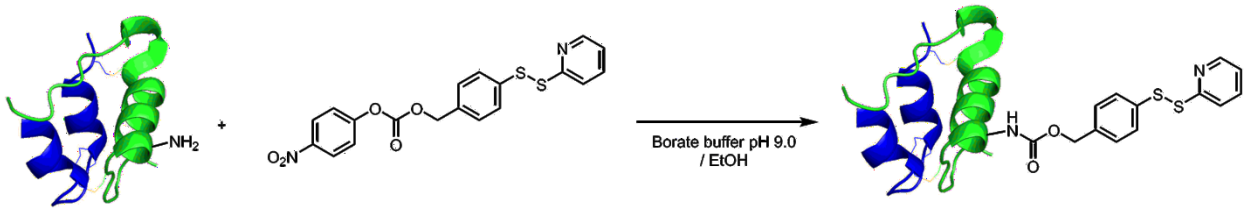

Insulin (0.5 mg, 8.5 x 10^{-5} mmol, 1 eq.) was dissolved in 250 µL borate buffer pH 9 and 50 µL EtOH. Linker **4** (0.4 mg, 8.5 x 10^{-4} mmol, 10 eq.) was dissolved in 100 µL EtOH and to this was added the insulin solution. The solution was mixed at 4 °C for 1 hour, then another aliquot of linker **4** (0.4 mg, 8.5 x 10^{-4} mmol, 10 eq.) dissolved in 100 µL EtOH was added. The solution was mixed for an additional 2 hours before buffer exchange with centriprep (MWCO 3 kDa) with borate buffer pH 9.5/EtOH then DPBS pH 7.4. MS (LC-MS) expected 5808, 6084, 6360, 6636 Da, found 5805, 6084, 6360, 6636 Da.

Kinetics of self-immolation of insulin-linker 4 conjugate

To insulin-linker **4** conjugate in DPBS pH 7.4 was added an equal volume 1.2 mM glutathione in DPBS pH 7.4. The mixture was monitored over time by HPLC (Zorbax SB300 C3 column, 10-95% MeCN/water +0.1% TFA over 15 min) (**Figure 4-38**).

Figures

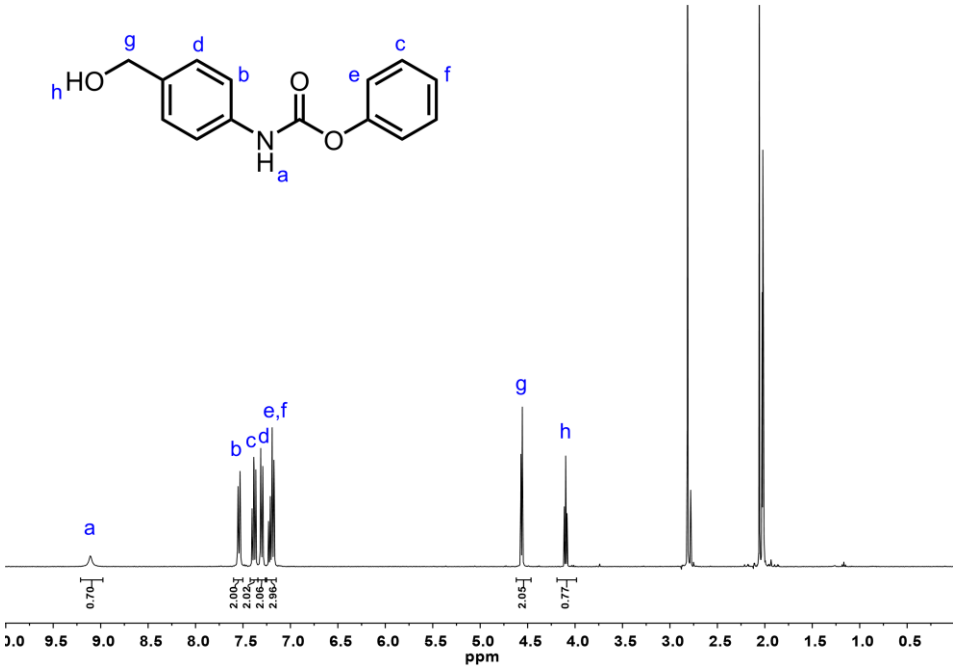

Figure 4-6. ^{1}H-NMR of phenyl (4-(hydroxymethyl)phenyl)carbamate in acetone-D6

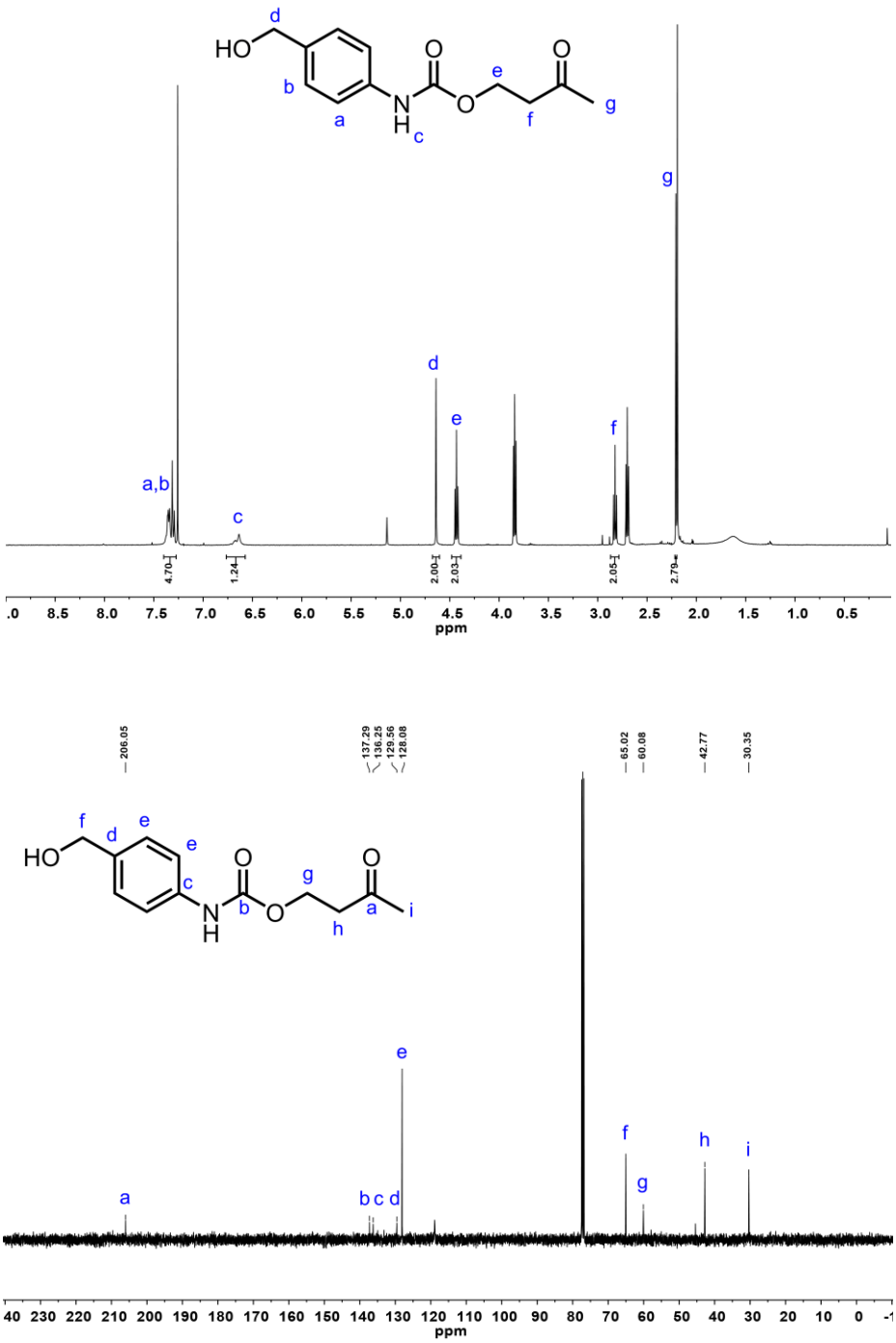

Figure 4-7. ^{1}H- and ^{13}C-NMR of 3-oxobutyl (4-(hydroxymethyl)phenyl)carbamate in acetone-D6

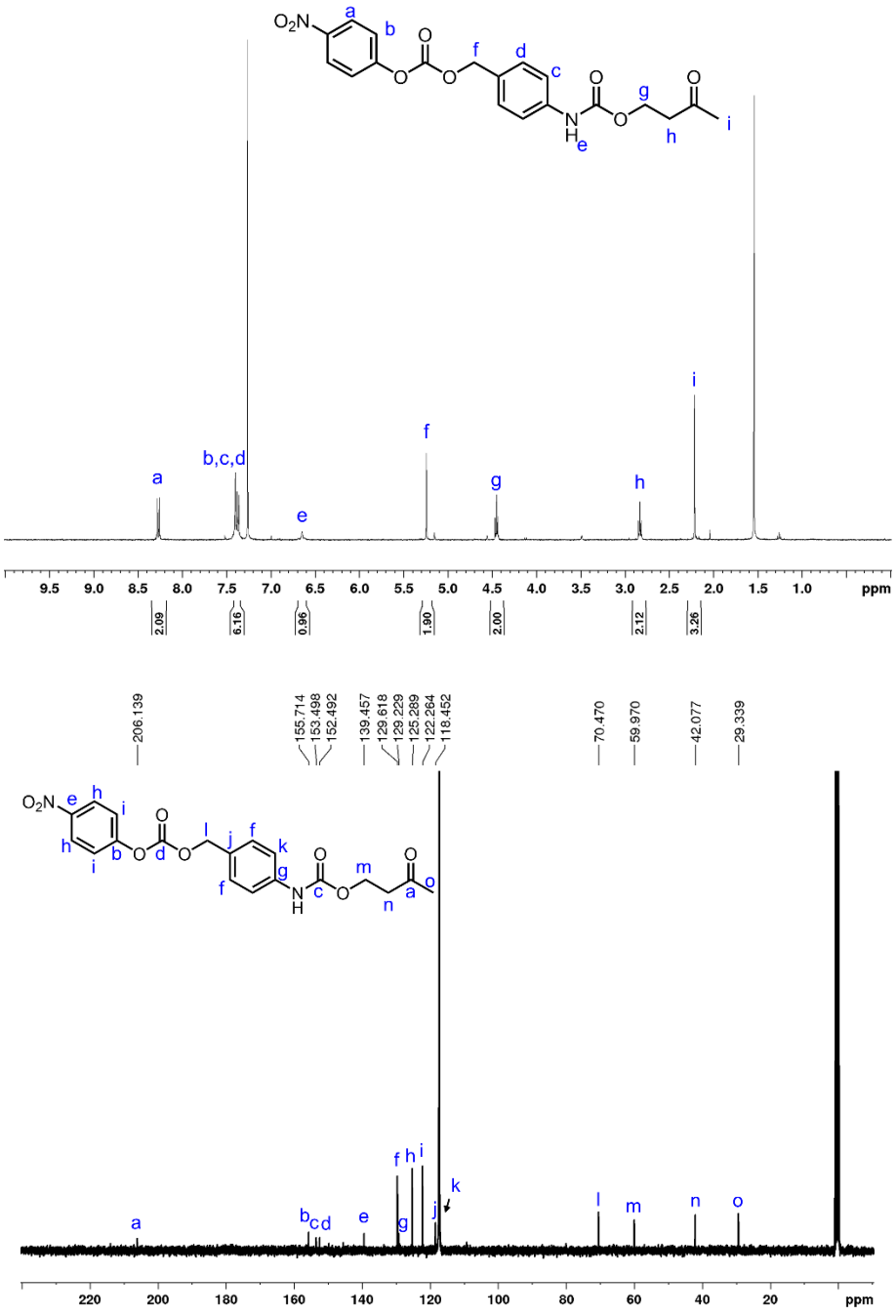

Figure 4-8. ^{1}H- and ^{13}C-NMR of linker **1** in $CDCl_3$

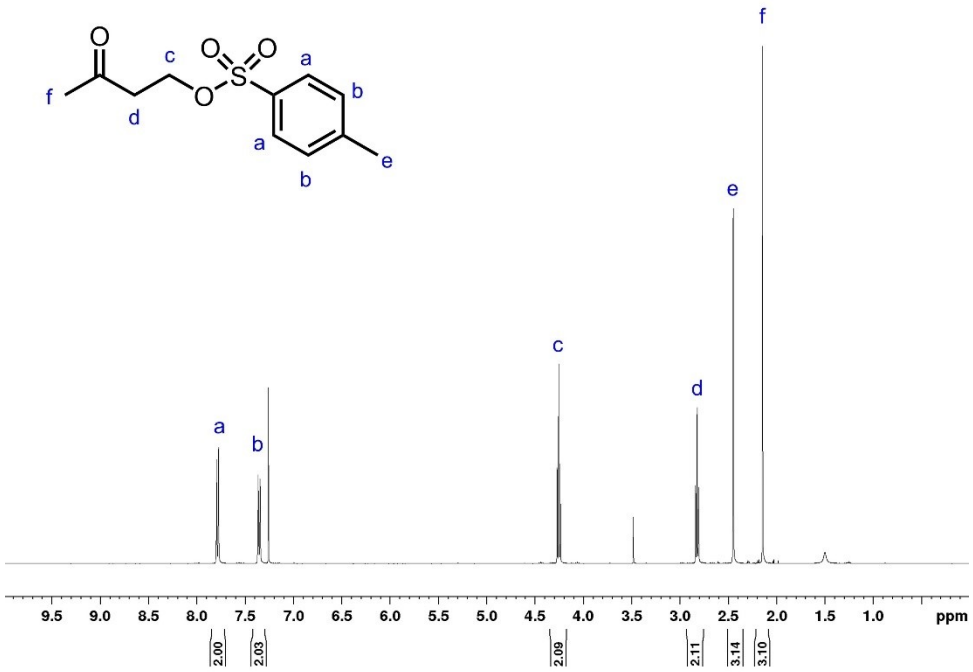

Figure 4-9. ^{1}H-NMR of 4-tosyloxy-2-butanone in $CDCl_3$

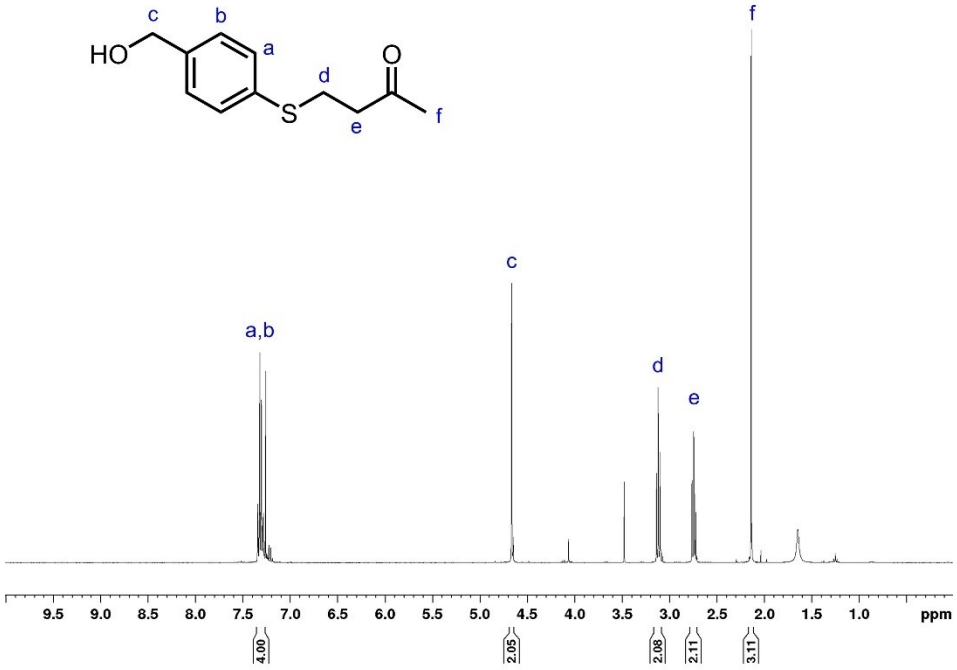

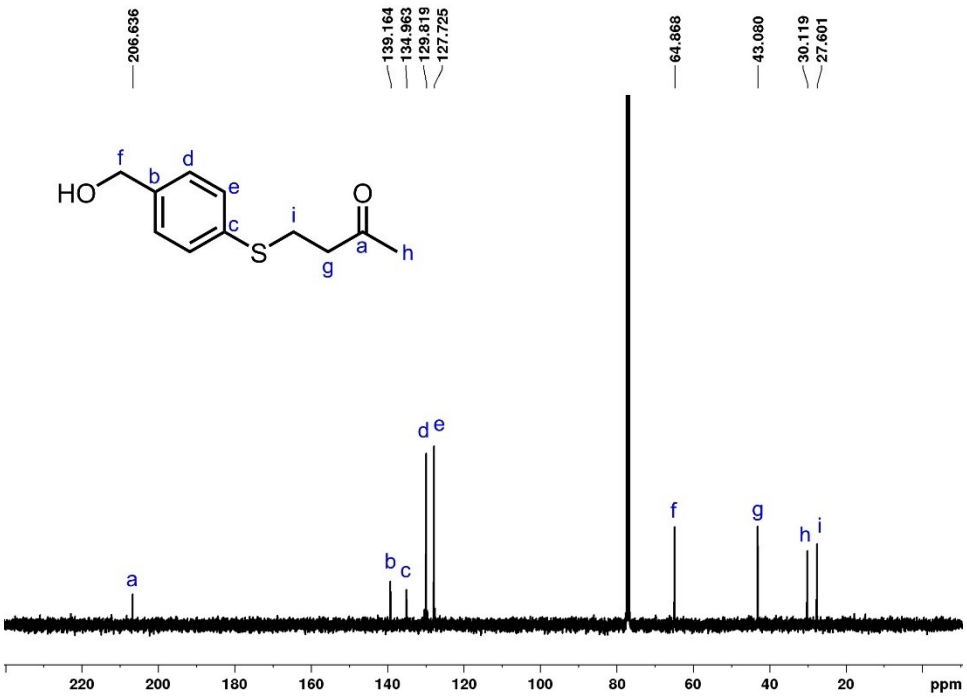

Figure 4-10. ^{1}H- and ^{13}C-NMR of 4-((4-(hydroxymethyl)phenyl)thio)butan-2-one in $CDCl_3$

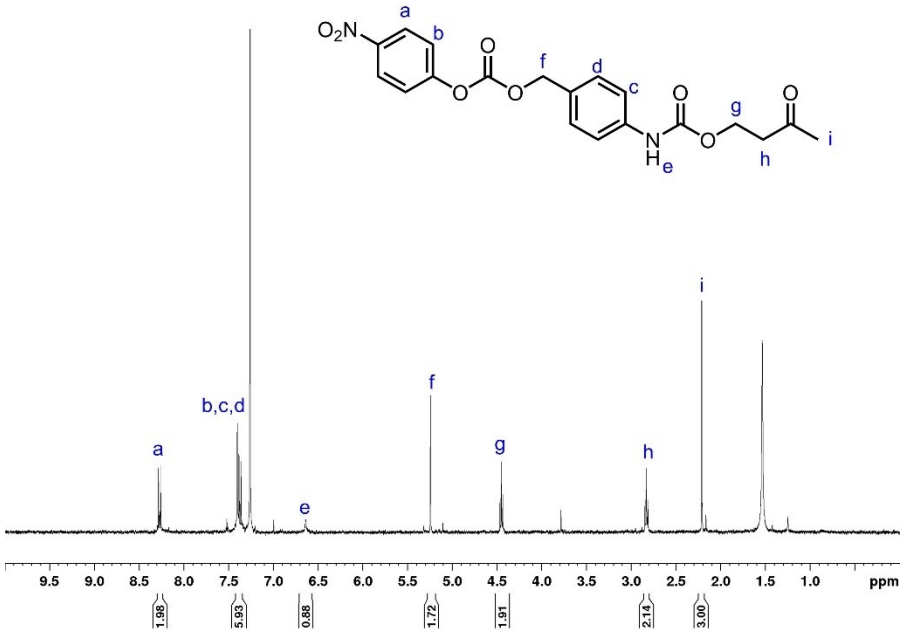

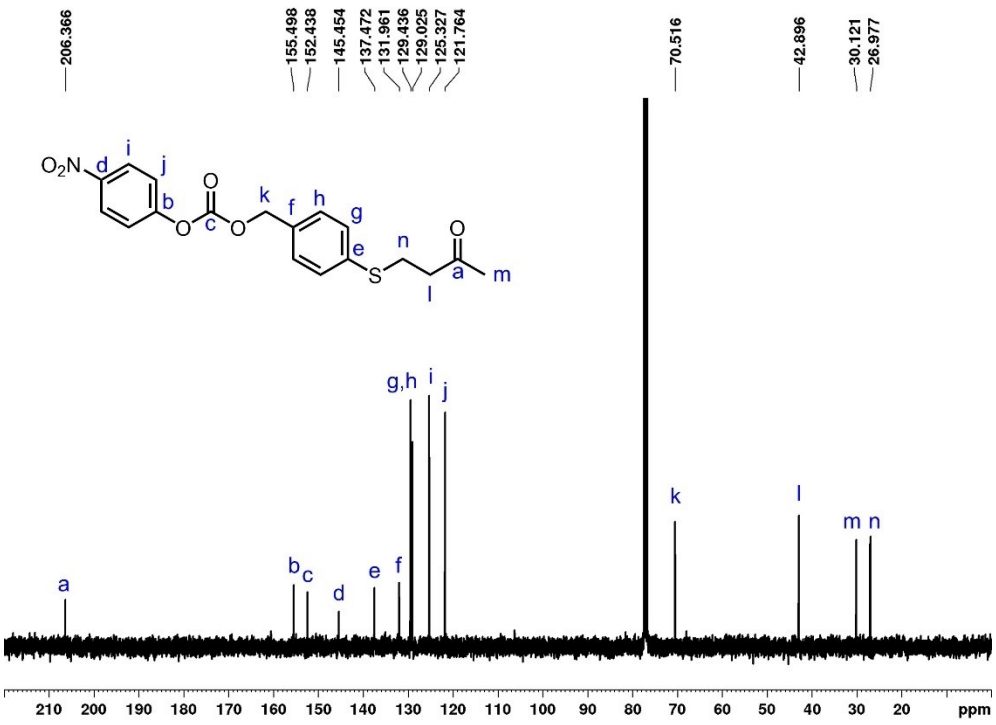

Figure 4-11. ^{1}H- and ^{13}C- NMR of linker **2** in $CDCl_3$

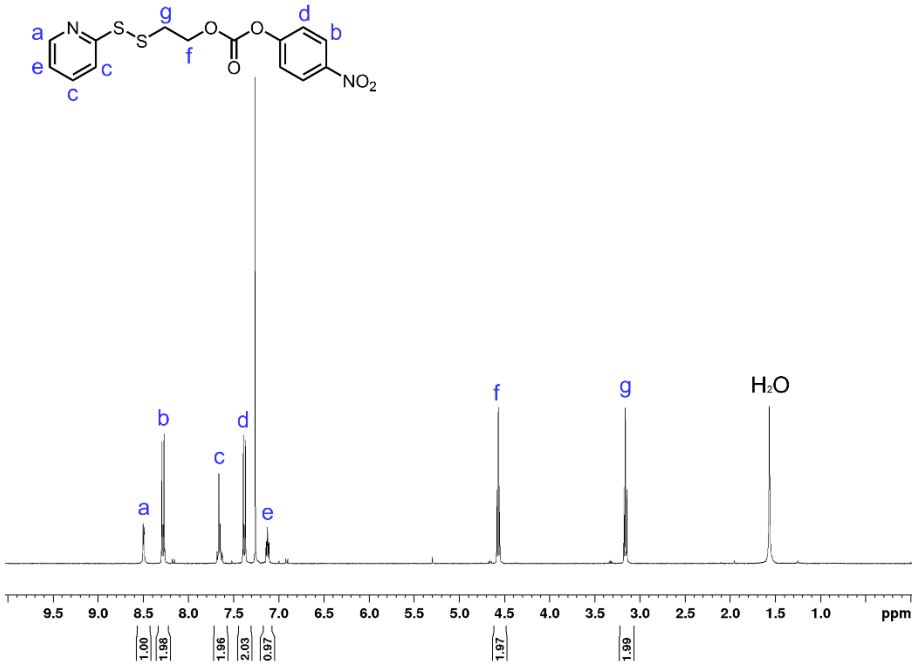

Figure 4-12. ^{1}H-NMR of linker **3** in $CDCl_3$

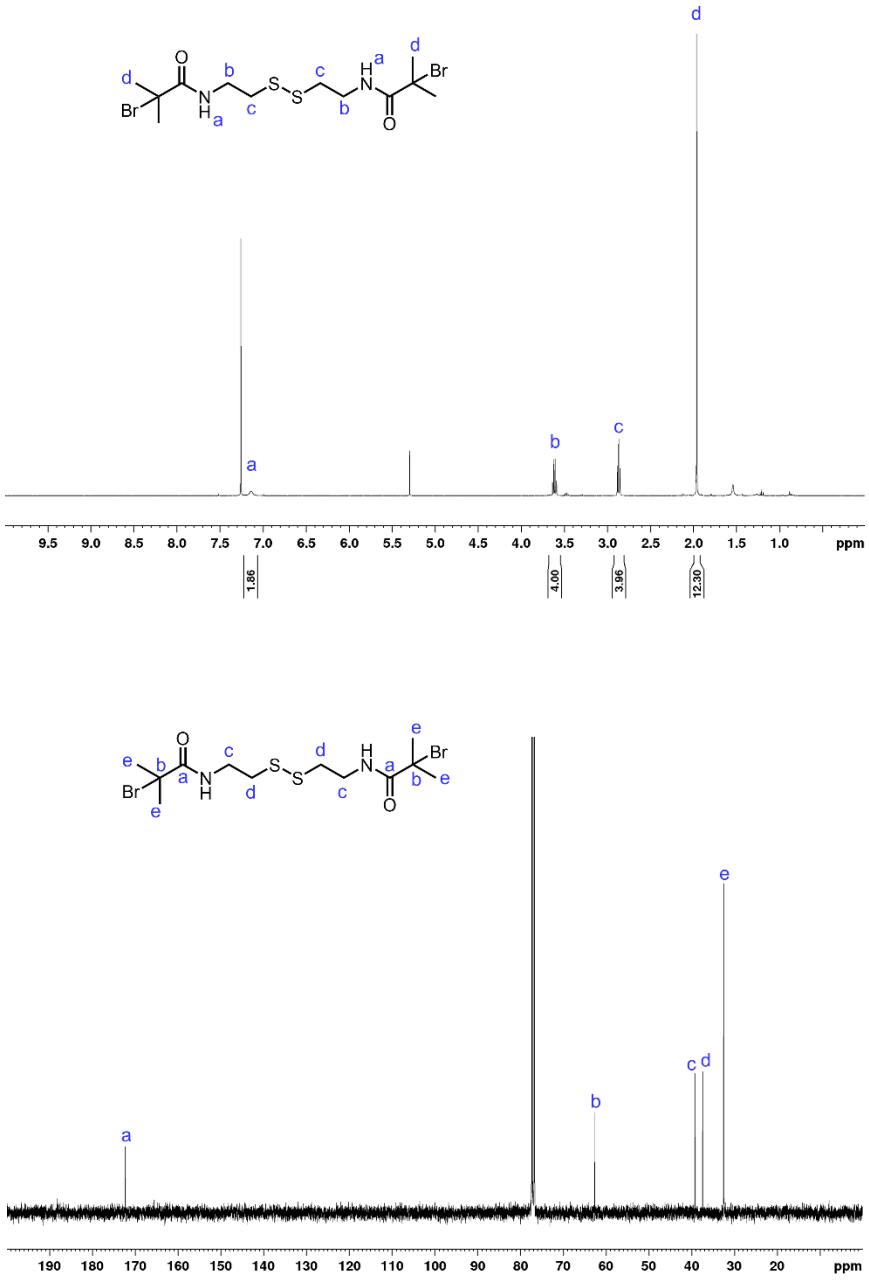

Figure 4-13. ^{1}H- and ^{13}C- NMR of cystamine bis initiator in $CDCl_3$

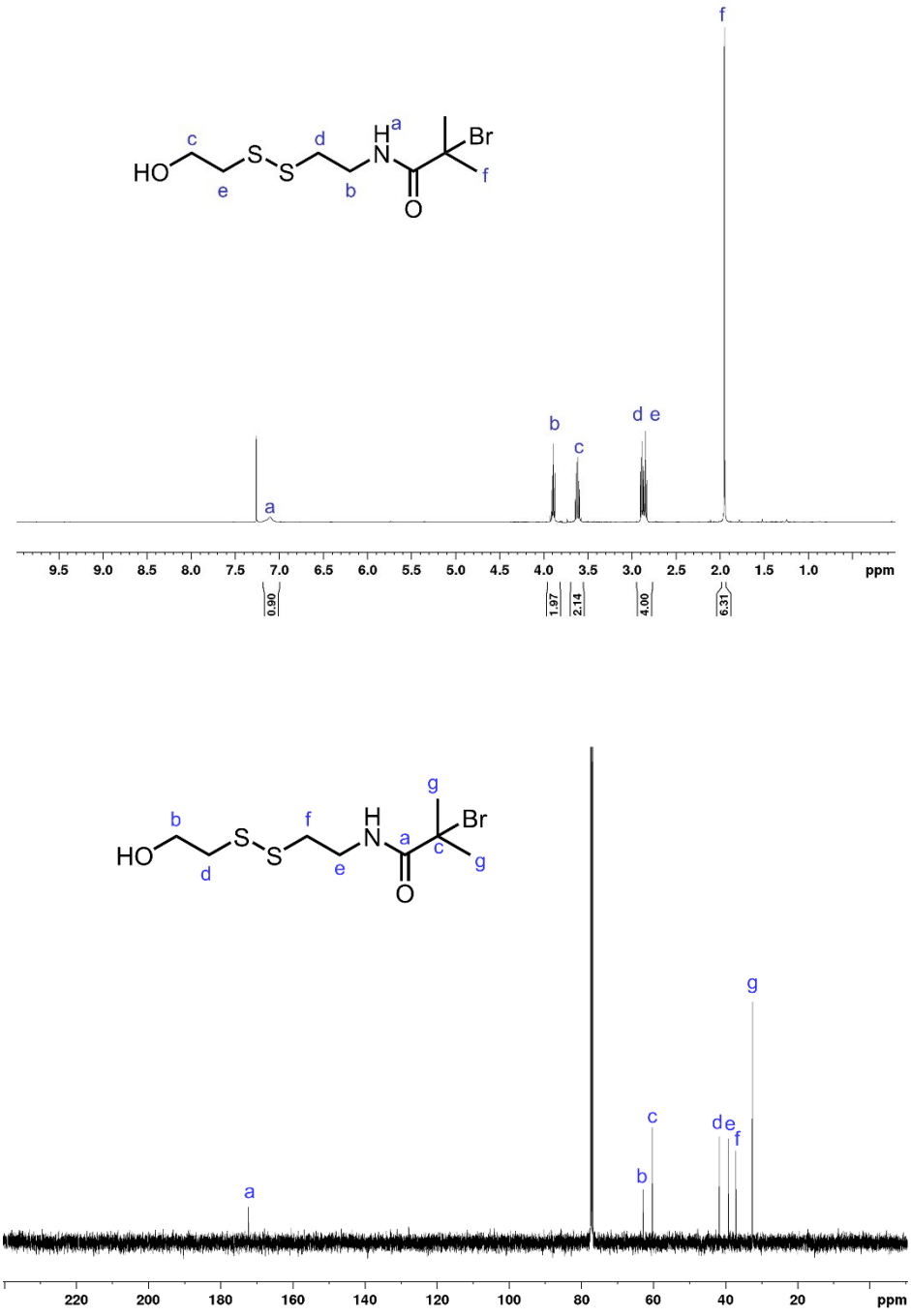

Figure 4-14. ^{1}H- and ^{13}C- NMR of 2-bromo-N-(2-((2-hydroxyethyl)disulfaneyl)ethyl)-2-methylpropanamide in $CDCl_3$

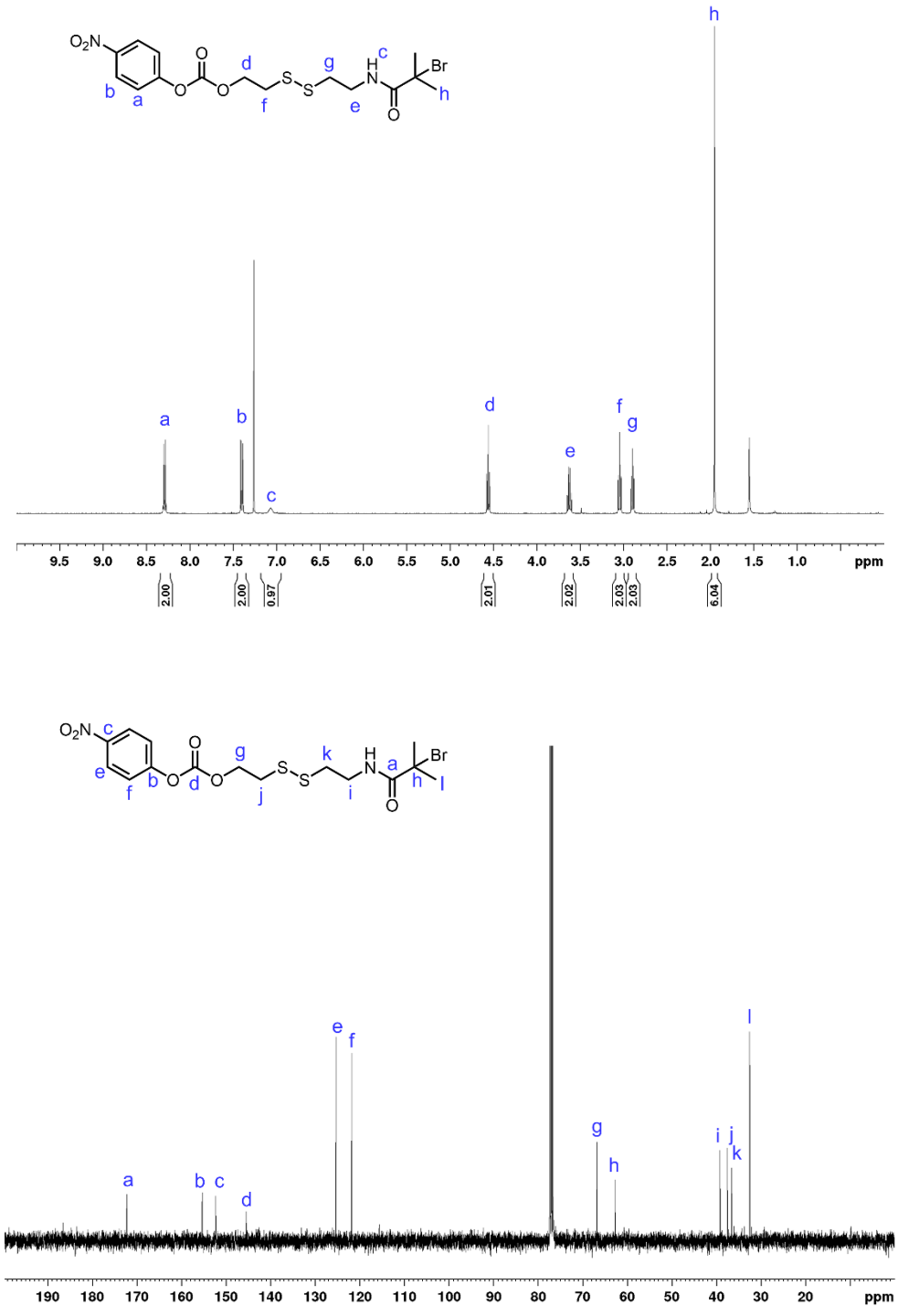

Figure 4-15. ^{1}H- and ^{13}C- NMR of linker **3** initiator in $CDCl_3$

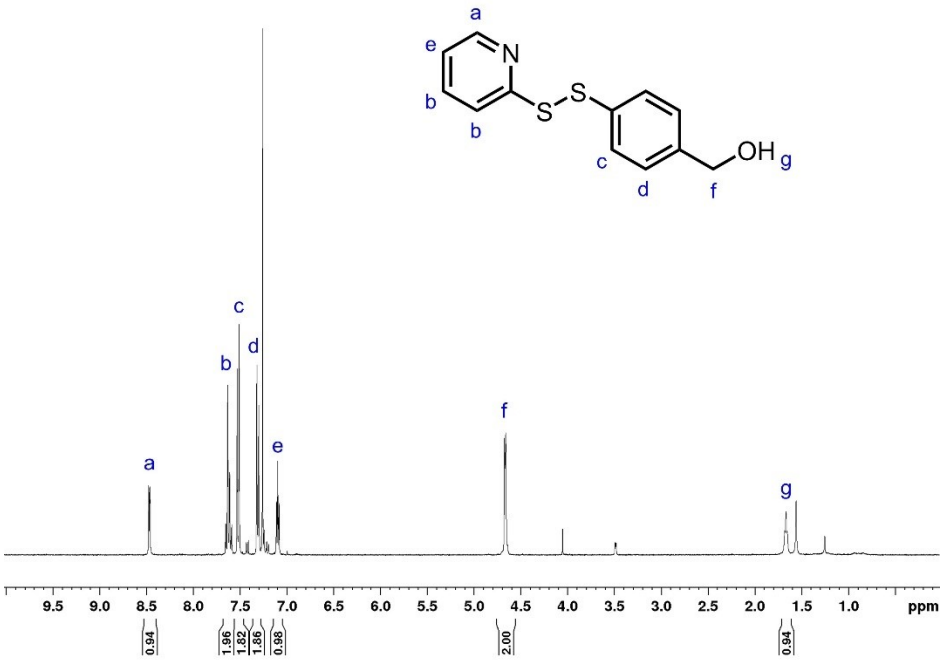

Figure 4-16. ^{1}H-NMR of PDS benzyl alcohol in $CDCl_3$

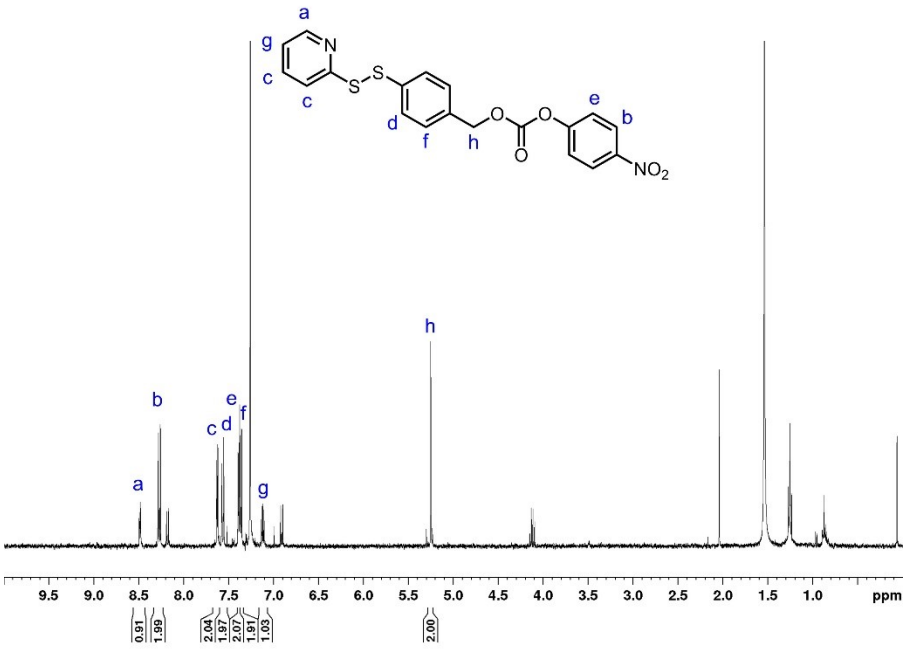

Figure 4-17. ^{1}H-NMR of linker **4** in $CDCl_3$

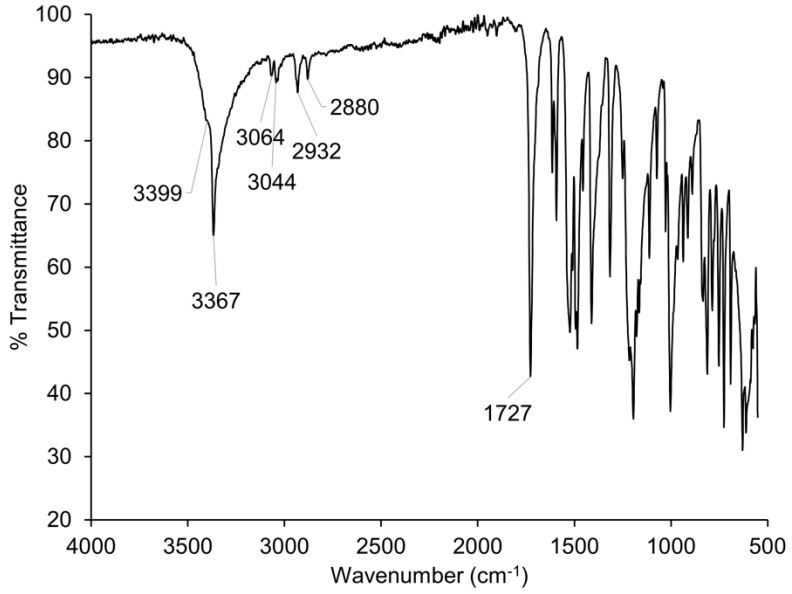

Figure 4-18. FT-IR of phenyl (4-(hydroxymethyl)phenyl)carbamate

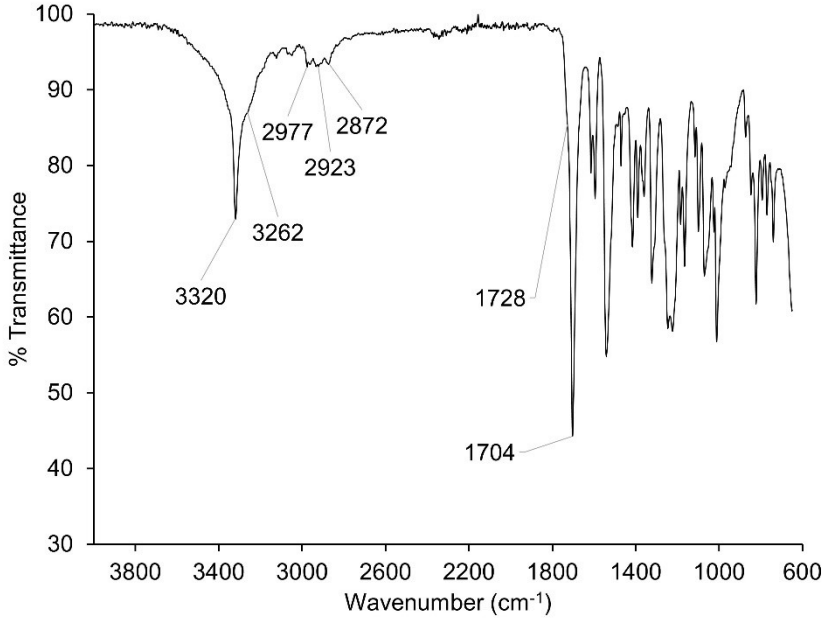

Figure 4-19. FT-IR of 3-oxobutyl (4-(hydroxymethyl)phenyl)carbamate

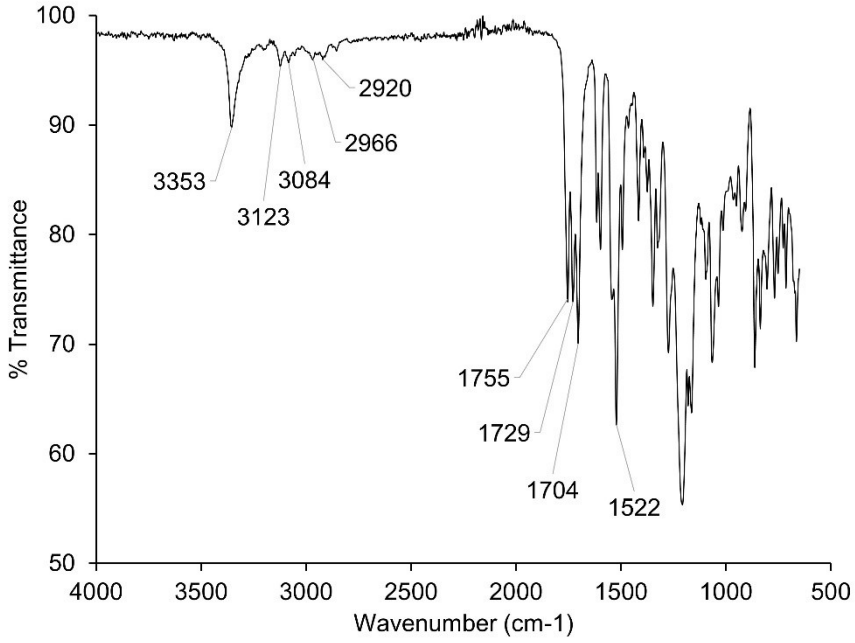

Figure 4-20. FT-IR of linker **1**

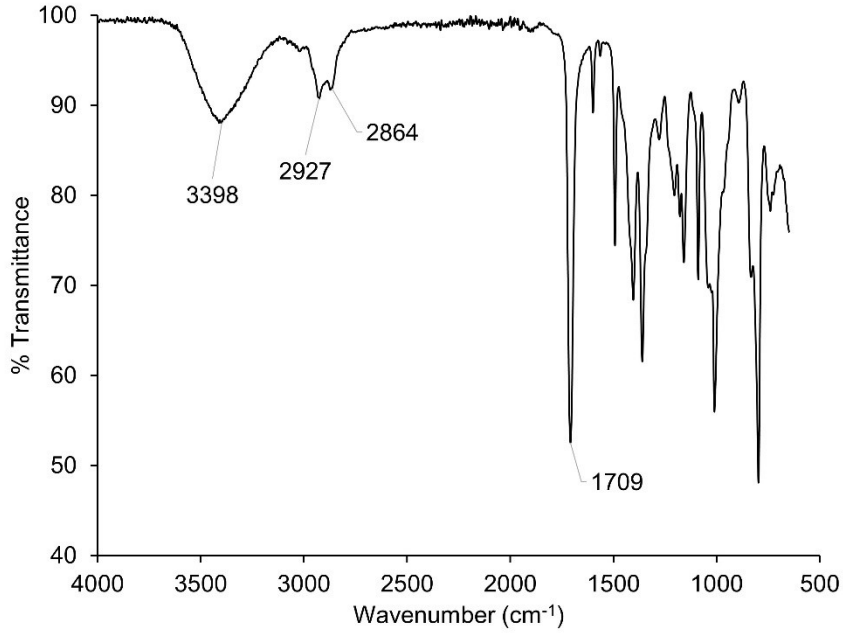

Figure 4-21. FT-IR of 3-oxobutyl (4-(hydroxymethyl)phenyl)carbamate

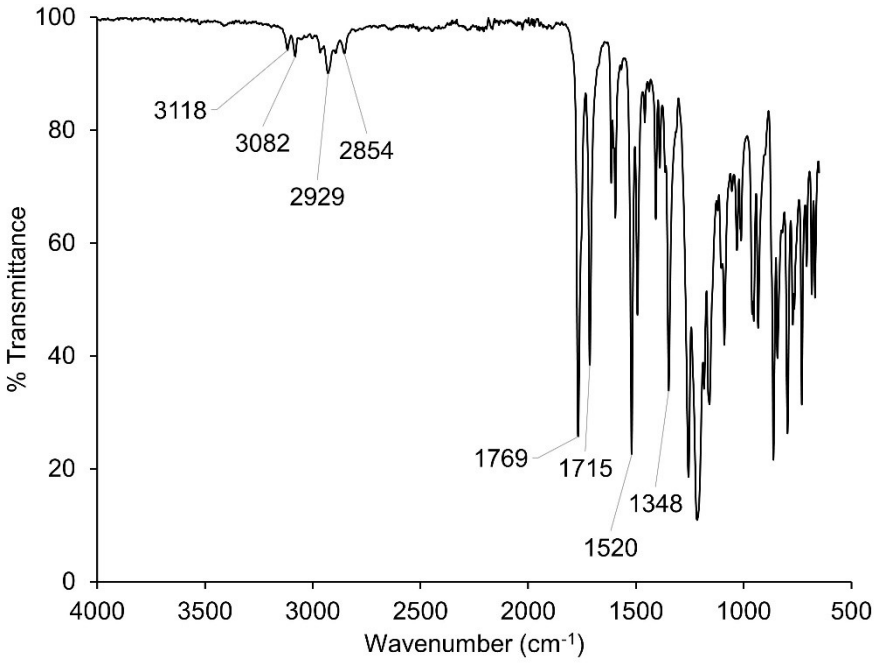

Figure 4-22. FT-IR of linker **2**

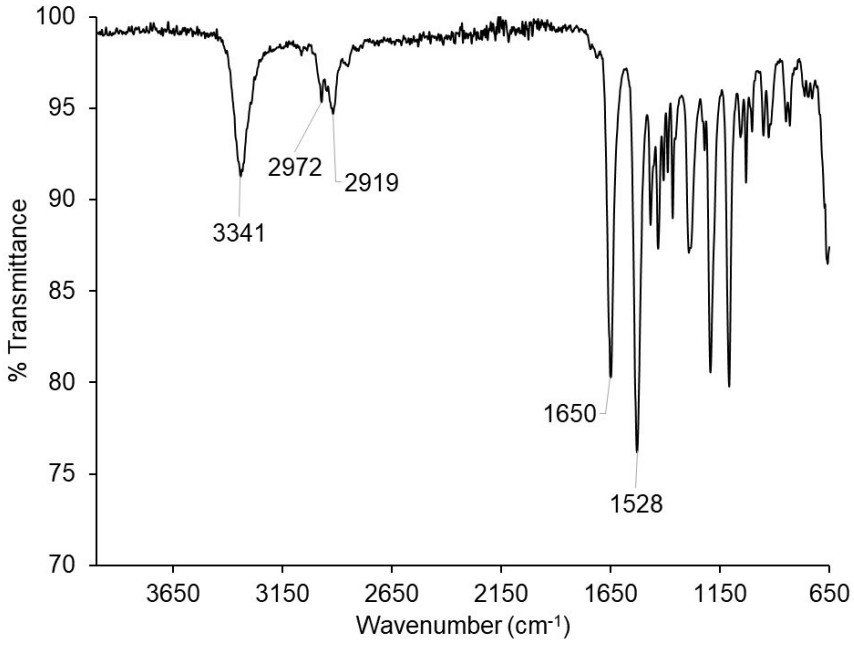

Figure 4-23. FT-IR of cystamine bis initiator

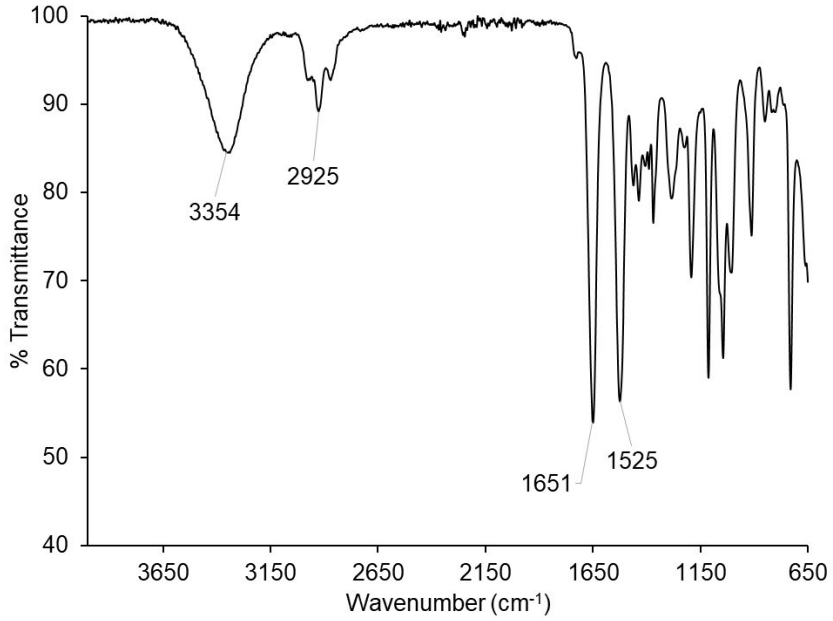

Figure 4-24. FT-IR of 2-bromo-N-(2-((2-hydroxyethyl)disulfaneyl)ethyl)-2-methylpropanamide

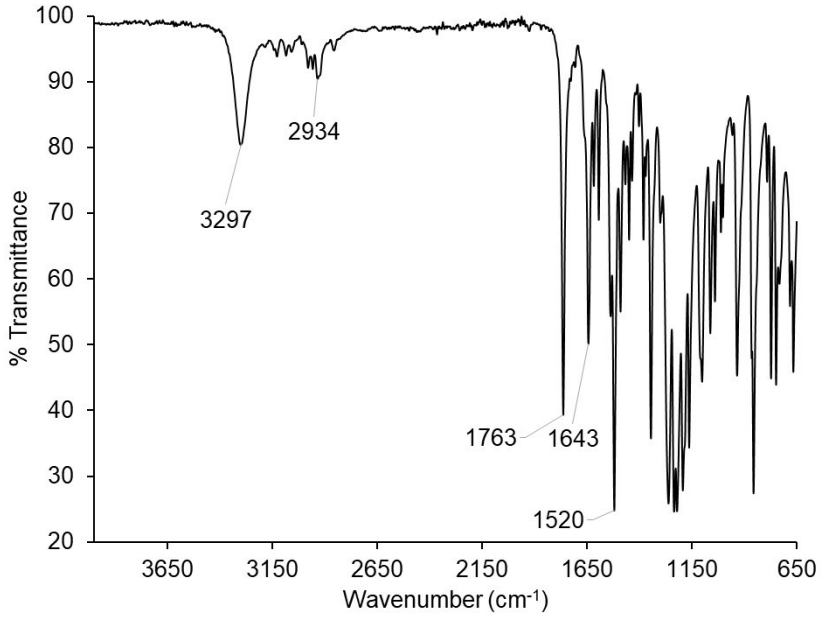

Figure 4-25. FT-IR of linker **3** initiator

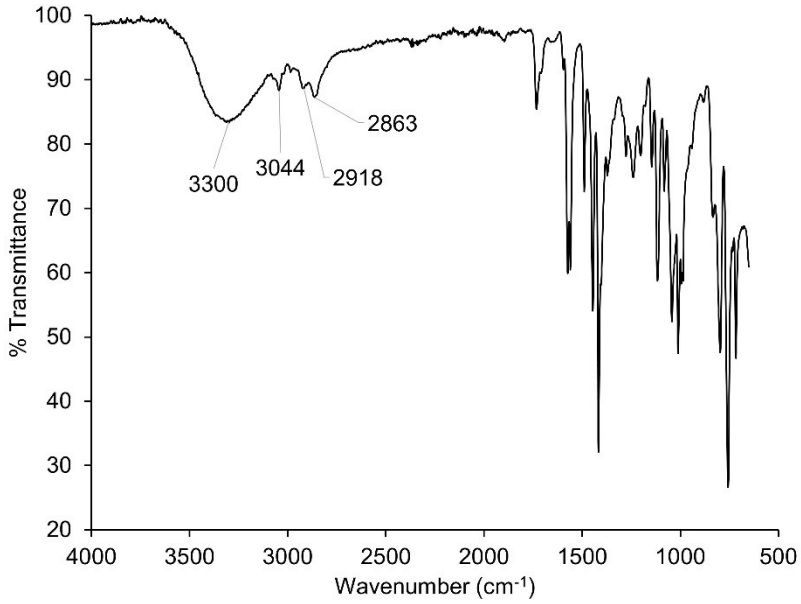

Figure 4-26. FT-IR of PDS alcohol

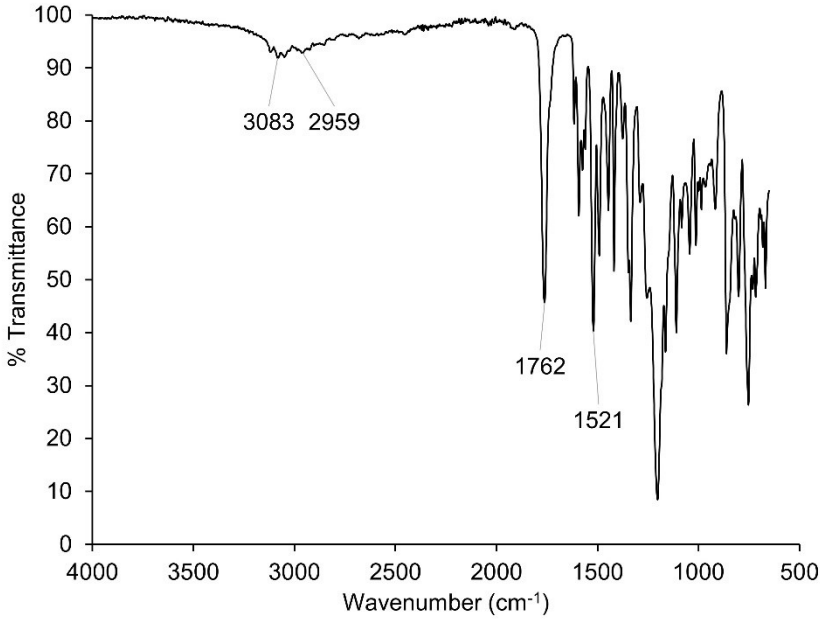

Figure 4-27. FT-IR of linker **4**

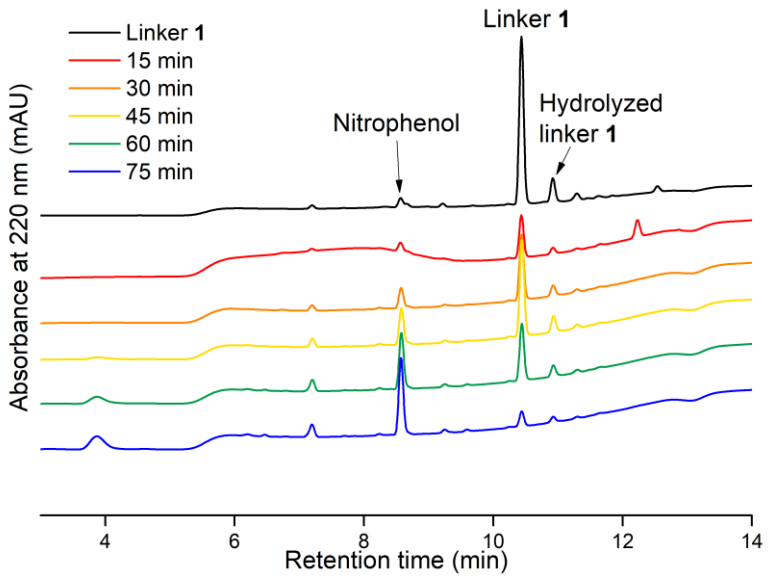

Figure 4-28. HPLC trace of linker **1** over time in borate buffer pH 9.0 only shows some hydrolysis.

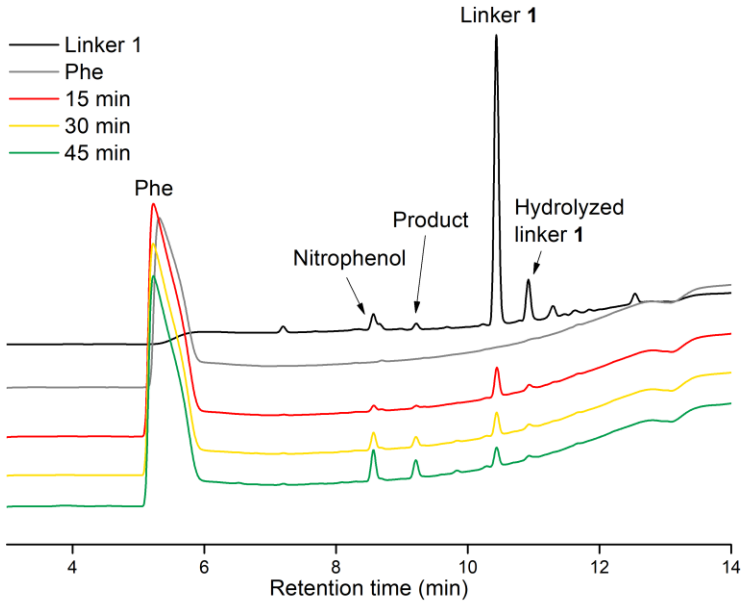

Figure 4-29. HPLC trace of linker **1** over time with Phe.

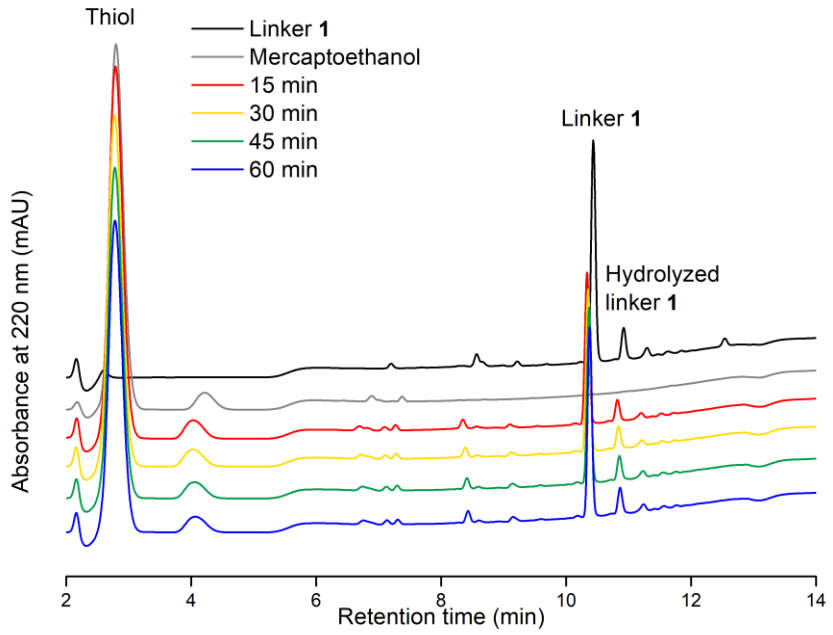

Figure 4-30. HPLC trace of linker **1** over time with β-mercaptoethanol shows β-elimination is not catalyzed by thiol.

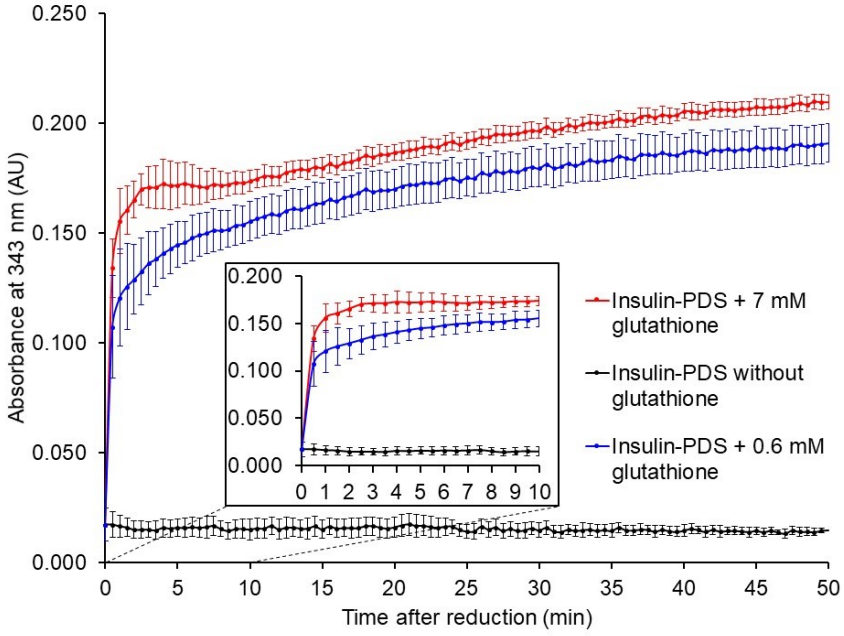

Figure 4-31. Absorbance from release of 2-pyridylthione during reduction of linker **3** with glutathione (n = 3).

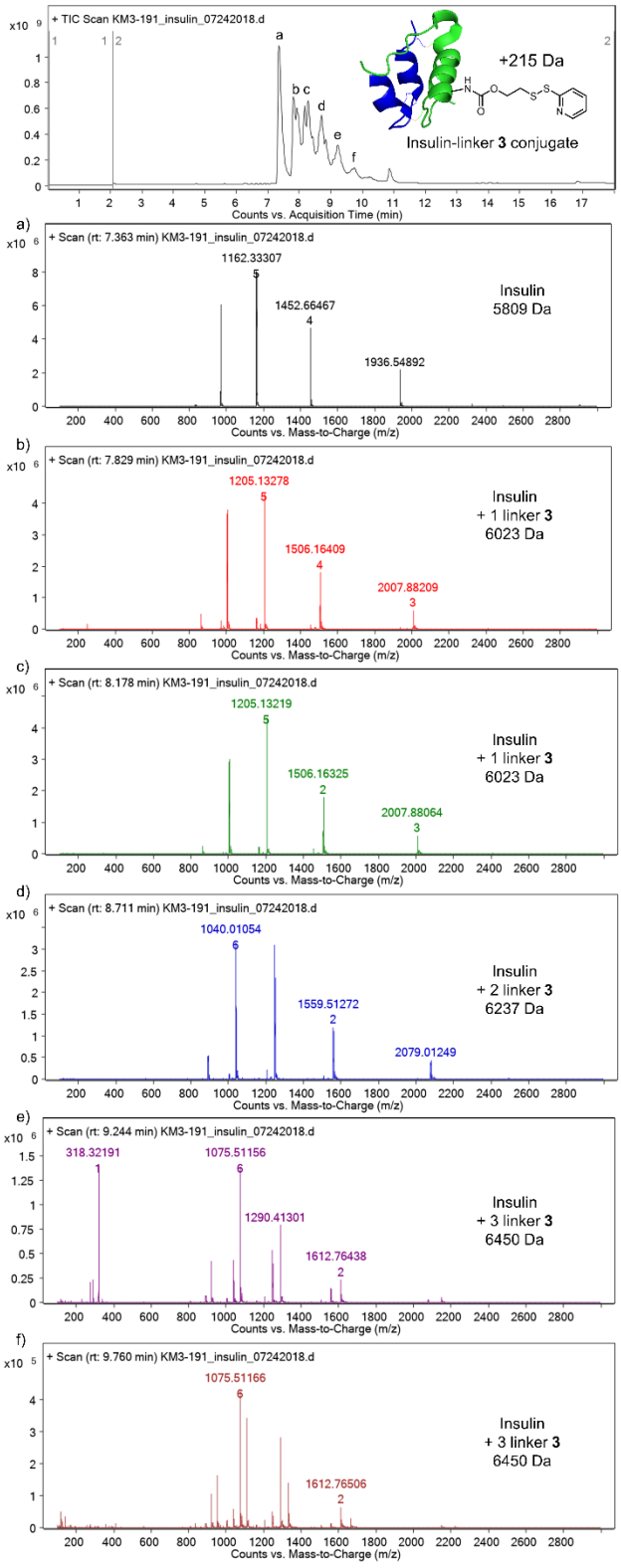

Figure 4-32. Characterization of insulin-linker **3** by LC-MS.

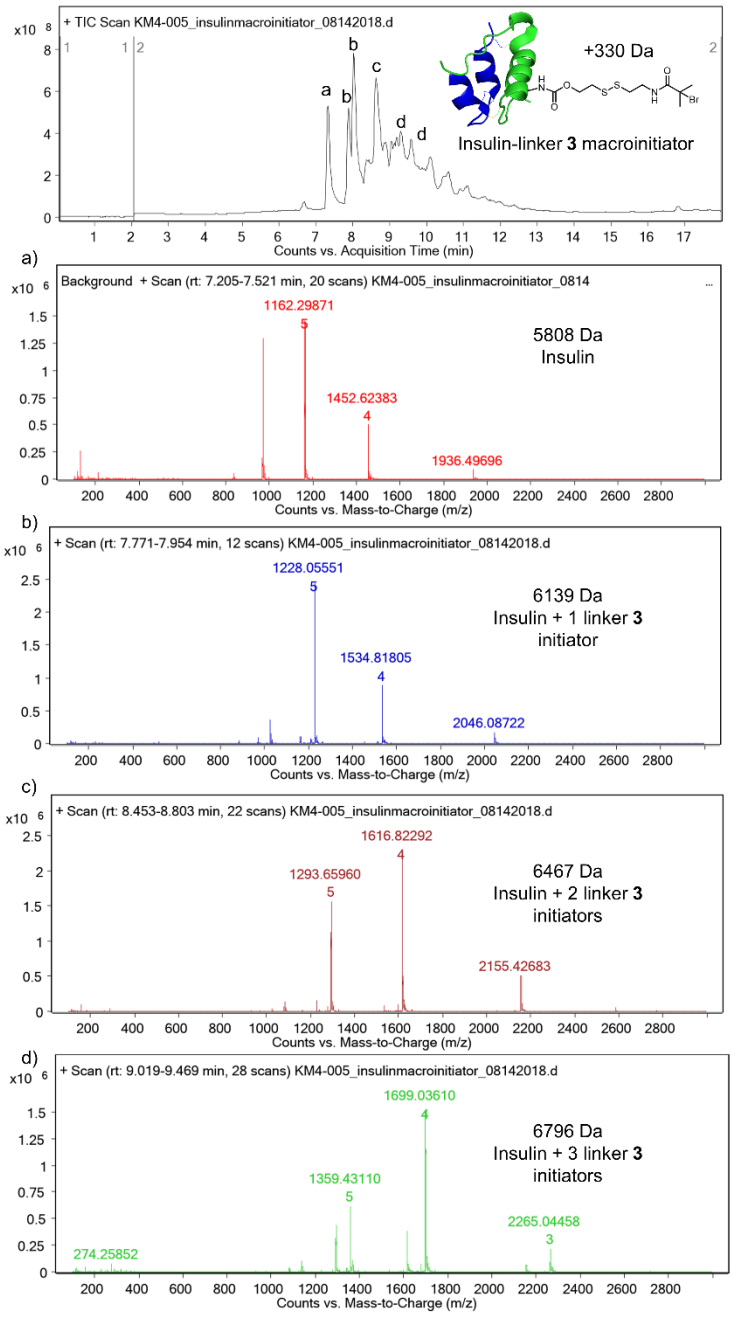

Figure 4-33. Characterization of insulin-linker **3** macroinitiator by LC-MS.

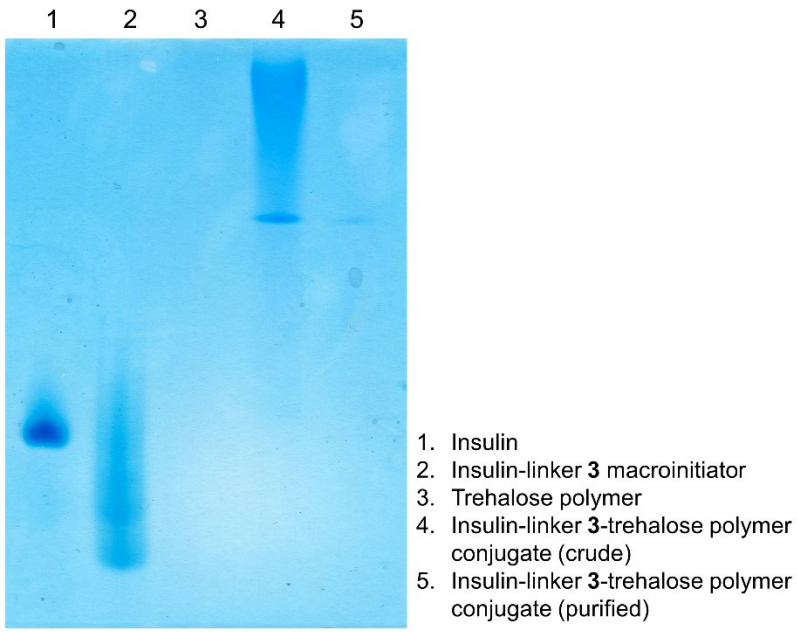

Figure 4-34. Native PAGE characterization of insulin-linker **3**-trehalose polymer conjugate.

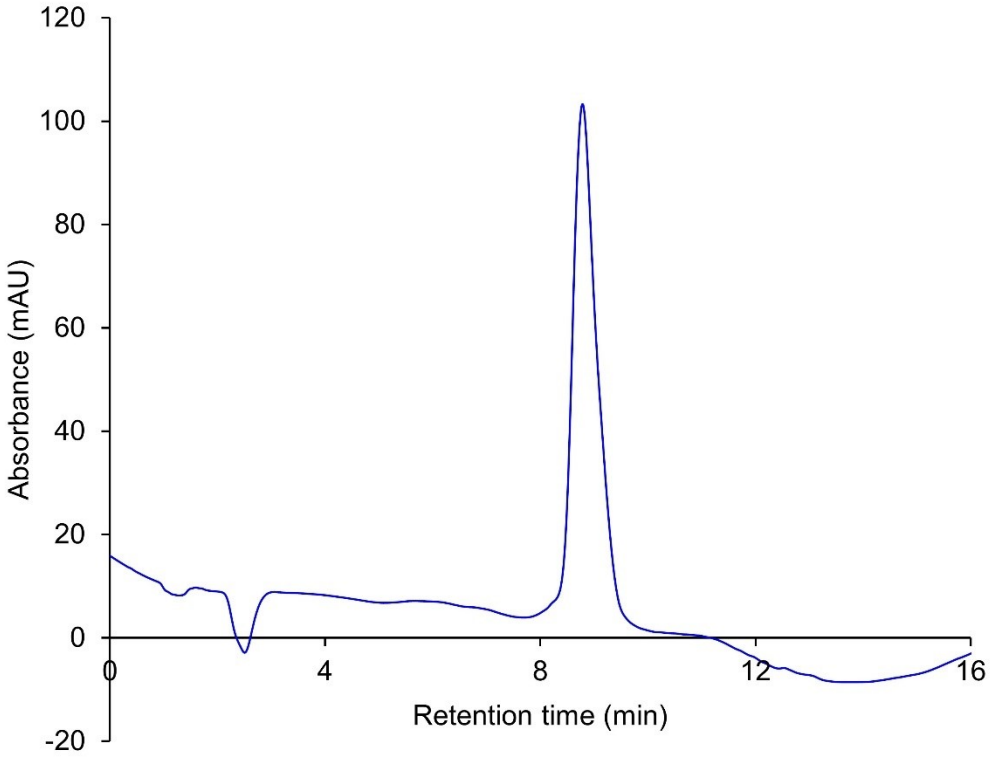

Figure 4-35. Analytical HPLC trace of insulin-linker **3**-trehalose polymer conjugate.

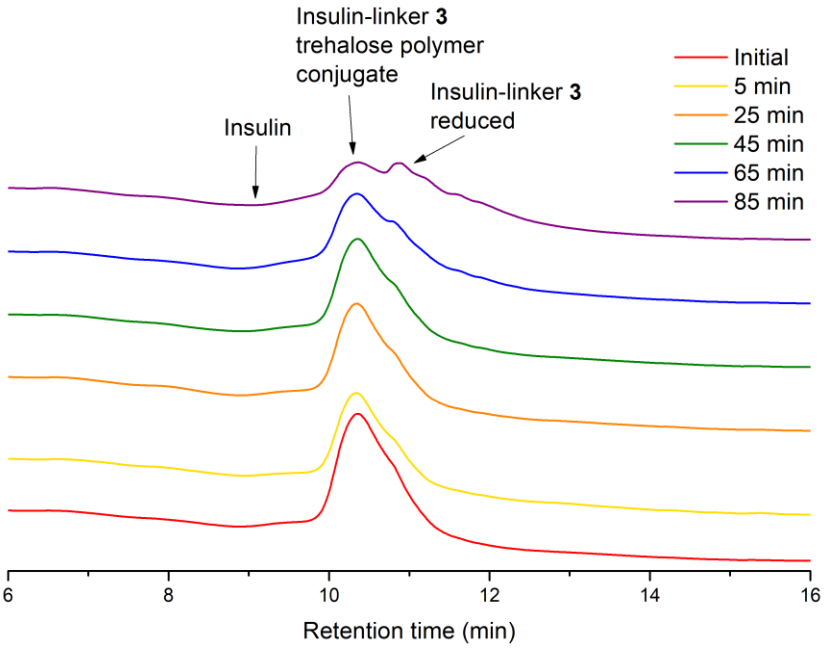

Figure 4-36. HPLC trace over time of insulin-linker **3**-trehalose polymer conjugate with 7 mM glutathione.

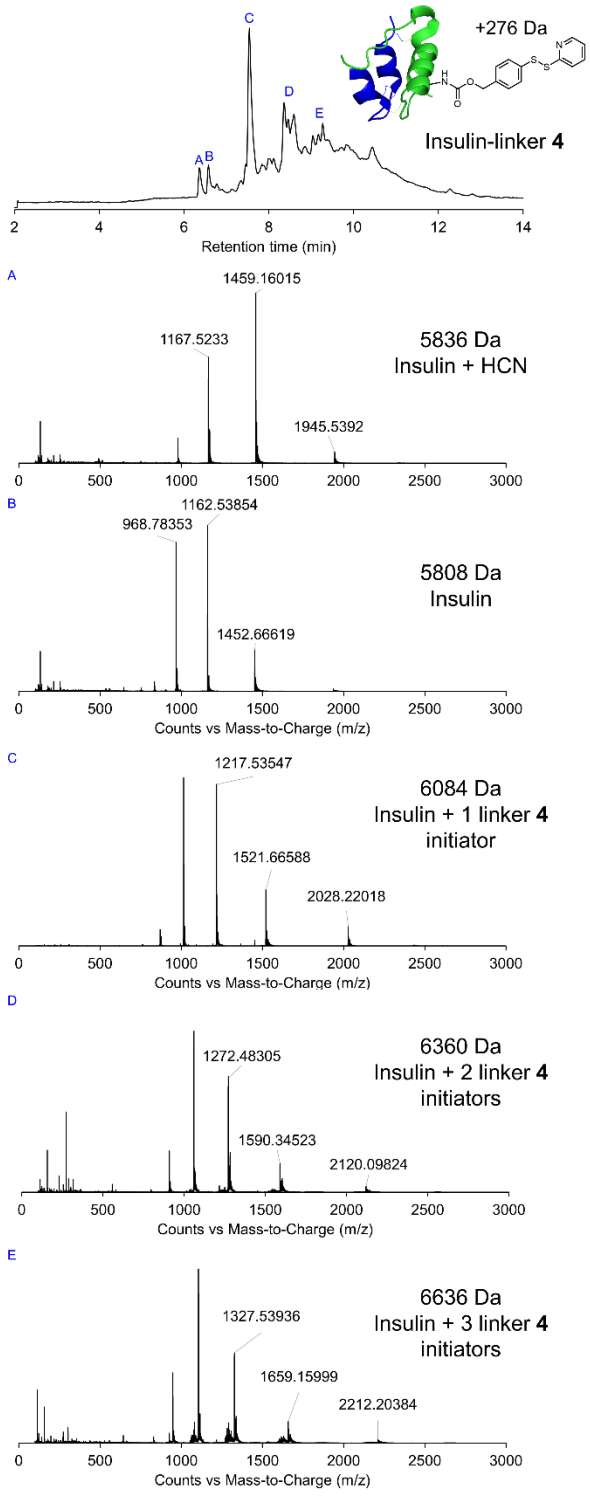

Figure 4-37. Characterization of insulin-linker **4** conjugate by LC-MS

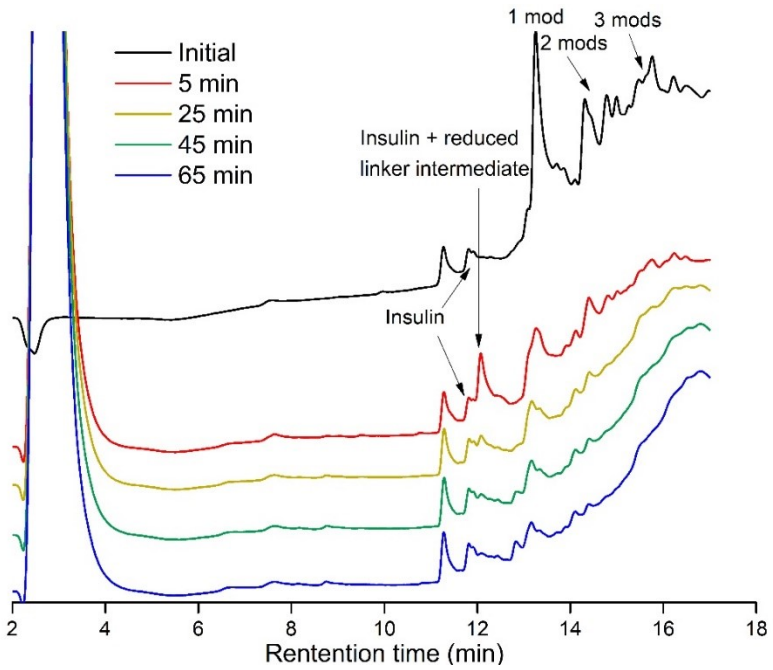

Figure 4-38. HPLC trace over time of insulin-linker **4** conjugate with 0.6 mM glutathione.

4.5 References

(1) Hirsch, I. B. Insulin analogues. *N. Engl. J. Med.* **2005,** *352*, 174-183.

(2) Freeman, J. S. Insulin analog therapy: improving the match with physiologic insulin secretion. *J. Am. Osteopath. Assoc.* **2009,** *109*, 26-36.

(3) Tibaldi, J. M. Evolution of insulin: from human to analog. *Am. J. Med.* **2014,** *127*, S25-S38.

(4) Brange, J.; Langkj, L.; Havelund, S.; Vølund, A. Chemical stability of insulin. 1. Hydrolytic degradation during storage of pharmaceutical preparations. *Pharm. Res.* **1992,** *9*, 715-726.

(5) Sluzky, V.; Klibanov, A. M.; Langer, R. Mechanism of insulin aggregation and stabilization in agitated aqueous solutions. *Biotechnol. Bioeng.* **1992,** *40*, 895-903.

(6) Liu, Y.; Lee, J.; Mansfield, K. M.; Ko, J. H.; Sallam, S.; Wesderniotis, C.; Maynard, H. D. Trehalose Glycopolymer Enhances Both Solution Stability and Pharmacokinetics of a Therapeutic Protein. *Bioconjugate Chem.* **2017,** *28*, 836-845.

(7) Mansfield, K. M.; Maynard, H. D. Site-specific insulin-trehalose glycopolymer conjugate by grafting from strategy improves bioactivity. *ACS Macro Lett.* **2018,** *7*, 324-329.

(8) Alouane, A.; Labruère, R.; Le Saux, T.; Schmidt, F.; Jullien, L. Self-immolative spacers: kinetic aspects, structure–property relationships, and applications. *Angew. Chem., Int. Ed.* **2015,** *54*, 7492-7509.

(9) Riber, C. F.; Smith, A. A.; Zelikin, A. N. Self-Immolative Linkers Literally Bridge Disulfide Chemistry and the Realm of Thiol-Free Drugs. *Adv. Healthcare Mater.* **2015,** *4*, 1887-1890.

(10) Blencowe, C. A.; Russell, A. T.; Greco, F.; Hayes, W.; Thornthwaite, D. W. Self-immolative linkers in polymeric delivery systems. *Polym. Chem.* **2011,** *2*, 773-790.

(11) Ducry, L.; Stump, B. Antibody− drug conjugates: linking cytotoxic payloads to monoclonal antibodies. *Bioconjugate Chem.* **2010,** *21*, 5-13.

(12) Gong, Y.; Leroux, J.-C.; Gauthier, M. A. Releasable conjugation of polymers to proteins. *Bioconjugate Chem.* **2015,** *26*, 1172-1181.

(13) Hollfelder, F.; Kirby, A. J.; Tawfik, D. S. Off-the-shelf proteins that rival tailor-made antibodies as catalysts. *Nature* **1996,** *383*, 60-63.

(14) Jourdain, N.; Carlón, R. P.; Reymond, J.-L. A stereoselective fluorogenic assay for aldolases: detection of an anti-selective aldolase catalytic antibody. *Tetrahedron Lett.* **1998,** *39*, 9415-9418.

(15) Boucher, G.; Robin, S.; Fargeas, V.; Dintinger, T.; Mathé-Allainmat, M.; Lebreton, J.; Tellier, C. Serum Albumin-Catalyzed Trigger System by Using a Tandem Kemp Elimination/β-Elimination Reaction. *ChemBioChem* **2005,** *6*, 807-810.

(16) Kikuchi, K.; Thorn, S. N.; Hilvert, D. Albumin-catalyzed proton transfer. *J. Am. Chem. Soc.* **1996,** *118*, 8184-8185.

(17) Sagi, A.; Weinstain, R.; Karton, N.; Shabat, D. Self-immolative polymers. *J. Am. Chem. Soc.* **2008,** *130*, 5434-5435.

(18) Weinstain, R.; Sagi, A.; Karton, N.; Shabat, D. Self-Immolative Comb-Polymers: Multiple-Release of Side-Reporters by a Single Stimulus Event. *Chem. - Eur. J.* **2008,** *14*, 6857-6861.

(19) Turell, L.; Radi, R.; Alvarez, B. The thiol pool in human plasma: the central contribution of albumin to redox processes. *Free Radicals Biol. Med.* **2013,** *65*, 244-253.

(20) Kaplowitz, N. The importance and regulation of hepatic glutathione. *Yale J. Biol. Med.* **1981,** *54*, 497-502.

(21) Xie, H.; Audette, C.; Hoffee, M.; Lambert, J. M.; Blättler, W. A. Pharmacokinetics and biodistribution of the antitumor immunoconjugate, cantuzumab mertansine (huC242-DM1), and its two components in mice. *J. Pharmacol. Exp. Ther.* **2004,** *308*, 1073-1082.

(22) Tolcher, A. W.; Ochoa, L.; Hammond, L. A.; Patnaik, A.; Edwards, T.; Takimoto, C.; Smith, L.; de Bono, J.; Schwartz, G.; Mays, T. Cantuzumab mertansine, a maytansinoid immunoconjugate directed to the CanAg antigen: a phase I, pharmacokinetic, and biologic correlative study. *J. Clin. Oncol.* **2003,** *21*, 211-222.

(23) Nagy, P. Kinetics and mechanisms of thiol–disulfide exchange covering direct substitution and thiol oxidation-mediated pathways. *Antioxid. Redox Signaling* **2013,** *18*, 1623-1641.

(24) Liu, Y.; Lee, J.; Mansfield, K. M.; Ko, J. H.; Sallam, S.; Wesdemiotis, C.; Maynard, H. D. Trehalose Glycopolymer Enhances Both Solution Stability and Pharmacokinetics of a Therapeutic Protein. *Bioconjugate Chem.* **2017,** *28*, 836-845.

(25) Boehnke, N.; Kammeyer, J. K.; Damoiseaux, R.; Maynard, H. D. Stabilization of Glucagon by Trehalose Glycopolymer Nanogels. *Adv. Funct. Mater.* **2018,** *28*, 1705475.

(26) Qiu, Y.; Li, D. Bifunctional inhibitors of mevalonate kinase and mevalonate 5-diphosphate decarboxylase. *Org. Lett.* **2006,** *8*, 1013-1016.

(27) Suma, T.; Cui, J.; Müllner, M.; Fu, S.; Tran, J.; Noi, K. F.; Ju, Y.; Caruso, F. Modulated fragmentation of proapoptotic peptide nanoparticles regulates cytotoxicity. *J. Am. Chem. Soc.* **2017,** *139*, 4009-4018.

(28) Batisse, C.; Dransart, E.; Sarkouh, R. A.; Brulle, L.; Bai, S.-K.; Godefroy, S.; Johannes, L.; Schmidt, F. A new delivery system for auristatin in StxB-drug conjugate therapy. *Eur. J. Med. Chem.* **2015,** *95*, 483-491.

Chapter 5. Glucose-Responsive Trehalose Hydrogel for Insulin Stabilization and Delivery

This chapter contains portions of an edited version of the following published paper reprinted with permission from: Lee, J., Ko, J. H., Mansfield, K.M., Nauka, P. C., Bat, E., Maynard, H. D., "Glucose-Responsive Trehalose Hydrogels for Insulin Stabilization and Delivery," *Macromol. Biosci*, **2018**, *18*, 1700372, 1-7.

5.1 Introduction

Diabetes is a growing problem in the United States, affecting an estimated 29 million or 9.3% of the population.[1] One of the main problems with insulin therapy is the instability of the protein to environmental conditions like elevated temperatures. Under these conditions, insulin forms degradation products such as aggregates that are not metabolically active, leading to possible patient harm from less effective doses and possible immunogenicity or waste and increased cost from disposal.[2-3] In addition, patients must self-administer insulin through multiple injections or infusions through an insulin pump per day after mealtimes to manage blood glucose.[4] Developing a delivery device responsive to the concentration of glucose in the blood could decrease the number of injections needed per day and simultaneously stabilize the protein would vastly improve patient quality of life and treatment compliance.

Nontoxic phenylboronic acids have been incorporated into materials for glucose sensing and delivery of insulin in response to glucose concentration.[5-6] _ENREF_7 Boronic acids are useful for glucose-responsive materials because they form dynamic covalent bonds with 1,2- and 1,3-diols such as in saccharides.[7] Two main mechanisms of insulin release have been employed: swelling and competitive displacement.[5-6] Swelling results from the change in charge of the boronic acid following binding of glucose, caused by the shift in equilibrium from the neutral trigonal to negative tetrahedral geometry, leading to an increase in osmotic pressure.[8] Alternatively, polymers containing boronic acids can crosslink with polymers bearing 1,2- or 1,3-diols to encapsulate insulin in situ.[9-11] _ENREF_12_ENREF_20 Subsequent displacement of the crosslinks by glucose leads to the release of insulin from the hydrogel.

Our group has synthesized polymers with trehalose side chains that have been shown to stabilize proteins to heat in solution and lyophilization as both excipients and conjugates.[12-15] Our

group reported the preparation of hydrogels by cross-linking trehalose polymers with boronic acid-functionalized 8-arm poly(ethylene glycol) (PEG).[12] Upon the addition of glucose, the network was disrupted due to boronic acid's preferential binding to glucose over trehalose, resulting in an accelerated dissolution of the hydrogel and release of insulin (**Scheme 5-1**). Because of the presence of the trehalose polymer in the hydrogel, insulin was stabilized to an accelerated heating assay. To our knowledge, a hydrogel that is both glucose-responsive and insulin stabilizing had not yet been reported until our group's account. These results demonstrated that the trehalose-boronic acid hydrogel can deliver insulin upon increase in glucose level, while also stabilizing the protein upon thermal stress. However, a significant amount of insulin was released when the hydrogel was incubated in solution without glucose. In this chapter, efforts to decrease the release of insulin in the absence of glucose (background release) through hydrogel structure alteration and gelation optimization are discussed.

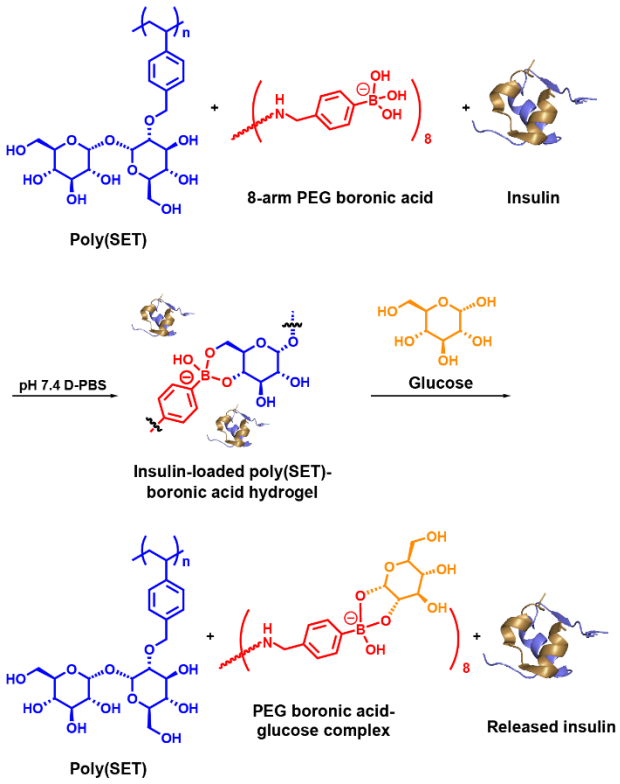

Scheme 5-1. Design for insulin delivery using trehalose-boronic acid hydrogel (insulin PDB ID: 4INS).

5.2 Results and Discussion

In previous work, a trehalose-based hydrogel was formed by cross-linking trehalose polymer with 8-arm PEG functionalized with 4-phenylboronic acid (**Scheme 5-1**).[12] The gelation occurred rapidly after mixing the solutions of the two components. It is viscous within a minute and forms the gel within 5 minutes. Insulin was also shown to be stabilized inside the hydrogel to heat (90 °C for 30 min) as measured by ELISA.[12] It is interesting to note that the hydrogel lost its water content under these conditions but could be rehydrated following exposure to heat (**Figure 5-1**), indicating that the network remained intact or readily reformed. We have observed that trehalose polymers stabilize proteins to both heat and removal of water (lyophilization).[14] We

hypothesize that the presence of the trehalose network stabilizes insulin in a similar manner even if the hydrogel is dehydrated during the heating process. Trehalose is known to bind strongly with water[16] and we have observed a large loss of water from trehalose polymers during the initial heat ramps in differential scanning calorimetry (DSC) (**Figure 5-13**). One of the proposed mechanisms of trehalose protein stabilization is preferential exclusion due to stronger water-trehalose interactions,[16] which may contribute to the stabilization capabilities observed for the hydrogel. Additionally, the trehalose polymer exhibited a glass transition temperature (T_g) of 118 °C, which is close to the reported T_g of 116 °C for trehalose.[16] Another proposed mechanism of trehalose protein stabilization is vitrification, where trehalose forms a glassy matrix around the protein upon drying.[17] This may also contribute to insulin stabilization in this case because trehalose and the trehalose polymer have similar T_g. Insulin was released in a glucose-responsive manner from the previously reported hydrogel, however significant background release of insulin was observed when no glucose was added.[12] Unintended release of insulin from the hydrogel without an increased glucose concentration is undesirable and could cause potentially dangerous hypoglycemia.

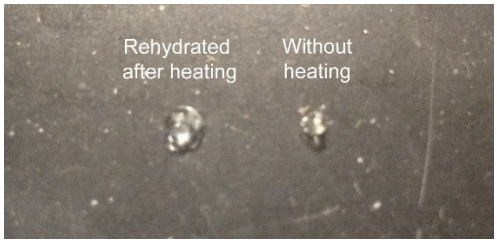

Figure 5-1. Photograph of gel before heating and rehydrated after heating.

We developed several strategies to address the issue of the high background insulin release from the trehalose-based polymeric hydrogel (**Figure 5-2**). We varied the pore size, boronic acid binding affinity, and electrostatic interactions in an effort to lower background release from

diffusion of insulin out of the hydrogel network as well as the slow dissolution of the hydrogel.

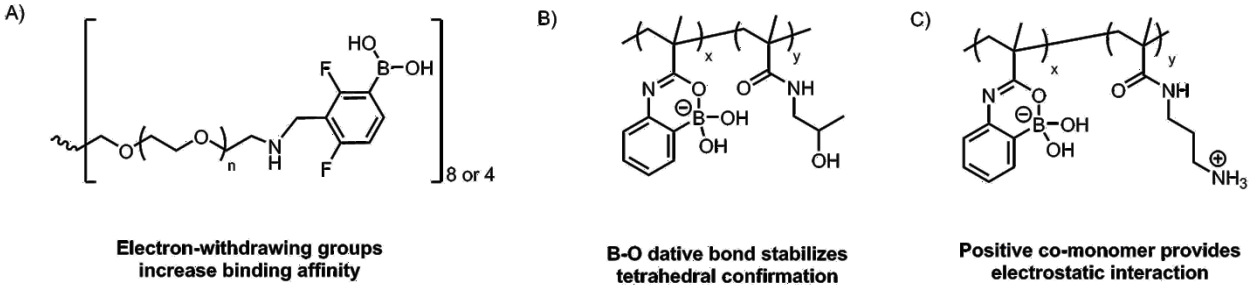

Figure 5-2. Summary of strategies developed to decrease background insulin release by forming a hydrogel with poly(SET) and boronic acid-containing polymers with (A) lower pK_a, (B) B-O dative bond stabilizing tetrahedral boronic acid conformation, or (C) positively charged amine comonomer.

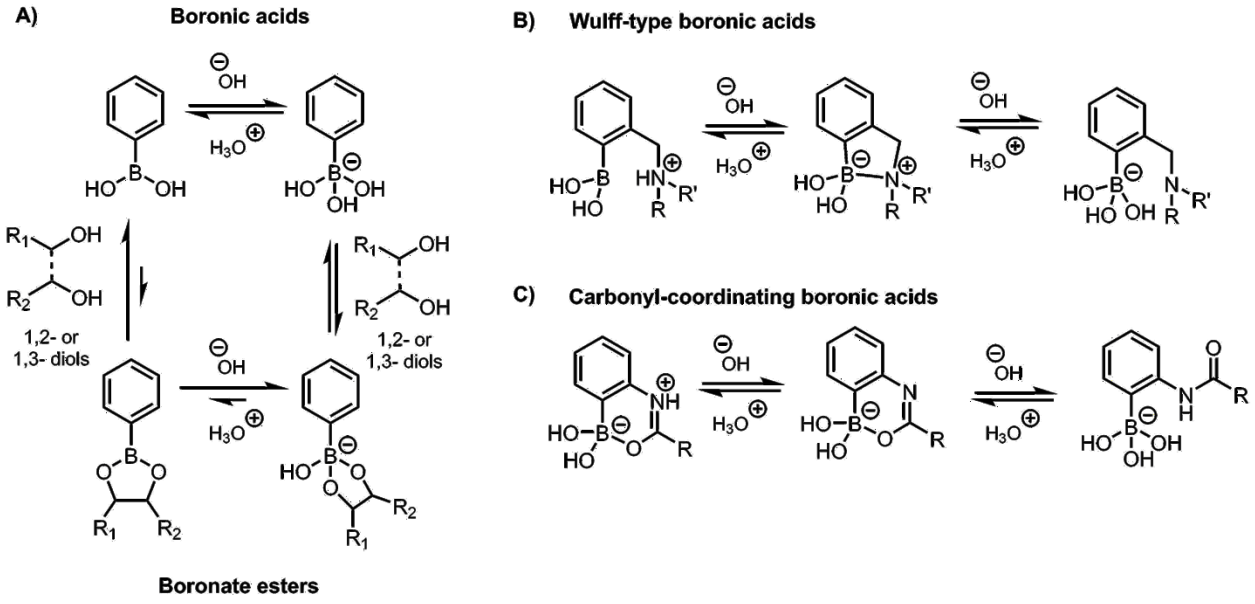

Figure 5-3. Equilibria of boronic acids. (A) The tetrahedral boronic acid geometry has a higher binding affinity with polyols which is stabilized through neighboring (B) amine or (C) carbonyl groups.

Boronic acids exist in an equilibrium in which the anionic boronic acid form exhibits a

higher binding affinity for polyols, as the trigonal boronate esters formed after complexation with polyols are hydrolytically unstable (**Figure 5-3 A** and **B**).[18] Lowering the pK_a of the boronic acid, through subtle changes in the electronics of the attached aryl substituents, shifts the equilibrium to favor the anionic tetrahedral binding geometry. Thus, lowering the boronic acid pKa increases the propensity for the boronic acid to form the corresponding boronate ester in the presence of a polyol. We chose 2,4-difluoro-3-formylphenylboronic acid (FPBA) (**Figure 5-2 A**) to replace 4-formylphenylboronic acid (PBA), which has a lower pK_a (approximately 7.6 compared to 8.0) and thus stronger binding to saccharides at neutral pH.[19-20] Two PEG amines with different molecular weight were chosen for modification with FPBA to investigate the effect of cross-linking density/pore size. The PEG amines, 10 kDa 8-arm PEG amine (used in our reported system[12]) and 2 kDa 4-arm PEG amine (for tighter cross-linking thus smaller pore size to minimize diffusion out of the network), were functionalized with FPBA by reductive amination as previously performed with PBA. However, upon addition of the trehalose glycopolymer, no gel formed with 8-arm PEG-FPBA. A gel formed using the 4-arm PEG-FPBA, which dissolved within 1 hour in D-PBS (**Figure 5-4**). This dissolution was deemed too fast to measure release of insulin in the gel. Therefore it was anticipated to be worse than the original with regard to background release and not explored further.

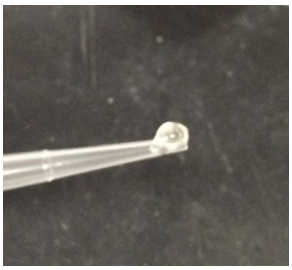

Figure 5-4. Photograph of 4-arm PEG-FPBA and p(SET) trehalose polymer hydrogel immediately after mixing.

The addition of neighboring atoms harboring non-bonding electrons, such as nitrogen and oxygen, promote the formation of the tetrahedral boronic acid form at neutral pH through donation of the lone-pair electrons into the empty p-orbital on boron (**Figure 5-3 C** and **D**).[21-23] We envisioned a trehalose glycopolymer hydrogel formed with a co-polymer incorporating phenylboronic acids with a carbonyl that could form a B-O dative bond to increase the polyol binding strength would be advantageous with regard to minimizing background release. Additionally, we hypothesized this design could increase the cross-link density by increasing the spatial density of boronic acid moieties on the polymer. Free radical polymerization of 2-acrylamido phenylboronic acid pinacol ester and 2-hydroxypropyl methacrylate followed by deprotection with trifluoroacetic acid (TFA) resulted in poly(2-hydroxypropyl methacrylate-co-methacrylamidophenylboronic acid) (p(HPMA-co-PBA)) (**Figure 5-2 B**). This polymer formed a hydrogel upon addition of the trehalose glycopolymer in an initial gelation test. The weight loss of gel was accelerated during incubation in D-PBS buffer with increasing concentrations of glucose (**Figure 5-5 A**). Insulin release was then quantified using FITC-labeled insulin with different volume ratios of trehalose polymer to p(PBA-co-HPMA), but 90% or more of the FITC-

insulin was released without glucose in solution after 2 hours for all condition (**Figure 5-5 B**).

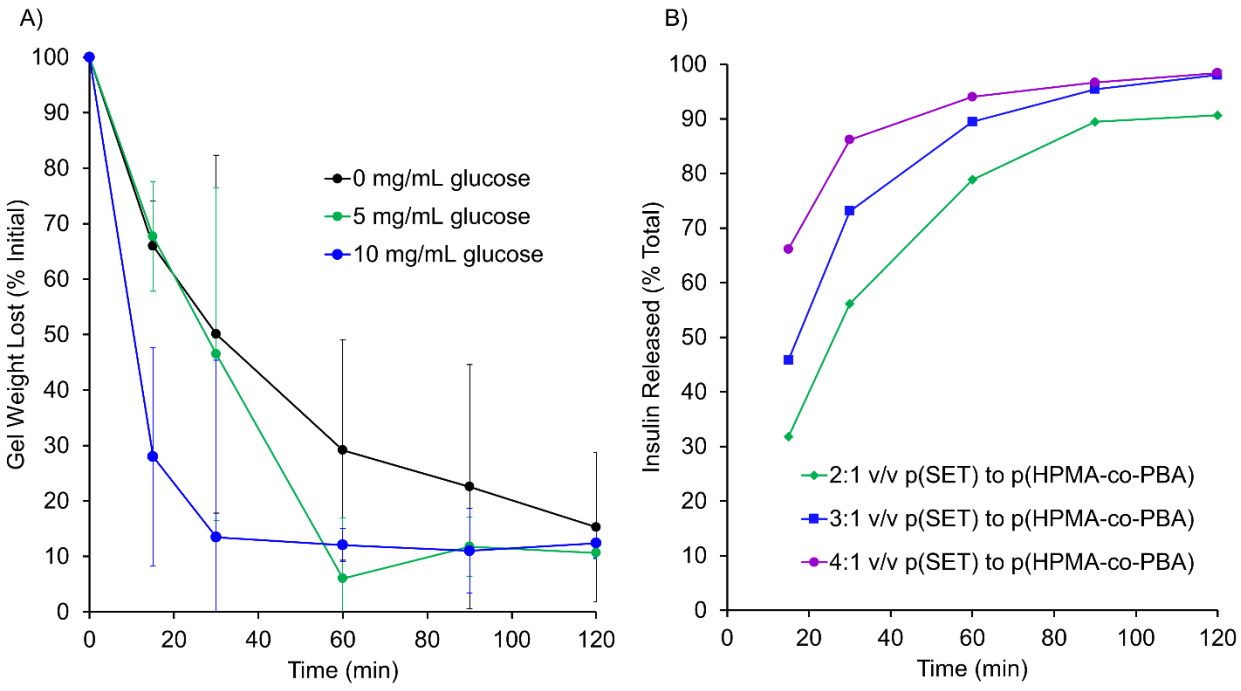

Figure 5-5. Examination of the effects of stabilizing the boronate ester using B-O dative bond on hydrogel properties. (A) Dissolution kinetics of hydrogel (n = 3) with various glucose concentrations at 1:1 v/v p(SET) to p(HPMA-co-PBA) and (B) FITC-insulin release from hydrogels (n = 1) at various volume equivalents p(SET) to p(HPMA-co-PBA) at 37 °C in DPBS buffer pH 7.4.

Insulin has an isoelectric point (pI) of 5.3 and is negatively charged under biologically relevant conditions (pH 7.4).[24] We next envisioned that synthesis of a co-polymer bearing monomers with amine groups or phenylboronic acid would help entrap insulin in the hydrogel network through the electrostatic interactions imposed by the pendant amine groups which would exhibit positive charge at neutral pH. Consequently, we synthesized a co-polymer with a protected amine and boronic acid via free radical polymerization, and deprotected with TFA to yield a

poly(N-(3-aminopropyl) methacrylamide-co-methacrylamidophenylboronic acid) (p(APMA-co-PBA) (**Figure 5-2 C**). The polymer had 33% PBA incorporated by ^{1}H-NMR. This co-polymer formed a robust hydrogel with the trehalose glycopolymer upon an initial gelation test and showed accelerated insulin release from the hydrogel with increased glucose concentration (**Figure 5-6 A**). Moderate background release was observed that was comparable to the original 8-arm PEG-phenylboronic acid system under the initially tested conditions (1:7 p(SET):p(APMA-co-PBA)). Insulin release was analyzed with hydrogels made from different ratios of trehalose glycopolymer and p(APMA-co-PBA) (**Figure 5-6 B**). The lowest background release was observed using 1:6 p(SET):p(APMA-co-PBA), which exhibited 60% insulin release in the absence of glucose. However, these results were only slightly better than the 70% insulin release observed in our original system.[12] These experiments suggest that the background insulin release is difficult to prevent with simple physical entrapment.

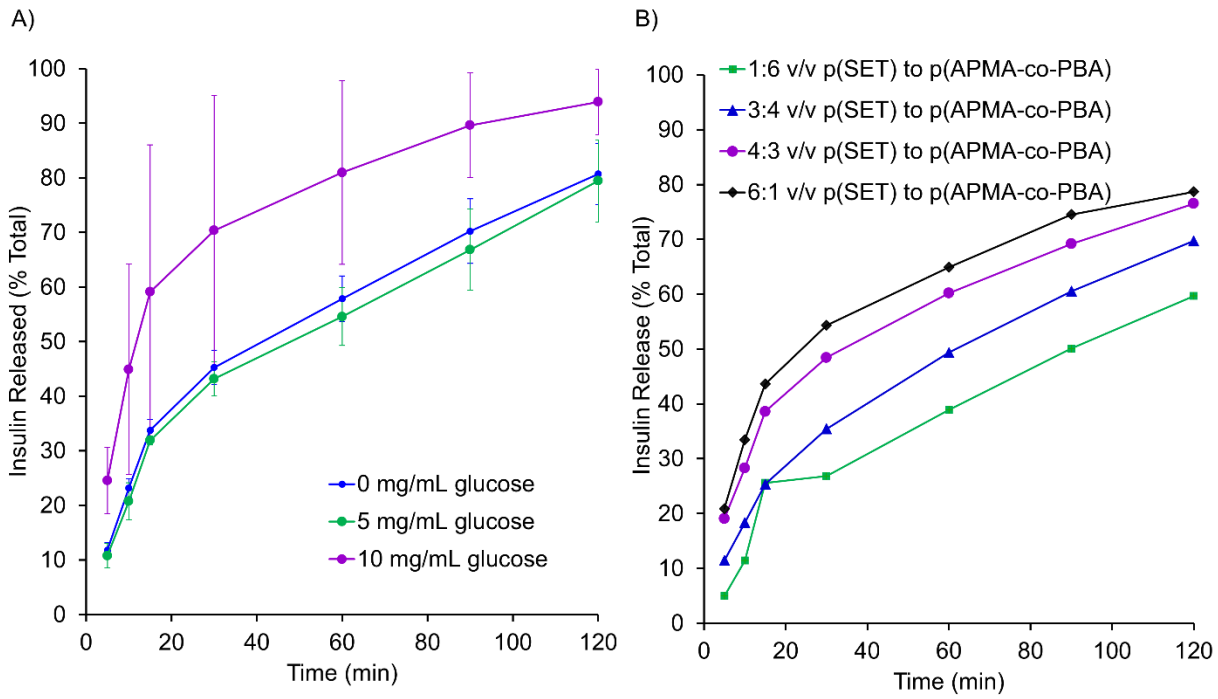

Figure 5-6. Investigation into the effects of altering co-polymer electrostatics on insulin release. (A) FITC-insulin release from hydrogels (n = 3) at various concentrations of glucose at 1:7 v/v p(SET) to p(APMA-co-PBA) solutions and (B) optimization of background insulin release from hydrogels (n = 1) at different volume ratios p(APMA-co-PBA) to p(SET) trehalose glycopolymer in D-PBS buffer pH 7.4 at 37 °C.

In our previous studies, we hypothesized that the hydrogel formation was aided by the multivalency of the polymers, effectively strengthening the weak interaction of trehalose with the polymer bearing the phenylboronic acids.[12] We hypothesized that changing the identity of the boronic acid to increase the binding affinity of phenylboronic acid to trehalose would strengthen the gel network and decrease background release. However, strategies to increase the binding affinity did not lower the background insulin release and in some cases resulted in weaker hydrogels. We believe this may result from changes in solubility when altering the identity of the

boronic acid or design of the cross-linker, which affected the strength of the gel network. The inclusion of charged monomers in the cross-linker to utilize electrostatic interactions resulted in the lowest background release of insulin without glucose in solution, though the amount of insulin released was only slightly lower than in our previous report. Diffusion of insulin out of the network in addition to the gradual dissolution of the hydrogel present challenges to all the strategies we have tested thus far. Because phenylboronic acid forms dynamic covalent bonds with polyols, the cross-linking of the hydrogel network is not permanent and undergoes dynamic rearrangement. Additionally, the affinity for phenylboronic acid binding to trehalose is weak (K_b = 2.57 M^{-1} for glucose vs. 0.48 M^{-1} for trehalose).[12] We believe these properties to be the major contributing factor limiting background release optimization.

5.3 Conclusion

This chapter details efforts to improve the unwanted background release of a glucose-responsive hydrogel for insulin delivery and stability. Several strategies were employed to lower the amount of insulin released during incubation in buffer in the absence of glucose and included varying the phenylboronic acid binding strength, increasing the cross-link density of the gel, and incorporating electrostatic interactions. Altering the identity of the phenylboronic acid and targeting smaller pore size did not improve the background release. Incorporation of cationic amine comonomers in a phenylboronic acid-containing polymer decreased the background insulin release after optimization of gelation conditions. However, this was a small improvement to the original design, suggesting a fundamental limit to background optimization because of the weak trehalose-phenylboronic acid interaction and the dynamic nature of the hydrogel network.

5.4 Appendix D

Materials

Materials were purchased from Sigma-Aldrich and Fisher Scientific and were used without purification unless noted otherwise. Recombinant human insulin was purchased from Sigma-Aldrich. Trehalose was purchased from The Healthy Essential Management Corporation (Houston, TX), and was azeotropically dried with ethanol and kept under vacuum until use. Azobisisobutyronitrile (AIBN) was recrystallized from acetone before use. 8-arm and 4-arm PEG amines were purchased from Jenkem Technology (Allen, TX). Human insulin ELISA kit was purchased from Mercodia (Uppsala, Sweden). Styrenyl ether trehalose monomer was prepared using the previously reported procedure.[14] 2-Methacrylamidophenylboronic acid pinacol ester was synthesized by Jeong Hoon Ko as previously reported.[22] p(SET) was prepared by Juneyoung Lee as described previously.[12] Poly(2-hydroxypropyl methacrylate-co-methacrylamidophenylboronic acid) was synthesized by Jeong Hoon Ko.

Analytical techniques

Nuclear Magnetic Resonance (NMR) spectra were recorded on a Bruker AV 400 MHz spectrometer. Gel permeation chromatography was conducted on a Shimadzu HPLC system equipped with a refractive index detector RID-10A and two Polymer Laboratories PLgel 5 μm mixed D columns (with guard column). Lithium bromide (0.1 M) in N,N-dimethylformamide (DMF) at 40 °C was used as the solvent (flow rate: 0.6 mL/min). Near-monodisperse poly(methyl methacrylate) standards (Polymer Laboratories) were employed for calibration. Preparatory reverse phase high performance liquid chromatography (HPLC) was carried out on a Shimadzu HPLC system equipped with a UV detector using a Luna 5 μm C18 100 Å column (preparatory:

5 μm, 250 x 21.2 mm) with monitoring at λ = 215 nm and 254 nm. Isocratic solvent system (water:methanol = 50:50) was used as the mobile phase at a flow rate of 10 mL/min. Fluorescence measurement was made on a FlexStation II (Molecular Devices). DSC for characterization of nanogel VPTT was conducted on a Mettler Toledo DSC3+ with ~5 mg polymer in 40 μL aluminum pans with three linear gradient heat ramps (-50 to 270 °C, 270 to -50 °C, -50 to 280 °C) with a heating rate of 10 °C/min.

Reductive amination of 8-arm PEG-amine with 4-formylphenylboronic acid

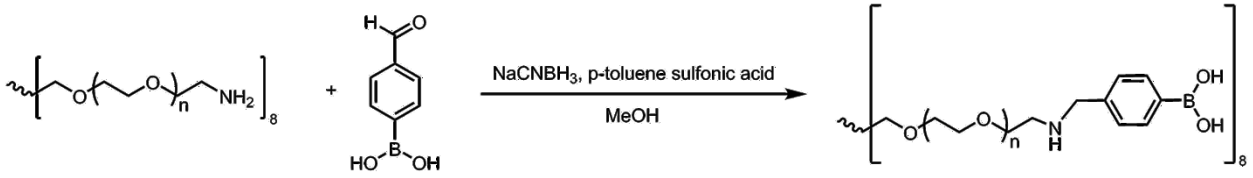

8-arm PEG amine (240 mg, 10 kDa, 24 μmol) and 4-formylphenylboronic acid (70.3 mg, 0.36 mmol) were dissolved in 1.7 mL of anhydrous MeOH in a dram vial. $NaBH_3CN$ (22.7 mg, 0.36 mmol) was added and the reaction was stirred at 25 °C (wrapped in foil). After 5 days the reaction solution was purified by dialysis (MWCO 3.5 kDa) against MeOH for 3 days. MeOH was removed and the polymer was recovered after lyophilization from water to yield 241.6 mg (91 % yield). ^1H NMR (400 MHz in D_2O) δ: 7.75 (16 H), 7.41 (16 H), 3.69 (908 H).

Reductive amination of 4- or 8-arm PEG-amine with 2,4-difluoro-3-formylphenylboronic acid

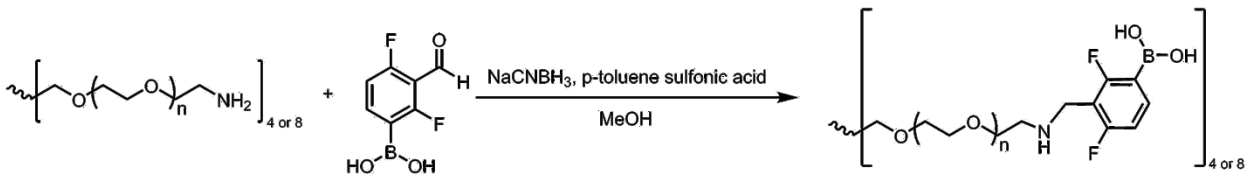

4-arm PEG amine (2 kDa, 100 mg, 0.05 mmol) or 8-arm PEG amine (10 kDa, 500 mg, 0.05 mmol), 2,4-difluoro-3-formylphenylboronic acid (74 mg, 0.40 mmol), *p*-toluenesulfonic acid (1.33 mg, 0.001 mmol), and sodium cyanoborohydride (31 mg 0.49 mmol) were dissolved in methanol (0.7 mL) and stirred for 3 days at 23 °C. The solution was precipitated into cold diethyl ether, decanted, and the solvent was removed in vacuo. The product was purified by dialyzing against H_2O (MWCO 3.5 kDa). For 8-arm PEG-FPBA: ^{1}H NMR (400 MHz in D_2O) δ: 7.63 (8H), 7.02 (8H), 3.72 (944 H). For 4-arm PEG-FPBA: ^{1}H NMR (400 MHz in CD_3OD) δ: 7.55 (4H), 7.36 (4H), 6.88 (4H), 3.61 (280H).

Co-polymerization of tert-butyl (3-methacrylamidopropyl)carbamate and 2-methacrylamidophenylboronic acid pinacol ester

2-Methacrylamidophenylboronic acid pinacol ester (66 mg, 0.229 mmol), tert-butyl (3-methacrylamidopropyl)carbamate (222 mg, 0.919 mmol), and AIBN (0.65 mg, 3.9 μmol) were dissolved in anhydrous DMSO (0.70 mL). The solution underwent four cycles of freeze-pump-thaw, and polymerization was initiated by immersing the flask into an oil bath at 70 °C. The polymerization was monitored by ^{1}H-NMR and was quenched at 70% conversion by exposure to oxygen and freezing in liquid N_2. The polymer was purified by dialyzing against H_2O (MWCO

3.5 kDa). ^{1}H NMR (400 MHz in CD_3OD) δ: 7.58-6.81, 6.72, 2.88, 1.34, 0.74. M_n= 1.8 kDa (by GPC), Đ = 1.15.

Deprotection of *tert*-butyl (3-methacrylamidopropyl) carbamate and 2-methacrylamidophenylboronic acid pinacol ester co-polymer

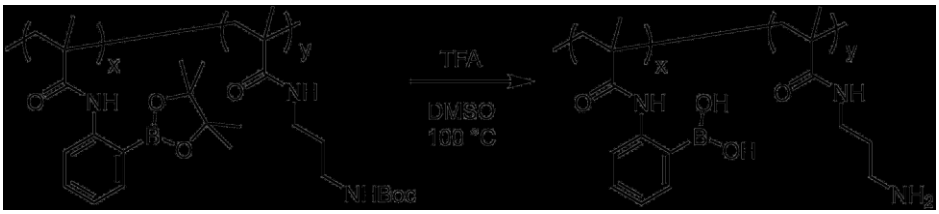

To 60 mg polymer, 1.6 mL 1:1 DMSO:TFA was added and the mixture was stirred 22 h at 100 °C. Deprotection was confirmed by ^{1}H-NMR and the polymer was purified by dialyzing against H_2O (MWCO 3.5 kDa). ^{1}H NMR (400 MHz in D_6DMSO) δ: 7.70, 7.21, 6.74, 6.40, 2.88, 1.36, 0.74. IR: ν = 3552, 2972, 2931, 1686, 1641, 1577, 1517, 1479, 1448, 1390, 1363, 1320, 1274, 1252, 1164, 1118, 1069, 1039, 1024, 953, 860, 761.

Gelation test of PBA polymers with trehalose polymer

The poly(SET) (500 mg/mL) and PBA polymer (200 mg/mL) stock solutions were prepared in D-PBS, pH 7.4. The gels were prepared by adding 9:1 ratio p(SET) to PBA polymer stock solutions for a total of 23 µL and incubating at room temperature for 1 h. Gelation was tested by visual inspection and manipulation with a plastic pipette tip.

FITC labeling of insulin

Insulin labeling with fluorescein isothiocyanate isomer I (FITC) was performed by dissolving insulin (0.65 mg, 0.112 µmol) and FITC (3.48 mg, 8.94 µmol) in 0.33 mL of 1 M

sodium bicarbonate buffer, pH 8.3. The mixture was stirred for two hours, and free FITC was removed by repeated centrifugation through a membrane using Centriprep tubes with molecular weight cut-off (MWCO) of 3 kDa. Typical degree of labeling was approximately 0.7 FITC per insulin as determined by UV absorbance.

FITC-labeled insulin release from trehalose hydrogel

FITC-labeled insulin (13.22 mg/mL in Dulbecco's phosphate-buffered saline D-PBS, pH 7.4) was added to the trehalose polymer (500 mg/mL). The PBA containing polymer was dissolved in D-PBS at 200 mg/mL concentration. Next, various volume of each stock solution for a total of 10 μL were added to an Eppendorf Lo-Bind centrifuge tube. The tube was agitated on a ThermoShaker (Allsheng Instruments, China) at 1,500 rpm at 21 °C for 1 h. The gels were transferred into a 24-well plate filled with 1 mL D-PBS and left to hydrate for 30 min. Next, the gels were transferred to a 96-well plate that had been blocked with 1% wt/vol bovine serum albumin (BSA) in D-PBS to prevent protein adsorption and filled with 0.3 mL of D-PBS containing 0, 5, or 10 mg/mL glucose. At each time point, all the solutions were aliquoted and the wells containing the gels were immediately refilled with 0.3 mL of the same buffer. After the last time point, the wells were treated with 0.3 mL of D-PBS containing 100 mg/mL glucose and incubated at 37 °C for 5 min to completely dissolve the gels. All the solutions were then transferred for measurement, and fluorescence of the time point aliquots and the residual insulin in solutions recovered after gel dissolution was measured.

Hydrogel dissolution kinetics

The poly(SET) (200 mg/mL) and p(HPMA-co-PBA) (100 mg/mL) stock solutions were prepared in D-PBS, pH 7.4. The gels were prepared by adding 1:1 ratio p(SET) to p(HPMA-co-PBA) stock solutions for a total of 10 µL and incubating at room temperature for 30 min. The gels were hydrated in D-PBS for 1 h, and then transferred to 5 mL D-PBS containing 0, 5, or 10 mg/mL glucose. At each time point, gels were weighed and then replaced into respective buffers.

Figures

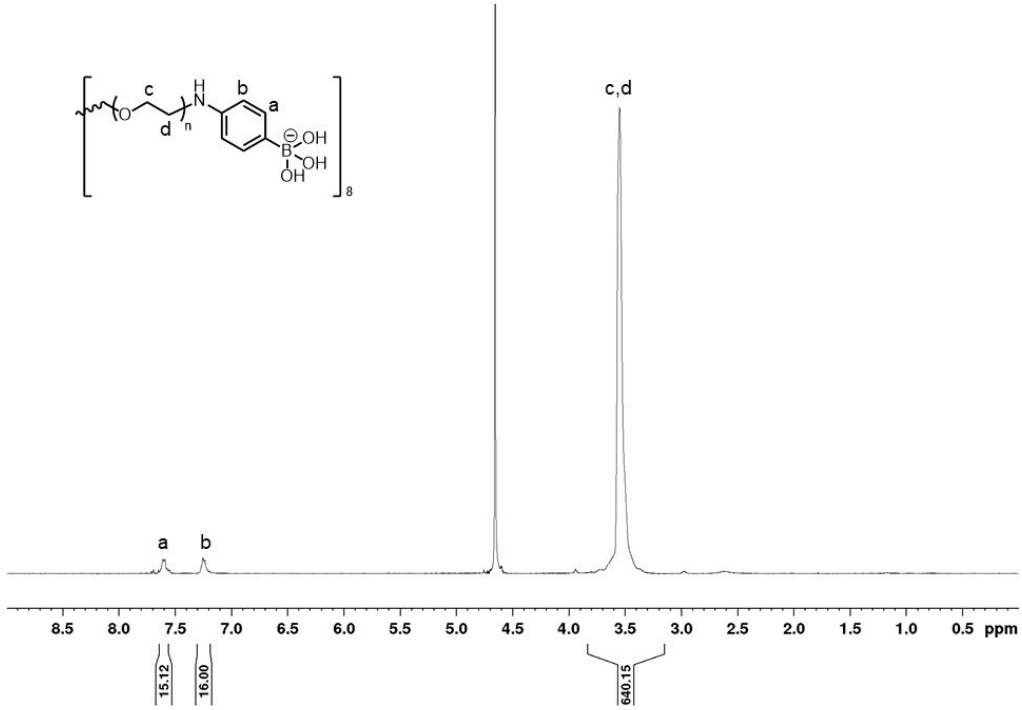

Figure 5-7. ^{1}H-NMR of 8-arm PEG-PBA (D_6DMSO).

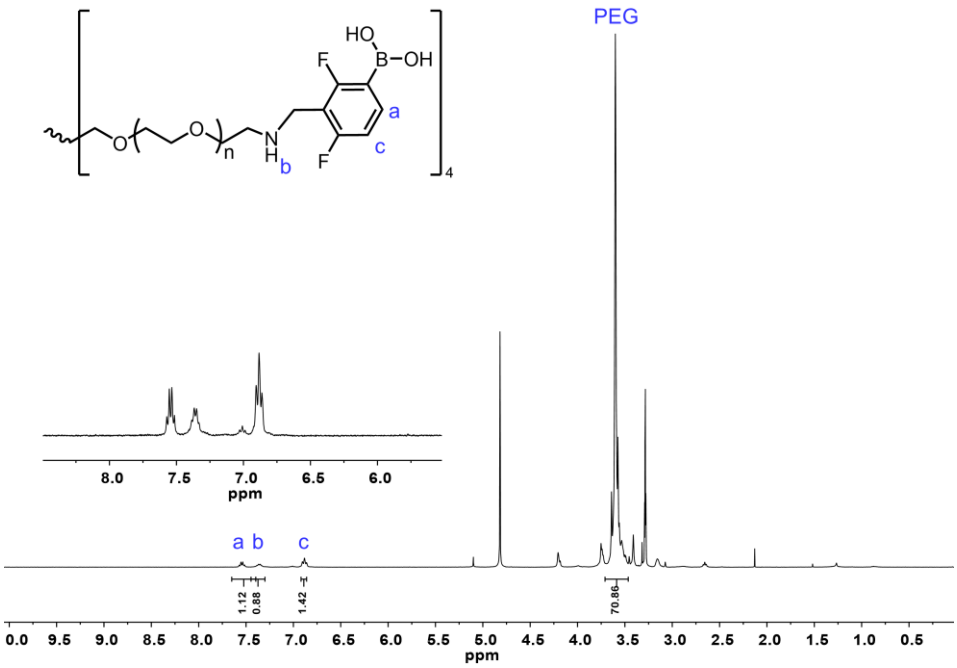

Figure 5-8. ^{1}H-NMR of 4-arm PEG-FPBA (CD_3OD).

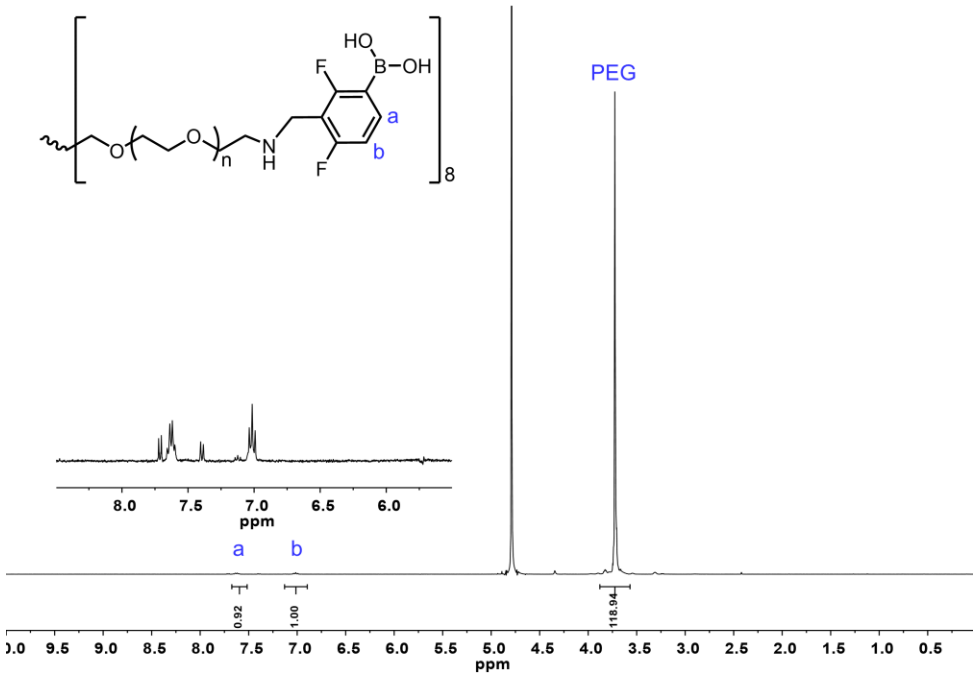

Figure 5-9. ^{1}H-NMR of 8-arm PEG-FPBA (D_2O).

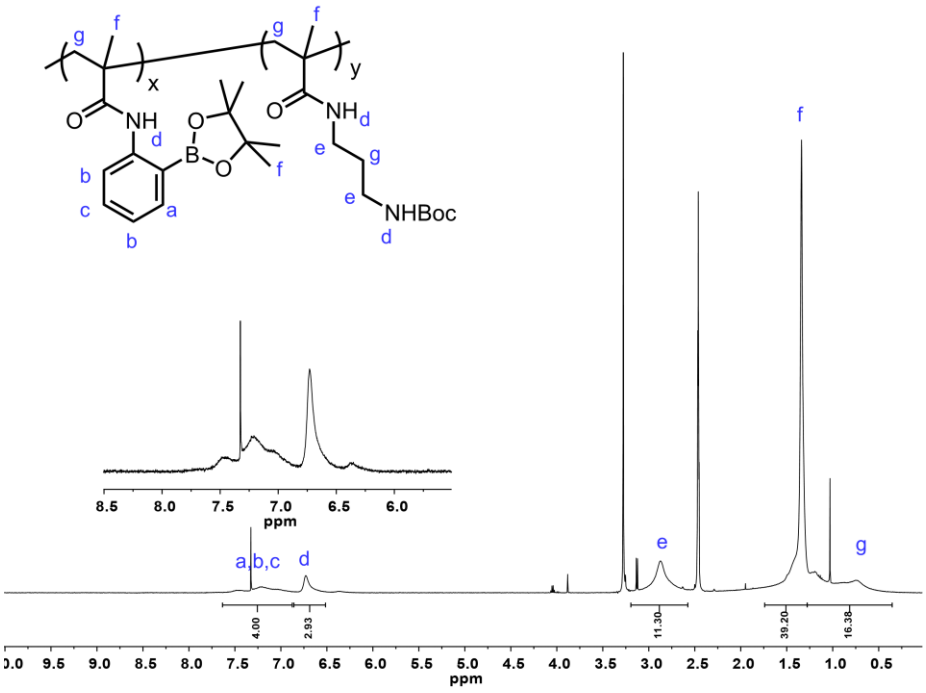

Figure 5-10. ^{1}H-NMR of p(APMA-co-PBA) before deprotection ($CDCl_3$).

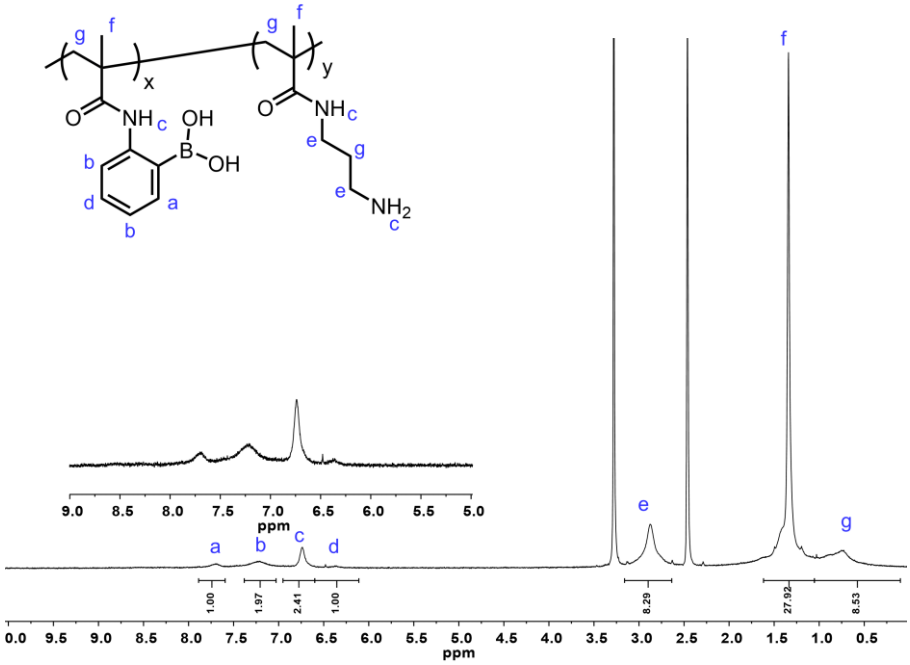

Figure 5-11. ^{1}H-NMR of p(APMA-co-PBA) after deprotection (D_6MSO).

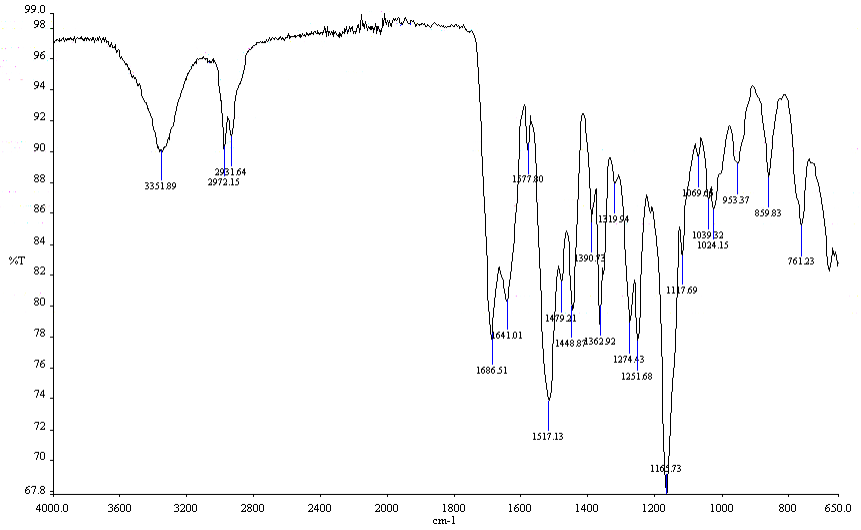

Figure 5-12. FT-IR spectrum of p(APMA-co-PBA)

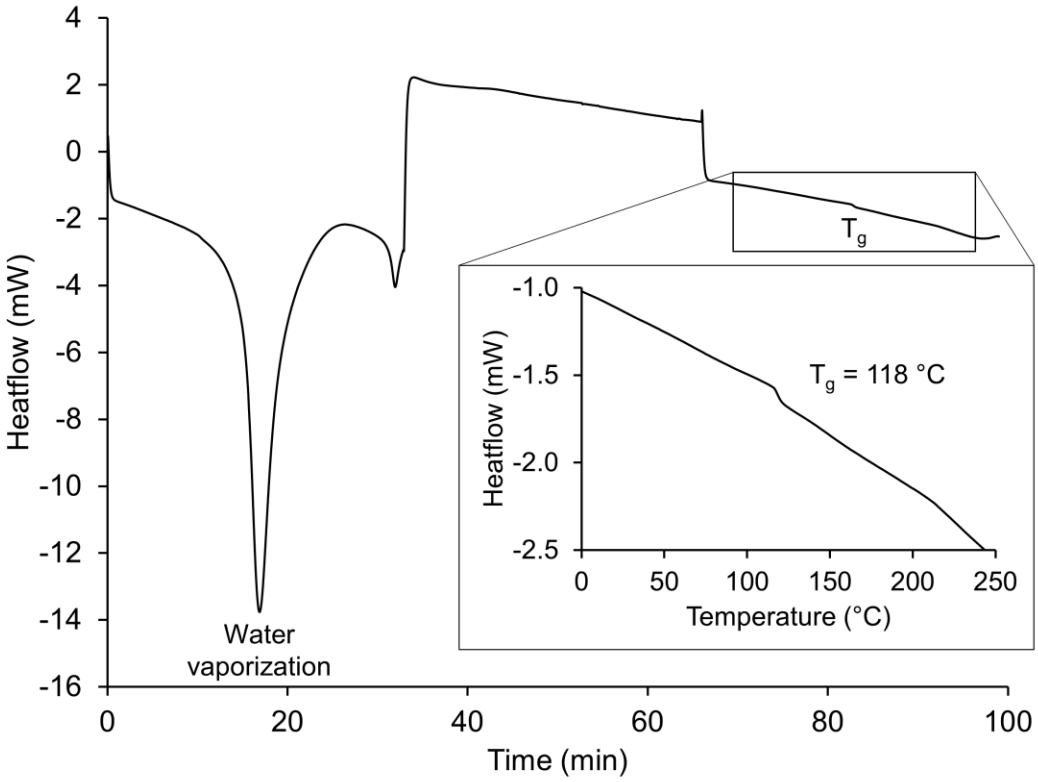

Figure 5-13. DSC trace with three linear gradient heat ramps (-50 to 270 °C, 270 to -50 °C, -50 to 280 °C, with rate of 10 °C/min) of trehalose polymer

5.5 References

(1) Pelegri-O'Day, E. M.; Lin, E.-W.; Maynard, H. D. Therapeutic protein–polymer conjugates: advancing beyond PEGylation. *J. Am. Chem. Soc.* **2014,** *136*, 14323-14332.

(2) Brange, J.; Langkj, L.; Havelund, S.; Vølund, A. Chemical stability of insulin. 1. Hydrolytic degradation during storage of pharmaceutical preparations. *Pharm. Res.* **1992,** *9*, 715-726.

(3) Oliva, A.; Farina, J. B.; Llabres, M. Influence of temperature and shaking on stability of insulin preparations: Degradation kinetics. *Int. J. Pharm.* **1996,** *143*, 163-170.

(4) Association, A. D. Standards of medical care in diabetes—2017 abridged for primary care providers. *Clinical Diabetes* **2017,** *35*, 5-26.

(5) Brooks, W. L. A.; Sumerlin, B. S. Synthesis and Applications of Boronic Acid-Containing Polymers: From Materials to Medicine. *Chem. Rev.* **2016,** *116*, 1375-1397.

(6) Wu, Q.; Wang, L.; Yu, H.; Wang, J.; Chen, Z. Organization of glucose-responsive systems and their properties. *Chem. Rev.* **2011,** *111*, 7855-75.

(7) Cambre, J. N.; Sumerlin, B. S. Biomedical applications of boronic acid polymers. *Polymer* **2011,** *52*, 4631-4643.

(8) Matsumoto, A.; Ishii, T.; Nishida, J.; Matsumoto, H.; Kataoka, K.; Miyahara, Y. A synthetic approach toward a self-regulated insulin delivery system. *Angew Chem Int Ed Engl* **2012,** *51*, 2124-2128.

(9) Bapat, A. P.; Roy, D.; Ray, J. G.; Savin, D. A.; Sumerlin, B. S. Dynamic-covalent macromolecular stars with boronic ester linkages. *J. Am. Chem. Soc.* **2011,** *133*, 19832-19838.

(10) Yesilyurt, V.; Webber, M. J.; Appel, E. A.; Godwin, C.; Langer, R. S.; Anderson, D. G. Injectable Self-Healing Glucose-Responsive Hydrogels with pH-Regulated Mechanical Properties. *Adv. Mater.* **2016,** *28*, 86-91.

(11) Dong, Y.; Wang, W.; Veiseh, O.; Appel, E. A.; Xue, K.; Webber, M. J.; Tang, B. C.; Yang, X.; Weir, G. C.; Langer, R. S. Injectable and Glucose-Responsive Hydrogels Based on Boronic Acid-Glucose Complexation. *Langmuir* **2016,** *32*, 8743-8747.

(12) Lee, J.; Ko, J. H.; Mansfield, K. M.; Nauka, P. C.; Bat, E.; Maynard, H. D. Glucose-Responsive Trehalose Hydrogel for Insulin Stabilization and Delivery. *Macromolecular Biosci.* **2018,** *18*, 1700372.

(13) Liu, Y.; Lee, J.; Mansfield, K. M.; Ko, J. H.; Sallam, S.; Wesderniotis, C.; Maynard, H. D. Trehalose Glycopolymer Enhances Both Solution Stability and Pharmacokinetics of a Therapeutic Protein. *Bioconjugate Chem.* **2017,** *28*, 836-845.

(14) Lee, J.; Lin, E. W.; Lau, U. Y.; Hedrick, J. L.; Bat, E.; Maynard, H. D. Trehalose Glycopolymers as Excipients for Protein Stabilization. *Biomacromolecules* **2013,** *14*, 2561-2569.

(15) Mancini, R. J.; Lee, J.; Maynard, H. D. Trehalose glycopolymers for stabilization of protein conjugates to environmental stressors. *J. Am. Chem. Soc.* **2012,** *134*, 8474-8479.

(16) Sakurai, M., Biological functions of trehalose as a substitute for water. In *Water and Biomolecules*, Springer: 2009; pp 219-240.

(17) Fedorov, M. V.; Goodman, J. M.; Nerukh, D.; Schumm, S. Self-assembly of trehalose molecules on a lysozyme surface: the broken glass hypothesis. *Phys. Chem. Chem. Phys.* **2011,** *13*, 2294–2299.

(18) Springsteen, G.; Wang, B. A detailed examination of boronic acid-diol complexation. *Tetrahedron* **2002,** *58*, 5291-5300.

(19) Lü, C.; Li, H.; Wang, H.; Liu, Z. Probing the interactions between boronic acids and cis-diol-containing biomolecules by affinity capillary electrophoresis. *Anal. Chem.* **2013,** *85*, 2361-2369.

(20) Yan, J.; Springsteen, G.; Deeter, S.; Wang, B. The relationship among pK a, pH, and binding constants in the interactions between boronic acids and diols—it is not as simple as it appears. *Tetrahedron* **2004,** *60*, 11205-11209.

(21) Wiskur, S. L.; Lavigne, J. J.; Ait-Haddou, H.; Lynch, V.; Chiu, Y. H.; Canary, J. W.; Anslyn, E. V. p K a Values and Geometries of Secondary and Tertiary Amines Complexed to Boronic Acids Implications for Sensor Design. *Org. Lett.* **2001,** *3*, 1311-1314.

(22) Deng, C. C.; Brooks, W. L. A.; Abboud, K. A.; Sumerlin, B. S. Boronic Acid-Based Hydrogels Undergo Self-healing at Neutral and Acidic pH. *ACS Macro Lett.* **2015,** *4*, 220-224.

(23) Yang, X.; Lee, M. C.; Sartain, F.; Pan, X.; Lowe, C. R. Designed boronate ligands for glucose-selective holographic sensors. *Chem. - Eur. J.* **2006,** *12*, 8491-8497.

(24) Wintersteiner, O.; Abramson, H. A. The isoelectric point of insulin electrical properties of adsorbed and crystalline insulin. *J. Biol. Chem.* **1933,** *99*, 741-753.

Chapter 6. Glucose-Sensing Nanogels (G-SENs) for Glucagon Encapsulation

6.1 Introduction

Glucagon is a therapeutic peptide used to treat emergency hypoglycemia in diabetics, usually in response to insulin overdose.[1-2] The peptide is insoluble at neutral pH and instable in aqueous solutions, rapidly forming cytotoxic fibrils.[3-4] For this reason, therapeutic glucagon is packaged as a lyophilized powder that must be reconstituted in dilute acid just prior to use.[1] Because glucagon is used in emergency response to severe hypoglycemia, administration of this kit can be intimidating and requires another person to inject the drug when the patient is incapacitated, which can sometimes lead to inadequacy in dosing.[5] A newly FDA-approved nasal glucagon now on the market addresses this issue and is shown to be effective and easier to administer but has lower bioavailability and requires a larger dose to be effective.[6-7] Additionally, a stable ready-to-use glucagon formulated in DMSO was recently approved, though there are issues with discomfort stemming from the organic solvent.[8] Glucagon administration that mimics the endogenous response to prevent dangerously low blood glucose has not yet been realized and yet would be very important for the regulation of glucose for persons with diabetes.

A variety of glucose-responsive materials have been synthesized for insulin delivery, but only a few examples of responsive delivery of glucagon exist.[9] Many glucose-responsive materials use phenylboronic acids as glucose sensing units. Phenylboronic acids can form dynamic covalent bonds with 1,2- and 1,3-diols, including those on glucose. The affinity of binding can be tuned by the inclusion of electron-withdrawing substituents on the phenyl ring that lower boronic acid pK_a or through dative bonds with neighboring nitrogen or oxygen that stabilize the tetrahedral boronic acid geometry that favors binding.[10-11] The first example of glucose-responsive glucagon delivery was published during the course of this study and utilized a nanogel embedded in a microneedle

patch. The mechanism consists of a transition from a 1:1 to a 1:2 complexation between glucose and boronic acids resulting in a more cross-linked material, reducing the nanogel volume and squeezing out glucagon at low glucose concentrations.[12] Glucagon delivery in response to insulin concentration was also demonstrated using a glucagon-insulin aptamer conjugate that enabled competitive displacement from an immobilized insulin scaffold.[13]

Nanogels presenting a novel mechanism of contraction upon addition of glucose were recently reported. These nanogels were synthesized by copolymerizing thermoresponsive N-isopropyl acrylamide (NIPAM) with acrylic acid (AA), which was modified with 2-aminophenylboronic acid (2-APBA) post-polymerization.[14-15] Unlike similar nanogels utilizing 3-aminophenylboronic acid that become more soluble from the increase in effective charge after binding with glucose due to the change from neutral trigonal to negative tetrahedral form,[16] the 2-APBA-bearing nanogels became less soluble in the presence of glucose. The selected phenylboronic acid does not change charge upon binding because the B-O dative bond inherently stabilizes the negative tetrahedral geometry.[11] Instead, glucose acts as an additive, structuring water in its proximity, that changes the hydration of the pNIPAM chain to shift the lower critical solution temperature (LCST) of the polymer and volume phase transition temperature (VPTT) of hydrogels.[17-19] Incorporation of boronic acid in the polymer chain effectively concentrates the saccharide near the thermoresponsive polymer, amplifying this effect (**Scheme 6-1**).

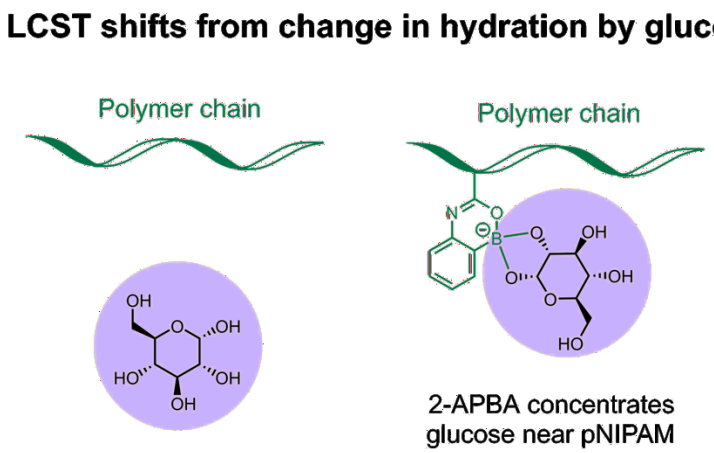

Scheme 6-1. Mechanism of LCST shift for 2-APBA copolymers with glucose as additive.

Herein, we describe the preparation of nanogels for the glucose-responsive delivery of glucagon (**Scheme 6-2**). The nanogels were synthesized using either NIPAM or poly(ethylene glycol) methacrylate (PEGMA) as the thermoresponsive elements. Characterization of these nanogels revealed glucose-dependent shifting of the VPTT below relevant physiological temperatures. During the loading process, native glucagon degraded and could not be released upon lowering glucose to swell the nanogels. Using a soluble glucagon analog, improved loading was achieved without degradation of the peptide.

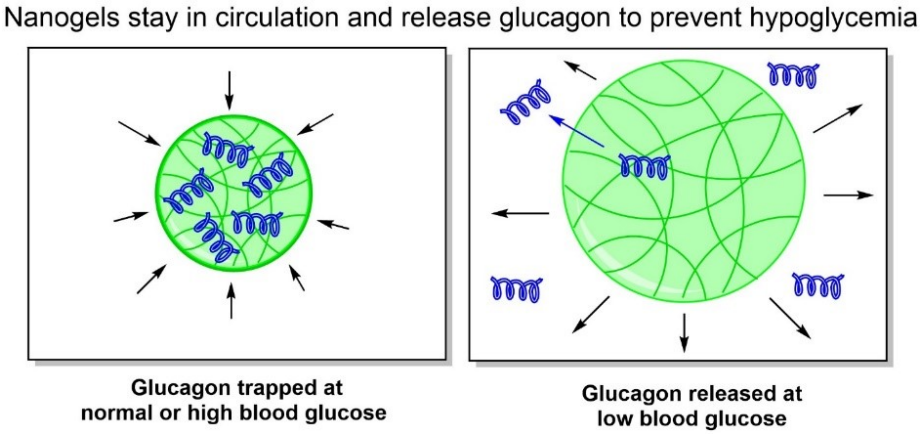

Scheme 6-2. Overview of nanogel for glucose-responsive glucagon delivery

6.2 Results and Discussion

We envisioned using nanogels that would collapse upon addition of glucose to encapsulate glucagon in situ. Nanogels would swell when blood glucose approached the counterregulatory threshold (70 mg/dL), releasing glucagon by diffusion out of the nanogel network to prevent hypoglycemia.[6] Diameters between 100 and 200 nm were targeted for extended circulation in the blood to control blood glucose for approximately 24 h.[20]

NIPAM nanogels were synthesized as previously reported (**Scheme 6-3 A**), with N-isopropylmethacrylamide (NIPMAM) as a comonomer to tune the VPTT to a physiologically relevant temperature.[15] Precipitation polymerization with NIPAM, NIPMAM, AA, and *N,N′*-methylenebis(acrylamide) (BIS) crosslinker at 70 °C with 2 mM SDS was found to give uniform nanogels with a diameter of 132 nm at 20 °C. Lower concentration of SDS (1 mM) resulted in larger nanogels with a diameter of 324 at 20 °C. Nanogels were functionalized post-polymerization by EDC coupling with 2-APBA as a glucose-sensing moiety. The nanogels were characterized by ^{1}H-NMR and FT-IR and thermo- and glucose-responsivity was characterized by DSC (Appendix E: **Figure 6-4**, **Figure 6-6**, and **Figure 6-8**). Full coupling of the AA with 2-APBA was confirmed by ^{1}H-NMR. VPTT was determined to be approximately 38 °C by DSC, which is physiologically relevant. NIPAM nanogels with 15% 2-APBA content were found to have the best glucose response with a sensitivity as low as 300 mg/dL and maximum size change of 31 nm in diameter by DLS. The nanogels were also responsive to other polyols, as determined by DSC (Appendix E: **Figure 6-8**), including xylose and poly(vinyl alcohol), which would enable glucagon loading without requiring glucose in the formulation.

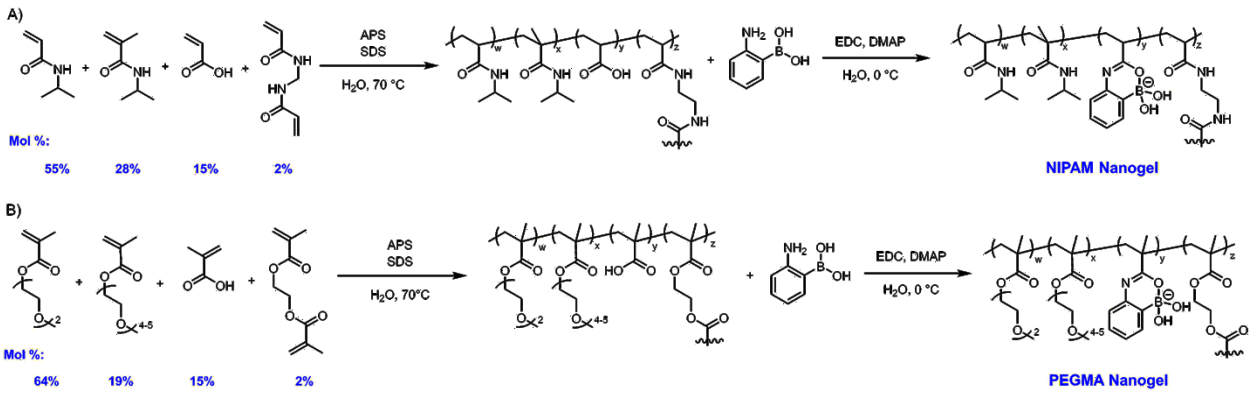

Scheme 6-3. Synthesis of (A) NIPAM and (B) PEGMA nanogels by precipitation polymerization and post-polymerization coupling of boronic acid.

Because of general concern about pNIPAM toxicity in vivo,[21-22] PEGMA nanogels were also prepared (**Scheme 6-3 B**). To tune the VPTT to a physiologically relevant temperature, the feed ratio of approximately 1 to 3 of 300 Da oligo(ethylene glycol) methyl ether methacrylate ($OEGMA_{300}$) and diethylene glycol methyl ether methacrylate (DEGMA) was selected based on previous reports tuning LCST and VPTT of OEGMA copolymers and gels.[23-24] Precipitation polymerization with $OEGMA_{300}$, DEGMA, methacrylic acid (MAA), and ethylene glycol dimethacrylate (EGDMA) crosslinker at 70 °C with 1.5 mM SDS resulted in uniform nanogels with a diameter of 246 nm at 20 °C and 103 nm at 40 °C. Higher concentrations of SDS did not yield nanogels with controlled size. PEGMA nanogels were functionalized with 2-APBA by post-polymerization coupling and characterized in the same manner as NIPAM nanogels (Error! Reference source not found., Appendix E: **Figure 6-5**, **Figure 6-7**, **Figure 6-9**, and **Figure 6-10**) and found to have a VPTT of approximately 43 °C by DSC.

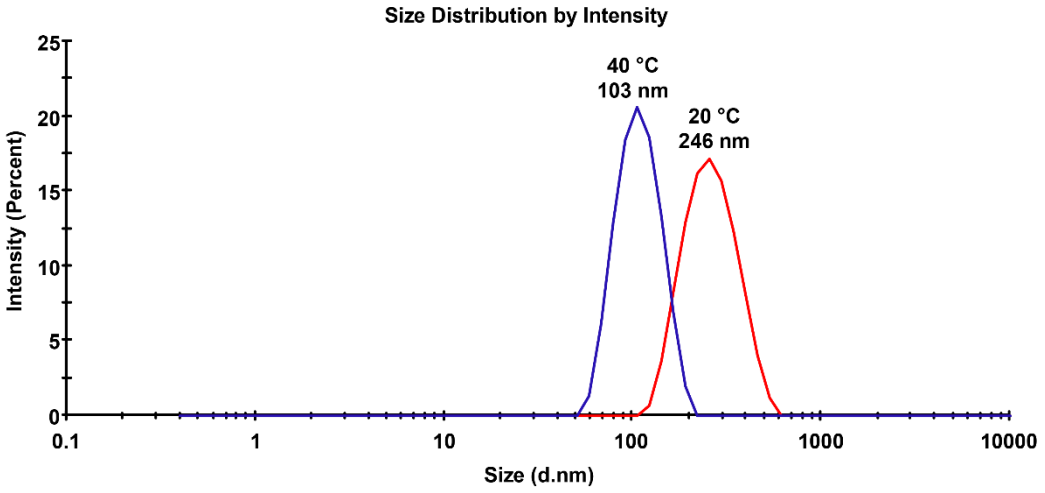

Figure 6-1. Characterization of PEGMA nanogels by DLS

In addition to the larger size and diameter change, PEGMA VPTT decreased by 14 °C with 10 mg/mL glucose by DSC compared to only 4 °C for NIPAM nanogels. The behavior of NIPAM and PEGMA in solution may lead to these observed differences. A study of saccharide effects on thermoresponsive polymers found a greater effect of glucose on the LCST of PEG-based Pluronics than pNIPAM.[17] Additionally, PEGMA lacks hydrogen bonding donors, such as the amide of NIPAM which is hypothesized to play a role in the hysteresis observed for pNIPAM upon cooling that is not observed with PEGMA.[24] The mechanism of nanogel collapse is dependent upon the hydration of the polymer chains with glucose acting as an additive. Thus, we hypothesize that the increase in structured water around glucose affects the hydration of PEGMA nanogels more than NIPAM nanogels because of the differences in hydrogen bonding and amphiphilicity of OEGMA, leading to the larger change in VPTT.

Glucagon loading into the nanogels was optimized using a three-step procedure (**Scheme 6-4**). First, the nanogels were incubated with glucagon in borate buffer pH 9.5 at 4 °C 14 h to maintain gel swelling, maintain peptide solubility and stability, and enable equilibrium diffusion.

Nanogels were then collapsed by adding 5 mg/mL glucose and heating to 37 °C. Glucagon that was not entrapped in the nanogel was then separated by wash steps using either centrifugal filtration or dialysis, maintaining the glucose concentration and changing the pH by introducing DPBS pH 7.4 in the final step. Loading efficiency (wt. loaded glucagon/initial wt. glucagon) and drug loading (wt. glucagon/total wt. of nanogel and glucagon) was determined indirectly by measuring the amount of glucagon in the washes by HPLC (Appendix E: **Table 6-3**). However, this method did not allow direct characterization of the amount of glucagon loaded in the nanogels. Additionally, very little peptide was detected when buffer was switched to DPBS pH 7.4 without glucose to stimulate release by enabling nanogel swelling. Similar results were also seen when borate buffer, stabilizing excipients, FBS, or blood were used throughout the loading and release steps, indicating that peptide solubility and partitioning in the buffer was not the issue but rather the instability (Appendix E: **Table 6-3**).

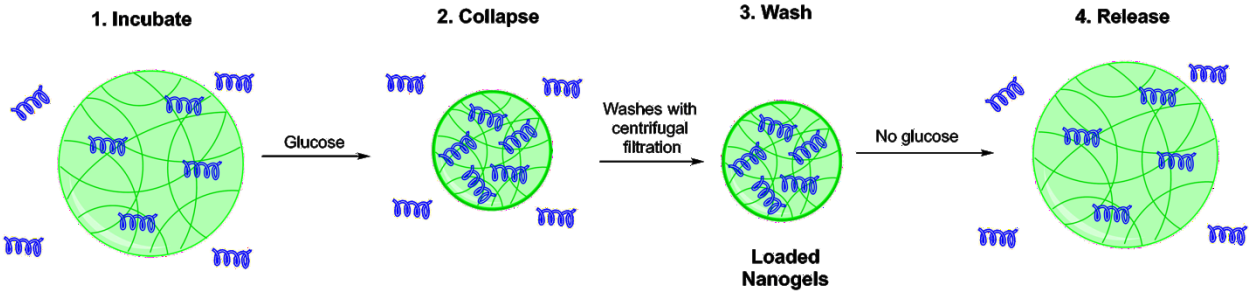

Scheme 6-4. Protocol to load glucagon into nanogels.

We hypothesized that a spectroscopic detection method would facilitate direct characterization of glucagon in the presence of the nanogels and increase assay throughput compared to HPLC. The fluorescamine assay is a method to quantify protein and peptide concentration via an increase in fluorescence upon binding of fluorescamine with primary amines. Additionally, it works under both basic and neutral pH, which were used during loading and

release. To test if this assay would be a viable detection method, it was used to quantify the amount of glucagon during each step in the loading protocol (**Scheme 6-4**), as well as the amount left with the nanogels in the filter at the end of the experiment (Appendix E: **Figure 6-11**). The amount of glucagon measured in the washes agreed with the HPLC method and the nanogel itself did not result in any background signal as expected. The amount of glucagon measured in the presence of the nanogels (directly measured, without the wash steps) was 47% of the expected. Fluorescamine is known to selectively react with solvent-accessible primary amines, resulting in lower fluorescence signal for amines blocked through interactions with nanoparticles.[25-26] However, this did not account for the 81% difference in expected versus measured glucagon in the nanogels at the end of the experiment. Thus, we hypothesized that the low percent detection of glucagon during the release experiment could be due to glucagon degradation in the nanogel.

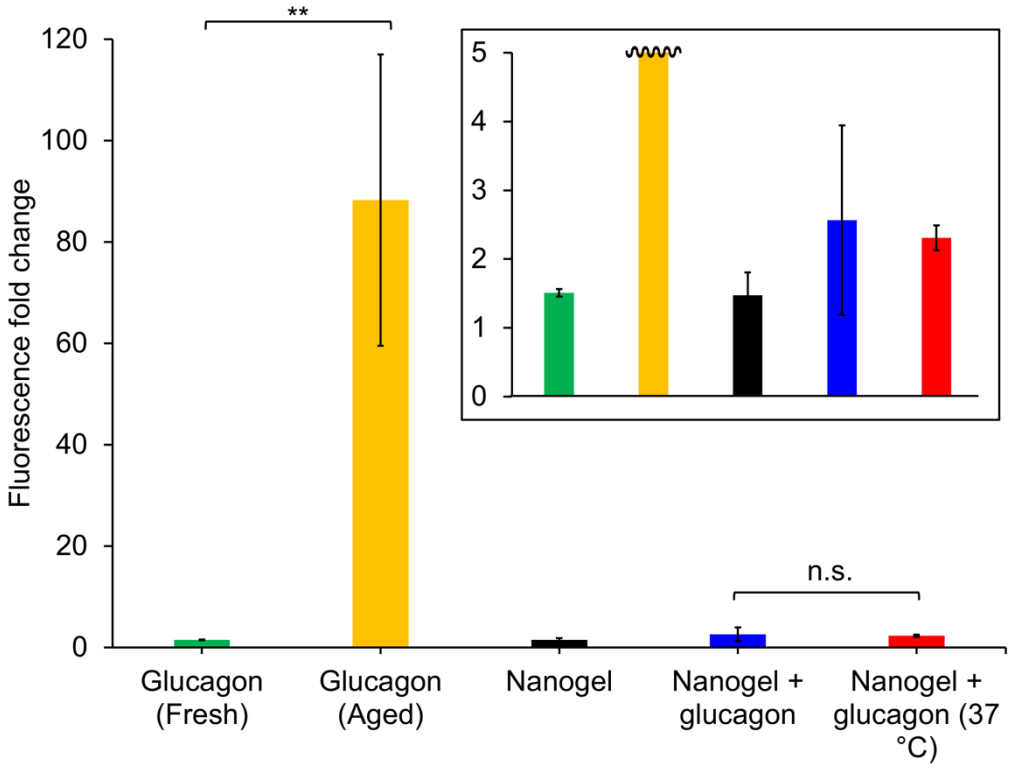

Figure 6-2. Stability of glucagon to fibrillation during loading using ThT assay to assess glucagon fibrillation in the presence of nanogel and during loading (n = 3, ** $p < 0.01$, n.s. $p > 0.1$).

Fibrillation is a major pathway of glucagon degradation in solution and may decrease the accessibility of glucagon's amines for fluorescamine binding, so the formation of fibrils during the loading conditions was investigated as a cause of the unexpectedly low signal in the nanogel. Thioflavin T (ThT) assay was used to quantitatively measure the extent of fibrillation during loading (**Figure 6-2**). Upon heating, glucagon forms fibrils which bind ThT, leading to a large fold increase in fluorescence signal. Glucagon in the presence of nanogel and after exposure to loading heat conditions did not significantly increase fluorescence, indicating that glucagon does not fibrillate during loading.

Scheme 6-5. Amino acid sequence comparing native glucagon and soluble glucagon analog with substitutions to eliminate deamidation site and lower isoelectric point.

Although this data indicates that glucagon does not fibrillate during the loading procedure, the low total detection of native glucagon could be due to shielding of the primary amines through chemical degradation. Glucagon also forms trimers and other higher order oligomers at high concentrations.[27-28] Steric blocking of amines upon formation of these aggregates from concentration of glucagon inside the nanogel during collapse could contribute to artificially low signal. To address these issues, a glucagon analog with improved solubility at neutral pH and greater stability was selected.[29-30] This analog has two amino acid substitutions at the C-terminus

that shift the isoelectric point to approximately 4.8 and eliminate a site of deamidation (**Scheme 6-5**). This change improves the solubility at neutral pH and could potentially disrupt glucagon self-interaction, which is known to occur at the C-terminus. Unlike the native glucagon, all of the soluble glucagon could be detected in the presence of either nanogel (directly measured, without the wash steps).

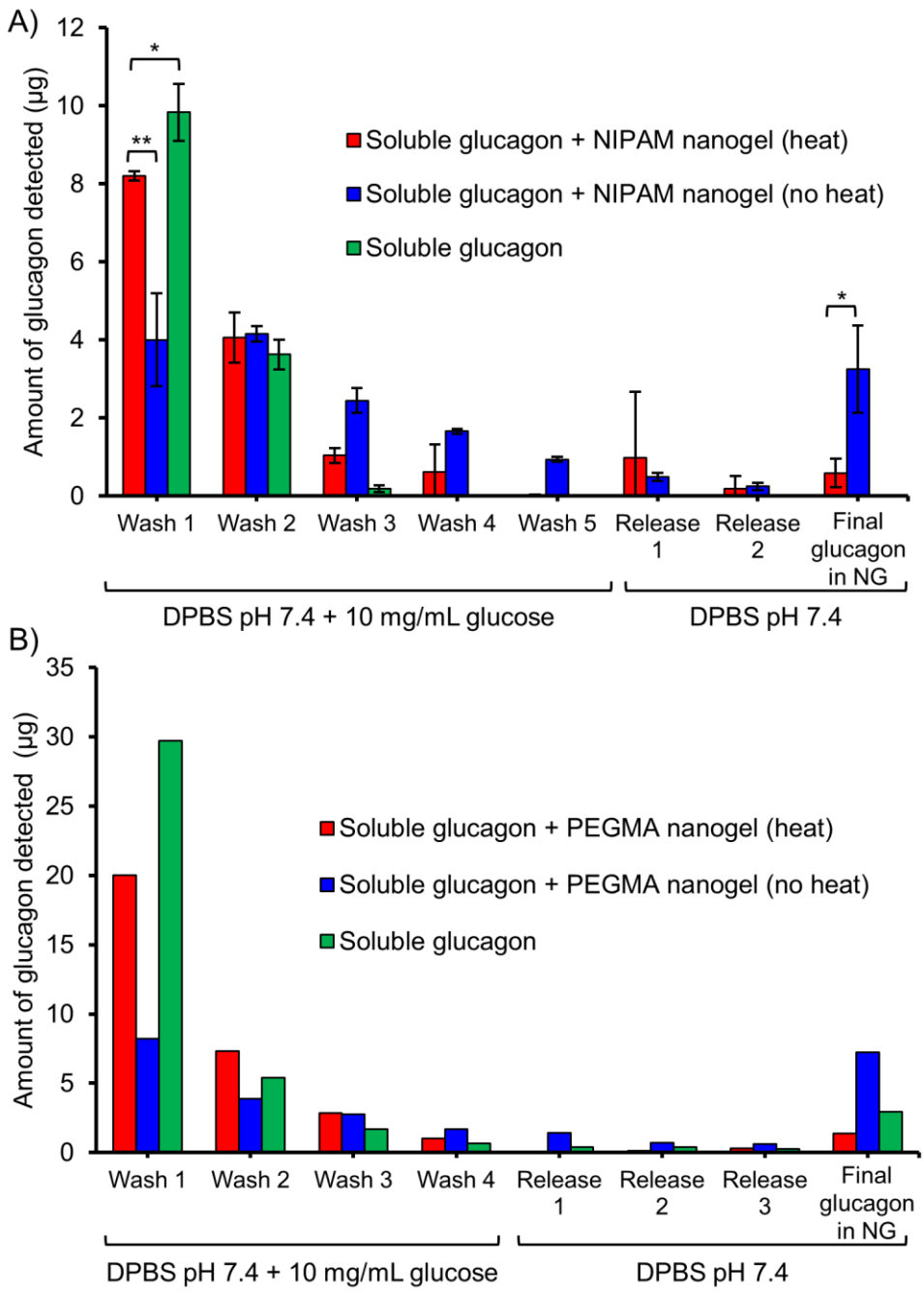

Figure 6-3. Amount of glucagon by fluorescamine assay during loading of soluble glucagon into (A) NIPAM nanogels (n = 3, * $p < 0.05$, ** $p < 0.005$) or (B) PEGMA nanogels (n = 1).

The soluble glucagon analog was loaded and released from the nanogel using the optimized centrifugal filtration procedure (**Scheme 6-4**) with and without the heating step to collapse the gel.

A control of just the soluble peptide was also included to assess stability and recovery during the centrifugation steps. Results for loading and release of the soluble glucagon in the nanogels is shown in **Figure 6-3** and summarized in **Table 6-1**. Loading efficiency and drug loading were again calculated indirectly from the amount of glucagon in the wash steps and the amount of glucagon released and in the nanogel left in the filter were determined from the fluorescamine assay. For the soluble glucagon control, 78% of the peptide was recovered in the wash steps, indicating good stability and passage through the membrane. Similar or higher recovery of the peptide was detected for the other conditions over the entire experiment. A difference in the amount of peptide in the first wash step in the presence of NIPAM nanogel was measured, with significantly more detected with the heating step (**Figure 6-3 A**). This also corresponded to the difference in loading efficiency and drug loading observed in **Table 6-1** comparing with and without heating. These data suggest glucagon may be squeezed out during the collapse upon heating. This squeezing-out mechanism has been observed for hydrophilic drugs in NIPAM hydrogels,[31] which agrees with our observation of this mechanism for the more hydrophilic glucagon analog. However, this difference could be due to degradation of native glucagon during the loading experiments. Very little release (< 3 μg) was observed for either nanogel condition when buffer was changed to DPBS pH 7.4 without glucose, same as for native glucagon. However, the amount of glucagon measured at the end of the experiment was significantly greater than the control, with 3.3 μg (17% of initial) detected in the NIPAM nanogels in the filter without heating. Similar results were seen with PEGMA nanogels (**Figure 6-3 B**) with a slight increase in the amount of soluble glucagon detected in the nanogel at 7.2 μg (25% of initial). This may be due to the larger change in diameter observed for PEGMA nanogels compared to NIPAM nanogels. Moreover, for all samples, a greater amount of the soluble glucagon (>77%) was accounted for

during the experiments than when native glucagon was studied, enabling more thorough characterization of loading and release.

Table 6-1. Summary of soluble glucagon loading and release into nanogels

	Loading efficiency (%)	Drug loading (wt. %)	Amount detected in release (µg)	Amount detected in filter (µg)	Recovery (% total detected)
Soluble glucagon	–	–	–	–	78
NIPAM (no heat)	39	0.3	0.7 ± 0.1	3.3 ± 1.1	77
NIPAM (heat)	25	1.6	1.2 ± 1.7	0.6 ± 0.3	81
PEGMA (no heat)	25	2.2	2.7	7.2	78
PEGMA (heat)	4	0.4	0.4	1.4	91

Although loading and detection was improved using the glucagon analog, a greater amount of glucagon release at low glucose concentrations is still needed. Additionally, a higher amount of glucagon in the final nanogels was observed without the heating step to collapse. These data indicate the peptide may be squeezed out during the collapse of the nanogel. This phenomenon has been observed for hydrophilic molecules encapsulated in NIPAM networks[31] and this mechanism was used for release of glucagon from nanogels.[12] To address these challenges, work using reversible covalent loading of glucagon into the nanogels is ongoing to avoid squeezing out. Additionally, self-assembled nanoparticles using block co-polymers containing the same glucose-responsive polymers as the nanogels are under investigation to improve the release of glucagon at low concentrations of glucose.

6.3 Conclusion

We have developed glucose- and thermo-responsive NIPAM and PEGMA nanogels for glucagon delivery. Nanogels were synthesized by precipitation polymerization and characterized by DLS and DSC. PEGMA nanogels were found to be larger in size and have a larger overall change in diameter upon collapse than NIPAM nanogels. Initial attempts at loading native glucagon resulted in low release and overall detection of the peptide. ThT assay showed glucagon was not fibrillating during loading but the fluorescamine assay indicated accessibility of primary amines was decreased from either chemical degradation or peptide interactions. Loading was improved for both nanogels using a more stable and soluble glucagon analog, though release of glucagon at low glucose concentrations was not changed. Overall, these materials exhibit dual stimuli-responsive materials and provide a basis for glucose-responsive glucagon delivery should the loading, stabilization and release be optimized. Work investigating strategies to address the low release of glucagon and squeezing-out mechanism is ongoing in the group.

6.4 Appendix E

Materials

All chemicals were purchased from Sigma-Aldrich and Fisher Scientific and were used without purification unless noted otherwise. Native glucagon was purchased from MedChemExpress or Biomatik. Soluble glucagon analog was purchased from Biomatik. Liquid monomers were purified by passage over basic alumina before used in polymerizations. For polymerizations, water was sparged with argon 30 min prior to use.

Analytical techniques

Nuclear Magnetic Resonance (NMR) spectra were recorded on a Bruker AV 400 MHz spectrometer. DSC for characterization of nanogel VPTT was conducted on a Mettler Toledo DSC3+ with 80 µL 10 mg/mL solution in 100 µL aluminum pans with gradient of 10 to 90 °C and a ramp rate of 5 °C/min. DLS for characterization of nanogel size and temperature response was conducted on a Malvern Nanozetasizer in 20 mM DPBS pH 7.4. Analytical HPLC for detection of glucagon was conducted on an Agilent 1260 Infinity II LC System equipped with a UV detector using Poroshell C18 column and a gradient solvent system (water:acetonitrile = 75:25 to 40:60 + 0.1 % trifluoroacetic acid over 17 min at 1 mL/min). Fluorescence in fluorescamine assay and turbidity for nanogel temperature response characterization was measured on a Tecan M1000 plate reader.

Synthesis of NIPAM nanogel

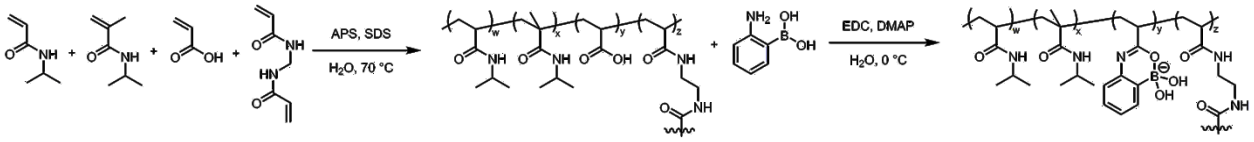

In a 3-neck round-bottom flask under argon, NIPAM (428 mg, 3.8 mmol, 27.1 equiv), NIPMAM (245 mg, 1.9 mmol, 13.8 equiv), AA (75 mg, 1.0 mmol, 1 equiv), N,N'-methylenebis(acrylamide) (21.5 mg, 0.14 mmol, 1 equiv), SDS (58 mg, 0.2 mmol, 1.4 equiv), water (9.5 mL), and a stir bar were added. The flask was placed in a 70 °C oil bath and stabilized under argon for 1 hour. APS (43 mg, 0.15 mmol, 1.07 equiv) dissolved in water (0.5 mL) was added to the flask to initiate the reaction. Polymerization was ended after 7 h by exposure to oxygen and removal from heat source. The nanogel was purified by dialysis (6-8 kDa MWCO) against water 3 days. To a round bottom flask under argon, 10 mL of NIPAM nanogel

(0.12 mmol acrylic acid, 1 equiv) was added. To the flask, 2-APBA (305 mg, 1.8 mmol, 10 equiv), EDC (410 mg, 2.6 mmol, 15 equiv), and DMAP (4.3 mg, 35 μmol, 0.2 equiv) were added successively. The reaction proceeded at 0 °C in an ice bath for 4 hours under argon. The product was purified by dialysis (6-8 kDa MWCO) against water for 3 days. ^{1}H NMR (400 MHz in D_2O) δ: 7.44, 7.20, 6.97, 3.76, 1.83, 1.52, 1.01. IR: ν = 3302, 2971, 2930, 2675, 1634, 1524, 1449, 1387, 1367, 1216, 1173, 1130, 1028, 962, 885, 840, 763 cm^{-1}.

Synthesis of PEGMA nanogel

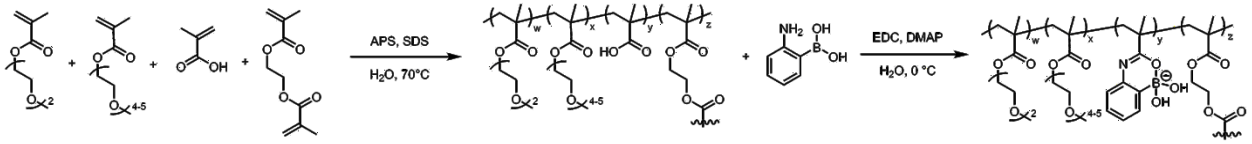

In a 3-neck round-bottom flask under argon, DEGMA (295 μL, 1.6 mmol, 1 equiv), $OEGMA_{300}$ (137 μL, 0.48 mmol, 0.3 equiv), methacrylic acid (31 μL, 0.37 mmol, 0.23 equiv), ethylene glycol dimethacrylate (8.7 μL, 0.046 μmol, 0.029 equiv), SDS (8 mg, 0.028 mmol, 0.017 equiv), water (24.5 mL), and a stir bar were added. The flask was placed in a 70 °C oil bath and stabilized under argon for 1 hour. APS (8.4 mg, 0.037 mmol, 0.023 equiv) dissolved in water (0.5 mL) was added to the flask and the reaction was initiated. Polymerization was ended after 20 h by exposure to oxygen. Gels were purified by dialysis (6-8 kDa MWCO) against water for 5 days. PEGMA nanogel (485 mg, 0.37 mmol acrylic acid, 1 equiv) suspended in 25 mL water was transferred to a round bottom flask under argon in an ice bath (0 °C). To this was added EDC (285 mg, 1.8 mmol, 5 equiv), DMAP (22.5 mg, 0.18 mmol, 0.5 equiv) and 2-aminophenylboronic acid (319.4 mg, 1.8 mmol, 5 equiv). The mixture was stirred at 21 °C for 16 hours before being quenched by exposure to oxygen. The nanogels were purified by dialysis (6-8

kDa MWCO) against water for 3 days. ^{1}H NMR (400 MHz in D_6DMSO) δ: 8.78, 8.33, 7.76, 7.30, 6.99, 3.98, 3.49, 3.23, 1.73, 0.91, 0.75. IR: ν = 3438, 2878, 1724, 1450, 1388, 1352, 1246, 1104, 1028, 944, 850, 750 cm^{-1}.

Loading and release of glucagon in nanogel

Glucagon (1 mg/mL in borate buffer pH 9.5 for native or DPBS pH 7.4 for soluble glucagon) and NIPAM or PEGMA nanogels (8-10 mg/mL in water) were combined in a LoBind tube at 1:1 volume ratio and incubated at 4 °C on the rocker for 16 h. Aliquots (200 µL) of nanogel or glucagon without nanogel were separated into LoBind tubes and to each was added borate buffer pH 9.5 (for native glucagon) or DPBS pH 7.4 (for soluble glucagon) with or without 10 mg/mL glucose. Samples were either heated at 37 °C for 30 min to collapse nanogels or kept at 4 °C. Samples were centripreped (MWCO 30 kDa) or dialyzed (MWCO 6-8 kDa) with the centrifuge at room temperature, refilling the reservoir with either borate buffer pH 9.5 + 10 mg/mL glucose for 3 washes then DPBS pH 7.4 + 10 mg/mL glucose for the final wash (native glucagon) or all washes with DPBS pH 7.4 + 10 mg/mL glucose. Filters were filled with DPBS pH 7.4 for release cycles and centripreped (MWCO 30 kDa) or dialyzed (MWCO 6-8 kDa). Filtrates and samples left in the centriprep filters were saved to analyze loading by fluorescamine assay, ELISA, or HPLC.

Fluorescamine assay

A 3 mg/mL stock solution of fluorescamine was prepared in DMSO. 80 µL of samples, calibrators, and buffer blanks were plated on a black 96-well plate. To each well was added 30 µL of the fluorescamine solution and the plate was incubated at 37 ˚C for 30 minutes. The fluorescence

(λ_{ex} = 380 nm, λ_{em} = 460 nm) was measured and the amount of glucagon in each sample was calculated using the calibrators.

ThT assay

ThT solution was prepared at 50 μM (0.0159 mg/mL) in 20 mM DPBS pH 7.4. Into a 96-well plate, 50 μL each sample was pipetted. To these was added 250 μL ThT solution and the plate was incubated at room temperature (21 °C) for 20 min. Fluorescence intensity was measured on the Tecan plate reader (λ_{ex} = 450 nm, λ_{em} = 482). Fold fluorescence change was normalized to the buffer control.

Statistical Analysis

For assessment of the statistical significance of differences, one-way ANOVA followed by two-tailed Student's t-test assuming unequal sample variance was employed. Results were considered significantly different if $p < 0.05$.

Figures

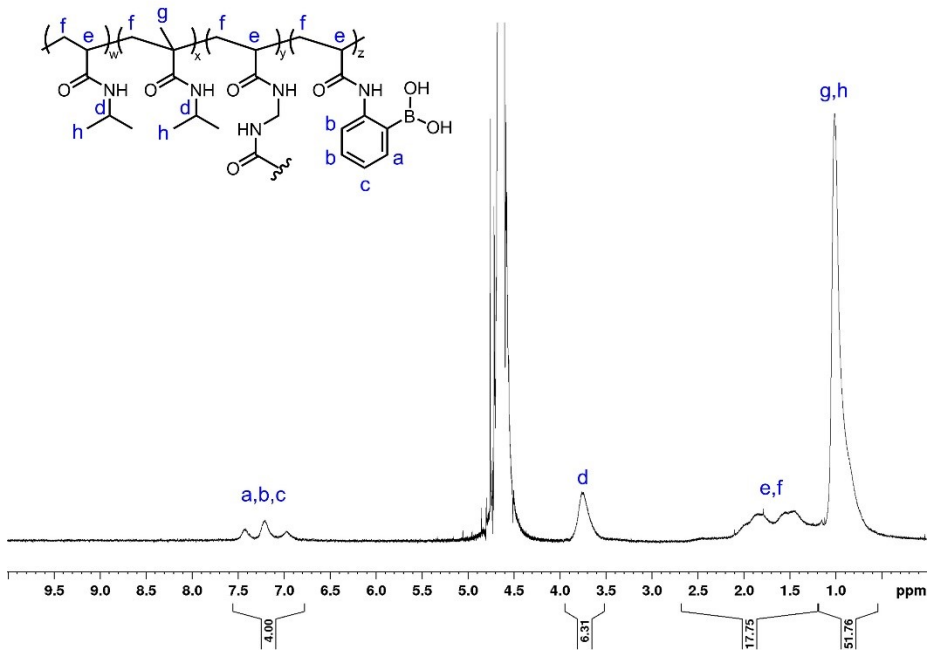

Figure 6-4. ^{1}H-NMR spectrum of NIPAM nanogel (D_2O)

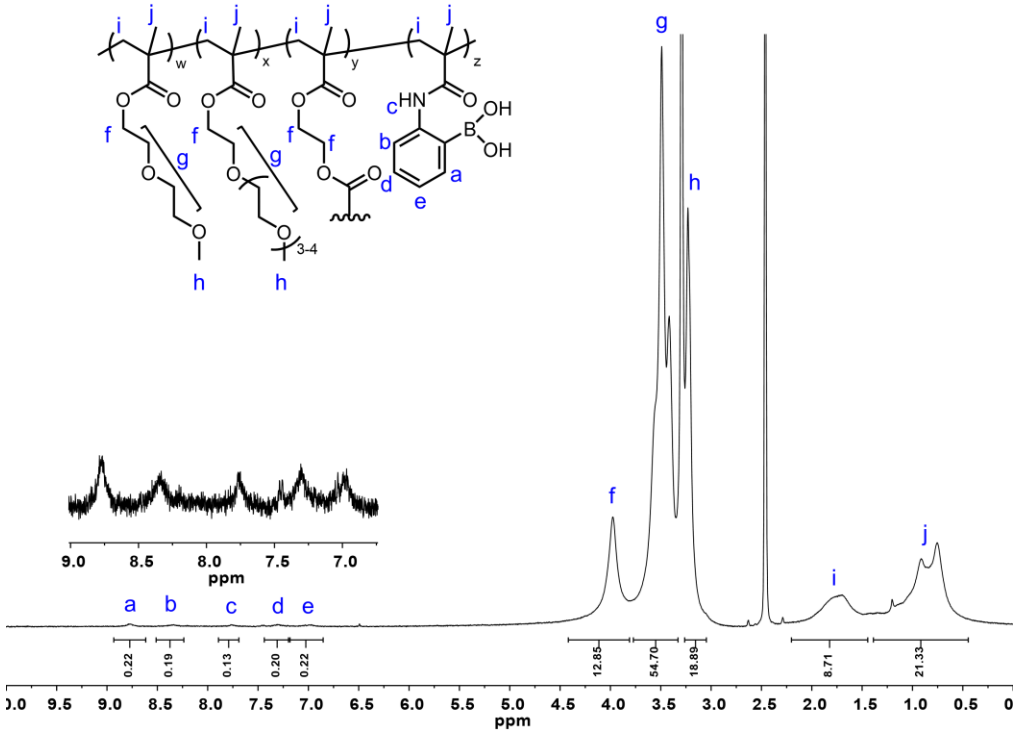

Figure 6-5. ^{1}H-NMR spectrum of PEGMA nanogel (D_6DMSO).

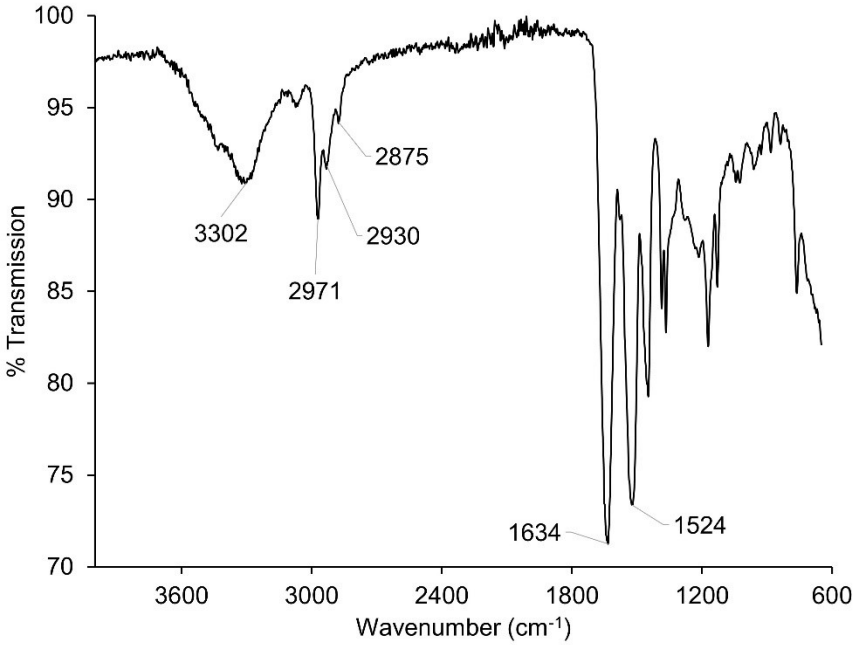

Figure 6-6. FT-IR spectrum of NIPAM nanogel

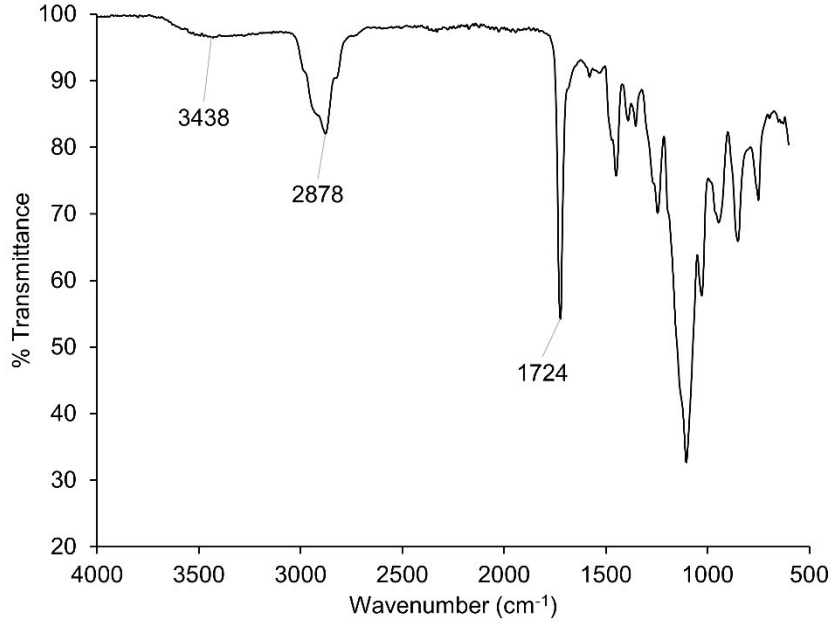

Figure 6-7. FT-IR spectrum of PEGMA nanogel

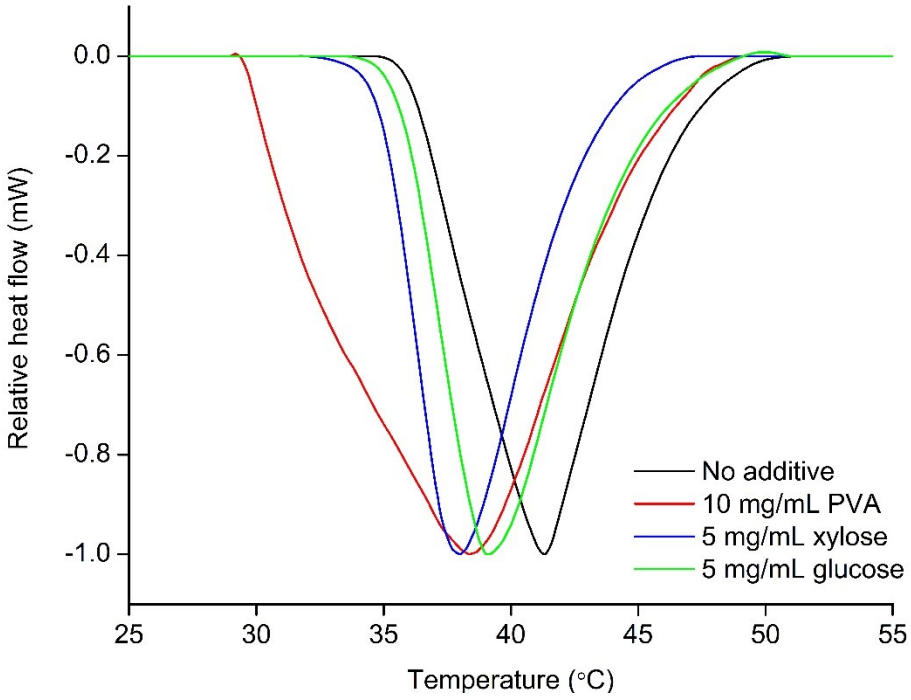

Figure 6-8. DSC of NIPAM nanogel with various polyols

Table 6-2. Characterization of NIPAM nanogel VPTT by DSC with various polyols

Condition	Onset (°C)[a]	VPTT (°C)[b]
No additive	34.8	41.9
10 mg/mL PVA	29.2	38.4
5 mg/mL xylose	33.5	38.1
5 mg/mL glucose	33.9	39.0

[a] Onset temperature was calculated from the initial change from baseline of the DSC peak, [b] VPTT was determined from the minimum of the DSC peak

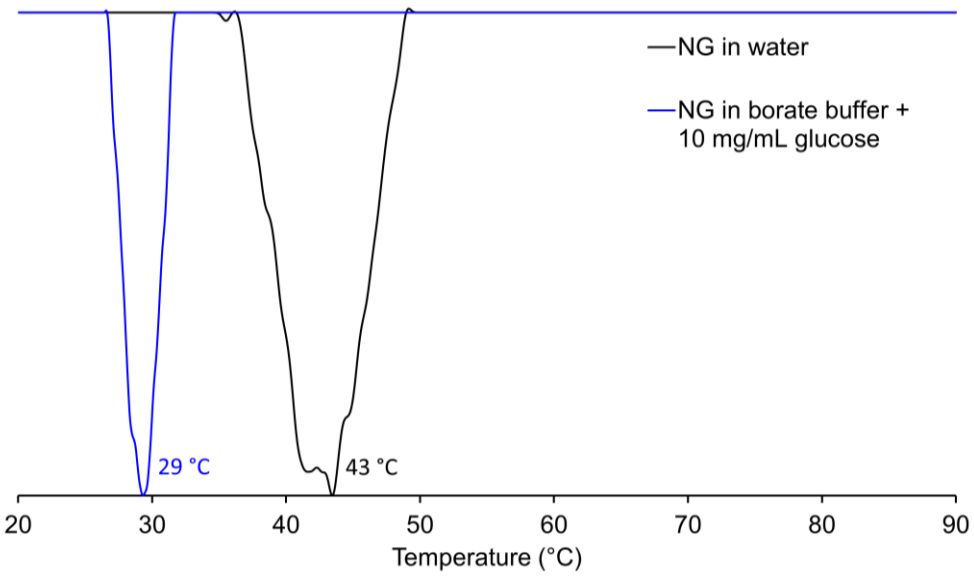

Figure 6-9. DSC of PEGMA nanogels with and without glucose

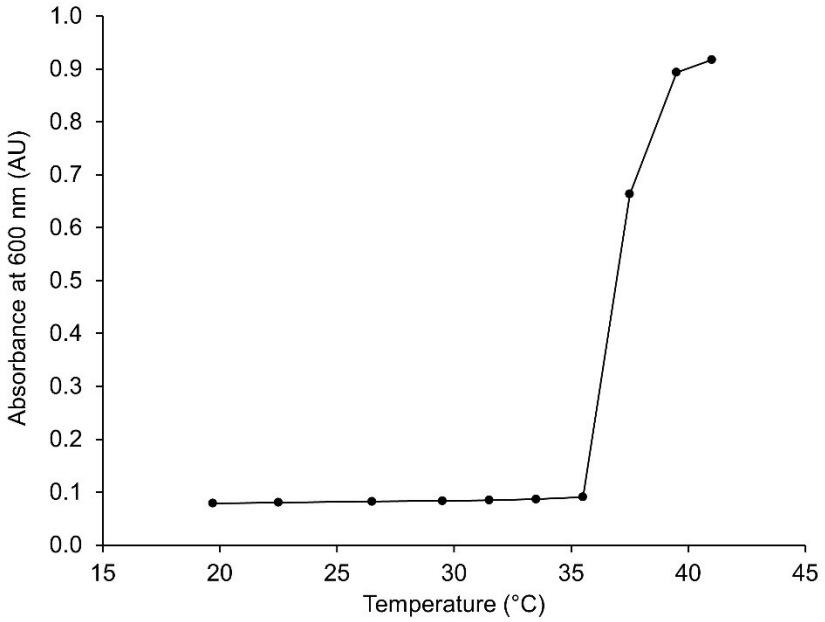

Figure 6-10. Turbidity of PEGMA nanogel VPTT by UV-vis

Table 6-3. Native glucagon loading and release with NIPAM nanogels

Condition	Loading efficiency (%)	Glucagon release (%) [c]
PBS [a]	83	2
Borate buffer [a]	79	7.7
Borate buffer with 0.1% SDS [a]	80	0.27
FBS [b]	98	0.2[d]
Dialysis in PBS [b]	97	0.7[d]
Whole blood [b]	81	0.8[d] – 4[e]

[a] HPLC, [b] ELISA, [c] Maximum glucagon released over 24 h, [d] 37 °C, [e] 4 °C

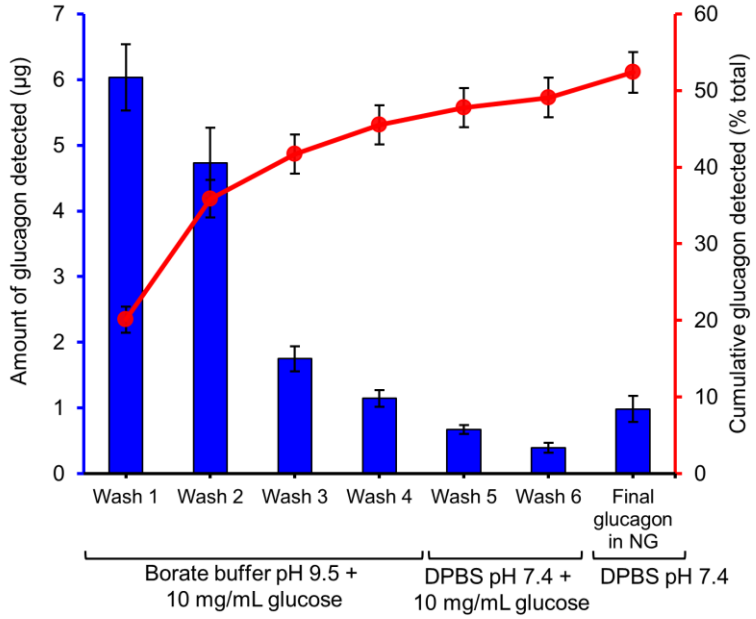

Figure 6-11. Amount of glucagon (blue) and cumulative glucagon detected over all steps (red) by fluorescamine assay during loading of native glucagon into NIPAM nanogels (n = 3).

6.5 References

(1) Eli Lilly and Company, Information for the Physician: Glucagon for Injection (rDNA Origin). 2018.

(2) Müller, T.; Finan, B.; Clemmensen, C.; DiMarchi, R.; Tschöp, M. The new biology and pharmacology of glucagon. *Physiol. Rev.* **2017,** *97*, 721-766.

(3) Joshi, A. B.; Rus, E.; Kirsch, L. E. The degradation pathways of glucagon in acidic solutions. *Int. J. Pharm.* **2000,** *203*, 115-125.

(4) Onoue, S.; Ohshima, K.; Debari, K.; Koh, K.; Shioda, S.; Iwasa, S.; Kashimoto, K.; Yajima, T. Mishandling of the therapeutic peptide glucagon generates cytotoxic amyloidogenic fibrils. *Pharm. Res.* **2004,** *21*, 1274-1283.

(5) Yale, J.-F.; Dulude, H.; Egeth, M.; Piché, C. A.; Lafontaine, M.; Carballo, D.; Margolies, R.; Dissinger, E.; Shames, A. R.; Kaplowitz, N. Faster use and fewer failures with needle-free nasal glucagon versus injectable glucagon in severe hypoglycemia rescue: a simulation study. *Diabetes Technol. Ther.* **2017,** *19*, 423-432.

(6) Eli Lilly and Company, BAQSIMI- glucagon powder. 2019.

(7) Seaquist, E. R.; Dulude, H.; Zhang, X. M.; Rabasa-Lhoret, R.; Tsoukas, G. M.; Conway, J. R.; Weisnagel, S. J.; Gerety, G.; Woo, V. C.; Zhang, S. Prospective study evaluating the use of nasal glucagon for the treatment of moderate to severe hypoglycaemia in adults with type 1 diabetes in a real-world setting. *Diabetes, Obes. Metab.* **2018,** *20*, 1316-1320.

(8) Wilson, L. M.; Castle, J. R. Stable liquid glucagon: beyond emergency hypoglycemia rescue. *J. Diabetes Sci. Technol.* **2018,** *12*, 847-853.

(9) Wang, J.; Wang, Z.; Yu, J.; Kahkoska, A. R.; Buse, J. B.; Gu, Z. Glucose-Responsive Insulin and Delivery Systems: Innovation and Translation. *Adv. Mater.* **2019**, 1902004.

(10) Brooks, W. L.; Sumerlin, B. S. Synthesis and applications of boronic acid-containing polymers: From materials to medicine. *Chem. Rev.* **2016,** *116*, 1375-1397.

(11) Yang, X.; Lee, M. C.; Sartain, F.; Pan, X.; Lowe, C. R. Designed boronate ligands for glucose-selective holographic sensors. *Chem. - Eur. J.* **2006,** *12*, 8491-8497.

(12) GhavamiNejad, A.; Li, J.; Lu, B.; Zhou, L.; Lam, L.; Giacca, A.; Wu, X. Y. Glucose-Responsive Composite Microneedle Patch for Hypoglycemia-Triggered Delivery of Native Glucagon. *Adv. Mater.* **2019,** *31*, 1901051.

(13) Yu, J.; Zhang, Y.; Sun, W.; Kahkoska, A. R.; Wang, J.; Buse, J. B.; Gu, Z. Insulin-Responsive Glucagon Delivery for Prevention of Hypoglycemia. *Small* **2017,** *13*, 1603028.

(14) Tang, Z.; Guan, Y.; Zhang, Y. Contraction-type glucose-sensitive microgel functionalized with a 2-substituted phenylboronic acid ligand. *Polym. Chem.* **2014,** *5*, 1782-1790.

(15) Tang, Z.; Guan, Y.; Zhang, Y. The synthesis of a contraction-type glucose-sensitive microgel working at physiological temperature guided by a new glucose-sensing mechanism. *Polym. Chem.* **2018,** *9*, 1012-1021.

(16) Zhang, Y.; Guan, Y.; Zhou, S. Synthesis and volume phase transitions of glucose-sensitive microgels. *Biomacromolecules* **2006,** *7*, 3196-3201.

(17) Kim, Y.-H.; Kwon, I. C.; Bae, Y. H.; Kim, S. W. Saccharide effect on the lower critical solution temperature of thermosensitive polymers. *Macromolecules* **1995,** *28*, 939-944.

(18) Kawasaki, H.; Sasaki, S.; Maeda, H.; Mihara, S.; Tokita, M.; Komai, T. Saccharide-induced volume phase transition of poly (N-isopropylacrylamide) gels. *J. Phys. Chem.* **1996,** *100*, 16282-16284.

(19) Shpigelman, A.; Portnaya, I.; Ramon, O.; Livney, Y. D. Saccharide-structure effects on poly N-isopropylacrylamide phase transition in aqueous media; Reflections on protein stability. *J. Polym. Sci., Part B: Polym. Phys.* **2008,** *46*, 2307-2318.

(20) Karg, M.; Pich, A.; Hellweg, T.; Hoare, T.; Lyon, L. A.; Crassous, J. J.; Suzuki, D.; Gumerov, R. A.; Schneider, S.; Potemkin, I. I., et al. Nanogels and Microgels: From Model Colloids to Applications, Recent Developments, and Future Trends. *Langmuir* **2019,** *35*, 6231−6255.

(21) N-Isopropylacrylamide, SDS, CAS No. 2210-25-5. ThemoFisher Scientific: Online.

(22) Cooperstein, M. A.; Canavan, H. E. Assessment of cytotoxicity of (N-isopropyl acrylamide) and poly (N-isopropyl acrylamide)-coated surfaces. *Biointerphases* **2013,** *8*, 19.

(23) Cai, T.; Marquez, M.; Hu, Z. Monodisperse thermoresponsive microgels of poly (ethylene glycol) analogue-based biopolymers. *Langmuir* **2007,** *23*, 8663-8666.

(24) Lutz, J. F. Polymerization of oligo (ethylene glycol)(meth) acrylates: Toward new generations of smart biocompatible materials. *J. Polym. Sci., Part A: Polym. Chem.* **2008,** *46*, 3459-3470.

(25) Ashby, J.; Duan, Y.; Ligans, E.; Tamsi, M.; Zhong, W. High-Throughput Profiling of Nanoparticle–Protein Interactions by Fluorescamine Labeling. *Anal. Chem.* **2015,** *87*, 2213-2219.

(26) Duan, Y.; Liu, Y.; Shen, W.; Zhong, W. Fluorescamine labeling for assessment of protein conformational change and binding affinity in protein–nanoparticle interaction. *Anal. Chem.* **2017,** *89*, 12160-12167.

(27) Wagman, M. E.; Dobson, C. M.; Karplus, M. Proton NMR studies of the association and folding of glucagon in solution. *FEBS Lett.* **1980,** *119*, 265-270.

(28) Oliveira, C. L. P.; Behrens, M. A.; Pedersen, J. S.; Erlacher, K.; Otzen, D.; Pedersen, J. S. A SAXS study of glucagon fibrillation. *J. Mol. Biol.* **2009,** *387*, 147-161.

(29) Chabenne, J.; Chabenne, M. D.; Zhao, Y.; Levy, J.; Smiley, D.; Gelfanov, V.; DiMarchi, R. A glucagon analog chemically stabilized for immediate treatment of life-threatening hypoglycemia. *Mol. Metab.* **2014,** *3*, 293-300.

(30) Chabenne, J. R.; DiMarchi, M. A.; Gelfanov, V. M.; DiMarchi, R. D. Optimization of the native glucagon sequence for medicinal purposes. *J. Diabetes Sci. Technol.* **2010,** *4*, 1322-1331.

(31) Coughlan, D. C.; Quilty, F. P.; Corrigan, O. I. Effect of drug physicochemical properties on swelling/deswelling kinetics and pulsatile drug release from thermoresponsive poly(N-isopropylacrylamide) hydrogels. *J. Control. Release* **2004,** *98*, 97–114.